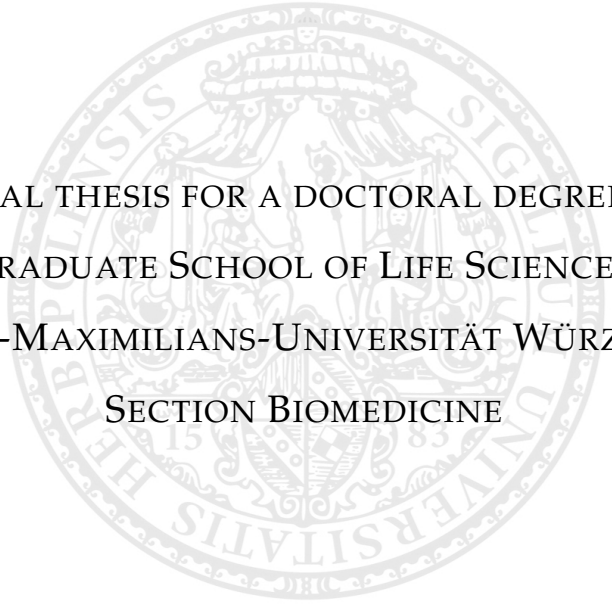

Doctoral thesis for a doctoral degree at the
Graduate School of Life Sciences,
Julius-Maximilians-Universität Würzburg,
Section Biomedicine

Mathematical Modeling of Cellular Signal Transduction

Mathematische Modellierung der zellulären Signaltransduktion

Submitted by
Gaby Wangorsch

from
Mellrichstadt

Würzburg, 2013

Submitted on: .....

Office stamp

Members of the Promotionskomitee:

Chairperson:	Prof. Dr. Manfred Gessler
Primary Supervisor:	Prof. Dr. Thomas Dandekar
Supervisor (Second):	Prof. Dr. Ulrich Walter
Supervisor (Third):	Prof. Dr. Jörg Schultz

Date of Public Defence: .....

Date of Receipt of Certificates: .....

To Thomas T.

in Memoriam

Acknowledgements

This doctoral thesis comprises research results arising from interdisciplinary collaborations of the Department of Bioinformatics at the University of Würzburg together with the University Hospital Würzburg. Starting in March 2008, I have been a fellow of the Graduate School of Life Sciences, section Biomedicine, and member of the special research area (SFB688) on mechanisms and imaging of cardiovascular cell-cell-interactions.

First and foremost, I would like to thank all the people who have accompanied and supported me over the last years.

All members of my supervisory committee Prof. Thomas Dandekar, Prof. Jörg Schultz and Prof. Ulrich Walter, for their support within the Doctoral Study Program "Life Sciences" of the Graduate School of Life Sciences.

My primary supervisor Prof. Thomas Dandekar, for giving me the opportunity to meet the dynamic research field at the interface between mathematics, biology and medicine. He supported me with his unwavering optimism and encouraging guidance during the conductance of my research.

My second supervisor Prof. Walter, the former speaker of the special research area (SFB688) on mechanisms and imaging of cardiovascular cell-cell-interactions, for offering such a comfortable and stimulating research environment. It was fascinating to immerse into the world of platelets, being tiny and anucleate blood cells but representing a pivotal regulatory target with regard to severe cardiovascular diseases. Following this, I am grateful for the funding by the DFG project SFB688.

My third supervisor Prof. Jörg Schultz for introducing me into the mysterious world of Perl, many helpful comments on my thesis and his persistent encouragement.

My external collaborators Prof. Harald Wajant (Division of Molecular Internal Medicine, Department of Internal Medicine II, University Hospital Würzburg) for sharing expert knowledge and data on inflammation signaling. Prof. Elke Butt, Dr. Jörg Geiger, Dr. Katharina Hubertus and Dr.

Stepan Gambaryan (Institute of Clinical Biochemistry and Pathobiochemistry, University of Würzburg) for fruitful discussions and providing data on platelets.
My former working group at the University of Freiburg for discussions and support in data-based mathematical modeling.
All associated members from the SFB688 for prosperous collaborations, in particular Prof. Stefan Frantz, Christina Pachel, Prof. Kristina Lorenz, Dr. Attila Braun, for starting and establishing interdisciplinary collaborations.
My internal collaborators, for helpful and stimulating discussions and meetings, showing that there is much more about Bioinformatics than BLAST and alignments; Tobias Müller and Marcus Dittrich for training and support in data analysis; Nicole Philippi and Muhammad Naseem for exchanging ideas on computational modeling of biological systems; Desi and Santosh - my brave "plateleteers" - for forming such a dense and interacting clot of mutual information exchange; every thrombus may become envious of.
All actual and former colleagues at the Department, especially Karin Lustre, Stefan Obermeier, Daniela Beißer, Christian Koetschan, Tina Schleicher, Alex the Great, Bärtierchen Frank, Michael Seidl, Astrid Fieselmann and the "plateleteers", for a very comfortable working atmosphere and many nice chats over some cups of coffee. Thanks for the unforgettable time also beyond room 116. Hopefully, the "interactions" we established during graduation will also have high edge scores in the future.
The LaTeX-command \usepackage[always]{coffee, chocolate} and Daniel for donating the essential, motivating Leberwurscht.
My "Stoogemer Mädels" together with the whole "Mühlfeld- and Werner-gang". The ties of our friendship are of incomparable value and helped a lot in managing the ups and downs in my life.
My brother Klaus, for proof-reading, for always taking care of his little sister and cheering me up with his music and extraordinary cooking experiments.
Lastly and surely the most, my entire family, especially my dear parents, for all their unconditional and perpetual love and support.

Abstract

A subtly regulated and controlled course of cellular processes is essential for the healthy functioning not only of single cells, but also of organs being constituted thereof. In return, this entails the proper functioning of the whole organism. This implies a complex intra- and inter-cellular communication and signal processing that require equally multi-faceted methods to describe and investigate the underlying processes.

Within the scope of this thesis, mathematical modeling of cellular signaling finds its application in the analysis of cellular processes and signaling cascades in different organisms. First, a comprehensive systemic analysis of signaling pathways in human platelets is presented. These tiny blood cells play a key role in thrombosis and hemostasis. Based on an integrative platelet-specific data base (PlateletWeb), I developed interaction networks, qualitative and quantitative models of antagonistic signaling pathways in the platelet. On the basis of phosphoproteomic data, this afforded the integration of potential substrates of key kinases into a functional network context. By means of a discrete dynamic model of central signaling cascades, I investigated the interplay between activatory and inhibitory signaling pathways towards the ultimate platelet aggregation. Extensive model simulations thereby documented the gradual activation of blood platelets to the point of aggregation. Data-based dynamic modeling of the inhibiting platelet cascade permitted quantitative model predictions of pivotal second messengers and yielded for the first time the quantification of central regulators. By comprehensively calibrating the dynamic model with time series data, I deciphered the feed-back regulation of second messengers (cAMP, cGMP) that lead to platelet inhibition. Model-based analyses of pathway cross-talks demonstrated the wide-ranging scope of pharmacological modulation, not only in the platelet but also in other cell types such as cardiomyocytes.

Inflammatory processes are regulated by a multitude of signaling cascades that are highly cross-linked as well. I here present a first mathematical model for simulating the apoptotic cross-talk between TNF receptors, crucial mediators of inflammatory processes. In this type of signaling, the detailed and receptor-specific formation of the signal at the respective receptor is also of prime importance. Here, simulations of a structure-orientated mathematical model offer valuable clues about the strengths of ligand-encoded signal that is created at the particular receptor.

Likewise, mathematical modeling and simulations are beneficial to decode the interplay of distinct phytohormones, as shown here using the example of *Arabidopsis* and pathogen *Pst* DC3000. Model-based forecasting together with profound validation by means of experimental data revealed multiple cross-talk for the hormone cytokinin with respect to plant immunity.

Lastly, models describing intra- and inter-cellular signaling of different liver cells demonstrate the impact of combining mathematical models to functionally analyze the liver as a holistic cellular system.

Within the framework of this thesis, I present mathematical methods for modeling cellular signaling cascades and their interplay in different organisms. Resulting models form the basis for a systemic description and analysis of cell-regulatory processes as well as for model-based predictions. This way, models guide further experimental investigation and are capable to indicate novel interaction points for pharmacological modulations.

Zusammenfassung

Das fein regulierte und kontrollierte Ablaufen zellulärer Prozesse ist essentiell für das gesunde Funktionieren einzelner Zellen, sowie der aus ihnen bestehenden Organe. Diese wiederum bedingen das Funktionieren des gesamten Organismus. Genauso vielschichtig wie die Kommunikation und Signalverarbeitung innerhalb und zwischen den Zellen, sind die Methoden um diese Vorgänge zu beschreiben und zu untersuchen.

Die mathematische Modellierung zellulärer Signalverarbeitung findet im Rahmen dieser Arbeit Anwendung in der Analyse zellulärer Prozesse und Signalkaskaden in verschiedenen Organismen. Zunächst wird eine umfassende systemische Analyse von Signalwegen in humanen Blutplättchen gegeben. Diese kleinen Blutzellen spielen eine Schlüsselrolle in Thrombose und Hämostase. Ausgehend von einer integrativen Blutplättchen-spezifischen Datenbank entwickelte ich Interaktionsnetzwerke sowie qualitative und quantitative Modelle zu antagonistischen Signalwegen der Blutplättchen. Auf der Basis von Phosphoproteom-Daten war es möglich, potentielle Substrate wichtiger Kinasen in einen funktionellen Netzwerkkontext zu setzen. In einem diskret-dynamischen Modell zentraler Signalkaskaden untersuchte ich das Zusammenspiel aktivierender und inhibierender Signalwege bis hin zur finalen Aggregation des Blutplättchens. Das durch intensive Simulationen gezeigte Verhalten belegt die schrittweise Aktivierung des Blutplättchens bis zur finalen Plättchen-Aggregation. Die datenbasierte, dynamische Modellierung der inhibierenden Kaskade konnte quantitative Vorhersagen bezüglich wichtiger sekundärer Botenstoffe im Plättchen erzielen, sowie erstmals wesentliche Regulatoren quantifizieren. Durch umfangreiche Kalibrierung des dynamischen Modells mit Zeitreihendaten entschlüsselte ich eine durch Rückkopplungsschleifen charakterisierte Regulierung der Botenstoffe (cAMP, cGMP), die zur Inhibierung des Plättchens führen. Modell-basierte Analysen zur Quervernetzung der inhibierenden Kaskade demonstrieren den breitgefächerten Spielraum für pharma-

kologischen Modulierung und zeigen neue molekulare Angriffspunkte auf, nicht nur in Blutplättchen, sondern auch in anderen Zelltypen wie beispielsweise der Herzmuskelzelle.

Entzündungsprozesse werden ebenfalls durch eine Vielzahl von Signalkaskaden geregelt, die miteinander stark wechselwirken. Ich präsentiere ein erstes mathematisches Modell zur Simulation der apoptotischen Wechselwirkung zwischen TNF-Rezeptoren, welche die Vermittlung von Entzündungsprozessen bewerkstelligen. Hierbei ist auch die detaillierte, Rezeptor-spezifische Entstehung des Signals von Bedeutung, welches über den Rezeptor weitergegeben wird. Simulationen eines strukturorientierten mathematischen Modells geben Aufschluss über die mögliche Stärke des Liganden-kodierten Signals am jeweiligen TNF-Rezeptor.

Ebenso nützlich ist die mathematische Modellierung und Simulation beim Entschlüsseln des Zusammenspiels verschiedener Pflanzenhormone, wie am Beispiel von *Arabidopsis* und dem Pathogen *Pst* DC3000 gezeigt wird. Modell-basierte Vorhersagen in Verbindung mit intensiver Validierung mittels experimenteller Daten konnten dabei dem Hormon Cytokinin eine Vielzahl vernetzter Effekte und Wechselwirkungen mit dem Pflanzenimmunsystem zuweisen.

Modelle zur Beschreibung von Signalwegen in und zwischen verschiedenen Typen von Leberzellen demonstrieren abschließend, wie eine Kombination von mathematischen Modellen die funktionelle Analyse der Leber als gesamtzelluläres System unterstützt.

Die vorliegende Arbeit präsentiert mathematische Methoden zur Modellierung zellulärer Signalkaskaden und deren Zusammenspiel in verschiedenen Organismen. Resultierende Modelle bilden die Grundlage für eine systemische Beschreibung und Analyse der zellregulierenden Vorgänge sowie für Modell-basierende Vorhersagen. Auf diese Weise geben sie Ideen für weitere Untersuchungen auf experimenteller Ebene und zeigen neue Ansatzpunkte für eine pharmakologische Modulation auf.

Table of Contents

Preface

MATHEMATICS IS BIOLOGY'S NEXT MICROSCOPE,
ONLY BETTER;
BIOLOGY IS MATHEMATICS' NEXT PHYSICS,
ONLY BETTER.

(*Joel E. Cohen*)

Mathematics and the life sciences have always been intertwined and already have a history of successful mutual interactions starting approximately 500 years ago. In 1628, physician William Harvey published his outstanding work "De Motu Cordis" (White, 1999) and set a pivotal milestone in the early history of biological quantitation. By meticulously observing the anatomy and dynamics of the heart, he could reasonably demonstrate that blood circulates in the body which was a revolutionary finding at that time. Moreover, the theoretical predictions based on mathematical calculations were scientifically confirmed in the following decades, illustrating the tremendous power of sensibly combining simple mathematics with thorough observations. Since then, all fields of mathematics have made remarkable progress, which has also enriched biology and all life sciences. Mathematics was and still is crucial for interpreting any kind of data. Or, to say it with Charles R. Darwin's words:

"*Mathematics seems to endow one*
with something like a new sense" (Bell, 1986).

The development of medical imaging, the theory of evolution or population-biological research are just some examples showing the benefit of mathematical approaches.

Conversely, mathematics has gained profit and progress through scientific and conceptual challenges from life sciences over the past years. Exemplary, the logistic equation for limited population growth (Verhulst, 1838), correlation (Pearson and Lee, 1903), Markov chains, statistics of language (Markov, 1906), the Hardy-Weinberg equilibrium in population genetics (Hardy, 1908; Weinberg, 1908), biochemical kinetics (Menten and Michaelis, 1913), the dynamics of interacting species (Lotka, 1925; Volterra, 1931), game theory (von Neumann and Morgenstern, 1953), threshold functions of random graphs (Erdoes and Renyi, 1960) or the sampling formula for haplotype frequencies (Ewens, 1972) show the diverse fields of mathematics which arose from biological problems.

Nevertheless, a quantitative and mathematically based description of biology has been very slow in development, moving the mathematician Gian-Carlo Rota to state this scathing remark:

> *"The lack of real contact between mathematics and biology*
> *is either a tragedy, a scandal, or a challenge,*
> *it is hard to decide which"* (Rota et al., 1986).

However, much has changed in the almost three decades since Rota's comment. This includes the rise of complete new disciplines in the field of computational life sciences such as bioinformatics and systems biology, the interdisciplinary union of data-based mathematical modeling and cell biology (Chuang et al., 2010).
We gain more and more insight into the complexity of biological systems, their multi-scale regulation and organization by accumulating loads of increasingly precise data. Technological advances (e.g. high through-put processing) and improved laboratory analysis methods have made biology a data-rich science demanding increasingly ingenious mathematical and computational concepts and tools. Computational methods based on a solid theoretical and numerical foundation have been established, especially tailored to investigate adaptive and dynamic systems in biomedicine. These techniques now allow for representing and analyzing large, multi-scale com-

plex systems and studying their emergent properties. Moreover, they offer tools to make both qualitative and quantitative predictions in order to investigate inherent system properties. Machine learning, numerics and bioinformatics support the efficient data mining and its analysis as well as the extraction of the most useful data from within an overwhelming amount. Advances in computer-aided approximation approaches and algorithms permit the simulation and optimization of large biological networks and help to reveal the dynamics of more focused non-linear systems. By novel physical, mathematical and computational methods, the folding of proteins and the binding between a ligand and its target site can be predicted, suggesting insights into highly specific molecular interactions. This in turn highlights points of interaction for targeted drug interventions.
The relevant disciplines complement each other in such a way that the "explosive synergy" (Cohen, 2004) among them will revolutionize not only biology and medicine but also other fields including environmental science, food production and drug development.

Modeling and simulation of intracellular molecular networks and cellular signal transduction is one challenging example how biology can inspire mathematical research and vice versa. The analysis of these cell communication processes has become an inevitable part of systems biological investigation. This thesis covers a set of examples of applied mathematical methods to model processes in cell biology and signal transduction in different cell types and organisms.

1 Introduction

DIMIDIUM FACTI, QUI COEPIT, HABET.
HE WHO HAS BEGUN HAS HALF DONE.

(*Horace*)

Models in Life Sciences

The use of models in cell biology is both, familiar and enigmatic. On the one hand, biologists always used models as an abstraction of reality such as diagrams, laws, graphs, plots, chemical formulas and relationships. In the same way, "model organisms" like yeast, *Arabidopsis thaliana*, *Escherichia coli*, *Drosphila melanogaster* or mice are extensively studied to understand particular biological phenomena. Their role lies in being similar to many organisms without being the same. Thus, one expects that discoveries will provide insight into the workings of other organisms as well.
On the other hand, a mathematical description of biological systems and processes can also be understood as a model, constituting a relatively new sector of the biological science. According to Eykhoff (1974), a mathematical model is "a representation of the essential aspects of an existing system (or a system to be constructed) which presents knowledge of that system in usable form." Mathematical models may take many forms and are particularly useful for a data-integrative study of interactions between different components of biological systems, and how these interactions holistically impact the function and behavior of a system. This systems biological way of modeling links fundamental chemical and physical principles, prior knowledge about the investigated system and experimental data to a powerful tool for extending and formalizing traditional cell biology.

Why Mathematical Modeling?

A very first step towards the comprehension of mechanisms in living cells is certainly unscrambling the genome of an organism, however, a more detailed picture is needed to really gather the regulatory properties of genetic, metabolic and cellular signaling networks. This is sustained by mathematical formulation, the generation of hypotheses and comparative validation with experimental data. Data-based calibrated models potentially lead to new hypotheses and predictions and represent a guided way of designing promising continuative experiments to explore questions that are not amenable to experimental inquiry. At the same time, experimental measurements are often too complex to be understood by visual inspection and can be brought into relation.
Generally two main steps are involved in the modeling process: First, the building of a model of the biological system of interest, a suitably structured representation that incorporates existing knowledge and experimental observations. Secondly, this established model can be subjected to various conditions as well as be allowed to evolve in time, a step typically called simulation, used to generate qualitative or quantitative predictions on the overall behavior of the system. Therefore, systems biological modeling approaches are also of great impact for medical investigation as well as drug development and discovery.

Modeling Approaches

Mathematical modeling approaches comply with two key properties of biological systems: their static structure and their dynamics. Thus, modeling approaches differ in the choice of suitable model structures:
Networks, the visualization of interaction graphs (e.g. protein-protein interaction networks) suitably represent the static structure and serve as a foundation for further integrative network analyses (Arrell and Terzic, 2012; Goh et al., 2007), the category of regression models uses algebraic equations (Seber and Wild, 1989), discrete Boolean models are composed of logical gates (Saez-Rodriguez et al., 2009), Bayesian networks (Jensen, 1996) and stochastic models (Turner et al., 2004; Gillespie, 2007) are based on probability distributions and continuous dynamic models comprise either ordinary differential equations (Aldridge et al., 2006) or partial differential equations (Murray, 2003) in the more general case, agent- and rule-based modeling

allows dynamic modeling trying to reduce combinatorial complexity which would occur when using an approach purely based on ordinary differential equations (Faeder et al., 2009). All approaches imply assumptions about the considered system, require certain types of measurements, and allow conclusions at different levels of accuracy and detail.

Modeling of Cell Signaling Processes

The term "biological system" allows various interpretations at different organization levels demanding individual ways and methods for their modeling and analysis. This comprises metabolic systems, cell cycle regulation, development and differentiation as well as intra- and intercellular signaling and cell communication. Most of the underlying involved processes are characterized by its dynamic behavior. This includes changes in gene expression patterns or profiles of metabolites as well as fluctuations of protein and hormone levels, especially in response to changed environmental conditions or drug modulation.
This thesis puts the main emphasis on modeling and analyzing cellular signal transduction, a highly dynamic process in both, time and space (Kholodenko, 2006; Timmer and Mueller, 2004). Cellular signaling is plugged into a complex system communication, governing basic but also cell-type specific cellular activities and coordinating cell actions in uni- and multicellular organisms. Starting with the activation of a cell surface receptor, intracellular signaling molecules are subsequently altered propagating the elicited initial signal to its targeted cell response. These signaling events do not necessarily proceed in a linear cascade that relay and regulate information from cell surface receptors to effectors such as transcription factors or targeted enzymes. Cellular signaling networks are constituted of highly connected modules regulating multiple functions in a context dependent manner including regulatory feedback (Jordan et al., 2000). Moreover, signaling cascades also interact with one another, forming a functional network complex in its organization and abundant in targets for signal amplification.
The cellular ability to sense and to correctly respond to its environmental conditions is essential for pivotal processes such as development, tissue repair, hemostasis, inflammation and immunity. Consequently, errors in cellular information processing are likely to cause severe diseases including cancer, autoimmunity, altered hemostasis and diabetes. Thus, a meticulous understanding of cell signaling, e.g. the identification of signaling modules

and hubs, is necessary for an effective therapeutic intervention and prevention of diseases.
Exemplary, blood platelets represent a pivotal target of pharmacological intervention in systematically affecting platelet signaling to protect from pathological effects due to impaired signaling. Platelets, also called thrombocytes, are small blood cells of major importance in playing a pivotal role in processes mainly connected with primary hemostasis and thrombosis: Under physiological conditions, they circulate quiescently in the blood. In case of a disruption of the vessel wall, platelets undergo a rapid shape change and activation process during which they adhere to the site of vascular injury and form a hemostatic plug. This protects against bleeding and seals smaller lesions. However, under pathological conditions, unwanted platelet aggregation and thrombus formation may cause a complete occlusion of the blood vessel. Consequently, this leads to disorders like myocardial infarction and stroke which represent the leading causes of death worldwide according to the World Health Organization (2011). Moreover, platelets also have impact on inflammatory processes, antimicrobial host defense, angiogenisis as well as on disorders like Diabetes Mellitus, cancer, Alzheimer's Disease or psychiatric disorders (Michelson, 2006). Thus, a deep understanding of platelet physiology, biochemistry, signal transduction and pathology is essential to eventually develop new strategies for pharmacological interventions.

Modeling Approaches Tailored for Analyzing Signaling Pathways

Traditionally, cell biological research has focused on studying individual parts of cell signaling pathways and gained enormous progress over the last three decades. However, the analysis of cell signaling networks requires a combination of experimental and theoretical approaches including the development and analysis of simulations. Computational models provide a basis to unravel the complex relationships between the stimuli and the cellular responses, and to reveal the underlying structure of cell signaling networks, and the mechanisms that are responsible for signal amplification.
To fulfill this task, a variety of different modeling approaches have emerged and have been adapted and partially find its application within this thesis. The range of modeling approaches is vast and highly dependent on the modeling task and the available data. For qualitative predictions of the behavior of a signaling network and to focus on the network structure, it is

useful to analyze Boolean networks. Here, logically connected nodes representing the signaling components are either in an "on" or "off" state. The logic interconnection can be interpreted as gates through which a signal is propagated (Morris et al., 2010). By translating these pure interaction networks into continuous dynamic systems, they also serve as basis for semi-quantitative modeling and prediction (Di Cara et al., 2007). Parametric, dynamic approaches and models focus on the time-resolved cell signaling, the change of signaling components, e.g. its protein concentrations over time and can serve for quantitative fore-casts (Becker et al., 2010; Timmer and Mueller, 2004). This is especially important for modeling and predicting to dose-dependent pharmacological effects (Iadevaia et al., 2010). Moreover, modeling enables data-based calibration and estimation of model parameters that are not accessible by experimental methods, but are crucial to verify whether a proposed molecular mechanism is correct or not.
Despite substantial progress in biochemistry, cell and molecular biology together with high-throughput techniques for detecting protein-protein interactions, data acquisition and experimental determination of kinetic parameters still represent a bottleneck in systems biological pathway analysis. Nevertheless, modeling and the use of data-driven computer simulations enables to rapidly test and generate hypotheses about functions of the signaling network and its structure, to simulate data and also to sustain the design of further efficient experiments.

Overview of this Thesis

In this thesis, we present mathematical models of signaling cascades at different scales and show how computational models can be applied to guide experimental design by model-based simulations, to investigate the structure of signaling networks, and to verify and test hypotheses concerning the regulation and signal propagation of investigated signaling networks.
First, relevant prerequisites are presented in Section 2. This forms the necessary background on cell signaling and mathematical modeling to understand and to establish the subsequent modeling applications. Foundations range from in-depth information on cell signaling to signaling characteristics focused on different cell-types and cellular processes. We thereby focus on the biology and function of blood platelets as this represents the relevant background for a comprehensive *in silico* platelet systems analysis. Additionally, it provides a short introduction into the computational analysis of

biological systems.
This is followed by the detailed description of used materials and relevant methods for data analysis and mathematical modeling of signal transduction in Section 3. As the choice of appropriate modeling approaches strongly depends on the modeling task and the available data, we applied different strategies for the pathway analyses. For studying the molecular interactions and relating signaling components within a signaling context we exerted static network analyses relying on cell-type specific data bases and phosphoproteomic studies. This sustains the establishment of suitable network topologies which then can be simulated either in a discrete or dynamic manner for further computational analyses and data-based validation.
In Section 4, the different and multi-scaled modeling approaches are implemented. More precisely, we investigated and analyzed signaling cascades of regulatory importance in special cell-types, the blood platelets (Section 4.1) but also in globally relevant, crucial cellular processes such as inflammation (Section 4.2). These biomedically and pharmacologically motivated models and approaches can easily be transferred to different cell-types to model organismic processes such as signaling in cardiomyocytes, plant immunity in *Arabidopsis* or to elucidate the cross-talk between different liver cells (Section 4.3).
The resulting conclusions and the applied approaches are critically inspected and compared in Section 5. We conclude with future prospects of mathematical modeling in systems and computational biology.

2 Foundations and Principles

THE ONLY SOURCE OF KNOWLEDGE IS EXPERIENCE.

(*Albert Einstein*)

2.1 Background: Cellular Signal Transduction

2.1.1 Transduced and Regulated Processes

Signal transduction in cell biology involves the binding of extracellular signaling molecules and ligands to receptors at the cell surface that trigger events inside the cell. Receptor activation upon ligand binding, inter-cellular communication or cellular stress responses cause the cell's ultimate responses (effect) to the messenger such as gene activation (Lalli and Sassone-Corsi, 1994) and altered metabolism (Rosen, 1987).
Diverse signal transduction processes influence the reaction of a single-celled organism to environmental chances (Kollmann et al., 2005), but also coordinate cell-cell communication (Fontana et al., 1986) and holistic regulation within multicellular organisms. Thus, signaling cascades are particularly involved in regulatory processes like aging (Kenyon, 2010), inflammation (Hotamisligil, 2006), cell cycle control (Malumbres and Barbacid, 2009), apoptosis and cell survival (Dragovich et al., 1998) and hormonal regulations (Santner and Estelle, 2009). Moreover, a variety of diseases such as diabetes (Hotamisligil, 2003), heart disease (Lorenz et al., 2009) and cancer (Sawyers, 2004) arise from impaired signal transduction processes, highlighting the biological and medical importance of this process. These triggered multiple responses are all directly due to changes in particular cell proteins - a highly dynamic process.

2.1.2 Typical Signaling Cascade and Main Constituents

Cellular signaling pathways comprise typical molecular constituents such as receptors, G proteins, phosphorylation cascades (MAP kinase cascade) and first and second messengers to receive and process signals. Albeit it exists a huge variety of signaling cascades, a typical sequence of signal transduction and its core modules are depicted in Figure 1. The general cellular signal transduction proceeds as follows.

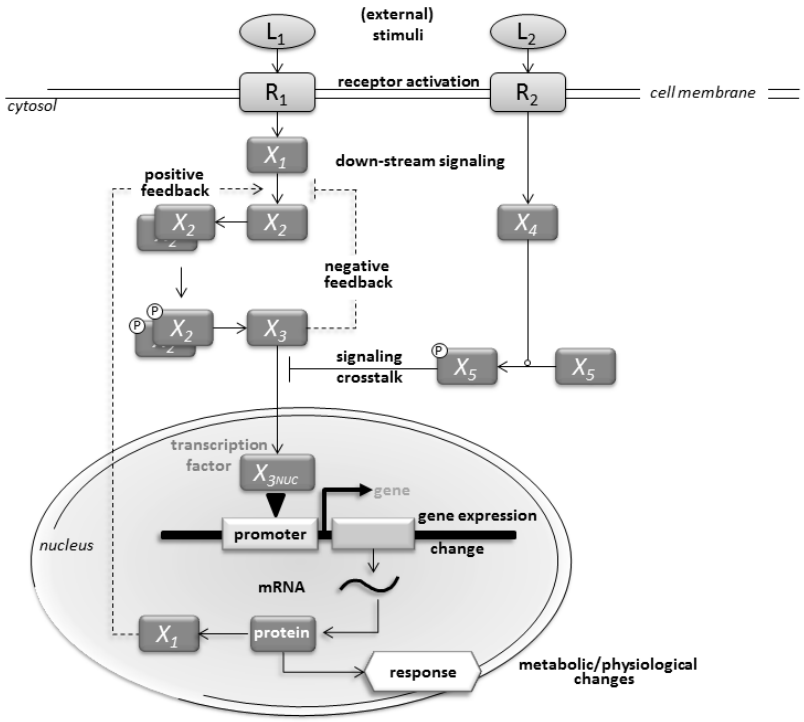

Figure 1: Signaling paradigm. Upon stimulation by a ligand or another kind of stimulus, the receptor gets activated and initiates the internal signaling propagation. This includes a series of protein phosphorylation state changes and the subsequent alteration of transcription factor activation. Thereby, the transcription rate of target genes is regulated, leading to a change in protein concentrations which in turn trigger the actual cellular responses to the initial signal. Figure construction follows Klipp et al. (2009).

A substance that acts as a ligand or physical stimulus (signal) binds to a transmembrane receptor which changes its state from susceptible to an activated state. This triggers an internal signaling cascade including a series of changes of phosphorylations states to propagate the signal. Phosphorylated or activated proteins may enter the nucleus to eventually de- or activate transcription factors. As a consequence, transcription factors change their binding properties to regulatory regions on the DNA which alters the

transcription rate of genes that lie downstream. This finally results in newly synthesized proteins or changes in protein concentrations causing the actual cellular response to the signal. In addition, several control mechanisms such as feedback and feed-forward activation and inhibition or cross-talk effects from different signaling pathways may potentially influence and regulate the signal cascade.

Ligand - Receptor Interactions There exist several concepts of the interaction between a ligand L and its receptor R. The simplest concept is the reversible binding, forming an intermediate active complex LR. This behavior is characterized by the dissociation constant

$$K_D = \frac{[L] \cdot [R]}{[LR]},$$

where $[L]$, $[R]$, and $[LR]$ denote the concentrations of the respective reactants. K_D can be derived from the law of mass action (see Section 2.3.3). Other receptors need to form a cluster to initiate the further signal propagation, or act through strategies that involve the mobilization and turnover of free receptors from intracellular pools or the internalization and degradation. These strategies are exemplary investigated by mathematical modeling for the information processing at the erythropoietin receptor (Becker et al., 2010).

G Proteins G proteins are involved in many signal cascades and play an essential role in the regulation of signal processing and mediation (Blumer and Thorner, 1991; Dohlman et al., 1991; Buck, 2000). Their name arise from the guanine nucleotides GDP (guanosine diphosphate) and GTP (guanosine triphosphate) they are bound to. They are heteromers consisting of three different subunits and are associated to cell surface receptors, the G protein-coupled receptors (GPCR). The activation and inactivation of G proteins follow a cycle. A G protein that binds GDP is inactive and the G protein α subunit (Gα) is associated with the G protein $\beta\gamma$ heterodimer (G$\beta\gamma$). Upon ligand binding to a GPCR, guanine nucleotide exchange is promoted: Gα releases GDP, instead binds GTP and dissociates from the G$\beta\gamma$ dimer. Both subunits Gα and G$\beta\gamma$ are free in order to activate their target proteins downstream the GPCR. There are several isoforms of each subunit which allow high combinatorial signal transduction options. They can be classified

according to their effects into subfamilies like the Gα_s- and Gα_i-subfamily, stimulating or inhibiting the production of cAMP from ATP, respectively. Hydrolysis of GTP enables the subunits to reassociate (Marks et al., 2009).

Second Messengers The intracellular signal transduction is often modulated by second messengers, which greatly amplify the signal strength. They can be grouped into water-soluble or -insoluble molecules or gases. Hydrophilic molecules like cyclic adenosine and guanosine monophosphate (cAMP and cGMP), inositol 1,4,5 trisphosphate (IP_3), or calcium ions (Ca^{2+}) are usually located within the cytosol or stored in special cellular organelles. Hydrophobic molecules such as diacylglycerol (DAG) and phosphatidylinositols are membrane-associated and diffuse from the plasma membrane into the intermembrane space to regulate membrane-associated effector proteins. Gases, e.g. nitric oxide (NO), carbon monoxide (CO) and hydrogen sulphide (H_2S) diffuse both through the cytoplasm and across cellular membranes to exhibit their effects. Normally, second messengers are enzymatically synthesized, activated or deactivated or released by opening of ion channels (Ca^{2+} signaling) (Nelson, 2009).

Feedback Regulations Signal cascades can exhibit special regulatory feedback features (see Figure 2) such as feed-forward loops and negative feedback. These features contribute to stability but also manifest interesting dynamics. Negative feedback is very common in transcription networks and also for regulating metabolic pathways. On cellular dynamics, negative feedback exhibits various effects such as the stabilization of systems states, the acceleration of response time or the introduction of oscillatory behavior (Hoffmann et al., 2002). Feed-forward loops often appear as motifs in transcriptional networks. One distinguishes two forms, coherent and incoherent feed-forward loops, which allow the differential regulation of a gene Z via two other genes (Mangan and Alon, 2003).

Signaling Cross-talk Signaling pathways cannot be considered separately, but influence each other at different scales: They can share pools of proteins, e.g. some proteins of one signaling pathway interact with proteins assigned to another cascade or an activated protein may have several targets that in turn affect different signal cascades (Fraser and Germain, 2009; Natarajan et al., 2006). Or, signal cascades may have the same target gene

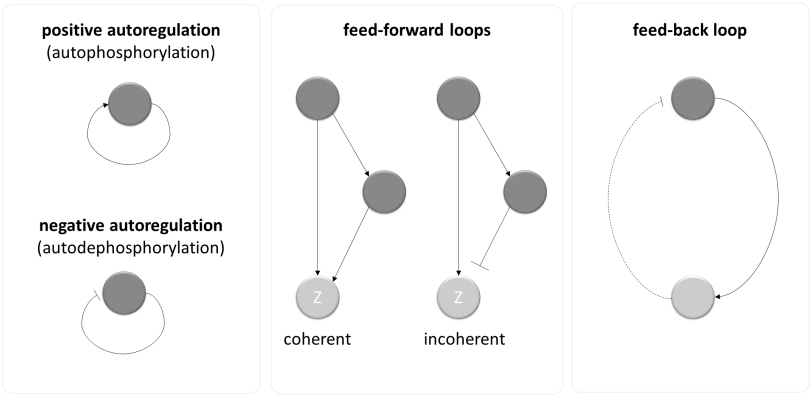

Figure 2: Motifs in signaling networks. Frequent regulatory network motifs include negative and positive autoregulation and feedback loops. Figure construction follows Marks et al. (2009) and Klipp et al. (2009).

as it is highly the case for the transcription factor NFκB (Oeckinghaus et al., 2011). These interactions may include feedback regulations or activatory and inhibitory effects also at the transcriptional level to alter the amplitude of a transduced signal. Cross-talk between signaling pathways provides for multiple non-linear responses to combinations of stimuli, but only little is known about the density of these interactions in any specific cell. Thus, the definition of a quantitative measure for signaling cross-talk is a crucial task. In the following we introduce the key concepts we applied for the analysis of signal transduction and its cross-talk.

2.1.3 Signaling in Inflammatory Processes

Exemplary, inflammation and inflammation-related diseases are highly connected with cell signaling processes at the molecular level. One has to distinguish between two types of inflammatory processes. The initial response of the body to harmful stimuli - acute inflammation - is achieved by the increased movement of plasma and leukocytes (in particular granulocytes) from the blood into the injured tissues. The inflammatory response is propagated and matured by a cascade of biochemical events that involve the local vascular system, the immune system, and various cells within the injured tissue. However, prolonged inflammation, the so-called chronic inflammation, can cause severe diseases such as rheumatoid arthritis or inflammatory bowel disease. Moreover, the onset of cancer (Coussens and Werb, 2002) and cardiovascular diseases (Pearson et al., 2003) have also been linked to inflammation. Therefore, a deep understanding as well as an investigation of inflammation and regulatory cross-talks (Beck et al., 2009), especially at

the molecular level, is indispensable in medical research.

Inflammation at the Molecular Level Inflammatory signaling progresses upon pro-inflammatory stimuli mediated by cytokines, such as interleukin-1 (IL-1), the tumor necrosis factor (TNF), interferon gamma (IFNγ), IL-12, IL-18. On the other hand, inflammation is resolved by action of anti-inflammatory cytokines including IL-4, IL-10, IL-13, IFNγ, and the transforming growth factor (TGF) (Hanada and Yoshimura, 2002). The intracellular signal transduction pathways that are triggered by cytokines ultimately lead to the activation of transcription factors such as NFκB, a tightly regulated process (Oeckinghaus et al., 2011). Under normal conditions, NFκB activation is transient and mediates the expression of genes being involved in inflammation and immunity (Vallabhapurapu and Karin, 2009), however its chronic activation is associated with human autoimmune diseases and cancer (Wang et al., 2009).
We focus here on NFκB regulating pathways that are mediated by TNF receptors. TNF is well known for its role in leading immune defenses that protect a localized area from invasion or injury. Additionally, TNF is also involved in controlling whether target cells live or undergo apoptosis. Besides the basic signaling steps described here, we present a mathematical model on TNF receptor cross-talk and clustering in Section 4.2.

TNF and its Receptors Tumor necrosis factor (TNF) plays a multifunctional role in inflammatory processes and the regulation of immune cells (Croft, 2009; Tracey and Cerami, 1993; Bradley, 2008). TNF can function in interacting with the death-domain-containing TNF receptor 1 (TNF-R1) and the non-death-domain-containing receptor 2 (TNF-R2), both belonging to the TNF receptor superfamily (Bazzoni and Beutler, 1996; Cabal-Hierro and Lazo, 2012; Tansey and Szymkowski, 2009). TNF-R1 is pervasively expressed in nearly all cell types of the body, whereas TNF-R2 expression is limited (Faustman and Davis, 2010) and is found especially in immune cells, endothelial and neuronal tissue (Grell and Scheurich, 1997). One can distinguish between the primarily produced membrane-integrated form of TNF (memTNF) and soluble TNF (sTNF) which can be released thereof by the metalloprotease TNF alpha converting enzyme (TACE). The two distinct forms of TNF bind to both, TNF-R1 and TNF-R2, but differ in their ability to stimulate the receptors: While both receptors can be fully activated by memTNF, the soluble form mainly stimulates TNF-R1 but has limited

capacity for triggering efficient TNF-R2 signaling (Grell, 1995; Grell et al., 1995). Due to its regulatory key role TNF and its signal transduction mechanisms, especially via TNF-R1, have been extensively studied (Chen and Goeddel, 2002; Jin and El-Deiry, 2005).

TNF-R1 Signaling Main down-stream effects of TNF-R1 mediated signaling involve the activation of NFκB (classical NFκB pathway) as well as the activation of caspases that result in cell death (apoptosis) as depicted in Figure 3.

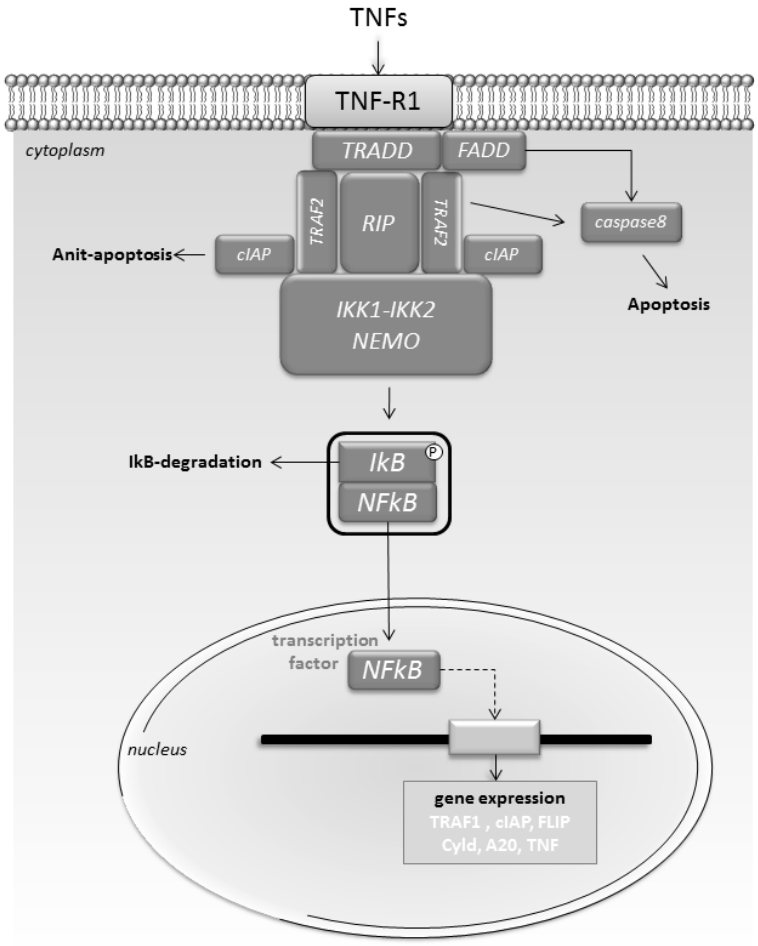

Figure 3: TNF -R1 signal transduction pathway. Binding of TNF with its receptor TNF-R1 results in the formation of a receptor-proximal complex containing the important adaptor proteins TRADD, TRAF2, RIP, and FADD. These adaptor proteins in turn recruit additional key pathway-specific enzymes (including the IKK1-IKK2-NEMO complex or caspase8) to the TNF-R1 complex, where they become activated and initiate downstream signaling events leading to apoptosis and canonial NFκB activation. Figure in adaption to (Chen and Goeddel, 2002) and Figure 1.

Upon the initial binding of the TNF trimer to the extracellular domain of TNF-R1, the adaptor protein TNF receptor-associated death domain (TRADD) is recruited, which itself recruits additional adaptor proteins such as receptor-interacting protein (RIP), TNF receptor associated factor 2 (TRAF2), and Fas-associated death domain (FADD). Subsequently, this triggers the activation of key enzymes being responsible for initiating further signaling events. The apoptotic branch is initiated by either a RIP-dependent or RIP-independent process involving caspase 8 resulting in active effector caspases that are responsible for apoptotic effects (Wang et al., 2008). This is opposed by anti-apoptic and pro-inflammatory signaling. TRAF2 recruits cellular inhibitors of apoptosis 1 and 2 (cIAP1, cIAP2), two anti-apoptotic proteins that also have ubiquitin protein ligase activity to the receptor (Mahoney et al., 2008). c-IAPs and both TRAFs contribute to the ubiquitination of RIP upon TNF-R1 stimulation via ubiquitin chains linked through lysine 63 (K63) (Wajant and Scheurich, 2011). The LUBAC (linear ubiquitin chain assembly complex), generates a recently detected type of linear polyubiquitin chain and specifically regulates the canonical NFκB pathway via the linear ubiquitination of RIP (Tokunaga and Iwai, 2012). Polyubiquitinated RIP serves as a docking site for both the TGFβ-activated kinase 1 (Tak1) and Tak1 binding proteins 2/3 (Tab2/3) heterocomplex and the inhibitor of κB (IκB) heterocomplex (Wu et al., 2006) including NFκB essential modulator (NEMO) (Ea et al., 2006). Upon assembly of this complex, Tak1 phosphorylates IKK2 that in turn phosphorylates IκB, an inhibitory protein that normally retains NFκB dimers (typically p50/p65) within the cytoplasm of unstimulated cells (Ghosh and Karin, 2002). IκB phosphorylation signals for its ubiquitination and proteasomal degradation allowing NFκB to translocate into the nucleus and regulate target genes. This involves the activation of the transcription of genes that promote inflammation as well as trigger the termination of NFκB activation (A20, Cyld). Exemplary, A20 can block activation of NFκB by the cytokine TNF through a ubiquitin-editing process (Wertz et al., 2004), modifying RIP that is thereby targeted for proteasomal degradation. Consequently, the activation of the IKK complex is prevented, which negatively regulates NFκB activation (Heyninck and Beyaert, 2005). Moreover, NFκB promptly induces the resynthesis of IκB and other inhibitory molecules, such as the cIAP molecules, thereby adding another layer for regulating the duration and amplitude of TNF signaling.

TNF-R2 Signaling In contrast, there is limited knowledge on the exact TNF-R2 associated signal transduction. Having no death domain, TNF-R2 mainly induces a long-lasting NFκB activation (Rothe et al., 1995a). Signaling starts with recruitment of the adaptor proteins TNF receptor-associated factor 1 (TRAF1) and TRAF2 (Rothe et al., 1995b) and cIAPs upon binding of TNF. TNF-R2 is preferentially activated by membrane-integrated TNF, whereas soluble TNF binds TNF-R2 but fails to properly stimulate TNF-R2 signaling (Grell et al., 1995). Down-stream, the classical (canonial) and non-classical (non-canonial) NFκB mobilization (via NFκB-inducing kinase (NIK)) promote the transcription of target pro-survival genes (Rauert et al., 2010; Marchetti et al., 2004). Furthermore, as it involves TRAF and cIAP molecules, the TNF-R2 signaling cascade is capable to mediate TNF-R1 signaling via regulatory cross-talk (Faustman and Davis, 2010; Fotin-Mleczek et al., 2002).

The TWEAK/Fn14 system The multi-functional cytokine TNF-like weak inducer of apoptosis (TWEAK) and its cognate receptor Fn14 are members of the TNF- and TNFR-superfamilies, respectively. Besides inflammation, TWEAK controls many cellular activities such as proliferation, migration, differentiation, apoptosis and angiogenisis (Winkles, 2008). The TWEAK-Fn14-axis resembles the one of TNF-R2 triggered by TNF, as the signaling cascade involves the recruitment of TRAF molecules a prime step, leading to NFκB activation and subsequent gene transcription (Saitoh et al., 2003). Like the TNF-TNF-R2-axis, TWEAK-Fn14 interaction can induce cell death (Nakayama et al., 2002), albeit the receptor itself has no death domain. Moreover, TWEAK acts specifically on Fn14, in comparison to TNF, which is capable to activate both, TNF-R1 and TNF-R2. Hence, the TWEAK/Fn14 system represents a valuable system for investigating the TNF receptor signaling cross-talk and for pinning out cross-talk specific regulations.

2.2 Platelet Biology and Signaling

2.2.1 Platelet Structure and Morphology

Among many cell types that are circulating in the blood, platelets are the smallest cells. Its diameter ranges from only $2.0\ \mu\mathrm{m}$ to $5.0\ \mu\mathrm{m}$, its thickness measures $5.0\ \mu\mathrm{m}$ resulting in a mean cell volume of 6 to $10\ \mathrm{fL}$ (Michelson, 2006). Platelets are formed and released by bone marrow megakaryocytes (Figure 4B) which are derived from hematopoietic stem cells (see Figure 4A). Thrombocytes are circulating in the blood for seven to ten days, before they are cleared by macrophages.

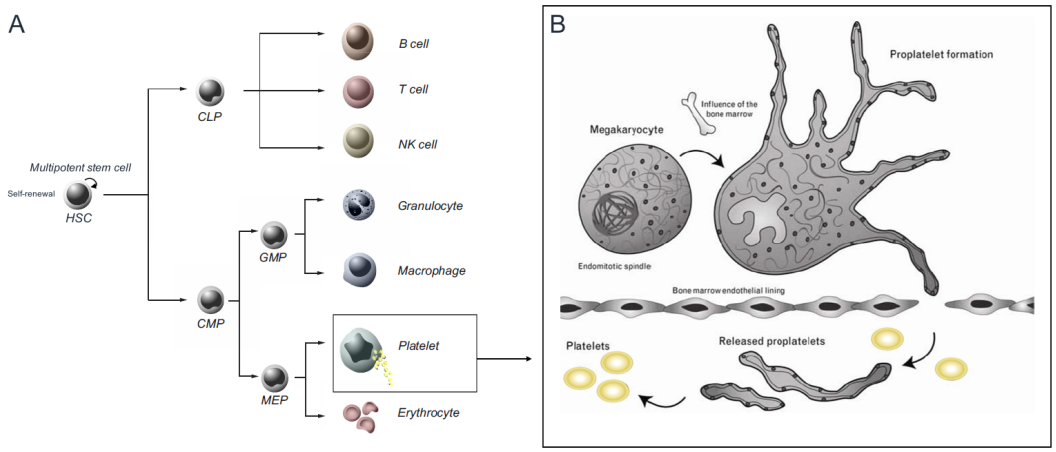

Figure 4: The hematopoietic stem cell (HSC) pathway (A) and platelet formation (B). Cell differentiation occurs through the common lymphoid progenitor (CLP), the common myeloid progenitor (CMP), the granulocyte/macrophage progenitor (GMP) and megakaryocyte/erythrocyte progenitor (MEP). Platelets originate from proplatelets, which are formed and released by bone marrow megakaryocytes (B). Subfigures adapted from Blank et al. (2008) and Battinelli et al. (2007).

Platelets are anucleate cell fragments and thus lacking a nuclear regulation. Nevertheless, platelets are highly communicative via divers surface receptors, signal transduction pathways and secreted messengers. Altogether, this ensures the intra- and inter-cellular information exchange and platelet functions.

Resting platelets have a discoid shape (Figure 5A) which rapidly changes upon activation to a more spherical shape with spiky pseudopods (Figure 5B).

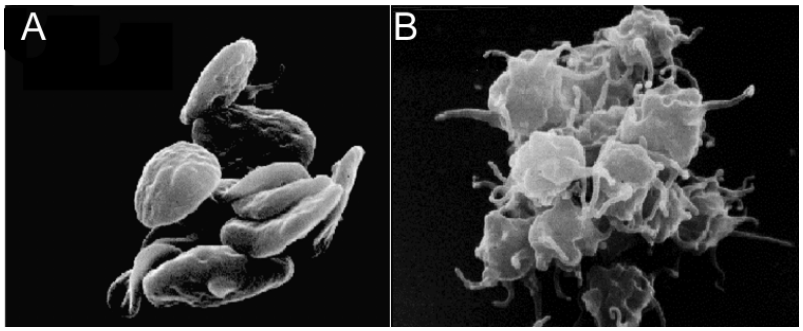

Figure 5: Shape change of platelets. Shape of resting platelets (A) and activated platelets (B). Figure adapted from Willoughby et al. (2002).

The plasma membrane encloses several components: internal membranes (open canalicular and dense tubular systems), a cytoskeleton (microtubules and microfilaments), mitochondria, glycogen granules, lysosomes and peroxisomes or storage granules. One distinguished between α-granules, which store matrix adhesive proteins including von Willebrand factor (vWF) and fibrinogen, and dense granules, containing small anorganic molecules (e.g. adenine nucleotides (ADP, ATP), serotonin, calcium and magnesium ions) (Michelson, 2006)
It is noteworthy that platelets contain messenger RNA (mRNA) even though at very low levels (Fink et al., 2003). [fill SAGE data analyis] This is not surprising, because due to the fact that platelets are anucleate they cannot transcribe mRNA to supplement the megakaryocyte-derived mRNA remaining in the thrombocyte. However, platelets are able to translate mRNA into proteins upon activation (Lindemann et al., 2001b), e.g. the inflammatory cytokine IL-1β (Lindemann et al., 2001a). This indicates a regulatory role of platelets in inflammatory processes (Weyrich et al., 2004). Nevertheless, the impact of protein synthesis in platelets is not clear.
The plasma membrane of thrombocytes is interspersed with multiple receptors and gylcoproteins that are essential for the activation but also the inhibition of platelets (Figure 6).

Circulating platelets are continually exposed to various activating factors such as fibrinogen, thrombin, collagen, ADP, thromboxane and vWF, but also inhibitory factors including ADPase, endothelial-derived nitric oxide (NO) and prostaglandin I_2 (PGI_2) (Ruggeri and Mendolicchio, 2007; Davi and Patrono, 2007; Varga-Szabo et al., 2008; Walter and Gambaryan, 2009). A subtle equilibrium between these opposing processes is essential for normal platelet and vascular functioning. In the following sections, the related thromboregulatory signal transduction events via surface proteins are intro-

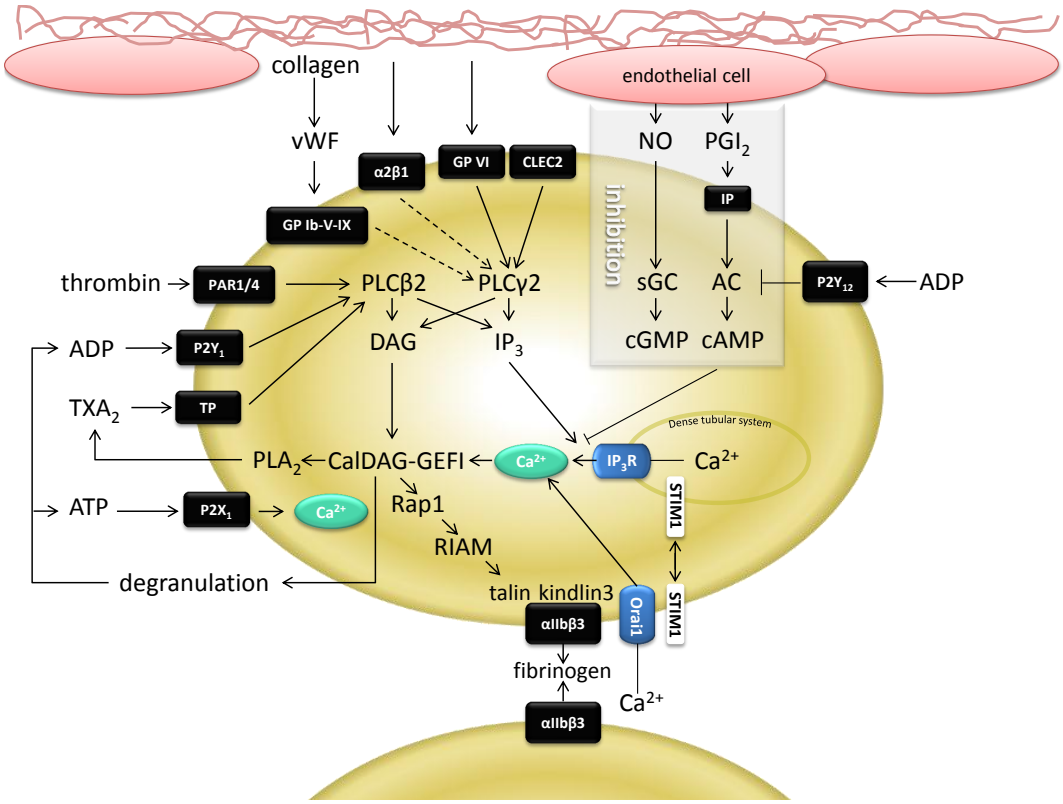

Figure 6: Major receptors and effectors involved in the inhibition, activation and aggregation of platelets. Platelet activation: Initial platelet tethering (binding of von Willebrand factor (vWF) with glycoprotein (GP) Ibα) allows the engagement of collagen receptors GPVI and integrin $\alpha 2\beta 1$. This thereby triggers the release of adenosine diphosphate (ADP) and thromboxane (TXA_2), which bind to the $P2Y_{12}$ and TP receptors, respectively. Consequently, levels of cytosolic Ca^{2+} and 1,2-diacylglycerol (DAG) are raised, which triggers a plethora of subsequent reactions including platelet shape change, granule secretion and aggregation. Platelet inhibition is mainly induced by endothelial-derived nitric oxide (NO) and prostaglandin I_2 (PGI_2) leading to the formation of cyclic nucleotides triggering inhibitory effects. Figure construction follows Broos et al. (2012).

duced. I will mainly focus on signaling pathways which are investigated by computational methods in this thesis.

2.2.2 Platelet Activation and Thrombus Formation

Platelet-activated generation of hemostatic plugs or thrombus formation comprises three steps: (1) platelet tethering and adhesion, (2) extended platelet activation and additional recruitment and aggregation of platelets and (3) firm adhesion, thrombus stabilization and growth (Figure 7).

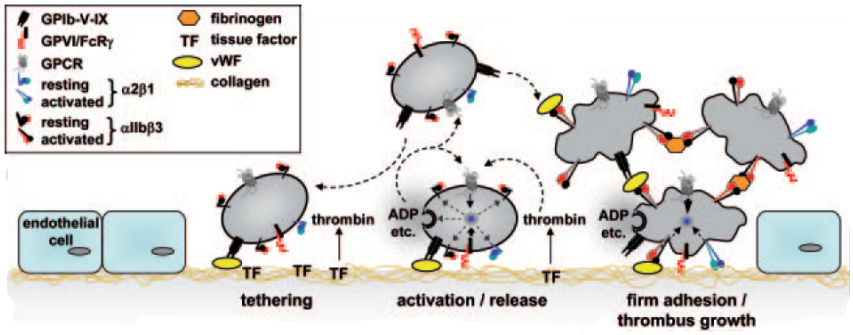

Figure 7: The three steps of thrombus formation. The initial contact (tethering) to the endothelial cell membrane (ECM) is mediated by the GPIbα-vWF interaction which thereby enables GPVI interaction with collagen. Consequently, this shifts integrins to a high-affinity state and triggers the release of adenosine diphosphate (ADP) and thromboxane (TXA_2). Concurrently, thrombin formation is locally triggered by tissue factor (TF) which additionally contributes to the activation of the platelet. Finally, activated $\alpha 2\beta 1$ and αIIb$\beta 3$ integrins trigger the firm adhesion to collagen, resulting in sustained GPVI signaling and enhanced procoagulant activity. Figure adapted from Varga-Szabo et al. (2008).

Platelet Adhesion

In the initial step of primary hemostasis, platelets interact with the exposed extracellular matrix (ECM). This matrix contains a large number of adhesive macromolecules including laminin, fibronectin, collagens, and vWF, serving as ligands for the different platelet surface receptors. Platelets roll, adhere and spread to form an activated monolayer of thrombocytes. Tethering and adhesion is mediated by the interaction between von Willebrand factor (vWF) with the GPIb-V-IX receptor complex as well as between the GPVI and GPIa proteins with collagen at injury sites. By this, adherent platelets get arrested and activated.

At low shear rates, e.g. in larger arteries and veins, platelets primarily adhere to collagen, laminin and fibronectin. Soluble vWF particularly interacts with the GPIbα of the GPIb-V-IX complex under conditions of high shear (Varga-Szabo et al., 2008), such as in small arteries or atherosclerotic vessels. Due to the fact that the binding of GPIbα to vWF has a fast off-rate, it is insufficient to mediate stable platelet adhesion. It rather maintains the platelet in close contact with the ECM. This so-called "rolling" of platelets facilitates the contact with the thrombogenic ECM protein collagen through the GPVI receptor and $\alpha 2\beta 1$ receptor. This triggers intracellular signals that shift platelet integrins to a high-affinity state. Additionally, this induces the release of adenosine diphosphate (ADP) and thromboxane A_2 (TXA_2) which function as secondary mediators in contributing to cellular activation together with locally produced thrombin.

Platelet Activation

There are two main pathways involved in platelet activation (Stegner and Nieswandt, 2011). GPVI and C-type lectin receptor (CLEC2) (May et al., 2009) transduce activation via tyrosine phosphorylation cascades occurring downstream of the receptor associated immunoreceptor tyrosine activation motif (ITAM). This leads to a full platelet activation. The other activatory pathway processes through soluble agonists including thrombin, ADP and TXA_2, which stimulate signal transduction through G protein-coupled receptors (GPCR) (Offermanns, 2006).

ITAM-coupled Receptors The major activating collagen receptor GPVI is associated with the FcRγ-chain, bearing an ITAM motif for signal transduction. The cross-linkage and clustering of GPVI by collagen leads to the activation of the Src tyrosine kinases Fyn and Lyn, which themselves are phosphorylating the ITAMs. This, but also the activation of CLEC2, enable the recruitment of Syk leading to the activation of phospholipase Cγ2 (PLCγ2) due to the tyrosine phosphorylation of its SH2 domains. Among other signaling proteins which have been implicated in GPVI-dependent platelet activation (e.g. Rap1. Rac1, Vav1, Vav3, PI3 kinase, Grb2, Gab2, Gads) the Bruton's tyrosine kinase (BTK) is essential for PLCγ2 phosphorylation *in vivo* (Liu et al., 2006), ultimately leading to calcium mobilization, degranulation, integrin activation and aggregation (Figure 6).

G Protein-coupled Receptors Platelet activation through GPCR are mostly triggered by ADP, thrombin and thromboxane. Thrombin activates through its protease-activated receptors (PARs), mainly PAR1 and PAR4. Thromboxane result from increased Ca^{2+} levels and associated activation of phospholipase A_2 (PLA_2) and signals through the TP receptor. PAR1, PAR4 and TP are coupled to G_q to activate PLCβ2, which is besides PLCγ2 a key protein in platelet activation and calcium mobilization (Stegner and Nieswandt, 2011).

ADP Signaling Adenosine diphosphate was one of the earliest identified platelet agonists and is also an important autocrine via secretion from platelet-dense granules. However, ADP associated receptors have only recently been definitively identified (Hechler and Gachet, 2011).

Released ADP is an important amplifier of platelet activation by acting on platelets through two G protein-coupled receptors $P2Y_1$ and $P2Y_{12}$. While the $P2Y_1$ receptor initiates platelet aggregation $P2Y_{12}$ is responsible for completion of the aggregation in response to ADP.
$P2Y_1$ triggers the mobilization of calcium from internal stores required for shape change and platelet aggregation (Hechler et al., 1998; Léon et al., 1999). This is mediated by its coupled G_q protein being responsible for the activation of PLCβ2 (Figure 6). In contrast, $P2Y_{12}$ is coupled to $G_{\alpha i2}$, that inhibits the adenylyl cyclase (AC). Hence, it prevents the formation of cyclic adenosine monophosphate (cAMP) which is crucial for triggering platelet inhibition (see Section 2.2.3). The G protein $G_{\alpha i2}$ also stimulates phosphoinositide 3-kinase β (PI3Kβ) leading to various downstream effects including the mobilization of calcium (Garcia et al., 2010).
Generally, all platelet-activating receptors trigger an elevation of calcium concentrations in the cytosol. Both, activated PLCγ2 and PLCβ2 convert phosphatidylinositol 4,5 bisphosphate (PIP2) to produce inositol 1,4,5 triphosphate (IP_3) and 1,2-diacylglycerol (DAG). While the latter activates protein kinase C (PKC) and is involved in Ca^{2+} entry from the extracellular compartment, IP_3 represents a critical molecule for the regulation of Ca^{2+} release in platelets (Stegner and Nieswandt, 2011).

Calcium Signaling Changes in cytosolic calcium level play a central role in signaling processes in almost all eukaryotic cells and also in platelet activation (Varga-Szabo et al., 2009). In platelets, elevations in intracellular Ca^{2+} contribute to a various steps of cellular responses including activation of integrins, granule release, cytoskeletal rearrangements essential for shape change and spreading as well as coagulant activity (Hathaway and Adelstein, 1979; Heemskerk et al., 2002; Mazzucato et al., 2002; Rink et al., 1982). The major pathway of Ca^{2+} entry pathway is a process referred to as store-operated calcium entry (SOCE). It involves receptor-mediated release of intra-cellularly stored Ca^{2+} which triggers the Ca^{2+} influx through the plasma membrane. The second main mechanism for Ca^{2+} entry is mediated by the direct receptor-operated calcium (ROC) channel, $P2X_1$. Besides, also non-SOCE mechanism exist in platelets, mediated by DAG which directly activates Ca^{2+} channels (e.g. canonial transient receptor potential channel TRPC6) in the plasma membrane (Hassock et al., 2002). Processes underlying calcium release from the stores has been well investigated. In contrast, mechanisms leading to calcium entry as well as signaling pathways

triggered by elevated intracellular Ca^{2+} remain mostly unknown (Varga-Szabo et al., 2009; Stegner and Nieswandt, 2011).

Calcium Store Release and SOCE The agonist-induced activation of phospholipase C isoforms leads to the formation of IP_3 which induces the calcium release from the intracellular stores by directly activating the IP_3 receptor (IP_3R). This Ca^{2+} release triggers the Ca^{2+} entry from the extracellular compartment (store-operated calcium entry). Recently, the stromal interaction molecule-1 (STIM1) (Grosse et al., 2007) and Orai1 (Braun et al., 2009; Bergmeier et al., 2009) were identified as important players in platelet SOCE. The transmembrane protein STIM1 acts like a Ca^{2+} sensor. Its EF-hand motif detects decreased Ca^{2+} levels in the intracellular stores. This opens the store-operated calcium (SOC) channels in the plasma membrane, allowing Ca^{2+} entry from the outside. Orai1 was recently detected as the major SOC channel on the platelet surface (Tolhurst et al., 2008), opened by STIM1.
As there is continuous leakage of Ca^{2+} from the intra-cellular stores, and already small increases in intracellular Ca^{2+} concentration would rapidly lead to platelet activation (Grosse et al., 2007; Rolf et al., 2001), counteracting mechanisms are of great importance. In platelets, two counteracting processes have been identified, ensuring the maintenance of a stable calcium concentration to keep platelets in a resting state in the circulation but also to bring the raised Ca^{2+} levels back to the basal amounts: The sarcoplasmic/endoplasmic Ca^{2+} ATPases (SERCAs) pump Ca^{2+} back to the intracellular stores and the plasma membrane Ca^{2+} ATPases (PMCAs) transport it out of the cell (Enyedi et al., 1986).

Firm Adhesion
Upon activation, the aggregation and spreading of platelets on the exposed ECM at sites of injury is mediated by the activated integrin α2bβ3 by building fibrinogen bridges (Varga-Szabo et al., 2008). These crosslinks between activated thrombocytes are responsible for thrombus growth and stabilization (Varga-Szabo et al., 2008).
The increased Ca^{2+} level in activated platelets triggers the activation of CalDAG-GEFI, the Ca^{2+} and diacylglycerol regulated guanine nucleotide exchange factor I (Crittenden et al., 2004). Subsequently, CalDAG-GEFI actives Rap1b, a small GTP binding protein which itself interacts with Rap1-interacting adapter molecule (RIAM) and talin (Rodius et al., 2008; Banno

and Ginsberg, 2008). This enables talin to the integrin β3-tail, inducing a conformational change of α2bβ3 now capable to bind fibrinogen and vWF (Shattil et al., 2010). Also kindlin3 was recently revealed as an important mediator of integrin activation and platelet aggregation (Moser et al., 2008).

2.2.3 Platelet Inhibitory Pathways and Regulation

Platelet activation is finely regulated through a plethora of cell signaling mechanisms and involves multiple waves of regulation leading to thrombus formation and protection from blood loss. However, in the absence of vessel injury or disease, inhibitory signals ensure that platelets stay in a quiescent state (resting platelet) and prevent uncontrolled aggregation. Strong inhibitory signals are derived from endothelial cells in producing and releasing bioactive NO and prostacyclin. In this connection, cyclic nucleotides play a pivotal role by mainly limiting platelet activation through two intracellular pathways regulated by either cAMP- or cGMP-elevating agents. The endogenous inhibitory effects on platelets are mediated by cGMP- and cAMP-dependent protein kinases, respectively (Figure 8). However, the exact mechanisms of cAMP/cGMP-mediated platelet inhibition are not fully understood. Many aspects of platelet activation can be blocked by cyclic nucleotides. This includes early activatory signals (Ca^{2+} release), adhesion, granule release, platelet aggregation and apoptosis (Rukoyatkina et al., 2011; Schwarz et al., 2001)

Besides the endothelium-derived platelet inhibition, receptors such as platelet-endothelial cell adhesion molecule-1 (PECAM-1) (Newman, 1999; Cicmil et al., 2002) and carcinoembryonic antigen cell adhesion molecule 1 (CEACAM1) (Wong et al., 2009) are known to be responsible for weak platelet inhibition. Recently, inhibitory mechanisms emerged which surprisingly involve intracellular receptors (e.g. retinoic X receptor (RXR), glucocordocoid receptor (GR), liver X receptor (LXR) or isoforms of the peroxisome proliferator-activated receptor (PPAR)) which are normally associated with the regulation of gene transcription (Jones et al., 2012). Additionally, inhibitory pathways including canonical Wnt signaling, Semaphorin 3A, endothelial cell specific adhesion molecule, and junctional adhesion molecule-A are emerging (Jones et al., 2012). As these inhibitory mechanisms played a minor role regarding the development and the purpose of mathematical models we established on platelet signaling, I will mainly focus on the endothelium-triggered inhibitory mechanisms in the following.

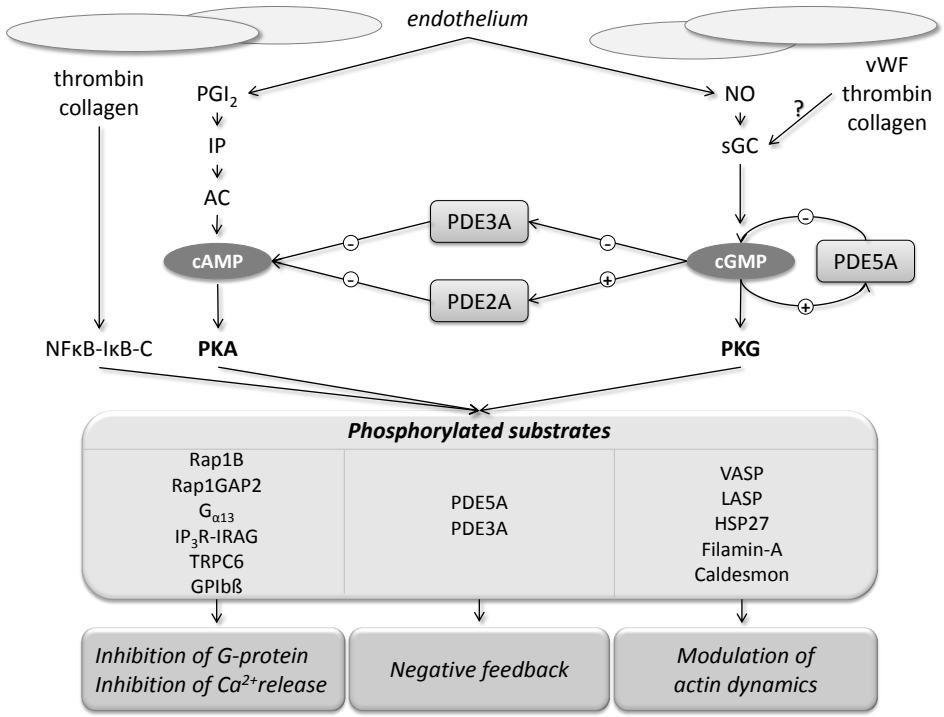

Figure 8: Model of cyclic nucleotide signaling network in platelets. Endothelial cells release prostacyclin (PGI_2) and nitric oxide (NO). PGI_2 binds to its IP receptor stimulating the synthesis of cAMP by adenylyl cyclase (AC). NO activates soluble guanylyl cyclase (sGC) leading to cGMP synthesis. Thrombin, von Willebrand factor (vWF) and collagen may also activate sGC but to a lesser extent than NO. cGMP inhibits PDE3A but activates PDE2A and PDE5A resulting in cGMP and cAMP degradation. cAMP stimulates the cAMP-dependent protein kinase (PKA). The C subunit of PKA is also associated with a NFκB-IκB complex, from which it can be set free upon thrombin and collagen signals. PKA and PKG phosphorylate substrates triggering platelet inhibition. They are functionally grouped (see Table 12). Glycoprotein (GP), heat shock protein 27 (HSP27), inositol 1,4,5-trisphosphate receptor (IP_3R), Lim and SH3 domain protein (LASP), phosphodiesterase (PDE), transient receptor potential channel 6 (TRPC6), vasodilator-stimulated phosphoprotein (VASP). Figure adapted from Smolenski (2012).

Cyclic Nucleotide Levels in Human Platelets

The most potent endogenous mechanism of platelet inhibition is mediated by the elevation of intracellular cyclic nucleotide levels of cGMP and cAMP. Since the 1960s, cAMP has been identified as a strong inhibitor of platelet aggregation (Kloeze, 1966; Marquis et al., 1969) and cGMP was found to inhibit platelet functions around 1980 (Mellion et al., 1981). In the resting state, basal concentrations remain at 4 µM (cAMP) and 0.4 µM (cGMP) (Eigenthaler et al., 1992). These levels can be modulated by adenylyl and guanylyl cyclases (AC, GC) which both synthesize cyclic nucleotides. In contrast, phosphodisterases downregulate cyclic nucleotide levels by degradation (Figure 8).

Regulation of Adenylyl and Guanylyl Cyclase Activity

There exist various isoforms of adenylyl cyclases (ACs), from which isoform AC3, AC6, AC7 (Dittrich et al., 2008) and AC5 (Lewandrowski et al., 2009) are expressed in human platelets. ACs are integral membrane proteins catalyzing the synthesis of cAMP from adenosine triphosphate (ATP) resulting in an increased level of intracellular cAMP. The activity of ACs is regulated by G-proteins: Inhibitory G-proteins such as $G_{\alpha i2}$ which is coupled to $P2Y_{12}$ (see section 2.2.2) reduce AC activity whereas stimulatory G-proteins G_{α_s} have an activatory effect on cAMP production. G_{α_s} is coupled to receptors for adenosine, β-adrenergic agents as well as to the IP receptor for prostacyclin (PGI_2) and prostaglandin receptors, which leads to the stimulation of cAMP formation upon ligand binding. Prostaglandins can modify platelet function through different prostanoid receptors which can be coupled to both activatory G-proteins like the IP receptor (for PGI_2) and to inhibitory G-proteins (Iyu et al., 2011; Hubertus, 2012).

In platelets, cGMP production is solely dependent on one single enzyme, the soluble form of guanylyl cyclase (sGC) which is sensitive to NO and other NO-generating agents. NO derives from endothelial cells where the endothelial NO synthase (eNOS) is located. Detailed analyses have been published of both mouse and human platelets, to rule out the presence of any significant nitric oxide synthase enzyme within platelets (Gambaryan et al., 2008; Ozüyaman et al., 2005; Rowley et al., 2011). Recently novel sources of NO have been identified in mice which might be of importance in platelet inhibition (Moore et al., 2010). NO is capable to stimulate sGC which in turn generates cGMP. Additionally, vWF, thrombin or collagen might activate sGC, resulting in a small increase in cGMP (Gambaryan et al., 2008; Zhang et al., 2011; Riba et al., 2006, 2005), but these findings could not be confirmed by all studies (Ozüyaman et al., 2005; Gambaryan et al., 2010; Marshall et al., 2004).

Platelet Phosphodiesterases

Platelet phosphodiesterases (PDEs) control cyclic nucleotide levels by PDE-mediated degradation. In human platelets, the isoforms PDE2A, PDE3A and PDE5A of phosphodiesterases are expressed (Haslam et al., 1999) and represent the major regulatory PDEs. Furthermore, PDE4D could be identified on proteomic level (Zahedi et al., 2008) as well as PDE7A, PDE8B and PDE9A on mRNA-level (Dittrich et al., 2006). PDE2 and PDE3 are

able to degrade both, cAMP and cGMP, whereas PDE5 specifically degrades cGMP. PDEs provide targets for feedback regulation of cyclic nucleotide signaling: cGMP has a regulatory impact on all three platelet PDEs (Figure 8). It stimulates PDE2 and PDE5 activity by binding to a specific cyclic nucleotide-binding domain, called GAF domain. In contrast, PDE3 activity is inhibited by cGMP because of competitive binding with cAMP at its catalytic site. PDE3 helps in maintaining low basal concentrations of cAMP in platelets (Dunkern and Hatzelmann, 2005; Feijge et al., 2004; Sim et al., 2004). It gets activated by the cAMP-dependent protein kinase (PKA)-mediated phosphorylation, providing a negative feedback loop for cAMP signaling (Macphee et al., 1988; Zhang and Colman, 2007). The main function of PDE5 is the regulation of cGMP levels. PDE5 enables a negative feedback on cGMP levels: cGMP activates PDE5 and cGMP-dependent protein kinase (PKG) additionally phosphorylates PDE5 resulting in an increased catalytic activity of PDE5 and also long-term desensitization of cGMP responses (Mullershausen et al., 2003).

cAMP/cGMP-dependent Protein Kinases

The translation of cAMP and cGMP levels into protein phosphorylation patterns is the major role of cAMP- and cGMP-dependent kinases. PKA is composed of four subunits, two have a regulatory and two have a catalytic function. Upon cAMP binding to the regulatory subunits, the catalytic subunits dissociate from the heterotetrameric complex and phosphorylate their substrates, leading to the suppression of platelet activation (Eigenthaler et al., 1992). Furthermore, Gambaryan et al. (2010) could show that the stimulation of human platelets by collagen and thrombin activates a distinct feedback inhibitory mechanism based on cAMP-independent activation of PKA. This activation process involves the release of the catalytic PKA-subunit from a NFκB-IκB complex.

PKG combines regulatory and catalytic subunits within one molecule which dimerizes upon cGMP binding (Hofmann, 2005; Lohmann and Walter, 2005). The dimeric complex then fulfills further processes leading to platelet inhibition.

There is some evidence for localized cyclic nucleotide function in platelets (Wilson et al., 2008; Bilodeau and Hamm, 2007) as it is known for many other cell types. A-kinase anchoring proteins (AKAPs) often coordinate localized cAMP signaling as recently reviewed in Vandamme et al. (2012).

AKAPs bind PKA and other signaling components such as phosphodiesterases, forming subcellular cAMP signaling compartments. In this regard, particularly AC5 and AC6 can be targets for PKA-mediated cAMP feedback inhibition (Iwami et al., 1995; Beazely et al., 2005; Chen et al., 1997). These adenylyl cyclases directly interact with AKAP 79/150 which facilitates the phosphorylation of AC5 and AC6 by PKA to inhibit cAMP synthesis (Bauman et al., 2006). Mass spectrometry-based screening recently revealed seven AKAP isoforms (AKAP1, AKAP2, AKAP7, AKAP9, AKAP10, AKAP11, and microtubule-associated protein 2) to be present in platelets (Margarucci et al., 2011). At the transcriptomic level, data analysis suggests the expression of AKAP5, AKAP8, AKAP8L and AKAP13 in platelets (Rowley et al., 2011). Regarding PKG, its substrate IRAG represents up to now the only known platelet G-kinase anchoring protein (GKAP) (Antl et al., 2007).

Substrates of PKA and PKG

Several steps in platelet activation and aggregation including adhesion and granule release are inhibited by cAMP and cGMP signaling cascades (Smolenski, 2012; Schwarz et al., 2001). The functional outcome of blocked platelet activation is transduced by PKA and PKG (Figure 8). Table 12 (Annex B.3) lists PKA and PKG substrates, their phosphorylation sites and proposed roles.

Here, I will focus on the vasodilator-stimulated phosphoprotein VASP as it is a suitable protein to monitor cyclic nucleotide-dependent PKA/PKG activation *in vitro* and *in vivo* and to analyze cross-talk between different receptor signaling pathways (Schwarz et al., 1999). Furthermore, information on phosphorylation kinetics is available (Eigenthaler et al., 1992; Butt et al., 1994; Smolenski et al., 1998) VASP therefore constitutes a suitable protein especially for computational dynamic modeling (Section 4.1.4). VASP was one of the first substrates of PKA and PKG that were discovered in platelets (Halbrügge and Walter, 1989). Its main phosphorylation sites are Ser157, preferentially phosphorylated by PKA, and Ser239, preferred by PKG (Smolenski et al., 1998). Against both sites, phosphosite specific antibodies have been developed, which have been widely used as markers of cyclic nucleotide activity, not only in platelets but also in other cells (Smolenski et al., 1998; Schäfer et al., 2003).

Platelet activation induces actin cytoskeletal reorganization that results in platelet shape change and is crucial for the secretion of intracellularly stored

granules. Apart from other downstream effects of VASP, it is an important regulator of actin dynamics as phosphorylated VASP inhibits its binding to F-actin and decreases F-actin bundling *in vitro* (Harbeck et al., 2000). VASP also regulates platelet activation in mediating NO-dependent inhibition of platelet adhesion to the vessel walls (Hauser et al., 1999; Massberg et al., 2004). Moreover, VASP is involved in directing the inhibitory effects of PKA and PKG to fibrinogen binding and further platelet aggregation but does not trigger the inhibition of Ca^{2+} release and granule secretion (Aszódi et al., 1999). In this connection, integrin β_3 might control the PKA-mediated phosphorylation of VASP on site Ser157 (Worth et al., 2010).

2.3 Mathematics of Biological Systems Analysis

2.3.1 Interaction Graphs

The study of networks and graphs has gained importance in all fields of science requiring the analysis of complex relational data. It reaches back to the year 1736 when Leonard Euler found the solution to the noted problem "Seven Bridges of Königsberg" (Euler, 1736). Euler introduced the mathematical description of vertices and edges which is deemed to be the foundation of the so-called graph theory, the field of mathematics that became the framework of complex network analysis and theory. Biological systems and networks such as signaling systems can formally be represented as graphs. A graph G is defined as a tuple (V, E), with V being as set of vertices and $E \subseteq V \times V$ being a set of edges:

$$G = (V, E).$$

Edges can be interpreted as the relation between vertices connecting them in a directed or undirected manner (see Figure 9).

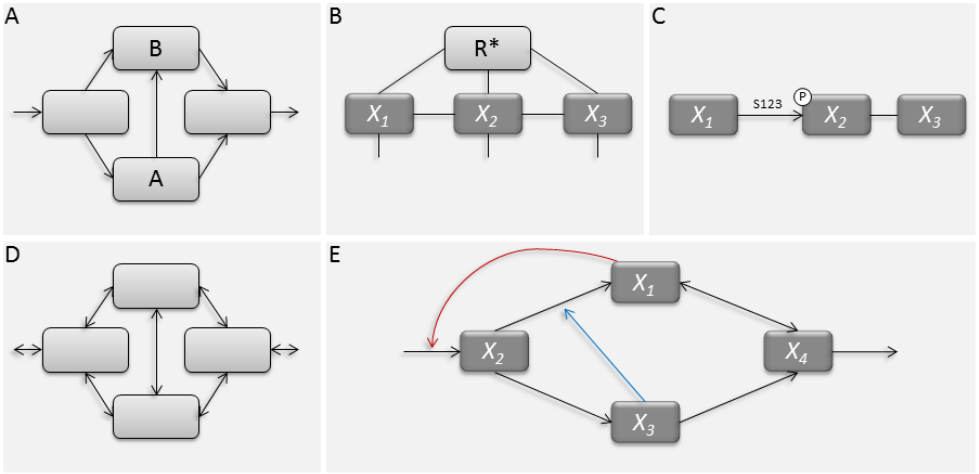

Figure 9: Types of generic networks. (A) Directed graph (gene A regulates the expression of gene B). (B) Undirected graph (protein-protein interaction network). Proteins X_1, X_2, X_3 form an interacting complex at the activated receptor R*. (C) Graphical interpretation of phosphorylation: Kinase X_1 phosphorylates protein X_2 at site S123, which then interacts with protein X_3. Static networks may also contain bidirectional edges (D) or regulation (E) such as inhibition (red arrow) or activation (blue) including feedback loops.

Adapted to cell biology, vertices can represent signaling components such as genes and proteins (kinases, enzymes), ligands or receptors. Protein-protein interaction (PPI) networks are typically formulated as undirected

graphs (Figure 9B). In contrast, transcriptional regulatory networks are typical examples of a directed graph. Here, nodes denote genes and edges represent interactions between them. As a gene A might regulate the expression of gene B but the opposite is not inevitably the case, the choice of a directed graph is reasonable (Figure9A). A directed edge can also be interpreted as a node-to-node activation or phosphorylation process (Figure 9C), mapped onto a PPI network. Static networks may also include bidirectional interactions (edges) (Figure 9D) and regulatory effects such as this inhibition or activation of a protein interaction by a protein (node) and feedback loops (Figure 9E).
The representation of a signaling pathway as a graph allows the analysis of its structural properties by means of graph-theoretical techniques (Barabási and Oltvai, 2004; Newman, 2003). The static, graphical representation also allows relating signaling components of interest with a functional (sub)network of signal transduction and revealing contextual interactions. Thus, static analyses focus more on the connectivity of system components and their interactions in assigning a functional and regulatory meaning. In this thesis, we focus on analyzing platelet signaling components of interest together with their functional network context applying *PlateletWeb* (Boyanova et al., 2012), a platelet-specific workbench.

2.3.2 Boolean Networks

The history of Boolean networks applied to biological processes reaches back to Stuart A. Kauffman. In his seminal paper (Kauffman, 1969), he proposed large-scale random Boolean models as generic models of gene regulatory networks. These networks are later referred to as Kauffman networks. Kauffman's models of gene regulation are one of the simplest kinds of models for complex dynamic systems. Here, genes are described by binary variables which take only discrete values 0 or 1. These binary states can be understood in the sense of gene regulation as "off" (0) and "on" (1) or to interpret them more meaningfully as "inactive" and "active", or "not expressed" and "expressed."
Boolean network models are a special case of discrete dynamic models. Simulation of those networks is done in discrete time steps. At each timepoint, the value of a variable is deterministically calculated by so-called update rule, the Boolean functions. Thereby, the state of a variable in the next time-step depends upon the values of (a subset of) the other variab-

les (inputs) at the previous time-point. The average number of inputs per variable is defined as the (mean) connectivity of the Boolean model. The update rules are often expressed in terms of Boolean operators, including logical *NOT* ($\neg$), *AND* ($\wedge$) and *OR* ($\vee$), where the name of these models come from. The operators are named after George Boole, a British mathematician and philosopher, who is deemed to be the inventor of Boolean logic (Boole, 1847, 1854). Thus, Boolean models code the complex system of gene regulation or signal transduction in terms of classic binary choices in a discrete, deterministic and parameter-free way. These choices are not based on any kinetic or biophysical law. Here, the state of a variable is determined by an abstract combination of inputs from other variables.
In terms of complexity, Boolean networks lie between static network models and continuous dynamic models (Kahlem and Birney, 2006), making them a tractable and powerful approach to modeling large-scale biological systems. After assembling the individual network components and regulatory interactions involved in a system into a coherent network representation, Boolean models can serve to describe the qualitative temporal behavior of a system. Furthermore, they can be used to understand how perturbations may alter its behaviors and lead to predictive testable hypotheses especially valuable in large-scale systems which are poorly understood (Assmann and Albert, 2009; Gross, 2006).
Several small- and medium-scale Boolean models of biological processes have been developed representing an integrative part of many systems biology research projects (Saez-Rodriguez et al., 2007, 2009; Samaga et al., 2009; Schlatter et al., 2009). They focus on the analysis of biological processes including signaling systems with the main goal of generating hypothesis and qualitative predictions about possible regulatory interactions. Boolean networks represent an intuitive approach towards assessing signaling systems. Here, networks comprise hardwired connections and signaling events that happen on a discrete time scale. Boolean update rules can be understood as "gates" through which the signal is proceeding over the network (Morris et al., 2010).

2.3.3 Dynamic ODE-based Modeling

It is probably one of Newton's major achievements to have developed the language of differential equations and dynamical systems to describe the statement of his laws of gravity and motion. Ever since, this language was

applied in many fields of science, including biochemistry and biomathematics to formulate dynamic processes. Dynamic modeling aims at formulating a set of mathematical equations which are able to predict computationally the dynamic behavior of a real system, e.g. of a signaling network (Swameye et al., 2003). The dependence of certain properties on time and space can deterministically be described by a set of ordinary differential equations (ODE).

Ordinary Differential Equations The dynamic behavior of a (biological) system comprising several variables x_i can be approximated by a system of ordinary differential equations (ODEs) (see Equation 2.1). Exemplary, it can be derived from the reaction mechanism and describes the time-resolved behavior away from equilibrium. Mathematically, the change in concentration of a variable x_i over time t can be represented as a function f_i

$$\frac{\mathrm{d}[x_i]}{\mathrm{d}t} = f_i(x_1, x_2, \ldots, x_n, p_1, p_2, \ldots, p_l, t) \qquad i = 1, \ldots, n. \tag{2.1}$$

where x_i denotes the variables (e.g. concentrations) and p_j $(j = 1, \ldots, l)$ represents the set of parameters (e.g. enzyme concentrations, kinetic constants) as detailed in the following Section.

2.3.4 Biochemical Reaction Kinetics

Law of Mass Action Deterministic kinetic modeling of biochemical reactions is based on the mass action law, which was introduced by Guldberg and Waage in the nineteenth century (Guldberg and Waage, 1864, 1879). The law of mass action governs reaction rates in biochemical systems. It states that for reactions in a homogeneous medium the reaction rate is proportional to the probability of a collision between molecular reactants. This in turn is proportional to the concentration of the reactants to the power of the molecularity according to the specific reaction.
Assuming a simple balance equation where two substrates S_1 and S_2 form a product P and vice versa

$$S_1 + S_2 \rightleftharpoons 2P. \tag{2.2}$$

Thus, the reaction rates of the forward reaction ν_+ and backward reaction ν_- result in

$$\nu_+ \;=\; k_+ \cdot [S_1] \cdot [S_2] \qquad \text{and} \qquad \nu_- \;=\; k_- \cdot P^2.$$

The proportionality factors k_+ and k_- are also called kinetic or rate constants. Thus, the net reaction rate ν can be expressed by

$$\nu \;=\; \nu_+ - \nu_- \;=\; k_+ \cdot [S_1] \cdot [S_2] - k_- \cdot [P]^2 \tag{2.3}$$

or in a more general way:

$$\nu \;=\; \nu_+ - \nu_- \;=\; k_+ \cdot \prod_i [S_i]^{m_i} - k_- \cdot \prod_j [P_j]^{m_j}.$$

Here, m_i and m_j denote the molecularities of the substrates S_i and the products P_j, respectively (Heinrich and Schuster, 1996). In equilibrium, reaction rate ν_+ equals ν_- so that one can declare the equilibrium constant K characterizing the ratio of substrate S_{eq} and product concentrations P_{eq} in equilibrium:

$$K = \frac{k_+}{k_-} = \frac{\prod [P_{eq}]}{\prod [S_{eq}]}.$$

Regarding reaction (2.2), the dynamic behavior of substrate and product concentrations over time t (see Equation 2.3) ensues from the system

$$\frac{\mathrm{d}[S_1]}{\mathrm{d}t} \;=\; \frac{\mathrm{d}[S_2]}{\mathrm{d}t} \;=\; -\nu \qquad \text{and} \qquad \frac{\mathrm{d}[P]}{\mathrm{d}t} \;=\; 2\nu.$$

The time course of the reactants S_1, S_2 and P is then obtained by integrating the ODEs.

Michelis-Menten Kinetics In 1913, Michaelis and Menten proposed a mathematical model (Menten and Michaelis, 1913) approximating the kinetics of enzyme reactions. The enzymatic reaction mechanism involves an enzyme E binding to a substrate S to form a enzyme-substrate complex ES, which in turn is converted into a product P and the enzyme E. This may be represented schematically as

$$S + E \underset{k_{-1}}{\overset{k_1}{\rightleftharpoons}} ES \xrightarrow{k_2} E + P,$$

where k_1, k_{-1} and k_2 denote the rate constants and the double arrows represent the reversible enzyme-substrate binding process. The Michaelis-Menten theory allows a quantitative description of the rate of enzymatic reactions by relating reaction rate ν to the concentration of a substrate S. It can be derived by applying the law of mass action, which states that the rate of a reaction is proportional to the product of the concentrations of the reactants. This leads to a system of four non-linear ordinary differential equations that define the rate of change of reactants over time:

$$\frac{\mathrm{d}[S]}{\mathrm{d}t} = -k_1 \cdot [S] \cdot [E] + k_{-1} \cdot [ES] \tag{2.4}$$

$$\frac{\mathrm{d}[E]}{\mathrm{d}t} = -k_1 \cdot [S] \cdot [E] + (k_{-1} + k_2) \cdot [ES] \tag{2.5}$$

$$\frac{\mathrm{d}[ES]}{\mathrm{d}t} = \underbrace{k_1 \cdot [S] \cdot [E]}_{\text{complex formation}} \quad \underbrace{-(k_{-1} + k_2) \cdot [ES]}_{\text{complex dissociation}} \tag{2.6}$$

$$\frac{\mathrm{d}[P]}{\mathrm{d}t} = k_2 \cdot [ES] = \nu, \text{ with } \quad k_{+/-1} \gg k_2. \tag{2.7}$$

The overall reaction rate ν is given by the negative decay rate of the substrate as well as by the rate of product formation:

$$\nu = -\frac{\mathrm{d}[S]}{\mathrm{d}t} = \frac{\mathrm{d}[P]}{\mathrm{d}t}. \tag{2.8}$$

The ODE system (Equation 2.4 - 2.8) can not be solved analytically so that several assumptions have been used for reformulation:
The so-called *quasi-equilibrium* (Briggs and Haldane, 1925) between a free enzyme and the enzyme-substrate complex reflects that the reversible conversion of enzyme and substrate to the complex is much faster than the subsequent dissociation into enzyme and product ($k_{+/-1} \gg k_2$). Thus, the latter reaction does not disturb the balance between complex formation and degradation (quasi-steady state) so that

$$\frac{\mathrm{d}[ES]}{\mathrm{d}t} = 0.$$

To justify this assumption, the initial substrate concentration $[S]_0$ has to be much larger than the enzyme concentration because otherwise, the steady state will never be reached. Thus, reaction rate k_2 dominates the velocity of the overall reaction and $\nu = \frac{\mathrm{d}[P]}{\mathrm{d}t} = k_2 \cdot [ES]$ (Equation 2.7). Furthermore, we regard the total enzyme concentration $[E_{tot}]$ as constant, meaning an en-

zyme may be free or part of the complex but is never produced or consumed in the reaction. Consequently, substituting E with $E_{tot} - ES$ and exploiting the quasi-equilibrium

$$\frac{\mathrm{d}[ES]}{\mathrm{d}t} = k_1 \cdot [S] \cdot [E] - (k_{-1} + k_2) \cdot [ES] = 0,$$

the following condition for the concentration of ES arises from Equation 2.6:

$$\begin{aligned}
& k_1 \cdot [S] \cdot ([E_{tot}] - [ES]) - (k_{-1} + k_2) \cdot [ES] = 0 \\
\Leftrightarrow \quad & k_1 \cdot [S] \cdot [E_{tot}] - k_1[S] \cdot [ES] - (k_{-1} + k_2) \cdot [ES] = 0 \\
\Leftrightarrow \quad & k_1 \cdot [S] \cdot [E_{tot}] - (k_1 \cdot [S] + k_{-1} + k_2) \cdot [ES] = 0 \\
\Leftrightarrow \quad & [ES] = \frac{k_1 \cdot [S] \cdot [E_{tot}]}{k_1 \cdot [S] + k_{-1} + k_2} = \frac{[S] \cdot [E_{tot}]}{\underbrace{\left(\frac{k_{-1} + k_2}{k_1}\right)}_{K_\mathrm{m}} + [S]}.
\end{aligned} \tag{2.9}$$

Substituted in Equation 2.7, this results in the Michaelis-Menten equation

$$\nu = \frac{k_2 \cdot [S] \cdot [E_{tot}]}{\left(\frac{k_{-1}+k_2}{k_1}\right) + [S]} = \frac{V_\mathrm{max} \cdot [S]}{K_\mathrm{m} + [S]}, \tag{2.10}$$

with enzyme-specific Michaelis-Menten constant $K_\mathrm{m} = \frac{k_{-1}+k_2}{k_1}$ and maximal velocity $V_\mathrm{max} = k_2 \cdot [E_{tot}]$. At high substrate level, all free enzyme molecules are occupied and bind to a substrate. Thus, the maximal reaction velocity V_max can be expressed by

$$\nu = k_2 \cdot [ES] \equiv k_2 \cdot [E_{tot}] = V_\mathrm{max}. \tag{2.11}$$

The Michaelis-Menten constant K_m is a measure for the affinity of an enzyme towards its substrate. It is equal to the substrate concentration which yields the half-maximal reaction rate: Putting $K_\mathrm{m} = [S]$, Equation 2.10 results in

$$\nu = \frac{V_\mathrm{max} \cdot [S]}{[S] + [S]} = \frac{V_\mathrm{max}}{2}.$$

Figure 10 shows typical time courses for $[S]$, $[E]$, $[ES]$ and $[P]$ as well as for the reaction rate ν.

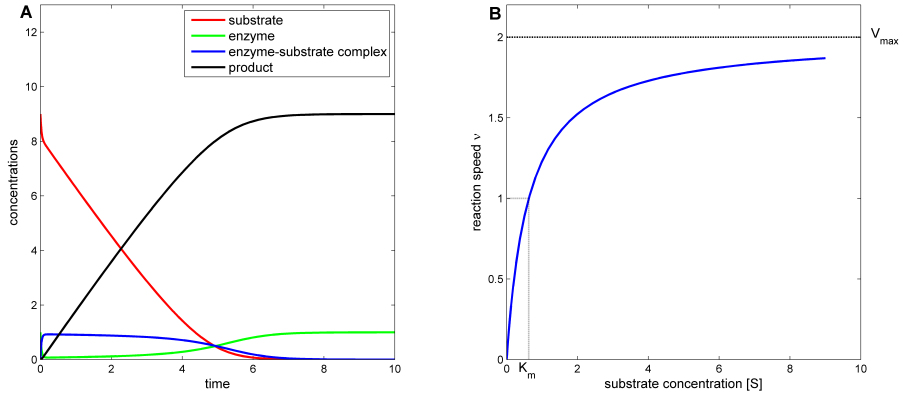

Figure 10: Time courses (Michaelis-Menten kinetics). (A) Solution of the ODE system (Equation 2.4 - 2.7) over time. (B) Plot of the reaction speed ν versus substrate concentration. Dashed lines indicate K_m and V_max values. Utilized parameters: k_1 = 4, k_{-1} = 0.5, k_2 = 2, K_m = 0.625, V_max = 2, $[S]_0$ = 9, $[E]_0$ = 1, $[ES]_0 = [P]_0$ = 0.

Hill Equation The binding of reactants, e.g. of a substrate to its enzyme may positively or negatively influence the affinity to further ligands (cooperative binding). The Hill-equation

$$\nu = \frac{V_\mathrm{max} \cdot [S]^h}{K_\mathrm{m}^h + [S]^h}, \tag{2.12}$$

accounts for cooperative binding (Figure 11A). A Hill-coefficient h larger than 1 corresponds to positive cooperativity, where the binding of one reactant facilitates binding of another reactant. In contrast, $h < 1$ denotes negative cooperativity, where binding of further reactants is made more difficult (Cornish-Bowden, 2012).

Enzyme Inhibition Michaelis-Menten kinetics is modified in case of inhibition of both, the substrate and the enzyme. A comprehensive list can be found in Cornish-Bowden (2012). We applied the following Michaelis-Menten-like rate equation to model the drug-mediated competitive enzyme inhibition of platelet enzymes (Floreani et al., 2003)

$$\nu = \frac{V_\mathrm{max} \cdot [S]}{\left(1 + \frac{[I]}{k_i}\right) \cdot K_\mathrm{m} + [S]}. \tag{2.13}$$

Modified reaction rates upon different concentration of an inhibitor I and its characteristic inhibition constant $k_i = 0.5$ are displayed in Figure 11B.

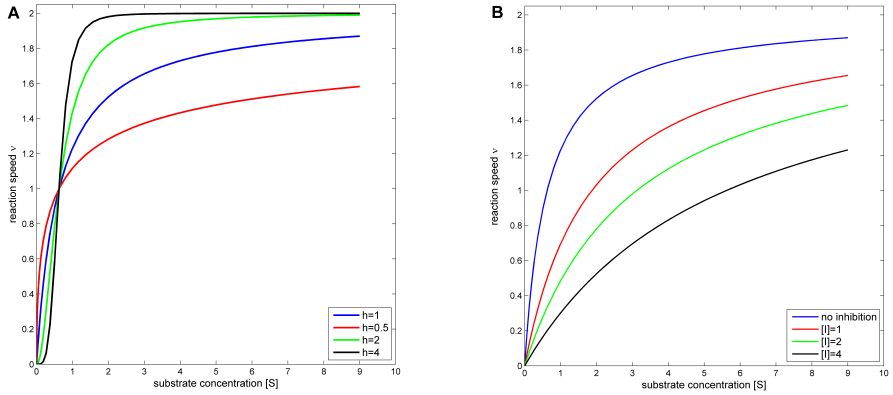

Figure 11 : Time courses: (A) Hill equation (B) Competitive enzyme inhibition. (A) Reaction rate ν for different Hill coefficients h = 0.5, 1, 2, and 4 showing cooperative binding behavior (Equation 2.12). Utilized kinetic parameters (see legend of Figure 10). (B) Influence of different concentrations of an competitive inhibitor I and inhibition constant $k_i = 0.5$.

Conventional equations for (enzyme) kinetics are based on the mass-action law, a mathematical model that explains and predicts behaviors of *solutions* in dynamic equilibrium. Thus, the question is whether it also holds under dimensionally-restricted *in vivo* conditions. There are several approaches (Kopelman, 1988; Savageau, 1995; Schnell and Turner, 2004; Grima and Schnell, 2006; Chen et al., 2010) trying to adjust the kinetic assumptions to the disordered media within cells.

3 Materials and Methods

IT DOESN'T MATTER HOW BEAUTIFUL YOUR THEORY IS,
IT DOESN'T MATTER HOW SMART YOU ARE.
IF IT DOESN'T AGREE WITH EXPERIMENT, IT'S WRONG.

(*Richard P. Feynman*)

3.1 Platelet Preparation and Immunoprecipitation

Concentration-dependent experiments with human platelets were of key importance with respect to data-based modeling. Moreover, we suggested experiments by computer-based model predictions. Therefore, chemicals and measurement methods are briefly described in the following. These experiments have been performed in the laboratory of the Institute of Clinical Biochemistry and Pathobiochemistry, Würzburg.

Platelet preparation Human platelets were washed (Aktas et al., 2003) and prepared as detailed in Geiger et al. (1998) to reduce leukocyte contamination. In brief, after informed consent whole human blood was drawn by venipuncture from volunteers. They had not been treated with any platelet or cyclic nucleotide affecting drugs in the past two weeks. Blood was collected in weakly acidic citrate/dextrose buffer (4:1 v/v) and centrifuged at 300 xg for $10\ \mathrm{min}$ at $20\ ^{\circ}\mathrm{C}$. Subsequently, the obtained platelet rich plasma was centrifuged (380 xg, $20\ \mathrm{min}$ at $20\ ^{\circ}\mathrm{C}$). The platelet pellet was resuspended in HEPES buffer ($145\ \mathrm{mM}$ NaCl, $5\ \mathrm{mM}$ KCl, $1\ \mathrm{mM}$ $MgCl_2$, $10\ \mathrm{mM}$ HEPES, $10\ \mathrm{mM}$ glucose, pH 7.4) resulting in a final cell density of 10^8/mL. Experiments were conducted by incubation of the platelet suspension at $37\ ^{\circ}\mathrm{C}$ with the respective compounds and for the time. For clarity and vali-

dation of the data, all experiments were repeated with at least three different preparations.

Chemicals For platelet inhibition, we used the following chemicals: Forskolin (Sigma, Munich, Germany), Iloprost (Schering, Berlin, Germany), Milrinone (Sigma, Munich, Germany) and Cilostamide (Tocris Cookson, Avonmouth, UK).

Measurement of cyclic nucleotide levels Levels of cyclic adenosine monophosphate (cAMP) and cyclic guanosine monophosphate (cGMP) were measured as follows: The stimulation of platelets with the respective compound was stopped by adding twice the sample volume of ice cold ethanol (100%). Afterwards, the precipitate was removed by centrifugation and washed again with 100 µL ethanol. The supernatants were combined and subsequently dried in the vacuum. The resulting dried platelet samples were dissolved and acetylated. Finally they were analyzed with cAMP or cGMP enzyme-immuno assays commercially available (ENZO Life Sciences, Loerrach, Germany) following the manufacturer's instructions.

Determination of phosphodiesterase concentrations Concentration of phosphodiesterase 2 (PDE2) and PDE5 were determined from calibration curves with lysates from recombinant expression systems (Butt et al., 1994). Briefly, *E. coli* BL21-T1 strain was transformed with plasmids which contain inserts coding for PDE2A (C-terminal fragment aa1-207 deletion, C-terminal His6-tag), PDE3A (aa675-1164 fragment, N-terminal GST-tag) or PDE5A (full length, C-terminal His6) and lysed after Isopropyl-β-D-thiogalactopyrano ß-sid (IPTG) induction. Afterwards, the resulting lysates were purified by affinity chromatography. The GST tagged PDE3A fragment was bound to a GST-sepharose column (Glutathione Sepharose 4B, Amersham Biosciences) and was eluted following the manufacturer's protocol. Similarly, the His6-tagged PDE2A and PDE5A were purified on a Ni-NTA column (Ni-NTA Superflow Kit, Quiagen) and eluted according to the manufacturer's protocol. The obtained protein content of the eluents was determined by the bicinchoninic acid (BCA) protein assay (Thermo Scientific) and dilution series were prepared. Subsequently, platelet lysates and dilution series of recombinant protein were submitted to acrylamide gel-electrophoresis and transferred on a nitrocellulose membrane. They were

detected with an appropriate antibody and chemoluminescence reaction (ECL plus, Amersham). The intensities of protein bands were quantified after scanning with ImageJ software (v1.43, NIH) and the platelet expression was quantified from the calibration curves which were obtained from the dilution series. Phosphodiesterase PDE2 and PDE5 were determined from calibration curves with lysates in over-expression systems (Butt et al., 1994). The quantitative PDE3 amount was taken from Eigenthaler et al. (1992), the kinetic and binding data from Butt et al. (1994) and Poppe et al. (2008).

VASP phosphorylation/immunoflourenscence Vasodilator-stimulated phosphoprotein (VASP) has two characteristic phosphorylation sites (pS239 and pS157) to monitor the corresponding cyclic nucleotide-dependent protein kinase activity. Both sites were determined according to Geiger et al. (2010) with the phosphosite specific antibodies 16C2 (pS239) or 5C6 (pS157) and the total VASP antibody IE273. A more detailed description can be found in the original publication (Wangorsch et al., 2011).

3.2 Static and Discrete Modeling Methods

3.2.1 Protein-protein Interaction Networks

The *PlateletWeb* knowledge base is a comprehensive human platelet repository for systems biologic analysis of platelets in the functional context of integrated networks (Boyanova et al., 2012) of protein-protein interactions. It integrates various information and data of the platelet proteome, transcriptome, site-specific phosphorylation reactions, disease associations, drugs, along with human protein-protein interactions (see Figure 12).

Database assembly Information on protein-protein interactions was obtained from the Human Protein Reference Database (HPRD; Version 9.0, April 2010) (Keshava Prasad et al., 2009) and the Entrez Gene National Center for Biotechnology Information (NCBI) server (Maglott et al., 2007). It was combined with data on protein phosphorylation from HPRD and PhosphoSite (Hornbeck et al., 2004). A comprehensive list of human kinases was extracted from Manning et al. (2002) and used for reference and validation of the HPRD phosphorylation data. Furthermore, integrated Drug data (DrugBank Version 3.0) (Knox et al., 2011) includes detailed information on drugs, drug targets and Gene Ontology (GO) information (GO database; Decem-

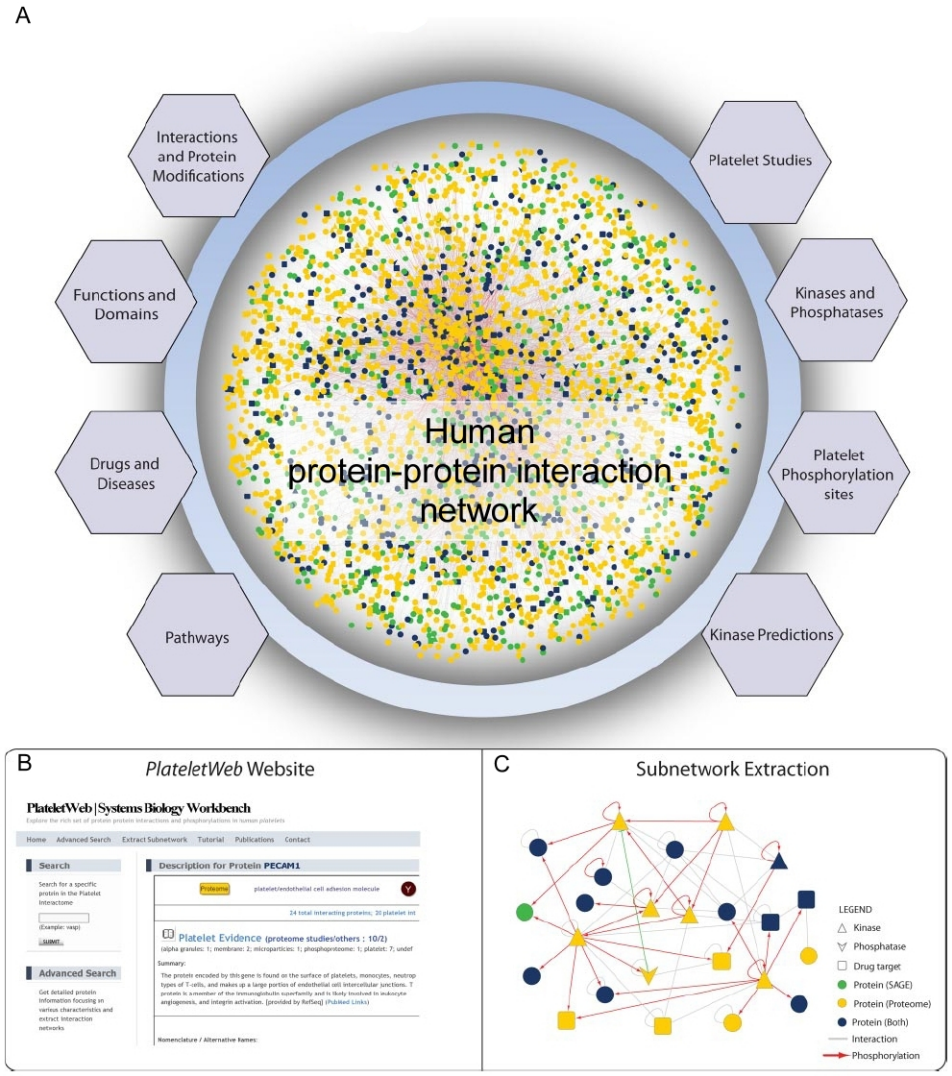

Figure 12: *PlateletWeb* - a platelet-specific knowledge base. (A) *PlateletWeb* combines data from various sources leading to a comprehensive resource for the platelet-specific integrated network analysis such as the investigation of signaling pathways, kinase distribution and functional enrichment in platelets. It includes data from protein-protein interactions and modifications complemented with drug and disease association data, pathway information, kinase-substrate data and predictions for kinases and transmembrane domains. (B) The systems biology workbench can be accessed online to interactively analyze platelet proteins and their related information. (C) The possibility to extract subnetworks allows in-depth analysis of multiple proteins with their modification type, kinase-substrate relationships and drug association. Figure adapted from Boyanova et al. (2012).

ber 2010) (Ashburner et al., 2000) can be accessed for functional enrichment analysis. A detailed listing of all integrated platelet data sources used is available in Boyanova et al. (2012).
The integrative database *PlateletWeb* provides the background for the investigation of signal transduction and involved proteins and interactions in humans and especially human platelets. The internet platform (`http://plateletweb.bioapps.biozentrum.uni-wuerzburg.de`) offers an interface for advanced data-mining and the visualization of subnetworks for functional network analyses. Extracted subnetworks comprise integrated information on site-specific phosphorylations and interactions of all investigated network proteins. Moreover, a novel network-based NetworKIN algorithm (Linding et al., 2007; Miller et al., 2008) is included to predict potential kinases for phosphorylation sites of which no associated kinase is known. This leads to a total kinase annotation of 95% of all phosphosites. Unraveling site-specific information of phosphorylation events is especially interesting for analyzing signal transduction cascades, as phosphorylating kinases play a main role in propagating a signal to its targets.
The extraction and graphical visualization of specific subnetworks allow placing proteins of interest in relationship to signaling modules involved in e.g. platelet activation or inhibition. As the visualization of particularly large networks is challenging, *PlateletWeb* features the export of created networks to Cytoscape (Shannon et al., 2003; Smoot et al., 2011) a well-established software for visualizing and analyzing biological networks.

3.2.2 Boolean Models

Methodologically, we typically apply the simplest Boolean algebra to analyze signaling pathways by Boolean modeling. Boolean variables are represented by a set of n binary elements $X_i, (i = 1, \ldots, n)$ having values 0 or 1 corresponding to the logical values FALSE and TRUE, connected by the logical operators $\wedge$ (AND), $\vee$ (OR) and $\neg$ (NOT). Thus, a Boolean function with n binary variables is a mapping $B : \{0,1\}^n \rightarrow \{0,1\}$ from the set of all n-tuples over $\{0,1\}$ to the binary output determined and based on logical operations from n binary inputs (Boole, 1848). Truth tables represent Boolean functions, wherein each row lists the respective combination of binary Boolean variables and according to the logical connection. For two variables this results in truth tables as defined in Table 1.

Table 1: Truth tables of the Boolean operators ¬ (NOT, negation) ∧ (AND, conjunction) and ∨ (OR, disjunction).

¬x	x=0	x=1
	1	0

x ∧ y	x=0	x=1
y=0	0	0
y=1	0	1

x ∨ y	x=0	x=1
y=0	0	1
y=1	1	1

Example Lets assume a small network of three Boolean variables X_1, X_2 and X_3, e.g. components of a signaling pathway logically connected. This small Boolean network model can easily be projected to a directed graph $G(V, E)$, and directly related to a pathway diagram commonly used for visualizing signaling pathways and biological regulatory systems (see Figure 13). Here, the node set V represent the Boolean variables and the edge set E is implicitly defined by the Boolean function set-up.

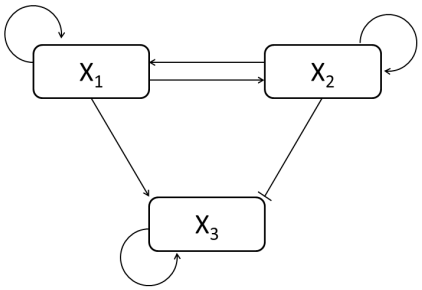

Figure 13: Boolean Network - an example. Simple Boolean network model comprising three Boolean variables X_1, X_2 and X_3, represented as a directed graph. Edges with sharp arrows denote positive, activatory effects, edges with blunt arrows represent negative effects towards their target nodes. In addition to the directed and signed graph, Boolean models contain more specific information, since the same diagram can correspond to several alternative Boolean functions (e.g. the specification of AND/OR connections).

Each edge has a sign specifying whether the input node has a positive or negative effect on the target node. As the network has three elements, it may show 2^N different states ($X_1X_2X_3$).
Assuming the update rules:

$$\begin{aligned} X_1(t+1) &= X_1(t) \wedge X_2(t) \\ X_2(t+1) &= X_1(t) \vee X_2(t) \\ X_3(t+1) &= X_1(t) \vee (\neg X_2(t) \wedge X_3(t)) \,. \end{aligned}$$

By updating the nodes' states at each time step synchronously, the model evolves over time following a trajectory of states, as represented in Table 2.

Table 2: Successively developed states for the Boolean network (see Figure 13). The states are synchronously updated at the same time point.

Current state (t= t_0)	000	001	010	011	100	101	110	111
Next state (t = t_0 + 1)	000	001	010	010	011	011	111	111

The model update according to the rules eventually reaches a steady state (fixed point) or a set of recurring states, commonly referred to as attractors. The set of initial states leading the model to a specific attractor is called the basin of attraction. Referring to the example model, the states (000), (001), (010), and (111) are fixed points (steady states) but in contrast, the states (000), (001), (100), (101), and (110) cannot be reached from a different state.

Software Several software packages have been developed that focus on qualitative modeling and the simulation of Boolean networks (Schlatter et al., 2011). Notably Genetic Network Analyzer (GNA) (De Jong et al., 2003), GINSim (Gonzalez et al., 2006), BooleanNet (Albert et al., 2008), MetaReg (Ulitsky et al., 2008), CellNetOptimizer (Saez-Rodriguez et al., 2009) and CellNetAnalyzer (CNA) (Klamt et al., 2007) have been shown to qualitatively reproduce the activation patterns of experimentally validated regulatory networks. For our analyses we applied CellNetAnalyzer, a MATLAB toolbox, capable to model, simulate and analyze metabolic as well as signaling networks. Besides others, CNA allows the involvement of a certain quantity by allowing stoichiometric assumptions within the modeled equations serving as update rules (see Equation 3.1). This feature extends the classical binarity of Boolean network being relevant for logical networks with multiple-valued discrete states.

$$X_1(t+1) = \neg X_2(t) \wedge 2X_3(t). \tag{3.1}$$

Additionally it allows the setting of different time scale for interactions. CNA facilitates the analysis of signaling networks solely on their network topology, i.e. independent of kinetic mechanisms and parameters in providing a powerful collection of tools and algorithms for structural network analysis.

3.3 Dynamic Transformations for Semi-quantitative Modeling

Simulations based on Boolean networks give a first idea of the signaling behavior, however, as stated in an *Editorial* in *Nature*: " ... to really understand ..., one needs to have numbers attached to the arrows, and equations relating to the numbers" (Campbell, 1999). In other words, the qualitative network structure one needs to be enriched with kinetic information to analyze the full signaling behavior. A first step towards this goal is the transformation of the qualitative network into a set of ordinary equations. The Java-based tool SQUAD (Di Cara et al., 2007) implements this step allowing the qualitative modeling using a set of non-linear ordinary differential equations.

SQUAD While data on the connectivity among molecules is becoming increasingly available, the stoichiometry and particular kinetic data of the biochemical reactions behind the majority of these connections remain scarce. Currently, this bottleneck is one of the major problems, especially when studying highly dynamic signaling cascades. To cope with this issue, a methodology called Standardized Qualitative Dynamical Systems was developed by Mendoza and Xenarios (2006), where SQUAD got its name from. Hybridizing discrete Boolean and continuous modeling methodologies, this approach masters the dynamic simulation of regulatory networks even in the absence of kinetic data.
In a first step, the network is converted into a discrete dynamical system, representing the network as a series of interconnected elements that have solely two possible activation states, 0 (inactive) and 1 (active). Based on this, the following set of Boolean equations completely describes the network.

$$X_i(t+1) = \begin{cases} (X_1^a(t) \vee X_2^a(t) \ldots \vee X_n^a(t)) \wedge \neg (X_1^i(t) \vee X_2^i(t) \ldots \vee X_m^i(t)) & i) \\ X_1^a(t) \vee X_2^a(t) \ldots \vee X_n^a(t) & ii) \\ \neg (X_1^i(t) \vee X_2^i(t) \ldots \vee X_m^i(t)) & iii) \end{cases}$$

Here, the set of activators of a node X_i are represented as $\{X_n^a\}$, whereas $\{X_m^i\}$ denotes the set of inhibitors affecting X_i. In case $i)$, X will be in an active state in the next time step if any of its activators and at the same time none of its inhibitors are acting upon it. Similarly, case $ii)$ or case $iii)$ holds,

if any of its activators or non of its inhibitors is acting upon it. To capture this connective information, SQUAD reads networks in xml-format, ideally created with CellDesigner version 3.5.1 (Funahashi et al., 2008) or other tools. The stable steady states of this network can be located using a Reduced Order Binary Decision Diagram (ROBDD) algorithm (Garg et al., 2007) in SQUAD.
In a second step, the software automatically converts the static network into a continuous dynamical system using the following set of differential equations:

$$\frac{\mathrm{d}X_i}{\mathrm{d}t} = \frac{-\mathrm{e}^{0.5h} + \mathrm{e}^{-h(\omega_i)}}{(1-\mathrm{e}^{0.5h})(1+\mathrm{e}^{-h(\omega_i-0.5)})} - g_i \cdot X_i, \quad \text{with} \qquad (3.2)$$
$$0 \leq X_i \leq 1, \qquad g_i, h \geq 0,$$

where the right-hand side is composed of two parts: an activation function and a term for decay. Activation can be expressed as a sigmoid function of ω, which represents the total input to the node:

$$\omega_i = \begin{cases} \left(\frac{1-\sum\alpha_n}{\sum\alpha_n}\right)\left(\frac{\sum\alpha_n X_n^a}{1+\sum\alpha_n X_n^a}\right)\left(1-\left(\frac{1+\sum\beta_m}{\sum\beta_m}\right)\left(\frac{\sum\beta_m X_m^i}{1+\sum\beta_m X_m^i}\right)\right) & i) \\ \left(\frac{1-\sum\alpha_n}{\sum\alpha_n}\right)\left(\frac{\sum\alpha_n X_n^a}{1+\sum\alpha_n X_n^a}\right) & ii) \\ \left(1-\left(\frac{1+\sum\beta_m}{\sum\beta_m}\right)\left(\frac{\sum\beta_m X_m^i}{1+\sum\beta_m X_m^i}\right)\right) & iii) \end{cases}$$

Analogous to the discrete system, function ω is written so that it describes different combinations of activatory and inhibitory inputs (cases $i)$ to $iii)$). These inputs are weights by $\alpha_n > 0$ and $\beta_m > 0$ so that ω is bounded in the closed interval $[0,\, 1]$. Initially, the weights and parameters h and g are assigned to default values, however, they may modified to fine-tune the dynamical behavior of the equations.

ODEfy Just for reasons of completeness, ODEfy also fulfills the task of transforming discrete into dynamic systems. CNA (version 9.9) comprises ODEfy (Krumsiek et al., 2010) a MATLAB- and Octave-compatible toolbox for the automatically transforming Boolean models into systems of ordinary differential equations. This is achieved by multivariate polynomial interpolation and optional application of sigmoidal Hill functions describing cooperativity and also applied in enzyme kinetics (see Section 2.3.3).

3.4 Data-based Dynamic Modeling

3.4.1 Approach

The different steps of the data-based modeling approach from model creation to the design of new experiments are displayed in Figure 14.

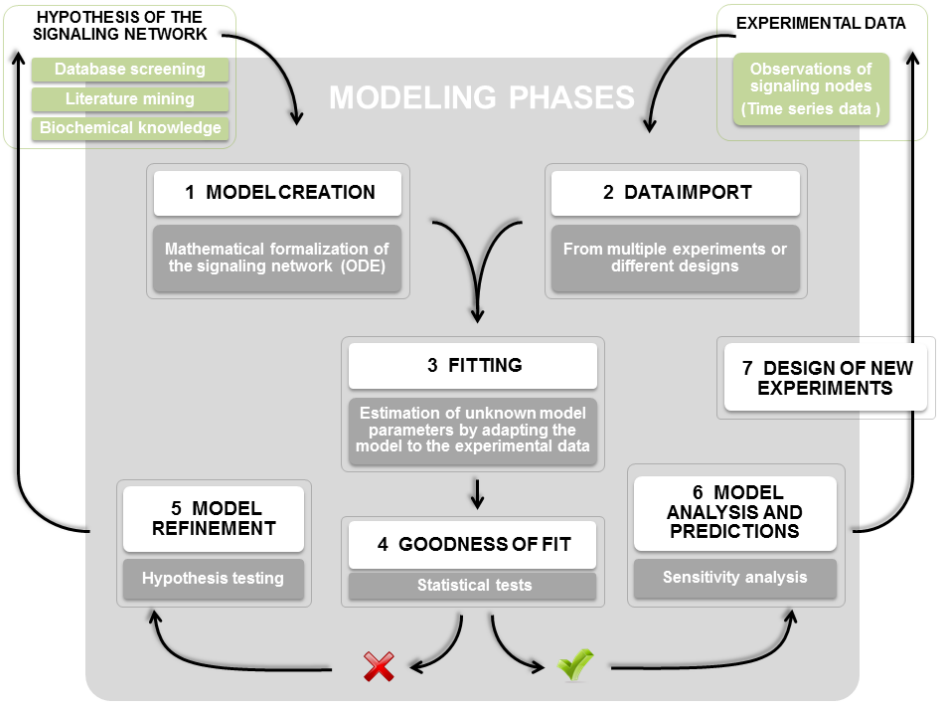

Figure 14: Modeling phases. Different modeling phases from the model creation to experimental design.

Finding the appropriate model structure and predictive model parameters the most crucial step in dynamic modeling. Moreover, the model complexity always needs to be supported by data, to finally result in a meaningful description of a biological process for quantitative model prediction and suggesting experimental designs (steps 6 and 7, Figure 14).
Having established a parametric set of ordinary differential equations (step 1, Figure 14), the parameters have to be determined, which is a crucial step and task. Usually it is preferable to use as much *a priori* information as possible to render the model more accurate. This includes the consultation of pathway data bases (e.g. Kyoto Encyclopedia of Genes and Genomes (KEGG), Ingenuity Pathways Knowledge Base (IPKB), Signal Transduction Knowledge Environment (STKE)) or screening of literature-based knowledge. However, biochemical parameter may unfortunately differ by orders of

magnitude according to the experimental conditions. Therefore it is difficult to decide whether discrepancies between experimental and simulated data arise from inadequate parameters of from an insufficient model (Timmer et al., 2000). One approach to solve this simulation dilemma is the parameter estimation and model selection from experimental data (steps 2 - 5, Figure 14). We applied this data-driven approach throughout the dynamic analysis of platelet signaling pathways (Section 4.1.4).

3.4.2 Fitting and Evaluating Dynamic Models

Section 3.4.2 introduces statistical methods to estimate parameters in a data-driven way. Experimental data is always prone to a certain measuring inaccuracy (noise). To explain the data most accurately, one can establish several models M_i of different complexity, each comprising a corresponding set of parameters $\theta = \{p_1, \ldots, p_r\}$. The evaluation and comparison of these models leads to the following questions: Which parameter set can explain the biological observations? Are these parameters identifiable, given the model and data? Which model gives a good fit to the data while having the least number of parameters to avoid overfitting? These questions can be answered by statistical methods being introduced in the following.

Maximum Likelihood Estimation

The least-square method and the method of maximum likelihood (ML), respectively, are common methods to fit a model to data while estimating the inherent model parameter $\theta = \{p_1, \ldots, p_r\}$. In other words, it exists a class of models M_i depending of a parameter vector $\theta_i \in \Theta \subset \mathbf{R}^r$. Vector θ determines the values which can be expected from the model $M = \{m_1, \ldots, m_N\}$. Principle of the ML method is to find the parameter vector θ_{ML} of a model with which the observed data $D = \{d_1, \ldots, d_N\}$ is the most plausible:

$$\theta_{ML} = \underset{\theta}{\operatorname{argmax}}(P(D|M, \theta)).$$

P represents the probability density of the observed data, given a model M and the parameter vector θ. In order to estimate θ_{ML}, one has to consider

$$\frac{1}{\sqrt{2\pi}\sigma_i} \mathrm{e}^{-\frac{(d_i - m_i)^2}{2\sigma_i^2}},$$

describing the dispersion of measured data values d_i around the model-

based values m_i. Note that one assumes Gaussian distributed measurement error ($N(0, \sigma_i^2)$).
Given a series on N independent measurements, the joined probability can be written as a product of Gaussian distributions:

$$L(\theta|D, M) := P(D|M, \theta) = \prod_{i=1}^{N} \frac{1}{\sqrt{2\pi}\sigma_i} \mathrm{e}^{-\frac{(d_i - m_i)^2}{2\sigma_i^2}}. \tag{3.3}$$

The so-called likelihood $L(\theta|D, M)$ is a function of θ. It provides upon maximization an optimal estimation θ_{ML} of model parameter with which the observed data is most plausible so that

$$L(\theta_{ML}|D, M) \geq L(\theta|D, M) \qquad \forall\, \theta.$$

It is often more convenient to maximize the log-likelihood

$$\begin{aligned} \mathcal{L}(\theta|M, D) &:= \log L(\theta|D, M) \\ &= -\sum_i \frac{(d_i - m_i)^2}{2\sigma_i^2} - N \log \sqrt{2\pi} - \sum_i \log \sigma_i \end{aligned} \tag{3.4}$$

with respect to θ or to minimize the negative log-likelihood. As the last two terms in 3.4 are constants and independent of θ that depend solely on the data and the error model, they can be neglected during the optimization process. Thus, the optimization problem is reduced to minimizing the sum

$$\sum_i \frac{(d_i - m_i)^2}{2\sigma_i^2}.$$

In other words, θ_{ML} is estimated so that the sum of squared error between data and model gets minimal (least-square method). The sum of squared errors is called χ^2-value and it holds: Assuming Gaussian distributed residuals $d_i - m_i$ or standardized residuals $\frac{d_i - m_i}{\sigma_i}$, respectively. Then, the sum of squared residuals is χ^2-distributed with $(N - r)$ degrees of freedom (Annex A.1):

$$\chi^2 = \sum_i \frac{(d_i - m_i)^2}{\sigma_i^2} \sim \chi^2_{N-r}. \tag{3.5}$$

The Kolmogorov-Smirnov test (Silvey, 1975) is a suitable test for normally distributed residuals.
Thus, the relation between χ^2-value and the optimized log-likelihood can

be formulated as:

$$\chi^2 = -2 \cdot \mathcal{L}(\theta_{ML}|M, D). \tag{3.6}$$

Goodness-of-fit

χ^2-values express the difference between data and model trajectories and therefore indicate the quality of the model fit, the goodness-of-fit. The smaller the value, the better the fit. Given a certain level of significance, this allows the statistical evaluation of the fit quality (χ^2-test). Besides, there are different goodness-of-fit measures to characterize statistically the fitting quality such as the Akaike's information criterion *AIC* (Akaike, 1973) and Bayesian information criterion *BIC* (Schwarz, 1978) and derivatives thereof (Burnham and Anderson, 2002) which can also serve as a basis for model selection (see section 3.4.3 and Annex A.3). Exemplary, the *AIC* measure

$$AIC = -2\mathcal{L}(\theta_{ML}|M, D) + 2 \cdot r = \chi^2 + 2 \cdot r, \tag{3.7}$$

directly penalizes the number r of free parameter to account for the problem of overfitting.

Multi-experiment Fitting

We used the MATLAB (2010) toolbox *PottersWheel* (Maiwald and Timmer, 2008) in order to fit our model to different time series data simultaneously, a useful feature for model calibration. Multi-experiment fitting is based on the assumption that kinetic system parameters stay unchanged if different initial values or input functions are applied. This way, the statistical power to estimate parameter values or to discriminate competing model hypotheses are strongly increased. The multi-experimental approach allows the estimation of global and local parameters. Global parameters are assigned to the same value for each experiment, reflecting structural parameters like rate constants. In comparison, local parameters obtain different values depending on the experiment.and helps to keep the model as parsimonious as possible.

The parameter estimation often leads to minimization problems which can be solved with a variety of global and local optimization algorithms. Here, we applied the trust region algorithm in logarithmic space (Coleman and Li, 1996) for multi-experiment fitting purposes.

The PottersWheel toolbox also features the conduction of fit sequences. Initial parameter values are repeatedly disturbed to a certain percentage and

subsequently fitted to the data. Thus, the distribution of estimated parameter values resulting from sequential fitting can be used for an identifiability analysis. This includes the evaluation of the χ^2 landscape which indicates local or global minima or the confidence intervals for each parameter, indicating how definite the parameters can be estimated from the data.

Parameter Identifiability

In parameter estimation it may occur that different sets of parameter may happen to agree equally well with the data or several parameters mutually compensate their effects, e.g. an increased value for parameter k_1 and a decreased value for k_2 may lead to the same time course of the observation. Then, the model might suffer from a so-called non-identifiability. One distinguishes between structural and practical reasons for non-identifiability:

Structural Non-identifiability If two parameters k_1 and k_2 only appear in a model only in form of a product or quotient $c = \frac{k_1}{k_2}$ they can not be determined independently from each. Thus, a maximum likelihood estimation may suffice to determine the quotient c but not the individual parameter values k_1 and k_2, respectively. This is referred to as structurally non-identifiable. The replacement of c by a new, possibly identifiable parameter k_3 may resolve the problem. Structural non-identifiability can result from several kinds of formulas and may be difficult to discover and to resolve. A data-based algorithm to identify linear and non-linear relations of arbitrarily many parameters is described in Hengl et al. (2007).

Practical Non-identifiability Even a structurally identifiable model may still comprise parameters which are practically non-identifiable if the data are not sufficient. There is either too few data available or the wrong kind of data is used to estimate the model parameters. Generally, if the number of parameters exceeds the number of measured data points, the parameters can not be clearly determined. Sontag (2002) gives a rule for the minimum number of experimental data needed to construct models of differential equations. An approach for identifiability analysis utilizing the profile likelihood was proposed by Raue et al. (2009).

3.4.3 Model Comparison and Selection

Selecting an adequate model structure is a crucial part of the modeling process for which no perfect solution exists. A suitable model renders possible new approaches to identify therapeutic strategies and to assess the feasibility of a research agenda minimizing the cost in terms of animals, time, and money. But in most cases, there exist more than one plausible model which supports the experimental data. Evidently, more complex models are advanced in fitting the observed data as they comprise more degrees of freedom (parameters). However for reasons of parameter estimation and calibration, one has to correct for the advantage of complex models. To find models with reliable parameter estimates and good potential for model predictions, there are different strategies including forward selection (bottom-up) and the top-down method. Following a bottom-up procedure, one starts with a very simple model which is extended until no significant improvement can be detected. The top-down method, in turn, takes a very complex model as starting point which is reduced until the fit gets significantly worse. For both procedures, a likelihood ratio test (LRT) can be applied to favor models with few parameters.

Likelihood Ratio Test (LRT)
The LRT (Vuong, 1989; Timmer and Mueller, 2004) compares two models M_1 and M_2 of different complexity by their maximal likelihood values. Reducing a model's complexity raises the question whether the reduced model sufficiently explains the data, or whether the more complex model is needed. We assume model M_1 is the more complex model comprising r_1 parameters and model M_2 is the reduced model having a set of r_2 parameters. The models are called nested, if model M_1 contains additional $r_1 - r_2$ parameters besides the r_2 parameters of model M_2. The comparison of the corresponding maximal likelihoods leads to hypothesis testing:
The null hypothesis H_0 states, model M_2 with its corresponding parameter set θ_2 describes the data equally well as the more complex model M_1 with additional parameters ($\theta_2 \subset \theta_1$). In contrast, the alternative hypothesis implies, that M_1 significantly improves the model fit to the data. Hypothesis testing compares the log-likelihoods of both models $\mathcal{L}(\theta_{1,ML}|M_1, D)$ and $\mathcal{L}(\theta_{2,ML}|M_2, D)$, respectively. As the more complex model always has a higher likelihood, it has to be tested whether the ratio of log-likelihoods is significant or not.

It can be shown that the log-likelihood ratio is χ^2-distributed with $r_1 - r_2$ degrees of freedom (see Annex A.1, A.2). For nested models M_1 and M_2 this yields

$$2(\mathcal{L}(M_1) - \mathcal{L}(M_2)) \sim \chi^2_{r_1 - r_2}. \tag{3.8}$$

Density functions and cumulative distributions of the χ^2 distribution with different degrees of freedom are displayed in Figure 15. For a given level

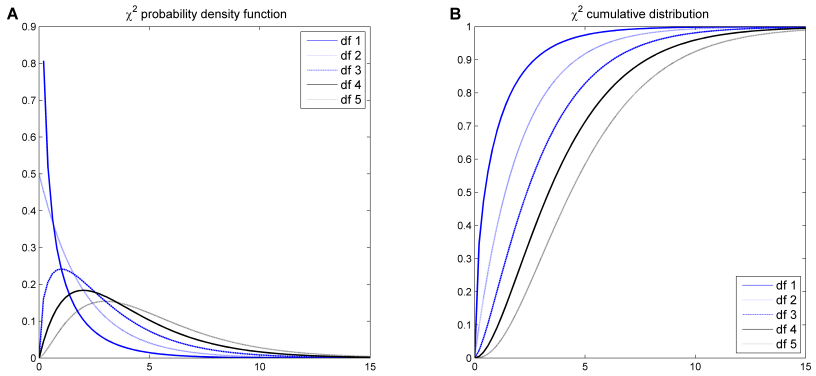

Figure 15: χ^2 distribution. (A) The probability density function according to different degrees of freedom (df). (B) The cumulative distribution functions.

of significance, this distribution is used for statistically testing, whether the null hypothesis can be rejected or not. However, the distributional result (3.8) only holds if the so-called standard conditions are given (Cox and Hinkley, 1974; Vuong, 1989). The most important conditions of these are:

1. The models M_1 and M_2 are nested.

2. The true parameters are not at the limit of the parameter space.

3. The parameters are identifiable under the null hypothesis.

For non-standard conditions and non-nested models however, one has to consider different strategies for model selection (Self and Liang, 1987; Hall and Wilson, 1991).

Akaike Information Criterion (AIC)

In the context of model selection, also criteria derived from information theory such as the Akaike information criterion (AIC) can be used (Akaike, 1973, 1974). It suggests to compare the models by

$$AIC = -2\mathcal{L}(\theta_{ML}|M, D) + 2 \cdot r = \chi^2 + 2 \cdot r, \tag{3.9}$$

and to choose the model with the smaller AIC value (see Annex A.3).

Sensitivity Analysis

Having established a suitable model structure with identifiable parameters, one may further predict and analyze how sensitive the model variables and observables themselves or their characteristics will react upon parameter changing. This may accompany the design of new experiments. Characteristic measures include the integral over a certain time period, the peak hight, last value or the area under the curve. This impact is quantified by calculated sensitivity values or control coefficients. We used the summation laws derived by Hornberg et al. (2005) and implemented in MATLAB to describe and quantify the influence of parameter change on the characteristics.

3.5 Rule-based Modeling

Rule-based modeling (RBM) is a powerful and increasingly popular approach that allows the use of available information about complex protein-protein interactions in a precise and compact manner. It is hence a convenient tool for constructing large executable models of complex cell signaling network, containing a starting set of molecules, with possible interaction behaviors defined by biochemical reaction rules. (Hlavacek et al., 2006; Faeder et al., 2009). Molecules are represented as structured objects whereas their interactions are defined as rules for transforming the attributes of these objects. A rule can be understood as an implicit definition of a class of reactions, all involving a common transformation. Thereby, RBM allows to systematically incorporate site-specific details about protein-protein interactions into a model for the dynamics of cellular signal cascades (Figure 16). The ability to involve site-specific information renders RBM a highly appropriate method, tailored to model complex binding and signal processing at a receptor comprising several binding domains such as the epidermal growth factor (EGF) receptor Danos et al. (2007) or the cluster formation upon ligand binding (Monine et al., 2010). The multiplicity of sites, e.g. possible phosphorylation states, the many ways that signaling molecules can combine and be modified, give rise to combinatorial complexity (Hlavacek et al., 2003), a problem modelers of signaling networks have to cope with.

The domain-oriented, rule-based approach addresses this problem as it provides a powerful alternative to approaches that require an explicit enumeration and description of all possible molecular species and reactions of a system such as ODE-based models. Rule-based models can appropriately be specified and analyzed on the basis of the BioNetGen language (Faeder et al., 2009).

Software Several RBM-related software is available (cf. Hlavacek et al. (2006); Faeder et al. (2009); Colvin et al. (2010)). We applied RuleBender (Xu et al., 2011a; Smith et al., 2012) for model implementation as it serves for editing, visualizing and simulating models based on BioNetGen language. Furthermore, this user-friendly tool can be combined with NFSim (Sneddon et al., 2011), a network-free stochastic simulator.

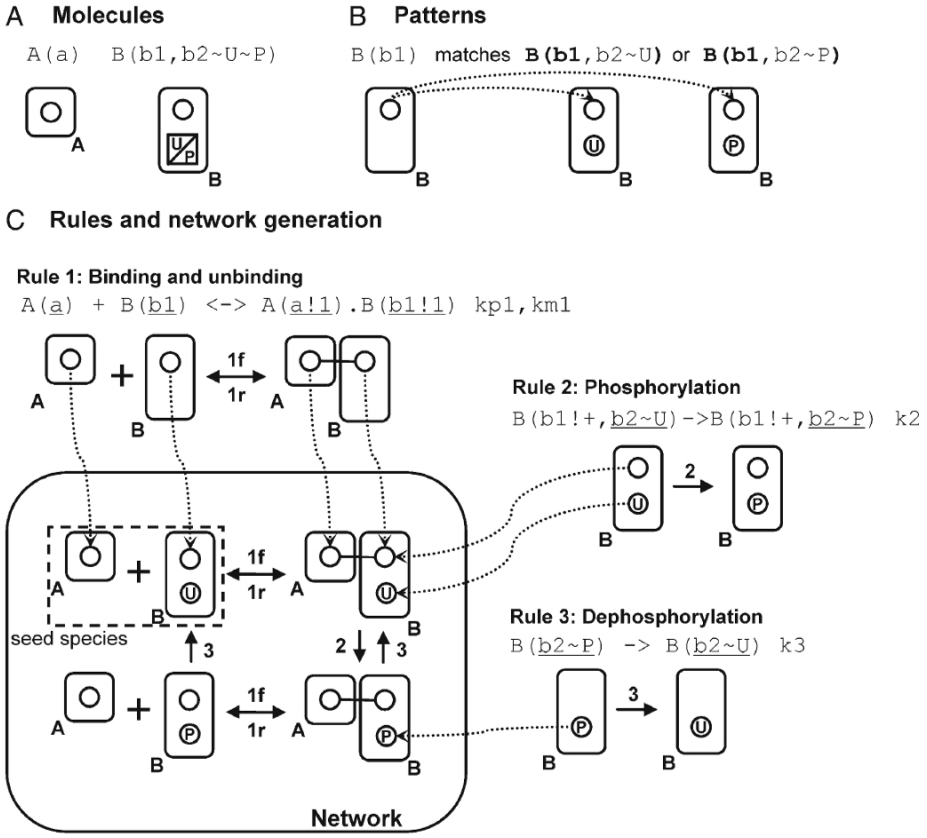

Figure 16: Concept of rule-based modeling. Rule-based modeling concepts and encoding in BioNetGen language. (A) Basic building blocks: Molecules, represented as structured objects, composed of components denoting functional elements of proteins such as domains. These elements may have associated states that describe covalent modifications or conformations (e.g. phosphorylations, ubiquitinations, bonds). Through bonds linking components of different molecules, they may be assembled into complexes. (B) Patterns: By using patterns, one can select particular attributes of a reacting molecules in species, here shown in bold. In the depicted example, the pattern selects all states of molecules of B that have a free $b1$ binding site. In particular, this is regardless of the phosphorylation or binding status specifying the $b2$ component of molecule B. (C) Rules and network generation: Rules represent the biochemical transformations which can occur in the system and are utilized to build up a network of species and related reactions (a complete description of the entire rule syntax is given in Faeder et al. (2009)). The reaction center, meaning the components that undergo direct modification, is underlined for reasons of clarity. The network is created as follows: By starting with the seed species, rules are applied in order to generate new reactions and species by mapping the described reactant patterns onto species and applying the implemented transformation(s) as specified. Species that have been generated by new reactions may be affected by other rules to again generate new reactions and species. This process continues until there is no new reaction or a stopping criteria is satisfied. Figure: Faeder et al. (2009)

4 Results

ALL MODELS ARE WRONG, BUT SOME ARE USEFUL

(*George Box*)

4.1 Systems Analysis of Platelet Signaling

4.1.1 Introduction

The small anucleate blood platelets are pivotal for the maintenance of hemostasis. This is achieved primarily by the formation of aggregatory blood clots (thrombi) in case of an injured endothelium of blood vessels. On the converse, thrombus formation has to be inhibited at times when the endothelium is undamaged. Impaired platelet signaling may disturb this subtle hemostatic balance leading to pathophysiological cardiovascular diseases as well as inflammatory processes and metastasis. Thus, a systemic description, examination and analysis is key to understand and control platelet signaling also under clinical conditions.

Data on the platelet and its proteome is rapidly accumulating due to advanced techniques including mass spectrometry (Garcia et al., 2004; Zahedi et al., 2008; Premsler et al., 2011) and systematic yeast two hybrid assays (Stelzl et al., 2005; Rual et al., 2005). The assembly of platelet-specific (phospho)proteome, transcriptome and interactome data together witch functional annotations and drug information form an integrative platform for the creation of an virtual *in silico* platelet model. Such a basis (Boyanova et al., 2012; Dittrich et al., 2008) allows the modeling of platelet signaling and interactions in more detail which potentially reveals biological functions or drug targets, building a bridge to pathophysiological processes. It deepens

the understanding of platelet (patho)physiology, biochemistry, signal transduction being essential to eventually develop new strategies for pharmacological interventions. This is supported by mathematical modeling and systems biological approaches, underpinning the drug developmental process (Nikolsky and Kleemann, 2010; Ramsey et al., 2010), (Chatterjee et al., 2010; Diamond, 2009).

Here, we present different methods for analyzing platelet signaling on different scales. This ranges from a global network-based approach to give systemic insights in cell signaling and the interlinking of signaling pathways (Section 4.1.2). Building on this static approach, we then zoom in on the Boolean modeling of specific signaling pathways of platelet inhibition and activation, bringing the temporal component to signal cascade models (Section 4.1.3). This is followed up by a dynamic ODE-based model which precisely describes platelet inhibition with focus on the feedback-regulated cAMP level. Calibrated by adaption to time series data, the model quantitatively serves as a predictor for testing anti-aggregatory drugs (Section 4.1.4).

4.1.2 Interactome, Subnetworks and Static Network Analysis

Cross-talk of Inhibitory and Activatory Pathways

The response of platelets to changes in the immediate environment is always a balance between activatory and inhibitory signals and related platelet signaling cascades. The cumulative effect of these signals is either platelet activation or quiescence (cf. Section 2.2). Besides the bivalent definite effect on the platelet, signaling cascades are highly interlinked (see Figure 17) and the unraveling of interactions represent a challenging subject of ongoing research. Exemplary, our experimental collaboration partners recently demonstrated cross-talk between platelet stimulatory and inhibitory pathways Gambaryan et al. (2010). They discovered that an activation of human platelets by vWF caused NO-independent activation of soluble guanylyl cyclase and stimulation of cGMP production and PKG. Thus, vWF which is mainly triggering platelet activation also initiates a feedback inhibitory pathway (Gambaryan et al., 2008).

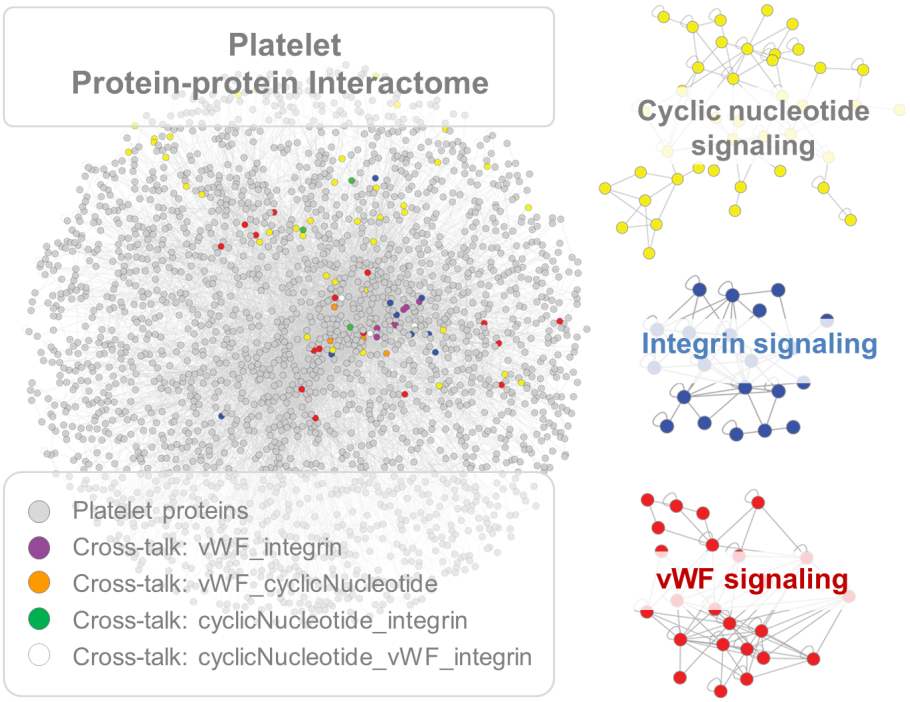

Figure 17: Main platelet signaling cascades and cross-talk. Graphical representation (subnetworks) of three main platelet signaling pathways: key nodes of cyclic nucleotide signaling (yellow), crucial for platelet inhibition; vWF signaling (red), and integrin signaling (blue) triggering the platelet activation. Platelet proteins are depicted in grey. Common proteins assigned to two or more pathways are shown with different colors: vWF_integrin (violet), vWF_cyclicNucleotide (orange), AcyclicNucleotide_integrin (green), cyclicNucleotide_vWF_integrin (white). Figure: Modified after Boyanova et al. (2012).

Integrative Subnetwork Extraction

Static network analysis and bioinformatical investigation of platelet-specific protein-protein interactions are a first step to gain insight into interactomics and platelet signaling. By offering functional, drug- and pathway-associations, the comprehensive platelet repository *PlateletWeb* (Boyanova et al., 2012) provides a first systemic insight into various aspects of platelet functionality, pharmacologic regulation and pathway interlinking. It allows an integrated network analysis sustaining a further inspection of cross-talking signaling proteins, their regulatory interactions and site-specific phosphorylations. This systems biological approach helps to underpin predictions or observations that have arisen from experiment. Particularly important candidates are set into a known or even novel or predicted network context highlighting their connections to platelet activation or inhibition, respectively.

Moving towards probing modulatory interactions, central activatory and inhibitory mechanism and main signaling cascades are extracted from the entire platelet interactome database. This results in enriched protein-protein subnetworks (see Figure 18) comprising pivotal network proteins whose connectivity show the information flow throughout the network.

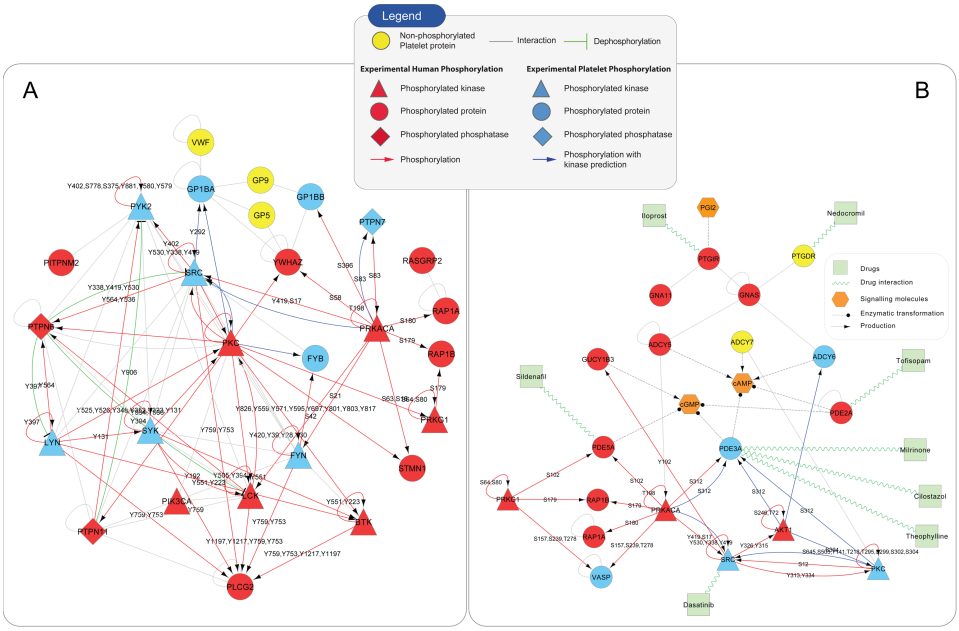

Figure 18: Platelet activatory (A) and inhibitory (B) subnetworks. For illustration of subnetworks we show the topology and key nodes of the activatory vWF cascade (A) and the inhibitory cyclic nucleotide signaling pathways (B). Proteins (circles) are trianglar if they constitute phosphorylated kinases, or diamond shaped in case they represent phosphorylated phosphatases. Human proteins (red) are blue-colored if they show platelet specific phosphorylations, and yellow-colored if they are non-phosphorylated. Protein-protein interactions (gray lines) are further divided into dephosphorlyation (green line) and phosphorylation (red arrow), specified by the corresponding phosphosite, a (de)phosphorylated serine (S), tyrosine (Y) or threonine (T) residue. If it exists a kinase prediction for such a phosphorylation, the arrow is blue-colored. Extracted subnetworks can be enriched with drug information (panel B, greenish modifications) or are manually refined by adding additional signaling molecules (orange nodes) or enzymatic transformations and reactions.

To further investigate cross-talk proteins and their functions, we focus on the integration of site-specific information of phosphorylations within the platelet interactome. Protein phosphorylation and dephosphorylation via kinases and phosphatases, respectively, are the most abundant and central mechanisms involved in the regulation of almost every cellular process (Sauro and Kholodenko, 2004). In eukaryotes, kinases phosphorylate at specific serine (S), threonine (Y) or tyrosine (T) residues thereby altering protein activities. This holds for anucleate platelets in particular, as phosphorylation events predominate the mediation of signal transduction.

Integration of Platelet Proteins into Signaling Contexts

By phosphoproteome analysis, recently several phosphorylation sites were identified in resting platelets which were located on potential PKA and PKG substrates. Involved in platelet inhibitory pathways, activated PKG and PKA antagonize platelet aggregation. Among the detected candidates for protein kinase substrates, CalDAG-GEFI, phosphatidylinositol transfer protein, membrane-associated 2 (PITPNM2) together with protein tyrosine kinase 2 (PYK2), nardilysin (NRD1) and stathmin (STMN1) are to be ranked highly interesting for further investigation according to our experimental collaborators. Exemplary, protein CalDAG-GEFI integrates signaling for platelet aggregation and thrombus formation (Crittenden et al., 2004) and plays a key role in the activation of Rap family GTPases involved in platelet integrin activation (Jeyaraj et al., 2011). The activation of PKA/PKG inhibits Rap activity, however the underlying mechanisms are not exactly known. We hypothesize that activated PKA is phosphorylating CalDAG-GEFI which inhibits Rap1 activity. Experimentally, we found that CalDAG-GEFI is a substrate for PKA/PKG and identified its *in vivo* phosphorylation site (Ser587). Bioinformatically, we support further investigations by predicting and analyzing the possible involvement of these proteins in platelet activatory and inhibitory signaling cascades (see Figure 19), critically modified and balanced by specific phosphorylations. Furthermore, potential kinases are predicated algorithmic-based (Linding et al., 2007; Miller et al., 2008) with respect to detected phosphosites, which hints at probable functional possibilities and may guide further experiments.

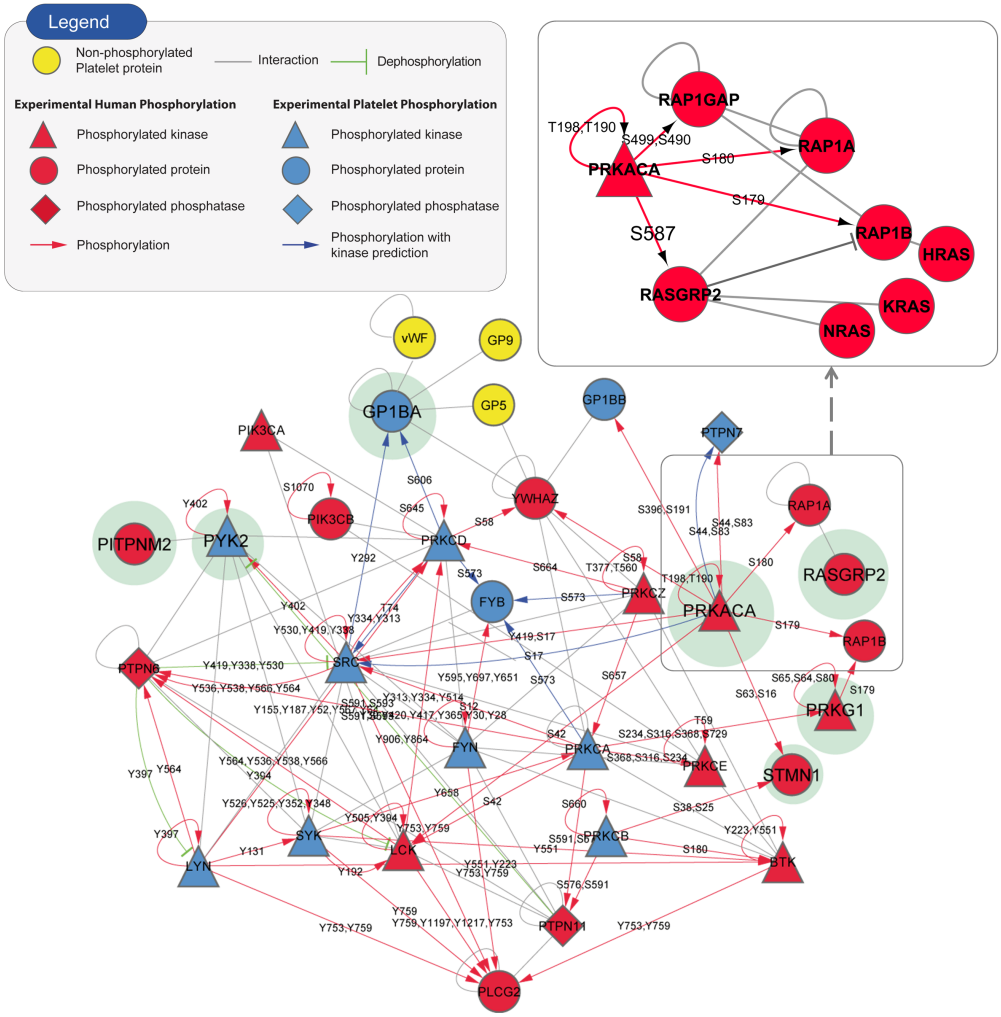

Figure 19: Network-integrated potential PKA/PKG substrates. Interesting proteins (named after gene name identifier) and potential PKA and PKG substrates (phosphatidylinositol transfer protein, membrane-associated 2 (PITPNM2); protein tyrosine kinase 2 (PYK2); CalDAG-GEFI (RASGRP2); stathmin (STMN1)) are integrated into the network context for platelet activation including PKA (PRKACA) and PKG (PRKG1). These central proteins are highlighted (green). Established protein-protein interaction network is superimposed with phosphorylation data (experimentally validated as well as predictions): Proteins (circles) are depicted in trianglar shape if they represent phosphorylated kinases, or diamond shaped in case they constitute phosphorylated phosphatases. Human proteins (red) are yellow-colored if they are non-phosphorylated and blue-colored in case they show platelet specific phosphorylations. Protein-protein interactions are represented by grey lines. Dephosphorlyations (green line) and phosphorylations (red arrow) are specified by the corresponding phosphosite, either a (de)phosphorylated serine (S), tyrosine (Y) or threonine (T) residue. Algorithm-based kinase predictions for such phosphorylation events are depicted by blue arrows.

4.1.3 A Boolean Model of Platelet Inhibition and Activation

Outline

As described in Section 4.1.2, we explored detailed data on the platelet (phospho)proteome and interactome to establish a simplified Boolean model of the central platelet cascades. Here, we focus on activatory pathways and its interplay with platelet inhibition. Activatory pathways are versatile to cope with diversified environmental conditions. Platelet activation and aggregation occurs on several activation levels including receptor activation, G-proteins and calcium mobilization, activation of central kinases and integrins as key steps (cf. Section 2.2). The interplay with the inhibitory cyclic nucleotide system manifests the behavior of the systems. Downstream of the receptor level, this results in a highly interlinked network of kinases, executing proteins and small molecules ensuring the signal responses. However, for the establishment of a predictive *in silico* model, it is indispensable to focus on key signal interactions of modulatory pathways (cf. Figure 18) out of a complex *PlateletWeb* of all protein-protein interactions within the platelet (Boyanova et al., 2012).
The analysis and simulations of the key-node focused model show the stepwise coalescence of different signaling events into a fully activated system state that includes positive feedback regulation. System stability analysis distinguishes the networks inherent biphasic threshold behavior: a subthreshold phase which is characterized by integration over different activatory and inhibitory conditions, opposed by a beyond threshold phase where counter-regulatory pathways are outweighted towards irreversible platelet aggregation. Model-based predictions are verified by monitoring phosphorylations marking different proposed activation phases.

Model Setup and Implementation

Focusing on the platelet interactome and key signaling nodes, we constructed a logically connected model of the key activating platelet cascades and modulatory inhibitory pathways (Figure 20).

Network Topology The network topology comprises a set of key nodes of each activating phase, that govern the overall-behavior of the respective sub-part. Starting with signal initiation, we include the collagen receptor GPVI, being a strong platelet activator. Upon stimulation, a cascade of kinases, including protein kinase C (PKC), Akt and Src is engaged, initially

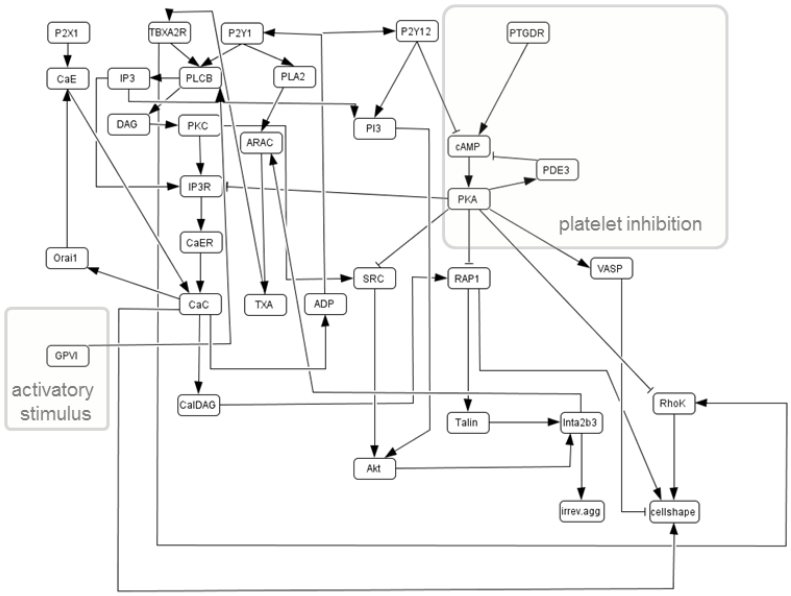

Figure 20: Boolean network represented as directed graph. Arrows denote activatory (→) and inhibitory (—|) effects on the corresponding target node. Pivotal key-nodes in the network context involved in different activatory and inhibitory platelet signaling cascades: collagen receptor (GPVI); phospholipase Cβ2 (PLCB); inositol-1,4,5-triphosphate (IP3); IP3 receptor (IP3R); 1,2-diacylglycerol (DAG); protein kinase C (PKC); thromboxane A2 (TXA); thromboxane receptor (TBXA2R); arachidonic acid (ARAC); ATP receptor (P2X1); ADP receptors (P2Y12, P2Y1); adenosine diphosphate (ADP); talin (Talin); phosphoinositide 3-kinaseβ (PI3); integrins (Inta2b3); phosoholipase A2 (PLA2); Akt kinase (Akt); prostaglandin receptor (PTGDR); cyclic adenosine monophosphate (cAMP); protein kinase A (PKA) and substrates phosphodiesterase 3 (PDE3), vasodilator stimulated phosphoprotein (VASP), Rap1, Src kinase (Src), Rho kinase (RhoK); cytosolic calcium (CaC); extra-cellular calcium (CaE); calcium in endoplasmatic reticulum (CaER); CalDAG-GEFI (CalDAG); calcium channel Orai1. Figure modified after Mischnik et al. (2013).

leading to a rearrangement of the platelet cytoskeleton (shape change) and the formation of unstable aggregates. At first, membrane-bound phospholipase Cβ2 (PLCB) gets activated, triggering the production of the second messengers inositol-1,4,5-triphosphate (IP3) and 1,2-diacylglycerol (DAG). IP3 diffuses through the cytoplasm, subsequently binding to its IP3-receptors at platelet organelle membranes, which causes the release of calcium ions from intra-cellular storage pools (Authi and Crawford, 1985), whereas DAG remains at the plasma-membrane potently activating of PKC (Lapetina et al., 1985). Besides shape change and the formation of pseudopodia, this results in the activation of CalDAG-GEFI (Crittenden et al., 2004) directly activating Rap1, thereby transmitting the signal via talin to integrin α2bβ3. Thus, integrin switches to the active state characterized by exposed fibrinogen binding sites. Activated PKC entails Src kinase phosphorylation (Liebenhoff et al., 1994), which potentially transmits the signal to the Akt

kinase (Xiang et al., 2010). The latter also receives signals from phosphoinositide 3-kinaseβ (PI3) and acts directly on integrin α2bβ3 (Kirk et al., 2000), which strengthens the platelet activation state. Increased intracellular calcium concentration also leads to the fusion of platelet granules with the plasma-membrane, thereby releasing small molecules such as ATP, ADP or serotonin and pro-coagulatory proteins into the extra-cellular space (Cattaneo et al., 1990). ADP subsequently binds to its receptors P2Y1 and P2Y12, further amplifying the kinase cascade, and inhibiting the cAMP-production by means of P2Y12 on the other hand (Cattaneo and Gachet, 2001). Thus, the inhibiting part (prostaglandin receptor (PTGDR)/cAMP/PKA-system) is suppressed, further increasing platelet activation. Emptying the calcium stores finally elicits a secondary calcium entry by means of Orai1, TRPC channels and ATP-receptor P2X1. A positive feedback loop from the activated integrin back to the inner side of the plasma-membrane stabilizes the activated system, by which phosoholipase A2 (PLA2) gets activated. As a result, thromboxane A2 (TXA) is synthesized from arachidonic acid (ARAC), catalyzed by cyclooxigenase (Jin et al., 2002) and released for binding at platelet thromboxane receptors (TBXA2R). This increases the pathway activity to the highest extent and switching the signal response from reversible to irreversible aggregation. In terms of the counter-regulatory, inhibiting pathway, protein kinase A (PKA) and its activating second messenger cAMP are to be designated as key nodes. Cyclic adenosine monophosphate (cAMP) production is triggered upon stimulation of prostaglandin receptors, here represented by PTGDR. cAMP exerts its main effects via its corresponding protein kinase PKA. It phosphorylates targeted serine and threonine residues on substrate proteins that prevent or reverse platelet activation (Smolenski, 2012) such as other kinases (Src), receptors (IP3R) and proteins linked to cytoskeletal organization like the vasodilator-stimulated phosphoprotein VASP (Abrahamsen et al., 2003; Murthy et al., 2002; Weber et al., 1999). cAMP levels are tightly regulated by means of several negative and positive feedback loops, comprising directly or indirectly modulation via phosphodiesterases (PDE3) and the ADP receptor P2Y12 (Feijge et al., 2004; Hechler and Gachet, 2011). This step-wise activation process is highlighted by transforming the known interactions into a multi-level Boolean network.

Implementation The multi-level connectivity and node selection was carried out in a literature-based way as well as according to *a priori* knowledge on platelet signaling (cf. Section 2.2). The logical model was implemented and simulated by means of CellNetAnalyzer (CNA) (Klamt et al., 2007) (see Annex B.1 Table 10 for key nodes and edges; Annex B.2 Table 11 for connectivity of the logical interaction hypergraph model). It can suitably be represented as a directed graph (Figure 20) denoting activatory and inhibitory effects on target nodes. Besides CNA for simulation in discrete time steps, we applied SQUAD (Di Cara et al., 2007) for semi-quantitative continuous simulations.

Model Simulation

The course of model simulation (CellNetAnalyzer) mimics the gradual platelet activation towards irreversible platelet aggregation over different time steps which is in accordance with *a priori* knowledge. The simulation involves four phases (Figure 21A-D), monitoring the propagating and activating signal throughout the network and time.

We start the model simulation from a point in phase space, where the activation levels of all pathway constituents are in the resting state (level 0). The first activation step (Figure 21A) comprises the initial binding of a strong activator to its receptor (GPVI) which competes with the inherent platelet inhibition (prostaglandin/cAMP pathway). Depending on the initial conditions, the subsequent signal transduction cascade activates integrin α2bβ3 to level 1 or 2 (if the initial inhibitory signals are absent). The second activatory step (Figure 21B) affects ADP being released as result of a calcium transient enhancing the signaling cascade. This heightens the integrin α2bβ3 activation state to level 2 or 3. The third step of platelet activation (Figure 21C) involves the store-operated calcium entry (SOCE). It is mediated by the release of calcium from intra-cellularly stored calcium pools which subsequently activates the calcium channel Orai1. This process further amplifies the activatory signal represented by integrin α2bβ3 activation of level 4. The final time-step (Figure 21D) comprises a positive feedback loop from integrin (level 4) strengthening the activatory signal and intercalating the synthesis of thromboxane (TXA) from arachidonic acid (ARAC). Thereby integrin achieves activation level 5 and forces the systems state towards irreversible aggregation.

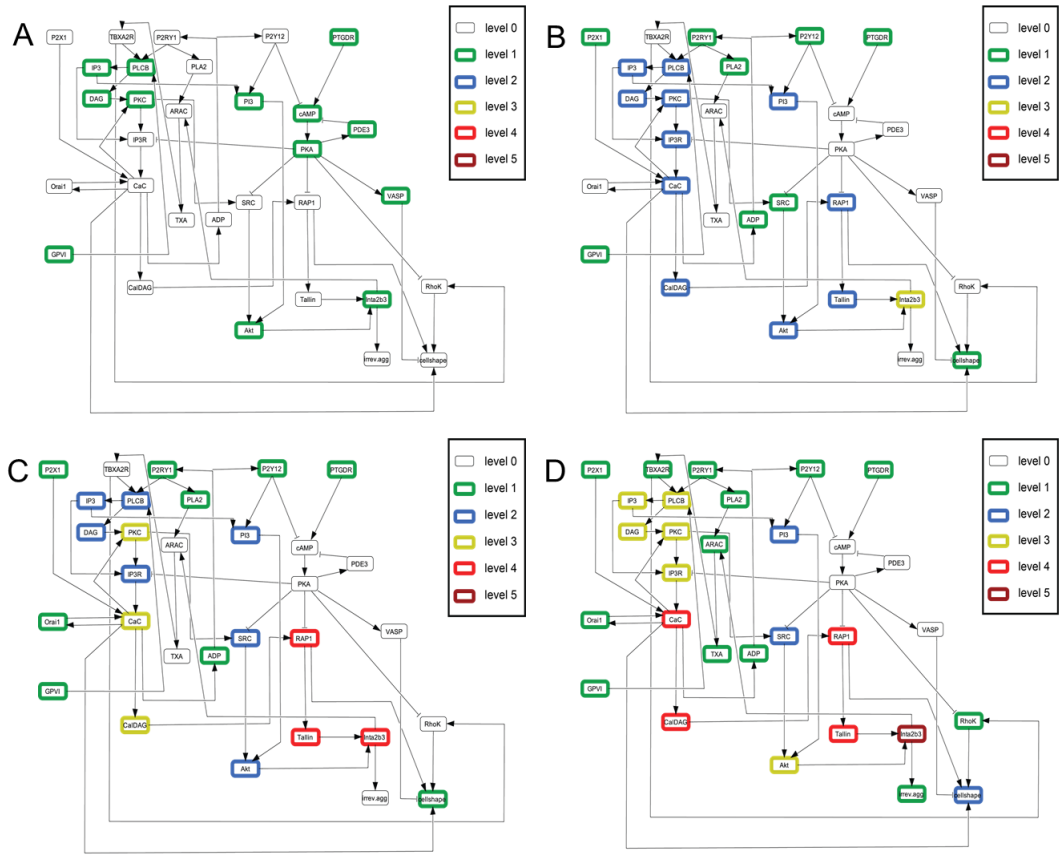

Figure 21: Different system states after logical steady state computation. (A)-(D): Boolean model represented as a directed graph (Figure 20). Arrows denote activatory (→) and inhibitory (—|) effects on the corresponding target node.
Appropriately added network functions coalesce (within 4 simulation time steps t_0, t_1, t_2, t_3) into a fully activated system (D) passing different intermediate systems states (A) to (C). (A): t_0. Solely reactions triggered by pure GPVI signaling are involved. (B): t_1. Effects from autocrine ADP signaling are added. (C): t_2. Signaling is complemented by store-operated calcium entry (SOCE). (D): t_3. Addition of a positive feedback loop established by integrin signaling results in the most driven system towards irreversible aggregation. Activation levels are color-coded (level 0 to 5 according to the CellNetAnalyzer simulation). Figure modified after Mischnik et al. (2013).

System Stability and Dynamic Behavior

To check for system stability and transformation to a continuous system for dynamic simulations of the logical network, we refer to the software SQUAD (Di Cara et al., 2007) (cf. Section 3.3)

Steady State Analysis The analysis of the discrete systems reveals two distinct steady states. A general off-state where all network nodes have an activation level of 0, which is opposed by an on-state, depicting the fully-excited system and being stabilized by positive feedback. Here, all network

nodes exhibit an activation-level of 1 (scaled activation units between 0 and 1), except those being involved in the platelet inhibitory cAMP-pathway (cAMP, PKA, VASP and PDE3).

Threshold Analysis Dynamic simulations indicated two phases of activation in the model: The first step is characterized by a sub-threshold behavior allowing rapid comparison and integration between different receptor signals and stimuli, both activatory and inhibitory. In a second phase, after inherent system thresholds were crossed and a specific signaling decision is made, all other pathways are competitively turned off.
To study this threshold behavior we combined several activatory and inhibitory stimuli and its combinations. We started from the resting (non-stimulated) off-state and excited the system with a GPVI-input pulse of strength 1. Activating the downstream cascade components, the signal is transduced towards integrin, which leads to aggregation and shape change. Akt kinase activity undergoes an initial increase, but diminishes as the activatory input via GPVI and thus Src signaling flattens. Due to the positive feedback, its activity increases again, ultimately leading to the fully activated enzyme (Figure 22A). A constant activatory impulse instead of the decaying GPVI-input drives the system straight to the on-state.
In the second scenario, the GPVI-pulse is accompanied by a half-maximal PTGDR input strength of 0.5. Akt kinase and calcium ions are slightly mobilized, but due to the inhibitory effect exerted by PKA, the system returns to its deactivated resting state (Figure 22B). Constant activatory and inhibiting inputs render the system oscillating (data not shown).
If the half-maximal PTGDR input is opposed by a stronger GPVI-pulse (Figure 22C), the system passes the integrative threshold, ending up in its maximal activation state. The minimal GPVI-value that leads to threshold-transgression, given a PTGDR inhibiting strength of 0.5, is estimated to 1.168. Here, the system is alternating between both, the on- and off-steady-state, respectively. Assuming a activating stimulus of 1.2 (Figure 22D) close to the threshold value, integration of the competing inputs proceeds, finally reaching the on-state. Akt kinase for instance receives activating signal via GPVI in accordance to the pure activatory scenario (Figure 22A), but as Src kinase also sustains inhibition via PKA, its activity tumbles until it reaches full mobilization. The dynamics of calcium levels occur as a result of coalescing IP3, Orai1 and PKA effects which could be reproduced by measurements (data not shown).

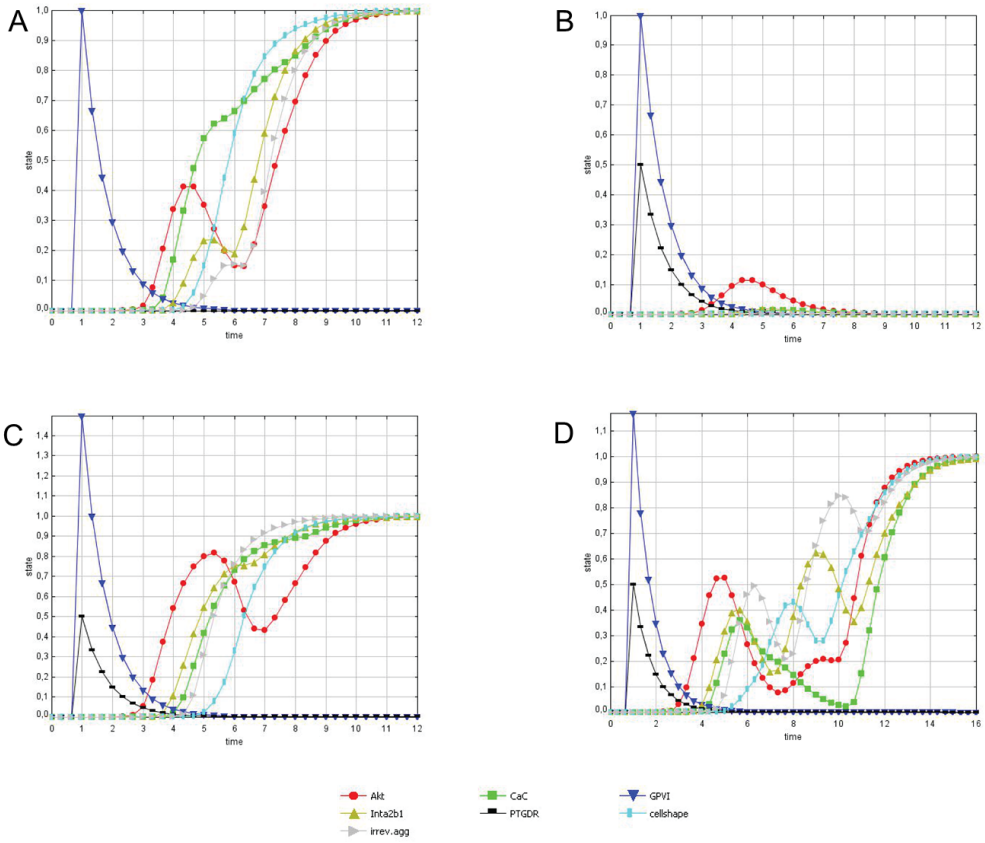

Figure 22 : Threshold analysis by dynamic simulation. (A): GPVI signal (input) with strength 1. System turns towards the on-state. (B): Combined activatory GPVI input with strength 1 and inhibitory prostaglandin (PTGDR) input with strength 0.5: System is forced to the off-state. (C): Combined GPVI input with strength 1.5 and inhibitory input via PTGDR with strength 0.5: System turns to the on-state. (D): GPVI input with strength 1.2 combined with PTGDR input with strength 0.5: System behavior is close vicinity of the threshold. Figure modified after Mischnik et al. (2013).

Different inhibitory input strengths together with the necessary activating input value to exceed the threshold are given in Table 3. Values denote full (≥ 1.0) or no (0.0) activation in arbitrary units.

The comparison of inhibiting and activating signals shows that the relative activating strength ($GPVI_{thr}$/PTGDR) that leads to threshold-crossing, decreases with elevating inhibiting inputs. Hence, this underpins the system ability to adapts for higher prostaglandin-concentrations by increasing its sensitivity for platelet activators.

Pharmacological Modulation and Validation

The power of mathematical models arises from the opportunity to simulate the effects of knock-out mutations or drugs. Exemplary, drug Clopidogrel influences platelet signal transduction in an anti-thrombotic way (Li et al.,

Table 3: Combinations of inhibitory and activatory input strengths $GPVI_{thr}$ to exceed the activation threshold. Table modified after Mischnik et al. (2013).

Inihibitory input via PTGDR	GPVI-value $GPVI_{thr}$	Relative activating strength $GPVI_{thr}$/PTGDR
0.25	0.946	3.784
0.5	1.168	2.336
0.75	1.456	1.941
1.0	1.625	1.625

2012). Therefore, it is of high medical relevance and widely applied in the treatment of heart diseases. Clopidogrel acts as an antagonist of the ADP receptor P2Y12, which entails both, a crucial activating effect on the platelet kinase machinery and the down-regulation of the inhibitory pathway branch by turning down the production of cAMP.
Within the logical network, P2Y12 is positively connected to PI3 kinase, and negatively to cAMP (Figure 20). Thus, a blocking of P2Y12 results in a remarkably weaker activation of all subsequent pro-thrombotic kinases after the activatory input, and a higher PKA activity, due to an increased cAMP level, which is in accordance with current experimental data (Haberstock-Debic et al., 2011; Iyú et al., 2011).
To further elucidate the kinase machinery being active within the different activation phases (Figure 21), we zoom into the phosphorylation events surrounding the respective kinases (Figure 23), according to experimental data (Boyanova et al., 2012). PKA is active during phase 0 and switches to level 0 during the following activation phases, which is in accordance with experimental data projected on the signaling network as depicted in Figure 23A, B. PKC is mainly active in phases 2 and 3 (Figure 23C,D). Akt becomes activated during phase 3 (Figure 23C), whereas Src kinase is moderately active during phase 1,2 and 3 (Figure 23B-D). Experimental data in terms of key phosphorylation events support this direction of signal processing (cf. Figure 23) and agree well with key activation steps postulated by the model. Findings resulting from Boolean and semi-quantitative modeling together with data validation has led to the publication entitled "A Boolean view separates platelet activatory and inhibitory signalling as verified by phosphorylation monitoring including threshold behaviour and integrin modulation" (Mischnik et al., 2013). My expertise in platelet signaling and modeling strategies sustained the model set-up and interpretation of resulting model simulations.

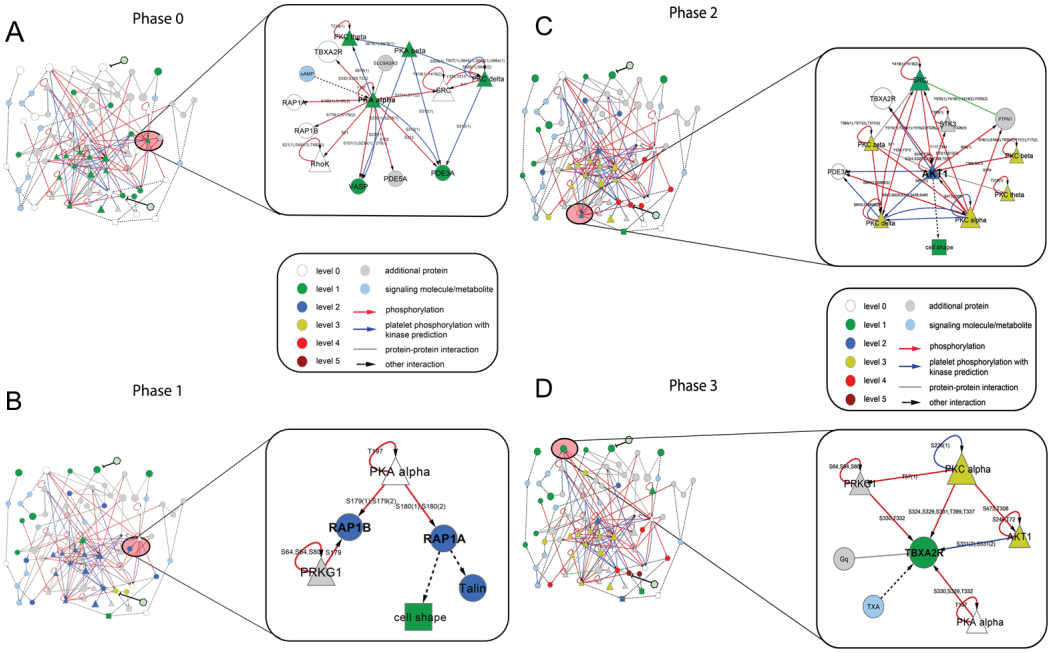

Figure 23 : Model validation : *PlateletWeb*. ADP signaling networks visualized and colored according to the postulated model phases of platelet activation ((A): phase 0; (B): phase 1; (C): phase 2; (D): phase 3). The key phosphorylation events according to experimental data are shown beside each network (phase 0: sub-network around PKA, phase 1: around Rap1A/RAP1B; phase 2: around Akt kinase (Akt1); phase 3: around the thromboxane receptor TBXA2R). Here, the Boolean model (Figure 20) is validated by data on phosphorylation, kinases and substrates not used for setting up the Boolean model but according to experimental data available from the *PlateletWeb* knowledgebase (Boyanova et al., 2012). Interactions (gray lines), site-specific phosphorylation events (red arrows with labeled sites) and dephosphorylation events (green lines) are extracted from literature studies based on the *PlateletWeb* knowledge base; kinase predictions (blue lines) were additionally considered. Kinases are depicted as triangles and proteins as circles. Phosphorylated proteins are represented in red, blue labels denote proteins from the initial ADP model network. Further proteins were added for maintaining the network structure and improving the visualization of the signal flow (for example G-proteins) but were not part of the Boolean model. Metabolites and small molecules such as NO and Ca^{2+} are presented in light blue circles. Figure modified after Mischnik et al. (2013).

4.1.4 Cyclic Nucleotide Signaling: A Dynamic Model

Synopsis

Cyclic nucleotides play a major role in platelet signaling, as they strongly mediate inhibition of platelets. This counterpart to platelet activation is crucial for countervailing unwanted platelet activation and therefore a pivotal target regarding the prevention of pathological platelet aggregation. Thus, platelet inhibition and its regulators are of great medical interest and object of pharmaceutical invention (antiplatelet therapies). Mathematical and pharmacodynamic modeling of thrombosis and hemostasis and associated signal transduction allows quantitative predictions upon drug modulation and supports the precise description of pivotal targets for pharmacological modulation.

I developed a dynamic mathematical model of the main inhibitory pathway in human platelets and its downstream effects. By means of a data-based *in silico* approach, we established a time-resolved description of the feedback regulation of cAMP levels which serves as a quantitative model for investigating combinatorial drug effects at multiple strengths. This includes dynamic effects of PDE-specific inhibitors (Milrinone, Cilostamide) and activators of adenylyl cyclase (Forskolin, Iloprost).

Modeling Approach and Model Setup

As kinetic information is available of most of the signaling components, as well as time-resolved quantitative data for validation, we opt for a data-based dynamic modeling approach offering model-based quantitative predictions such as drug effects. The dynamic model, based on a system of ordinary differential equations (ODEs) is set up following the data-based approach as described in Section 3.4. Starting with the most parsimonious model of basal cyclic nucleotide signaling in non-stimulated platelets we successively refined and adapted it to drug stimulation leading to platelet inhibition. This includes iterative model fitting to experimental time-series data and statistical testing for data-based model selection (Figure 24). Thus, careful validation resulted in the overall model topology of feedback-regulated cyclic nucleotide signaling depicted in Figure 25.

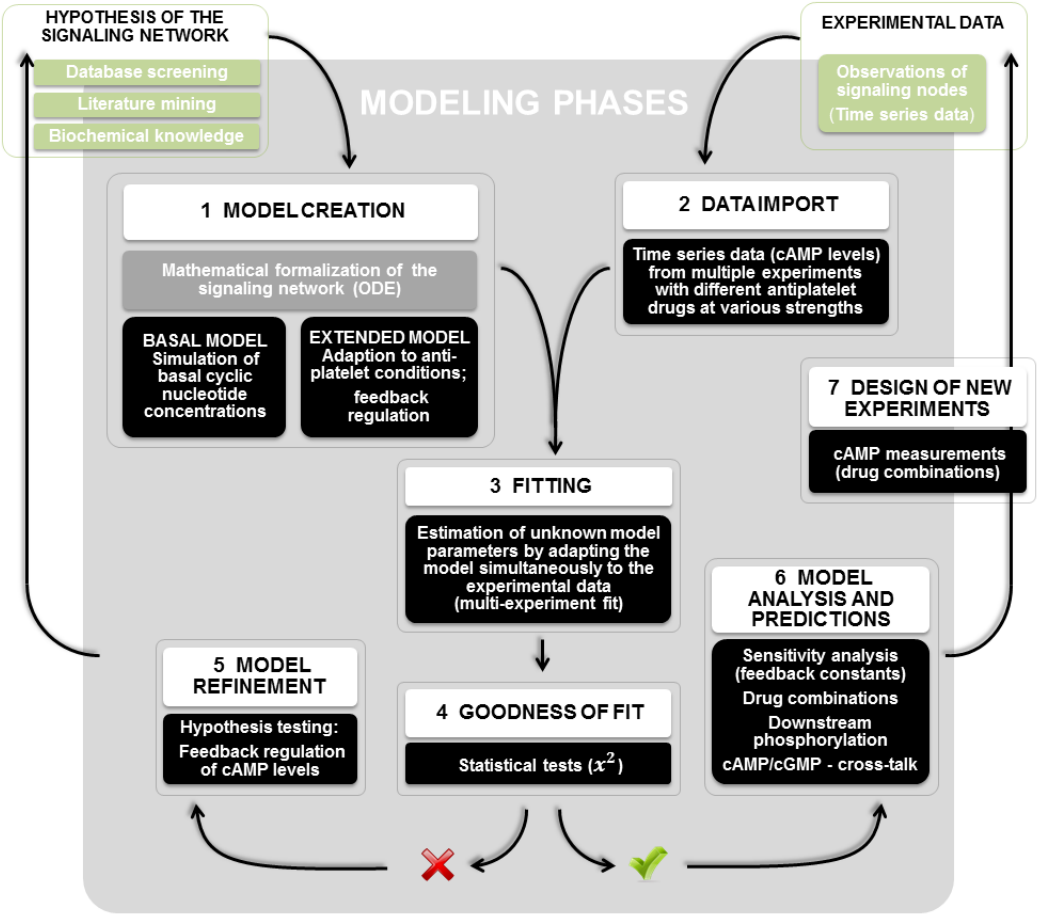

Figure 24: Model development processes. Modeling approach and main phases from the platelet signaling network creation to model-based design of new experiments leading to quantitative predictions (cf. Figure 14) Black boxes specify the steps tailored to the platelet study. Figure: modified after Wangorsch et al. (2011).

Formed by their corresponding cyclases, cAMP and cGMP are degraded by phosphodiesterases modulating the activation of cyclic nucleotide dependent protein kinases. They in turn mediate the respective inhibitory effects e.g. on VASP (cf. Section 2.2.3). Information about model components and enzyme isoforms in platelets, gathered from transcriptome and proteome databases (Boyanova et al., 2012; Dittrich et al., 2006) and literature mining are presented in Table 13 (Annex B.4).

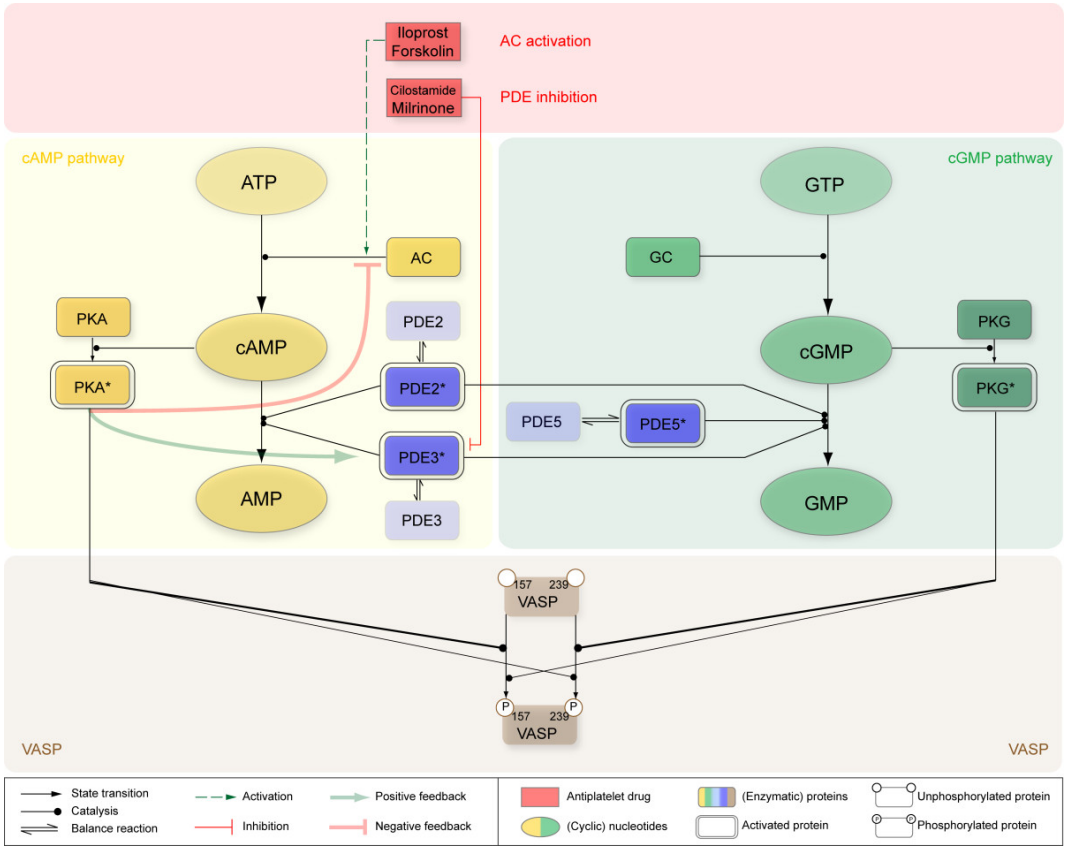

Figure 25: Topological scheme of the modeled branches of cyclic nucleotide signaling. Main components of cyclic nucleotide signaling pathways and their cross-talk and downstream effects are illustrated: Pivotal signaling components of the simplified cAMP signaling pathway are shown in yellow, major components of cGMP signaling branch in green. The three central cyclic nucleotide degrading phosphodiesterases (PDEs) are depicted in blue. Both, cAMP and cGMP signaling share in downstream effects on phosphoprotein VASP (brown). VASP is differentially phosphorylated at both phosphorylation sites, Ser157 and Ser239 upon cyclic nucleotide dependent activation of their corresponding protein kinases (PKA, PKG). Concentrations of cAMP and cGMP, respectively, react sensitively to pathway modulating compounds such as inhibitors of PDEs (Cilostamide, Milrinone) as well as adenylyl cyclase (AC) stimulating drugs (Iloprost, Forskolin) shown in red rectangles. This direct activation (green dashed arrow) and/or inhibition (red arrow) results in elevated cAMPs level which subsequently feeds back via cAMP-dependent PKA. This way, PDE3 gets phosphorylated (activatory feedback) and AC gets inhibitied. Feedback regulation is indicated by bold green and red colored arrows. Figure: Wangorsch et al. (2011).

Basal Model of Non-stimulated Platelets As experimentally observed (Eigenthaler et al., 1992), non-stimulated platelets show basal cAMP and cGMP levels of 4 µM and 0.4 µM, respectively, maintained by AC and GC as well as the three major platelet phosphodiesterases PDE2, PDE3 and PDE5 (Figure 26).

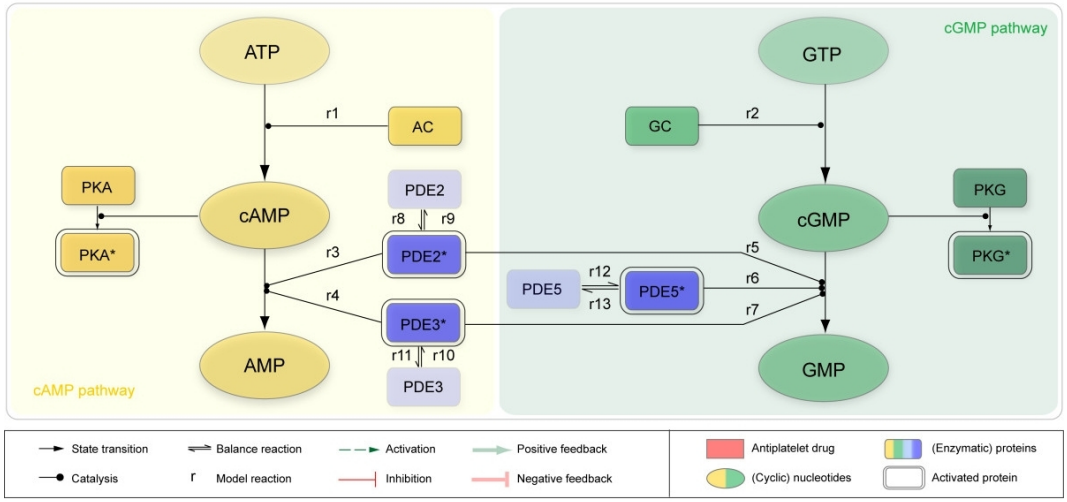

Figure 26: Reaction scheme (basal conditions). Reaction scheme representing assumed regulations to maintain basal concentrations of the cyclic nucleotides cAMP and cGMP in non-stimulated platelets. The constant generation of cyclic nucleotides by the corresponding cyclases AC and GC (reaction r1,r2) is in turn balanced by PDE-mediated degradation (PDE2, PDE3, cGMP-specific PDE5). This is accomplished by active phosphodiesterases (reactions r8-r13) degrading the cyclic nucleotides (reactions r3-r7). For explicit formulations of the underlying reactions (r1 - r13) see Table 4. Figure modified after Wangorsch et al. (2011).

Their enzymatic activity is modeled by Michaelis-Menten kinetics with kinetics constants detailed in Bender and Beavo (2006). Regarding PDE2 catalysis, cAMP shows a positive cooperativity resulting in a Hill coefficient of 2 (Matsumoto et al., 2003). Besides PDE2, essentially PDE3 (80%) provides the degradation of cAMP (Butt and Walter, 1997), whereas PDE5 mainly and specifically adjusts the level of cGMP.

Under basal conditions, we assume an overall guanylyl cyclase activity of $0.6 - 1.0$ µM/min and an AC activity of 7 ± 2 µM/min according to reported data (Hines and Tabakoff, 2005; Parsian et al., 1996; Juska and Farndale, 1999; Schmidt et al., 2001). The following set of ordinary differential equations covers these kinetic assumptions under basal conditions:

System of ODEs (basal conditions)

$$\frac{\mathrm{d}x_1}{\mathrm{d}t} = +\nu_1 - \nu_3 - \nu_4; \tag{4.1}$$
$$\frac{\mathrm{d}x_2}{\mathrm{d}t} = +\nu_2 - \nu_5 - \nu_6 - \nu_7; \tag{4.2}$$
$$\frac{\mathrm{d}x_3}{\mathrm{d}t} = +\nu_8 - \nu_9; \tag{4.3}$$
$$\frac{\mathrm{d}x_4}{\mathrm{d}t} = +\nu_{10} - \nu_{11}; \tag{4.4}$$
$$\frac{\mathrm{d}x_5}{\mathrm{d}t} = +\nu_{12} + \nu_{13}; \tag{4.5}$$
$$\frac{\mathrm{d}x_6}{\mathrm{d}t} = -\nu_8 + \nu_9; \tag{4.6}$$
$$\frac{\mathrm{d}x_7}{\mathrm{d}t} = -\nu_{10} - \nu_{11}; \tag{4.7}$$
$$\frac{\mathrm{d}x_8}{\mathrm{d}t} = -\nu_{12} + \nu_{13}; \tag{4.8}$$
$$\frac{\mathrm{d}x_9}{\mathrm{d}t} = +\nu_3 + \nu_4; \tag{4.9}$$
$$\frac{\mathrm{d}x_{10}}{\mathrm{d}t} = +\nu_5 + \nu_6 + \nu_7. \tag{4.10}$$

The reactions r and its rates ν are defined as given in Table 4. Dynamic variables x and constants k are declared in Table 5.

Table 4 : Reactions and rates for modeling the dynamics in cyclic nucleotide signaling under resting conditions, defined in the system of ODEs (cf. Equation 4.1 - 4.10).

Reaction	**Rate**
Basal AC influx of cAMP (r1):	$\nu_1 = k_{11};$
Basal GC influx of cGMP (r2):	$\nu_2 = k_{12};$
cAMP turnover via PDE2 (r3):	$\nu_3 = \frac{k_1 \cdot x_1^{k_{19}} \cdot x_3}{k_2^{k_{19}} + x_1^{k_{19}}};$
cAMP turnover via PDE3 (r4):	$\nu_4 = \frac{k_3 \cdot x_4 \cdot x_1}{k_4 + x_1};$
cGMP turnover via PDE2 (r5):	$\nu_5 = \frac{k_5 \cdot x_3 \cdot x_2}{k_6 + x_2};$
cGMP turnover via PDE3 (r6):	$\nu_6 = \frac{k_7 \cdot x_4 \cdot x_2}{k_8 + x_2};$
cGMP turnover via PDE5 (r7):	$\nu_7 = \frac{k_9 \cdot x_5 \cdot x_2}{k_{10} + x_2};$
(De)activation (r8 -r13):	$\nu_8 = k_{14} \cdot x_6;$
	$\nu_9 = k_{13} \cdot x_3;$
	$\nu_{10} = k_{16} \cdot x_7;$
	$\nu_{11} = k_{15} \cdot x_4;$
	$\nu_{12} = k_{18} \cdot x_8;$
	$\nu_{13} = k_{17} \cdot x_5;$

Table 5: Dynamic variables and constants implemented in the systems of ODEs (cf. Equations 4.1 - 4.10). Constants concerning the cAMP and cGMP turnover by PDE isoforms are extracted from Bender and Beavo (2006); Butt and Walter (1997).

Model parameter	Value	Foundations/assumptions	Reference
Dynamic variables			
x_1 : c(cAMP)	4μM	basal levels	(Eigenthaler et al., 1992)
x_2 : c(cGMP)	0.4 μM	basal levels	(Eigenthaler et al., 1992)
x_3 : c(PDE2) active	0.05 mg/l	model-based simulation experimentally: 63.46 mg/l	this study
x_4 : c(PDE3) active	2.3 mg/l	model-based simulation experimentally: 225 mg/l	this study
x_5 : c(PDE5) active	1 mg/l	model-based simulation experimentally: 1359 mg/l	this study
x_6 : c(PDE2) inactive	(63.46 - x_3) mg/l		
x_7 : c(PDE3) inactive	(225 - x_4) mg/l		
x_8 : c(PDE5) inactive	(1359 - x_5) mg/l		
x_9 : c(AMP)	μM; simulated		
x_{10} : c(GMP)	μM; simulated		
Constants			
k_1 : V_{max}PDE2	120 µmol/min/mg	cAMP turnover	
k_2 : K_mPDE2	50 μM	cAMP turnover	
k_3 : V_{max}PDE3	3 µmol/min/mg	cAMP turnover	
k_4 : K_mPDE3	0.2 μM	cAMP turnover	
k_5 : V_{max}PDE2	120 µmol/min/mg	cGMP turnover	
k_6 : K_mPDE2	35 μM	cGMP turnover	
k_7 : V_{max}PDE3	0.3 µmol/min/mg	cGMP turnover	
k_8 : K_mPDE3	0.02 μM	cGMP turnover	
k_9 : V_{max}PDE5	5 µmol/min/mg	cGMP turnover	
k_{10} : K_mPDE5	5 μM	cGMP turnover	
k_{11} : kcAMP	8 µmol/min	basal influx of cAMP	(Hines and Tabakoff, 2005) (Parsian et al., 1996) (Juska and Farndale, 1999)
k_{12} : kcGMP	1 µmol/min	basal influx of cGMP	(Schmidt et al., 2001) (Wu et al., 1995)
k_{13} : Deactivation PDE2			this study
k_{14} : Activation PDE2	k_{13} - k_{13} = 0		this study
k_{15} : Deactivation PDE3	for simulation of		this study
k_{16} : Activation PDE3	basal levels		this study
k_{17} : Deactivation PDE5	(resting state)		this study
k_{18} : Activation PDE5			this study
k_{19} : hPDE2	2	Hill coefficient	(Matsumoto et al., 2003) (Butt and Walter, 1997)

Estimation of PDE Concentrations Although kinetic parameters for many PDE isoforms are available, data on enzyme concentrations in human platelets is lacking. Therefore, we determined experimentally intra-cellular concentrations of the major PDE isoforms which yielded 63.46 mg/L (3.3 ng/10^7 platelets) for PDE2, 225 mg/L (11.7 ng/10^7 platelets) for PDE3 and 1359 mg/L (70.7 ng/10^7 platelets) for isoform PDE5. The total molar levels are calculated assuming a platelet volume of 5.2 fL (Eigenthaler et al., 1992). How-

ever, integrating the experimentally determined concentrations and kinetic assumptions, simulations from the basic model indicate that the basal levels of cyclic nucleotides cannot be maintained but are rather rapidly diminished (Figure 27). Mathematical calculations revealed a cAMP hydrolysis activity of 1846.1 μM/min for PDE3 isoform (75% of the total activity) and 642.9 μM/min concerning PDE2 ($\approx$ 25% of the total activity).

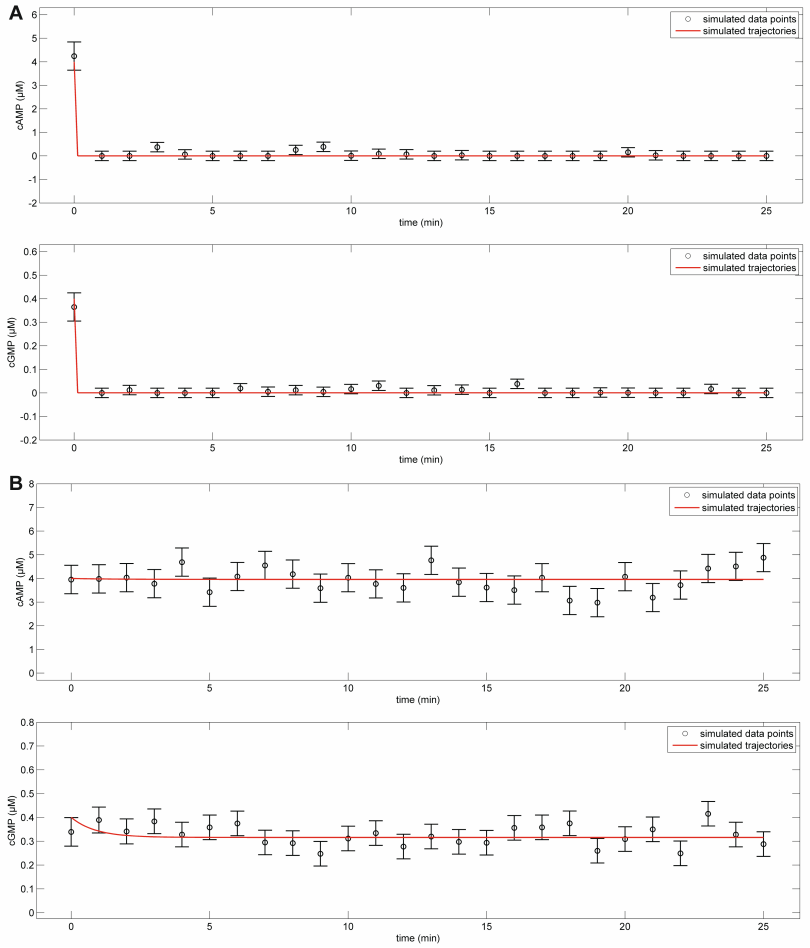

Figure 27: Simulated levels of cyclic nucleotides (human platelets) under resting conditions. Simulated time courses of basal cyclic nucleotide concentrations (cAMP, cGMP) over a time span of 25 minutes. (A) Experimentally quantified levels of cAMP-degrading PDE isoforms are assumed compared to calculated PDE concentrations (B) involving prior knowledge of kinetic constants and PDE turnover (Table 5). Black circles represent the simulated cAMP levels (y) at distinct time points together with calculated standard deviation (Gaussian distribution error: $0.10 \cdot y + 0.05 \cdot \max(y)$). Red curves denote the simulated model trajectories of cAMP and cGMP. The strong enzymatic activity of measured PDE concentrations would fail to maintain the basal levels of cAMP (4 μM) and cGMP (0.4 μM) in platelets. In contrast, they would be diminished fast. In contrast, the setting of calculated levels of active PDE concentrations for model simulation results in a precise reproduction of these basal levels. Figure modified after Wangorsch et al. (2011).

In fact, this would entail a total cAMP hydrolysis rate of 2.5 mM/min, which corresponds to a turnover rate of the entire cAMP pool in the platelet of 625 times per minute. These calculations suggest that not the total amount of PDE is enzymatically active but the main part of enzymes remains quiescent in the resting platelet. Parameter optimization constrained on a constant level of basal cAMP (4 μM) achieved 0.05 mg/l for PDE2 and 2.3 mg/l for PDE3, respectively, in terms enzymatically active PDE concentrations, precisely reproducing the cyclic nucleotide levels under resting conditions (Figure 27). This predicts an *in vivo* activity of 1.5 μM/min for PDE2 as well as 6.5 μM/min for PDE3, resulting in a total cAMP hydrolysis activity of 8 μM/min. Hence, either the enzyme activity under *in vivo* conditions is significantly lower compared to the *in vitro* activity and/or there are substantial amounts of cAMP degrading phosphodiesterases not being catalytically active. These assumptions are underpinned by the experimental evidence indicating the compartmentalization of PDE isoforms (Wilson et al., 2008; Baillie, 2009; Houslay, 2010). Thus, to incorporate all experimental findings, we extended the model by assuming the equilibrium between the active and inactive PDE state (Figure 26).

Model Adaption to Anti-platelet Conditions and Validation
After developing and calibrating the basal model of cyclic nucleotide signaling under resting conditions, we extended and adapted it to model pathway effects of drugs causing elevated cyclic nucleotide levels (anti-platelet effect). This was accompanied by time-resolved drug stimulation experiments, probing the effect of varying drug doses on the cAMP pathway branch.

Time Series Data from cAMP elevating Compounds Three independent cAMP measurements were quantified per distinct time point and drug dosage. Phosphodiesterase inhibitors like Milrinone and Cilostamide decrease the cAMP degrading action. Inhibition of PDE3 by Milrinone in doses of 1, 5, 10, 50 and 100 μM, or Cilostamide (0.5, 1, 5, 10, 50 μM) resulted in a slightly delayed increase in cAMP levels (Figure 28A, B, respectively). Milrinone treatment exerted a larger effect resulting in higher cAMP concentrations compared to those induced by administration of comparable doses of Cilostamide. Other anti-platelet drugs like Forskolin and Iloprost stimulate the cAMP production itself. Stimulation of the prostacyclin receptor

by Iloprost in doses of 1, 5, 10, 50 and 100 nM (Figure 28C) and an allosteric activation of ACs by Forskolin (1, 3, 10, 30, 100, 200, 500 μM) evoked a prompt and pronounced dosage-dependent cAMP increase (Figure 28D). Stimulation by the stable prostacyclin analog Iloprost thereby led to elevated cAMP plateaus with saturation beyond the administration of a drug dosage of 50 nM (Figure 28C). Similarly, stimulation by diterpene Forskolin (500 μM) provokes high cAMP concentrations and a plateau (700 μM cAMP) after a time span of approximately five minutes (Figure 28D).

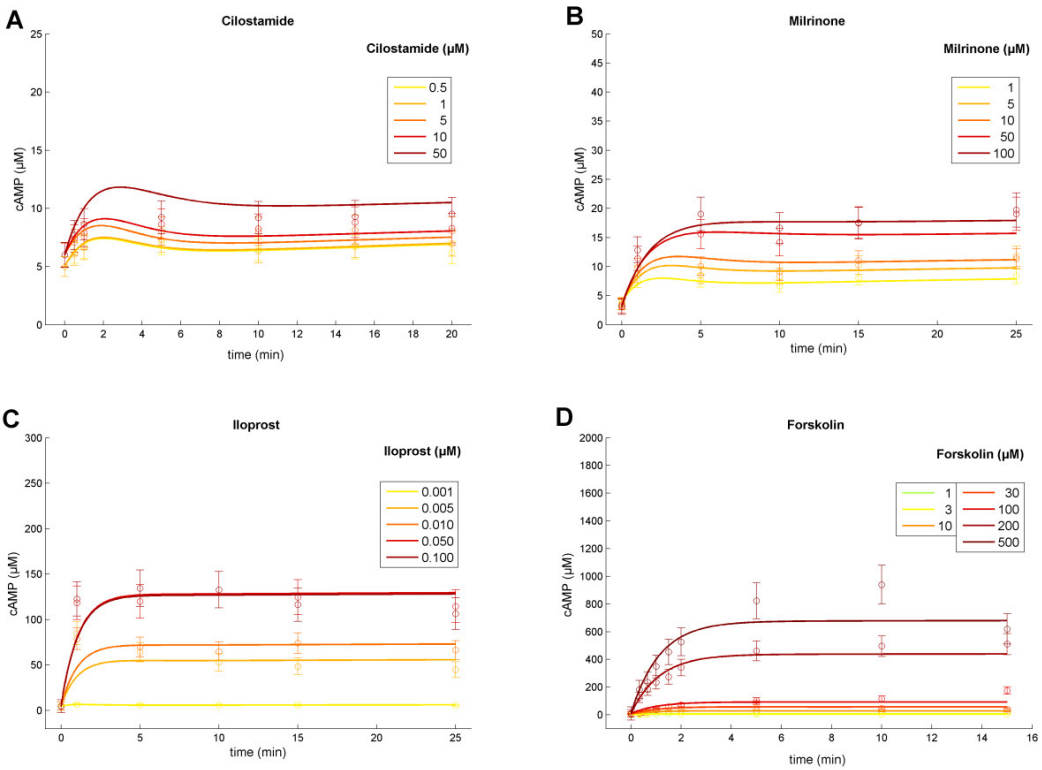

Figure 28: Multi-experiment data fit. cAMP time series: Administration of varying drug doses of cAMP elevating platelet drugs acting as PDE3 inhibitors (A: Cilostamide, B: Milrinone) and activators of adenylyl cyclase (C: Iloprost, D: Forskolin) caused increased cAMP levels. Depicted are means of three independent cAMP measurements (circles) together with the corresponding estimated standard error of the mean. Model trajectories: Depicted curves reflect predicted model trajectories of the optimized and calibrated ODE models. Models for PDE inhibition and AC activation were fit simultaneously to all available data (number of data points N =155) resulting in a significantly good model fit (χ^2 = 129.08) by precisely estimating a set of only 23 model parameters in total. Colors indicate the different shades of drugs. Figure: Wangorsch et al. (2011).

Adaption of the Model Structure To incorporate the entire range of time-resolved data, we iteratively expanded and refined the established basal model. This was statistically supervised by fitting the resulting models reflecting PDE inhibition and AC stimulation simultaneously to all collected data sets. We therefore modified the formula representing the enzymatic catalysis mediated via PDE3 by incorporating the kinetics for competitive inhibition (Figure 29A) as reported in Floreani et al. (2003) for this enzyme. This results in the observed Michaelis-Menten-like reaction rate:

$$\nu = \frac{V\text{max}(\text{PDE3}) \cdot c(\text{PDE3}) \cdot (\text{cAMP})}{(1.0 + \frac{u_i}{k_i}) \cdot K_m(\text{PDE3}) + c(\text{cAMP})}. \tag{4.11}$$

Here, u_i denotes the concentration of the respective PDE inhibitor (Milrinone, Cilostamide), whereas k_i represents the corresponding inhibition constant. These drug-specific constants function in adjusting the apparent K_m-value of the competitively inhibited enzyme.

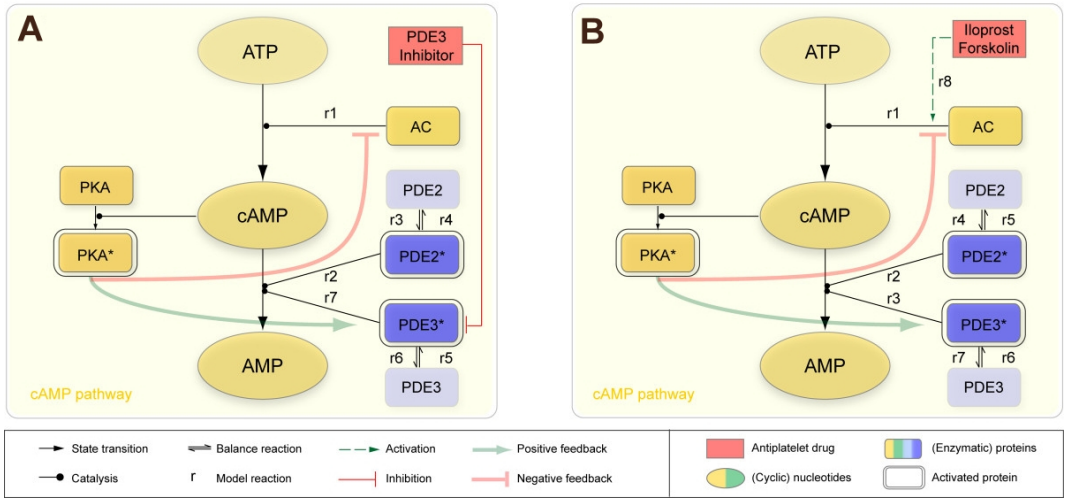

Figure 29: Reaction scheme (elevated cAMP conditions). Reaction scheme for feedback-controlled regulation of cAMP levels with regard to cAMP-elevating treatment (PDE3 inhibition, AC activation). (A) Modeled reactions concerning the inhibition of platelet PDE3 (competitive inhibition via Milrinone and Cilostamide). The cAMP influx (reaction r1) and cAMP degradation (reaction r2,r7) via active PDE2, PDE3 (reactions r3-r6) are counterbalancing each other. (B) Modeled reaction concerning the activation of AC via Iloprost and Forskolin. Elevated cAMP levels evoked by the increased AC activity (reaction r8) are enzymatically degraded (reaction r2,r3) which is mediated by active platelet PDEs (reactions r4-r7). Figure modified after Wangorsch et al. (2011).

To adapt for drug-stimulated AC activation, we introduced additional rates

$$\nu = x_{\text{Forskolin}}, \quad \nu = x_{\text{Iloprost}}, \tag{4.12}$$

respectively, representing the increased cAMP formation by adenylyl cyclase (Figure 29B). These rates have been estimated locally in a data-based way for the concentration of both AC activators, Forskolin and Iloprost. Details on the corresponding system of ODEs and rates are given in Annex B.5.

Parameter Optimization by Multi-experiment Fitting We conducted and evaluated a series of fit sequences by slightly disturbing all variable model parameters before the model was again adapted to time series. This way, the optimization process samples over the fitting ranges of unknown parameters chosen according to mean values extracted from literature if possible or selected a broad range for not limiting the parameter space during fitting (Annex B.5). Resulting multi-experiment fitting sequences provided us with χ^2 values, indicating the quality of model fits (Table 6).

Table 6: Model evaluation (feedback loops). We assumed the following competing hypotheses: H0 - no integrated assumption of feedback loops; H1 - positive feedback of cAMP-dependent PKA to PDE3 (one additional parameter); H2 - negative feedback of elevated cAMP levels to AC (one additional parameter); H3 - both assumptions (H1, H2) are implemented in the mathematical model (two additional parameters). To evaluate the model under each hypotheses, the χ^2-value, number of data points (N), number of estimated model parameters (p) and the Akaike information criterion (AIC) are calculated while fitting to time series data. Table: Wangorsch et al. (2011).

Hypotheses	χ^2	N	p	χ^2/N	AIC
H0	530.19	155	21	3.42	857.04
H1	185.52	155	22	1.2	514.395
H2	133.00	155	22	0.9	461.825
H3	129.08	155	23	0.8328	459.952

This reveals that the adapted model, according to equations 4.11 and 4.12, could not explain all experimental data (AIC, $\chi^2/N \gg 1$).

Statistical Hypothesis Testing and Model Selection Facing this discrepancy, we considered two possible regulations to further expand and refine the model: Feedback regulation of the cAMP level is known to be mediated through activation of PDE3 and inhibition of AC, which both have been observed by experiments (Macphee et al., 1988; Iwami et al., 1995; Murthy et al., 2002; Hunter et al., 2009; Chen et al., 1997). The cAMP-

dependent mechanism of PDE3 activation is indicated by possible PDE3 phosphorylation at Ser312, a PKA phosphorylation site, which is also reported in *PlateletWeb* (Boyanova et al., 2012), has shown up in a phophoproteomic study of resting human platelets (Zahedi et al., 2008).
We therefore modified the underlying model equations 4.11 and 4.12 by introducing a cAMP-dependent increase of the V_{max} value of characterizing the PDE3 enzyme activity:

$$V_{\text{max}}\text{new} = V_{\text{max}}(\text{PDE3}) + kf_1 \cdot c(\text{cAMP}). \tag{4.13}$$

Here, factor kf_1 weights the feedback exerted by cAMP resulting in a raised PDE3 activity. Analogously, we implemented a cAMP-dependent term for mimicking the AC inhibition in rate equations 4.12 for i = Forskolin and Iloprost, respectively:

$$\nu_{\text{new}} = x_i - kf_2 \cdot c(\text{cAMP}). \tag{4.14}$$

Feedback constant kf_2 adjusts the cAMP-mediated strength of this negative feedback loop.
Using likelihood ratio tests, we inspected whether both model refinements are statistically necessary to expand the model structure, thus to explain the observed data. During this statistical procedure we investigated competing nested pairs of models (Cox and Hinkley, 1994). The resulting p-values for testing hypotheses on both feedback loops are listed in Table 7.
We elaborated the following hypotheses: Positive feedback of cAMP-dependent PKA on PDE3 activity is present (H1), negative feedback of PKA inhibiting the AC activity (H2) or both feedback loops happen simultaneously (H3). They were tested against the null hypothesis stating that the parameter (kf_1, kf_2) with regard to each feedback loop equals zero (H0), meaning the feedback regulations are ignored. Although the assumption of one feedback solely (H1 or H2) enhanced the overall model fit significantly ($p < 0.05$), it failed in explaining all time-resolved data simultaneously. Thus, given a level of significance of 0.05, likelihood ratio tests of nested models evidenced a significantly better model fit to all data by the inclusion of both feedback assumptions (H3 vs H2, p = 0.0477; H3 vs H1, p = $5.80 \cdot 10^{-14}$).

Table 7: Hypothesis testing. Assuming the level of significance of 0.05, four competing hypotheses on feedback regulation are tested. For each test scenario, we therefore conducted the appropriate likelihood ratio test for nested models, based on χ^2-values of resulting model fit sequences (Table 6). This indicates the statistical relevance to select the model that integrates both additional feedback constants as it thereby explains all time-resolved data on cAMP elevating drugs. Table: Wangorsch et al. (2011).

Test scenario	p**-value**
H1 versus H0	$< 10^{-15}$
H2 versus H0	$< 10^{-15}$
H3 versus H1	5.80^{-14}
H3 versus H2	0.0477

Hence, we concluded that the inclusion of both feedback regulations statistically led to the most reasonable model structure. The adapted model resulted in model trajectories explaining all data simultaneously (Figure 28A-D) not differing significantly from the experimental data (χ^2/N = 0.8328 < 1; N = 155, number of data points). During the multi-experiment fitting procedure, a small set of 23 specific parameters were estimated from the data (Annex B.6, Table 18). The validated *in silico* model thus reflects pivotal processes of platelet inhibition and models correctly the experimental drug-stimulated measurements by considering low effective PDE concentrations, activation of PDE3 by PKA at increased cAMP levels and the negative feedback loop of PKA towards a degraded activity of adenylyl cyclase.

Simulation Studies and Model Predictions

Sensitivity Analysis For investigating the influence of model parameters on the platelet cAMP signal, indicating the state of inhibition, we analyzed several characteristics of this inhibitory signal. Results were shown exemplified for one PDE3 inhibitor (Cilostamide) and one AC stimulator (Iloprost) indicating that the cAMP signal is mainly controlled by the basal formation of cAMP in case of PDE3 inhibition (low and high dose; Figure 30A, B). Calculations also revealed that the impact of drug-specific and PDE-specific constants augments with the increase of the dosage of inhibitory drugs. For low-dose AC stimulation (Figure 30C), a similar sensitivity profile for parameters can be observed. This is opposed by the high dosage cage, where particularly the feedback constant kf_2 (AC inhibition) gains impact and outweighs the influential effect of basal cAMP formation (Figure 30D). These findings corroborate the crucial role of feedback regulation of the cyclic nucleotide levels in platelets.

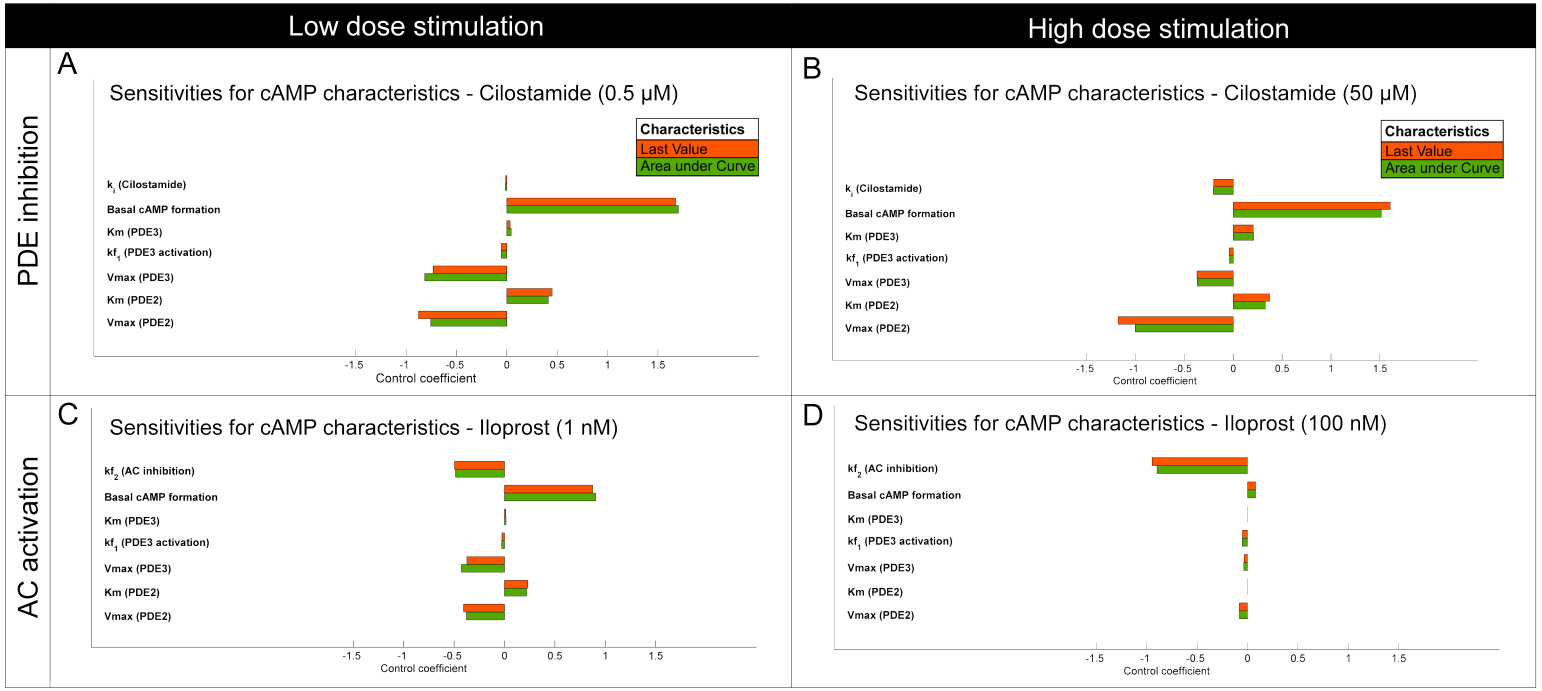

Figure 30: Detailed sensitivity analysis (high- and low-dose stimulation). Shown are parameter-dependent effects towards two distinct characteristics of the cAMP signal: *Area under Curve* (green) as a measure of the overall cAMP signal and *Last Value* (orange) denoting the magnitude of the cAMP plateau. PDE inhibition (A, B) and AC activation (C, D) were investigated separately and under low-dose (A, C) as well as high-dose inhibition (B, D) of the platelet. Control coefficients denote the tendency of the parameter-dependency of the characteristic value evoked by a change of parameter values. Coefficients indicate the increase of the signal property related to the increased parameter value. Calculating this ratio for all model parameters results in similar profiles for both signal characteristics per drug concentration. Furthermore, a main sensitivity of the cAMP signal to the basal formation of cAMP (PDE inhibition) is indicated, whereas the impact of drug- and PDE-specific constants raises with the increase of inhibitory drug doses. Low-dose AC stimulation (C) yield similar characteristic profiles, however for high-dose stimulation (Iloprost, 100 nM) the cAMP-dependent feedback constant kf_2 (feedback AC inhibition) outweighs the influence of the basal cAMP production (D). Figure modified after Wangorsch et al. (2011).

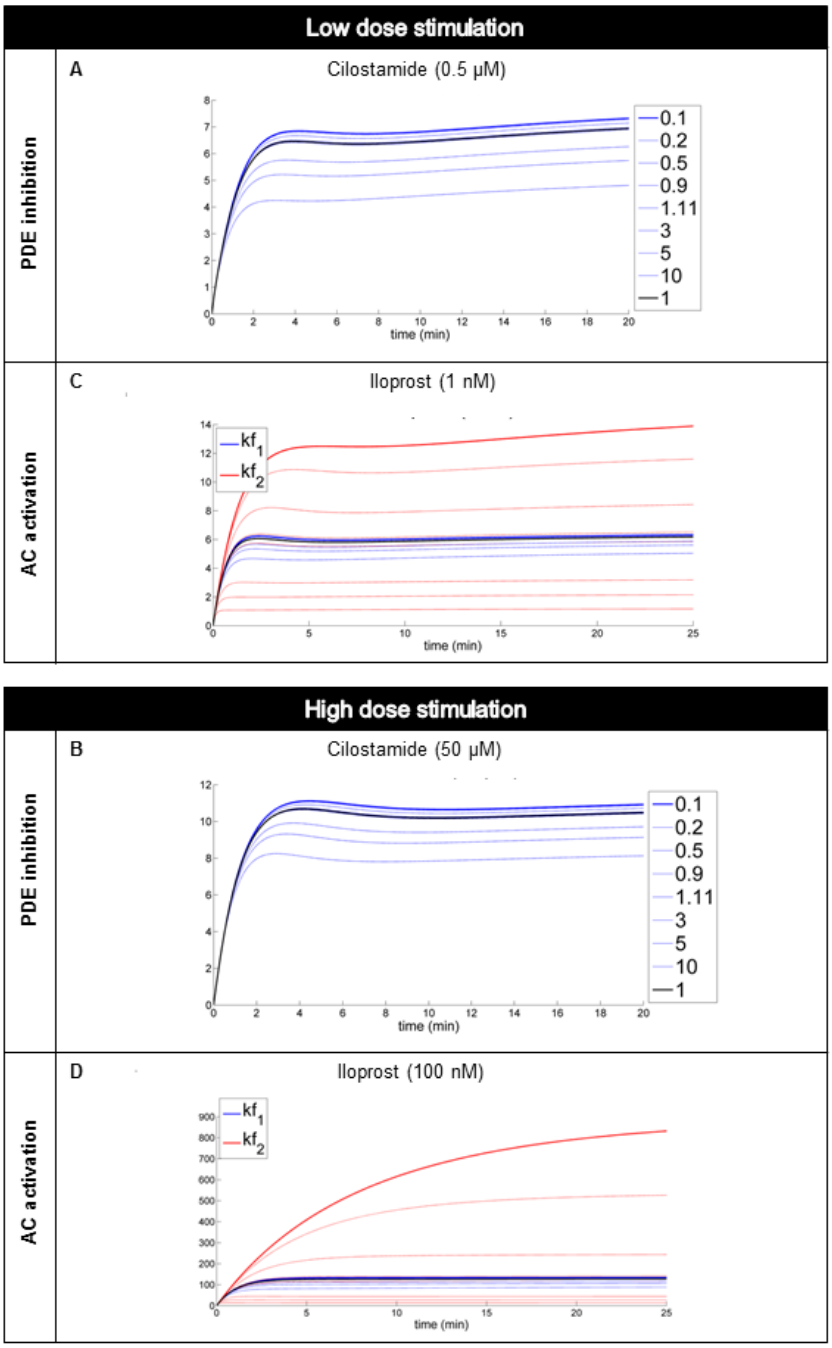

Figure 31: Sensitivity analysis of feedback constants. Sensitivity on the cAMP signal with respect to the feedback constants kf_1 (feedback activation of PDE3, blue) and kf_2 (feedback inhibition of AC, red, only modeled for AC stimulation conditions). To investigate strength-sensitive effects, constants were multiplied by factors ranging from $0.1, 0.2, 0.5, 0.9, 1.11, 3$ and 5 to 10. Black trajectories represent the effect on cAMP of the actual (fitted) parameter value (factor 1). Starting from low to high-dose inhibition of PDE3, simulations show that the variation of kf_1 cause cAMP signal spans ranging from 3 to 5 μM (A, B). Overall, the analysis indicates a high sensitivity of the cAMP signal to feedback constant kf_2 (C, D). Figure modified after Wangorsch et al. (2011).

It is equally interesting to investigate the potential effects of the feedback constants kf_1 (equation 4.13) and kf_2 (equation 4.14) on the model predictions for the cAMP signal. To highlight this, constants were perturbed (multiplication with factors ranging from 0.1 to 10) and the corresponding cAMP signals were plotted (Figure 31A-D). Variation of constant kf_1, describing the feedback activation of PDE3, resulted in cAMP signal spans ranging from 3 to 5 μM (Figure 31A, B). However, this range widely expanded up to 300 μM (500 μM Forskolin). Even at low concentration (1 nM) of Iloprost (Figure 31C), the cAMP signal is highly sensitive to perturbations concerning the AC feedback inhibition (constant kf_2). These findings are also reflected in the model selection procedure (Table 7) which again indicates a subtle feedback regulation of cAMP levels in platelets.

Prediction of Combined Drug Effects Having established a calibrated dynamic model on the basis of time-resolved data evoked by four distinct anti-platelet drugs at varying concentrations, it thus can be applied to predict and to study drug combination effects in detail. Here, we investigated the combined effects of PDE3 inhibitors (Milrinone and Cilostamide) and AC activators (Iloprost and Forskolin).
Explicitly, we experimentally measured cAMP levels caused by the effect of Iloprost and Cilostamide individually (Cilostamide: 10, 50, 100 μM; Iloprost: 2, 5, 20 nM) as well as the drug response on the cAMP level of all drug doses in combination (Figure 32A). The resulting cAMP plateaus which have been experimentally detected and reached for each drug combination are depicted in Figure 32C (black dots). The bar charts clearly revealed an over-additive effect of the two drugs when applied in combinations. Moreover, synergistic effects of PDE inhibitors in combination with Iloprost have been described to occur in human platelets (Nolte et al., 1994; Hanson et al., 2008; Netherton et al., 2002). We therefore embedded an additional cAMP-dependent constant k to capture this over-additive effect. Based on this, we forecast cAMP levels evoked by different drug combinations (Figure 32B-E): Simultaneous stimulation of AC and inhibition of PDE3 was exemplary simulated by combining Iloprost (2, 5 and 20 nM) and Milrinone (10, 50 and 200 μM; Figure 32B) or Cilostamide, respectively (Figure 32C). The surface of cAMP level resulted from interpolating the evoked cAMP plateaus at the corresponding drug combinations. Its origin marks the basal cAMP level, whereas each axis denotes the effect of each single drug solely.

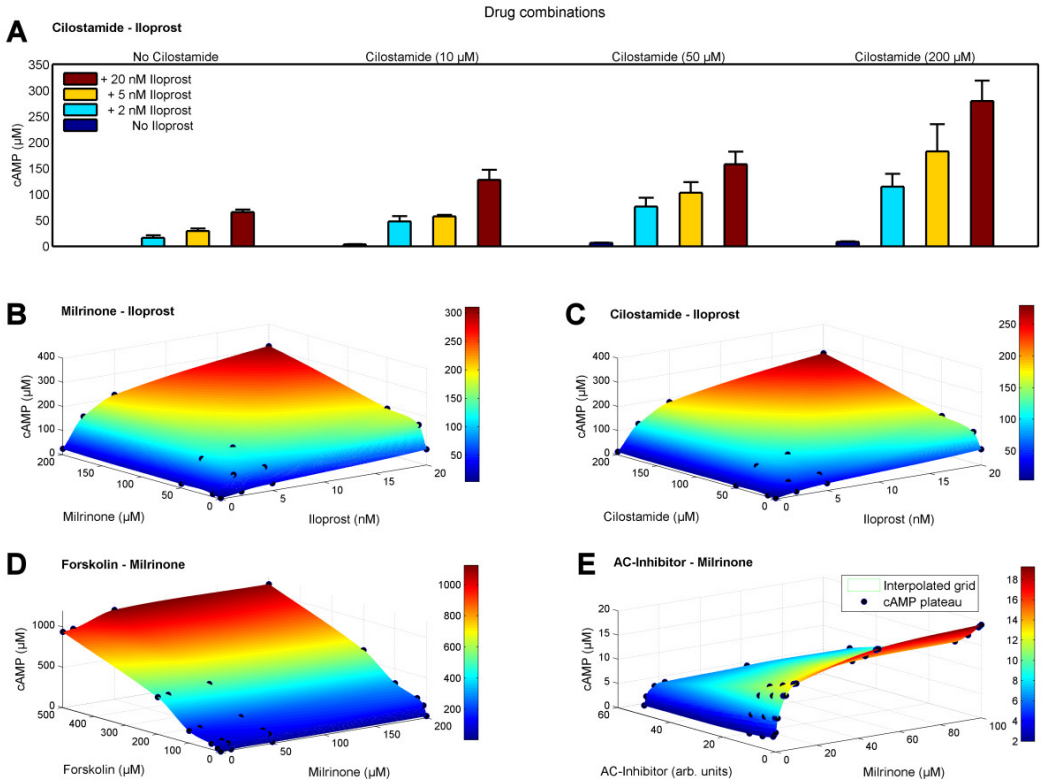

Figure 32: Predicted time course and experimentally measured cAMP levels under different combinatory drug conditions. Besides results solely based on model predictions (B, D, E), panel A and C show experimentally measured cAMP concentrations, indicated by black dots. Single effects of Cilostamide (drug doses range: 10, 50, 200 μM) and those in combination with Iloprost (drug doses range: 2, 5, 20 nM) on the cAMP level (A): The resulting evoked cAMP signals, depicted as the mean of triplicate measurements ($\pm$ SEM), successively rise due to the corresponding elevated drug doses. Moreover, this shows a clear synergistic effect. 3D-plots depict interpolated cAMP levels (z-axis; cAMP surface) of estimated or experimentally monitored plateaus of cAMP at various synergistically activating or inhibitory drug in combination (x- and y-axes): (B) Combination of Iloprost and Milrinone (AC activation, PDE inhibition); (C) combination of Iloprost and Cilostamide (AC activation, PDE inhibition); (D) of Forskolin and Milrinone (AC activation, PDE inhibition); (E) of Milrinone combined with an unspecified inhibitor of AC (PDE and AC inhibition). Dots mark (C) experimental measured cAMP level (mean) and accordingly predicted cAMP concentration levels (B, D, E) evoked after the administration of respective concentrations and combinations of drugs. See Table 19 (Annex B.7) for further details. Figure: Wangorsch et al. (2011).

In adaptation to quantitative data of experiments (Cilostamide and Iloprost combinations), we find the calculated cAMP level surface in close accordance to the measured cAMP concentrations (Figure 32C), resulting in k = 1.443 $\pm$ 0.004. The predicted cAMP levels describe the subsequent experimental measurements significantly better compared to assuming an additive effect of drug combinations (p < 0.05). This indicates a continuous synergistic effect of Cilostamide and Iloprost interaction potentiating the respective single drug stimulation (Figure 32A).
Furthermore we simulated combined effects of Forskolin and Milrinone by predicting cAMP concentrations affected by combining Forskolin drug doses (10, 30, 100, 200, 500 μM) with Milrinone doses of 10, 50 and 200 μM (Figure 32D). The resulting surface of cAMP level interpolates calculated cAMP level plateaus reached due to the distinct drug combination. Analogously, we predicted cAMP levels for the simultaneous inhibition of AC and PDE3 (Figure 32E) showing the successive decrease of elevated cAMP levels due to Milrinone (1-100 μM) by combining this PDE3-affecting drug with several doses of an inhibitor of AC (e.g. 2'5'Dideoxyadenosine; non-synergistic, k = 1). In addition, several important platelet drugs are given in Table 19 (Annex B.7), together with their specific parameters which serve as a basis for modeling and investigating effects of drug combinations.

Pathway Integration: Prediction of VASP Phosphorylation An important downstream effector of cyclic nucleotide signaling is the phosphoprotein VASP (Smolenski et al., 1998). It bears two major phosphorylation sites (Ser157 and Ser239) which both negatively regulate platelet aggregation down-stream of the cyclic nucleotide cascade. Since this protein is a major target for both, PKA (cAMP pathway) and PKG (cGMP pathway), respectively, VASP functions as integrator of input from these inhibitory pathway branches. It therefore represents a paradigm for complex combination effects regarding phosphorylation events and its monitoring. Here, we quantitatively capture the downstream effect on VASP by investigating phosphorylation events of individual VASP phosphorylation sites (Figure 33).

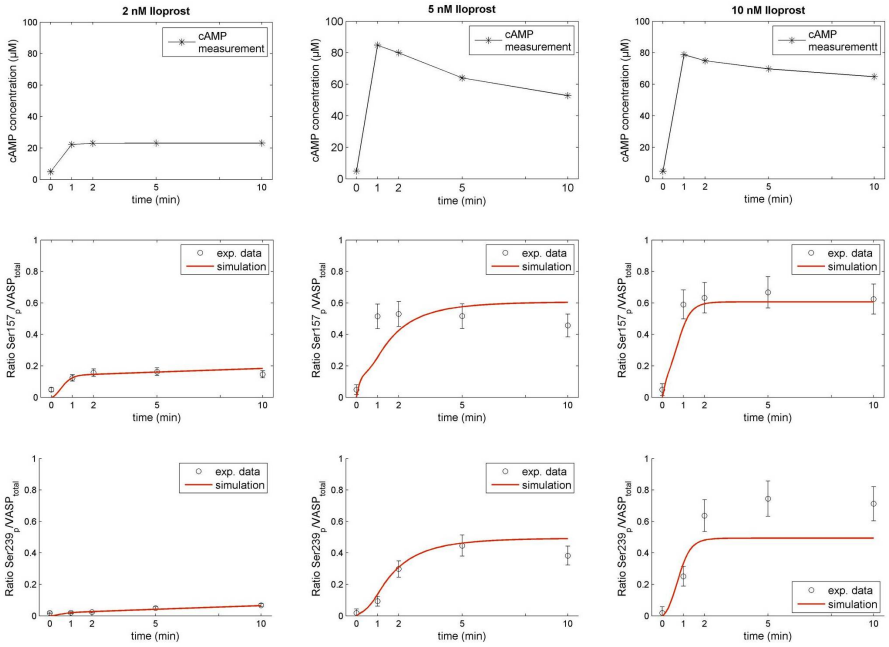

Figure 33: Time-resolved and dosage-dependent VASP phosphorylation evoked by cAMP elevating drugs. Ratios of phosphorylated VASP sites (Ser157, Ser239) to the total amount of VASP in platelets are experimentally measured after the administration of AC stimulator Iloprost in different doses (2 nM, 5 nM, 10 nM). Ratios are detected at distinct time points, indicated by black circles ± calculated standard deviation. The experimentally measured cAMP time course (top panel of each row) serves as model input for simulations. As indicated by data and model curves (red trajectories), VASP phosphosite Ser157 is phosphorylated prior to Ser239 by cAMP-dependent PKA . Figure: Wangorsch et al. (2011).

For this, we modeled the differential effect of PKA on both of these phosphorylation sites, including the assumption that site Ser157 is a 15-fold better substrate for phosphorylation by PKA than the phosphosite Ser239 (cf. Annex B.5). The latter is also targeted by the cGMP-dependent protein

kinase PKG (Smolenski et al., 1998; Butt et al., 1994). Moreover, this differential phosphorylation of protein kinase A has to be considered for the readout of diagnostic VASP assays (Geiger et al., 2010). Phosphosite-specific modeling resulted in a good fit to experimental measurements (Figure 33) allowing again predictions of effects for different drug strengths and combinations. However, modeled parameters were highly non-identifiable and could not be estimated definitively and independently from each other from the time-resolved data.

Probing Different Time-scales of Drug Stimulation To probe the signaling network sensitivity, we tested and simulated different perturbations and network cross-linking. We analyzed the model performance by probing different drug stimuli, e.g. inhibition of PDE2 with EHNA (1, 50, 100 μM) and PDE3 (Figure 34). Thereby, we varied different time-scales of drug stimuli (transient vs. long-term stimulation, concurrent vs. successive stimuli) and monitored the resulting effect on the cAMP level. Simulations showed that the network sensitively responds to transient stimuli even at low drug doses (Figure 34).

Transient Prostacyclin Stimulation Besides transient drug effects, also a transient prostaglandin receptor activation (Geiger et al., 2010) may occur under physiological conditions. This receptor is transiently activated by prostacyclin, having a half-life of less than 5 minutes (Gomberg-Maitland and Olschewski, 2008)) and being produced by the endothelium. Hence, in case of an injured vessel wall, some parts of the endothelium remain without prostacyclin production so that only a deficient signal is evoked and the platelet lacks inhibition. Similarly, patho-physiological conditions such as prostacyclin receptor mutations (Patrignani et al., 2008; Arehart et al., 2008) contribute to a differential platelet inhibition resulting in a decreased protection against unwanted platelet activation and aggregation. We monitored this gradual and transient platelet inhibition due to different prostacyclin doses (100, 200, 500nM) experimentally by detecting cAMP-dependent, time-resolved phosphorylation events on site Ser157 of VASP (Figure 35A). As Iloprost represents a prostacyclin-analogon, we reused the established AC inhibition model for model simulations. Instead of Iloprost, the model was perturbed by driving prostacyclin inputs (sine-pulse) of different amplitudes. Resulting model trajectories were in close accordance to the experimentally measured prostacyclin-dependent responses (Figure 35B).

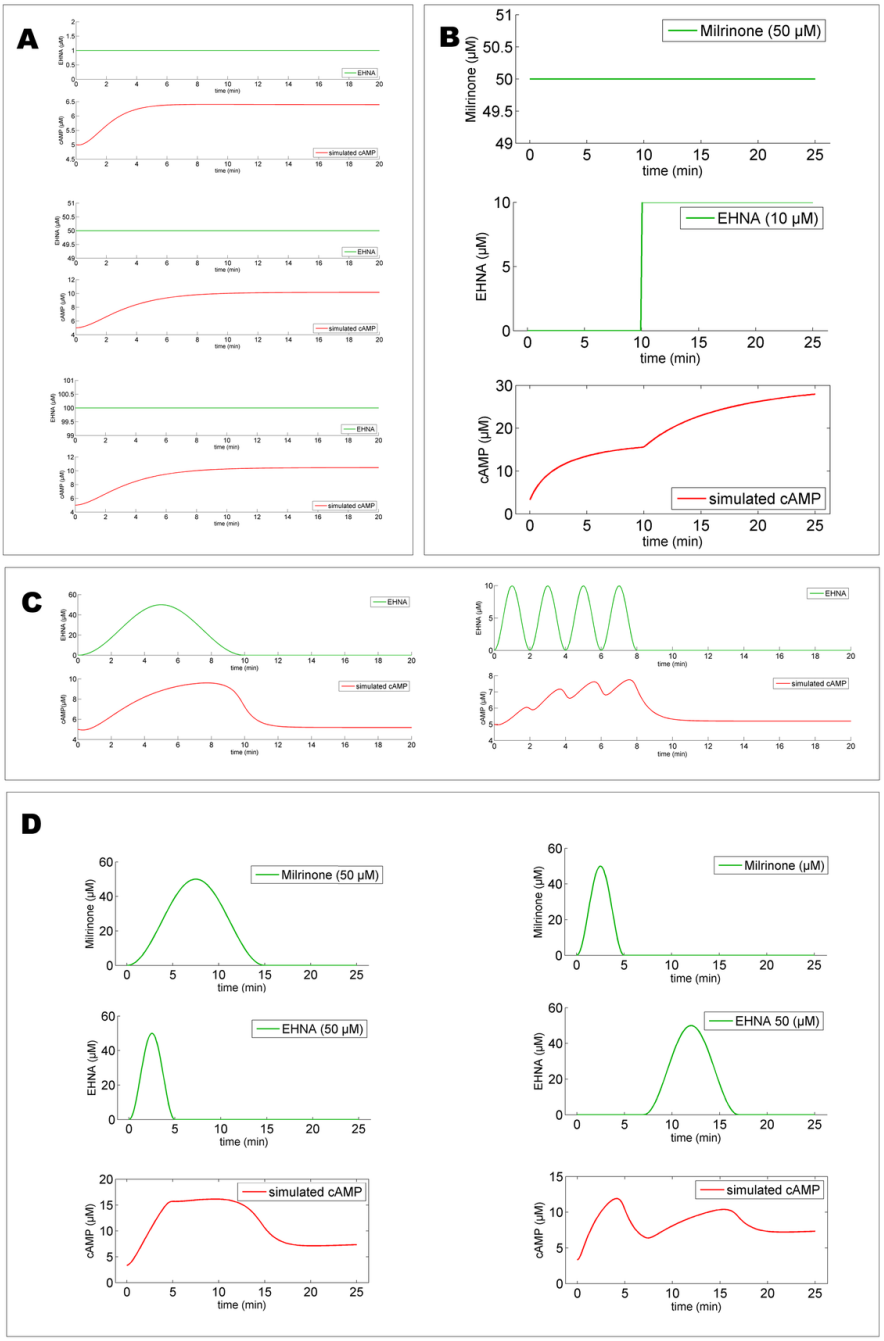

Figure 34: Simulations of different time-scales of drug stimuli. (A) Simulation of continuous inhibition of phosphodisterase 2 with EHNA, a specific inhibitor (assumed k_i-value: 0.7μM). Resulting model simulations show in increased cAMP plateau depending on the respective inhibitor concentration. (C) The stimulation period of a single transient drug stimulus (EHNA) is mirrored in the model-based predicted cAMP concentration, depending on the time delay between the stimulative sine pulses. Successive continuous stimuli have additive effects on the resulting cAMP concentration (B). This holds also if stimulation occurs simultaneously in successive transient drug stimuli (D). Additional to drug doses, the signal magnitude (cAMP level) depends on the time interval between single drug pulses as well, as exemplified here for pulses of one single or two different PDE inhibitors (Milrinone, EHNA). Figure: Wangorsch et al. (2011).

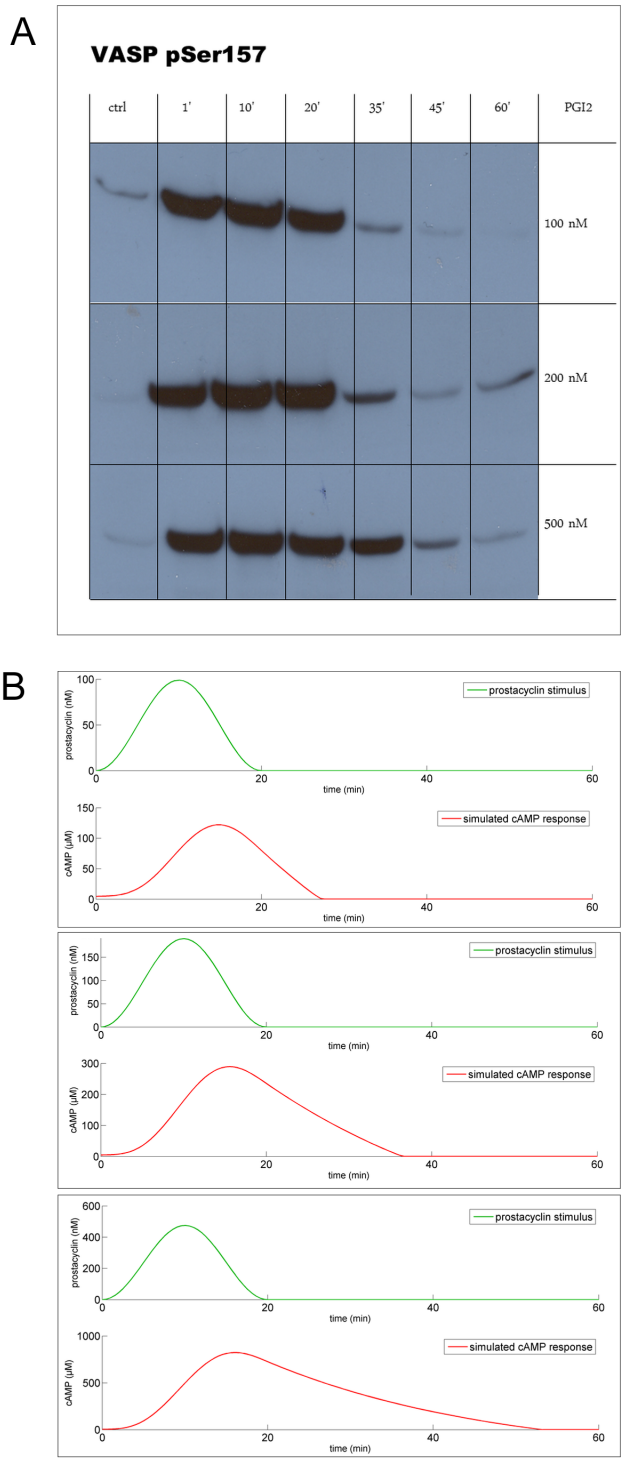

Figure 35: Probing transient prostacyclin stimuli. (A) Experimentally measured and (B) simulated responses to transient prostacyclin stimulations of various doses (100 nM, 200 nM and 500 nM). Transient effects on the cAMP level (B) and on the subsequent phosphorylation (VASP phosphorylation site Ser157 (A), are monitored. They increase and are prolonged with augmentation of the respective prostacyclin concentration. Figure: Wangorsch et al. (2011).

Cross-talk between cAMP and cGMP Signaling Branches Experimental data and model predictions evidenced that the cAMP signal and response in human platelets is highly specific. There is no cross-talk to the cGMP branch of the inhibitory pathway as indicated by the monotonous cGMP levels while stimulating with cAMP stimulating compounds (Figure 36). Even at very high cAMP concentrations raising up to the millimolar range e.g. evoked by extreme AC stimulation by Forskolin (500 μM), the cGMP concentrations remained almost totally unaffected (Figure 36A, C-D). Similarly, PDE3 inhibition by Cilostamide (50 μM) and Milrinone (100 μM) as well as AC stimulation (Iloprost, 100 nM) exclusively elevate the cAMP production (Figure 36B).

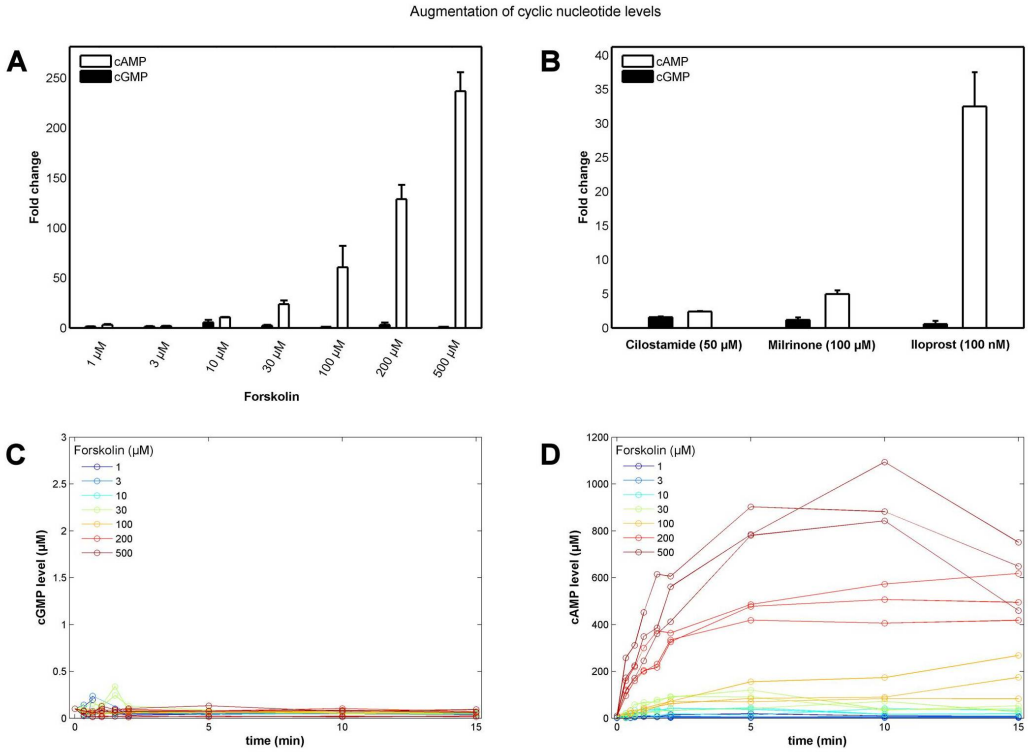

Figure 36: cAMP to cGMP cross-talk. (A) Bar plots depict fold changes (mean of three measurements ± SEM) of different cyclic nucleotide levels for cGMP (black) and cAMP (white) evoked by Forskolin stimulation (1-500 µM) with respect to the corresponding basal cyclic nucleotide levels. Strong stimulation by Forskolin result in high cAMP levels (A, D), however does not change low cGMP levels (C). Similarly, comparatively high doses of Cilostamide (50 µM), Milrinone (100 µM) and Iloprost (100 nM) solely leads to an increase in cAMP levels, leaving cGMP levels unaffected (B). Figure: Wangorsch et al. (2011).

Predicted Cross-talk from cGMP to the cAMP Branch In contrast to the finding that an elevation of platelet cAMP level has no effect on the cGMP pathway, the converse cross-talk has been described (Schwarz et al., 2001; Omori and Kotera, 2007; Aktas et al., 2002). It is mainly mediated through cross-linking of the platelet phosphodiesterases (Figure 37). Cyclic GMP evokes the activation of PDE2 but is also capable to reduce PDE3 activity, thereby affecting the cAMP pathway.

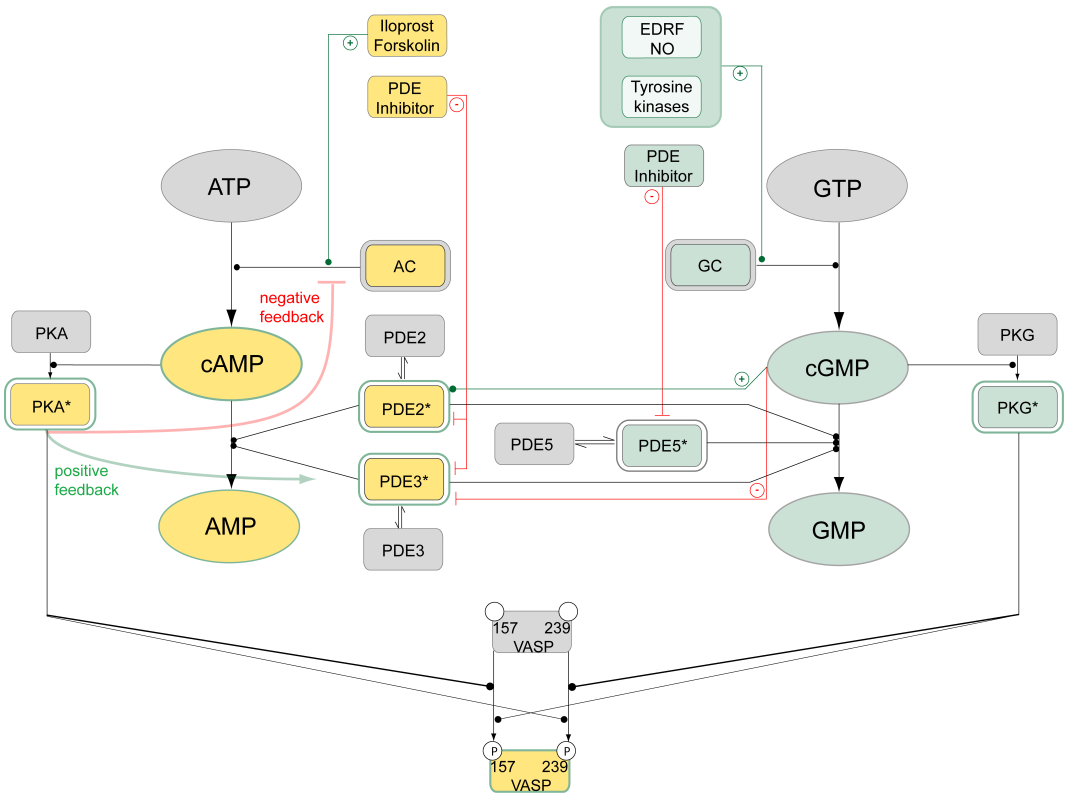

Figure 37: Pathway states and intermediate regulations. Different system nodes being involved in different cyclic nucleotide pathway stages are depicted: Resting state (gray nodes), activated cAMP path (yellow) and cGMP path (green) activated by endothelium-derived relaxing factor (EDRF) like nitric oxide (NO) or by tyrosine kinases and phosphodiesterase type 5 inhibitors. Components which are subsequently activated due to cGMP-evoked cross-talk are framed in green. Activatory effects (+) are depicted in green lines, inhibitory effects (-) in red. Figure: Wangorsch et al. (2011).

Therefore, we speculated on the effect of different cGMP concentrations by incorporating identified PDE interconnections into the model structure. The monitored cAMP levels are depicted in Figure 38. Predicted time-courses show that cAMP levels are highly dependent on actual cGMP concentrations in a both, dynamic and dose-dependent manner. Thus, future work will include the detailed modeling of the cGMP-branch including its cross-talk to the cAMP-pathway. Currently, time-resolved data concerning the

cGMP-to-cAMP cross-talk are collected by our collaborating team around Dr. Stepan Gambaryan at the Institute for Clinical Biochemistry and Pathobiochemistry. Exemplary, increased cGMP levels are evoked by inhibiting the cGMP-specific PDE5 in the human platelet. The effects of different doses of Silendafil, a potent PDE5 inhibitor, are measured quantitatively. The resulting time-series data can be used to train the appropriately extend dynamic model against.

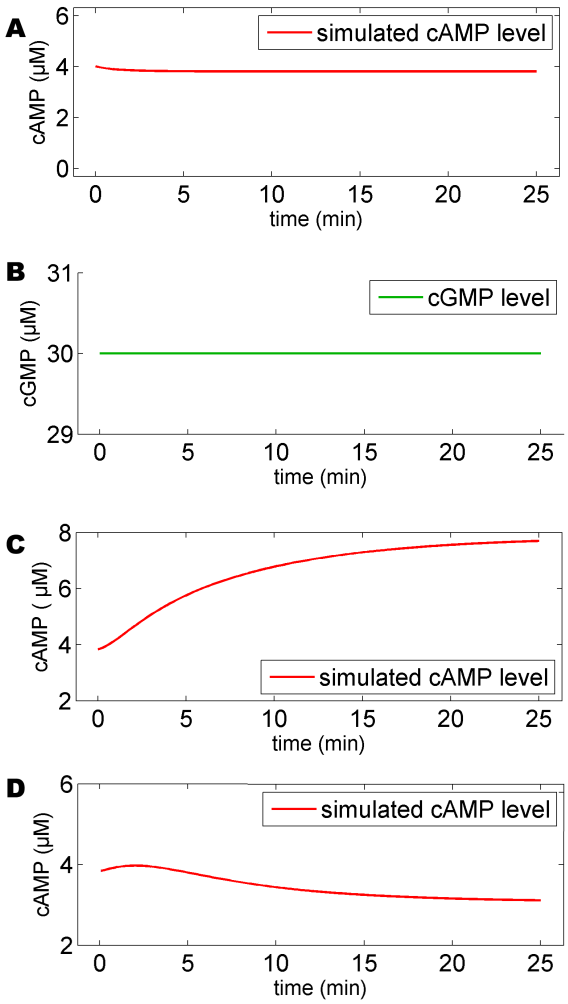

Figure 38: Modeling the potential cross-talk via cGMP. cGMP is known to potentially decrease (via PDE2-stimulation) or enhance (via inhibition of PDE3) cAMP responses. To model this cGMP-mediated cross-talk effect to PDE, we included two cGMP-dependent feedback constants (set to 0.1) in the basal model of nucleotide signaling. Assuming an constant additional cGMP stimulus of 30 µM (B), the cAMP concentration does not remain at basal level (A) but is increased (C). Thus, model-based cAMP predictions indicate a higher cGMP-dependency for PDE3 inhibition compared to PDE2 activation. However, the increase of the feedback constant representing the cGMP-dependent PDE2 activation (2.5 fold) leads to an intensified degradation of cAMP (D). Figure: Wangorsch et al. (2011).

The presented study on mathematically modeling the dynamic, feedback-regulated inhibitory signaling in human platelets has led to the publication "Time-resolved *in silico* modeling of fine-tuned cAMP signaling in platelets: feedback loops, titrated phosphorylations and pharmacological modulation" (Wangorsch et al., 2011). Besides assembling profound and specific information about platelet signaling, I established the entire model, conducted the data-based calibration, model-fitting and statistical testing and validation. Moreover, I suggested appropriate model-based predictions and simulations for probing the network sensitivity and strengthening the application-oriented impact of both, the model and approach.

4.2 Modeling Inflammatory Signaling

4.2.1 Introduction

Mammalian inflammatory signaling is an exquisite example demonstrating how cellular signaling pathways can be regulated to produce different yet specific responses to diverse inflammatory insults. NFκB represents a principal transcription factor and inflammatory mediator, whose activation is evoked by inflammatory signaling (cf. Section 2.1.3). Mathematical modeling with tight links to experiments have been instrumental in unraveling different forms of regulation in NFκB signaling as well as the underlying molecular mechanisms (Cheong et al., 2008), e.g. regulatory feedback or NFκB oscillations. This includes a variety of mathematical models mainly of the IκB - NFκB signaling module (Carlotti et al., 2000; Hoffmann et al., 2002) or IKK-focused models (Lipniacki et al., 2004), that are listed and compared in Cheong et al. (2008). The dynamics of molecular levels such as NFκB and their regulations are physiologically of immense importance and can quantitatively captured by mathematical modeling. Within this context, the exploration of signaling pathways *in silico* allows the description of how changes in signaling occur in space and time.

Adding to this, cross-talk between signaling modules and between entire signaling pathways is a central regulatory issue. Exemplary, NFκB is activation as a response to numerous inflammatory and non-inflammatory signals (Hayden and Ghosh, 2004). We here present a mathematical description of the TNF receptor interplay between TNF-R1 and TNF-R2 (Section 4.2.2). TNF-R2 influences TNF-R1 signaling by evoking an apoptotic cross-talk and by triggering a shift in NFκB activation.

Besides a detailed understanding of the down-stream signaling events of TNF receptors, a profound comprehension of the creation and processing of transduced signals is of equal importance. Ligand binding on the targeted receptor, e.g. TNF to TNF-R1, causes a variety of structural changes such as receptor clustering. Mathematical modeling sustains the identification of receptor properties determining the processing of ligand-encoded information (Becker et al., 2010). We show here first results of such a mathematical rule-base model on receptor cluster formation (Section 4.2.3).

4.2.2 Cross-talk Model of Inflammatory Signaling Pathways

TNF Receptor Cross-talk An interesting feature of the TNF-R1 and associated signaling events is the existence of extensive signaling cross-talk. This includes receptor signaling mediated by members of the TNF-receptor superfamily (Naudé et al., 2011; Nakayama et al., 2002) and other receptor types (Beyer and MacBeath, 2012). With respect to inflammatory signaling, this mainly affects the differential activation of the transcription factor NFκB (Oeckinghaus et al., 2011), being a critical regulator of immunity, stress responses, apoptosis and differentiation.

In the following, we focus on the interplay of TNF-R1 and TNF-R2 : The distinct signaling pathways initiated by TNF-R1 and TNF-R2 stimulation can mutually influence each other via signaling cross-talk (Figure 39). This maintains a delicate balance between cell survival and apoptosis (Thakar et al., 2006; Wajant, 2011; Wicovsky et al., 2009b,a).

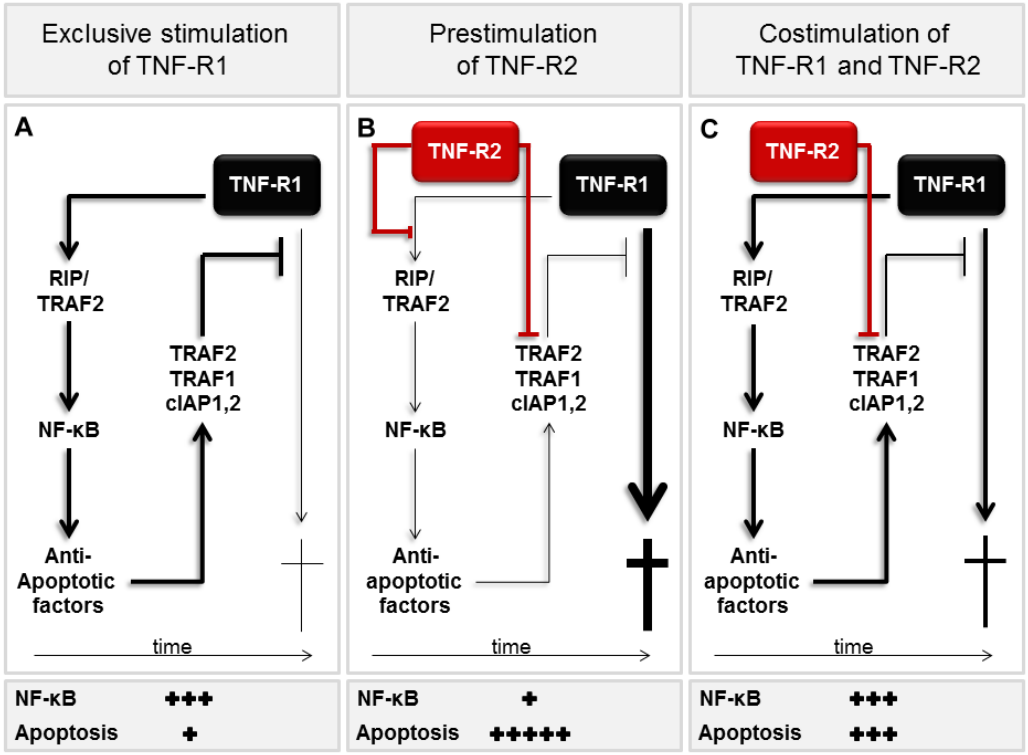

Figure 39: Apoptotic cross-talk. Signaling outcome of TNF-R1 is influenced by co- and prestimulation of TNF-R2, respectively, in a time-dependent manner. Signaling due to exclusive stimulation of TNF-R1 (A) is slightly shifted towards apoptosis if TNF-R2 is stimulated simultaneously (C). Prestimulation effects reduced NFκB signaling accompanied with a strong shift towards apoptosis (B). Figure: Modified after Fotin-Mleczek et al. (2002).

However, the molecular basis for the mutual interplay of these TNF receptors with the apoptotic pathway and the signaling cascades that lead to activation of NFκB is not fully understood. This pertains to the cross-talk in NFκB signaling pathways (Oeckinghaus et al., 2011) and to the direct cross-talk between both receptors (Cabal-Hierro and Lazo, 2012; Naudé et al., 2011). This emphasizes the need to set up mathematical models and *in silico* descriptions of signaling networks as a first step to better understand and predict cellular behavior in complex signaling settings.
In recent years, several signaling proteins have been identified for being capable to interact either directly or indirectly with domains of both receptors. Regarding the question of TNF receptor cross-talk, the TNF receptor-associated factor (TRAF)1 and 2 (Fotin-Mleczek et al., 2004; Wajant and Scheurich, 2001; Wicovsky et al., 2009a), as well as the cellular inhibitor of apoptosis proteins (cIAPs) are of special interest (Wajant, 2011). These adaptor proteins are suggested to form critical integration points for pro- and anti-apoptotic signals (Fotin-Mleczek et al., 2002). The balance between anti-apoptotic (TRAF1/TRAF2/cIAP1/cIAP2) complexes and proapoptotic (FADD/caspase-8) complexes being recruited to TNF-R1 might determine the signal transduction pathways activated through TNF-R1. This in turn induces either gene expression or apoptosis. Hence, these regulatory proteins make up potential targets for therapeutic intervention, e.g. in anti-cancer therapy (de Almagro and Vucic, 2012) or myocardial infarction (Schulz and Heusch, 2009).

Multi-valued Boolean Model Deciphering this molecular puzzle will greatly help to interpret the cause of specific outcome of TNF receptor signaling in distinct biological contexts. Approaching this issue, we developed a multi-valued Boolean model of TNF-R1 and TNF-R2 cross-talk that comprises signaling events as depicted in Figure 40.
We used the CellNetAnalyzer, for implementing the underlying logical connectivity between signaling nodes. Thereby we could capture two main features of the signaling cross-talk, (i) the stepwise apoptotic cross-talk effect regarding the different stimulatory scenarios (cf. Figure 39A-C) as well as (ii) the time-dependent component. A binary Boolean approach would have failed in modeling the multi-step apoptotic cross-talk effect, as nodes are assigned by just two values, either 1 (on) or 0 (off).

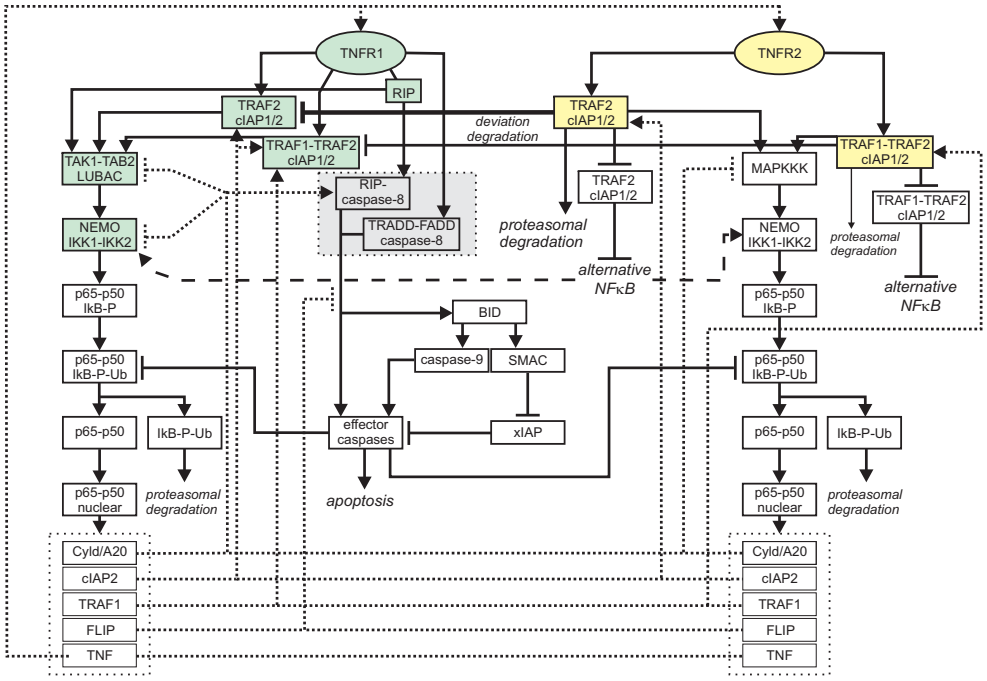

Figure 40: Network topology of TNF receptor cross-talk. Components that can physically be detected in the immunoprecipitates of TNF-R1 and TNF-R2, respectively, are depicted in green and yellow. Cytoplasmatic components are depicted in white. Gray box: TNF-R1- induced complex activating caspase8. Arrow thickness reflects its functional effect. Currently, a regulatory connectivity between the alternative NFκB pathway and cell death is not known. Therefore, it is just modeled as one single black box. Secondary processes resulting from NFκB activation are depicted with dashed lines. The activation of effector caspases through caspase8 is divided in a BH3 interacting-domain death agonist (BID)-dependent and direct activation. The activatory pathway via BID however is only relevant in cell having an abundance of X-linked inhibitor of apoptosis proteins (XIAPs). TNF-R1 mediates the activation of caspase8 in a RIP-independent and RIP-dependent manner. The latter is inhibited by k63-ubiquitinated NEMO which is of equal importance for NFκB signaling. A20 und Cyld are induced by NFκB and prevent the ubiquitination of NEMO via LUBAC. This way, NFκB is inhibited but the RIP-dependent caspase8 activation is sensitized. NFκB-induced FLIP inhibits both, the RIP-independent and the RIP-dependent pathway. The inhibition of NFκB signal transduction is indicated by blocking the p65-p50 activation.

Model development occurred in three steps. First we set up the reactions for the distinct pathways (TNF-R1, TNF-R2) separately. Therefore, we defined TNF-R1 and TNF-R2 stimuli (cf. Table 20, Reaction 27, 28) that specifically activate the distinct receptors. TNF in general would result in the activation of both receptor types and thus can serve for modeling the costimulation condition. Finally, the prestimulation condition was realized by setting a so-called 'time scale scenario' in CellNetAnalyzer that assures the update of logical reactions at a given, pre-defined time point. We assumed that first,

signaling molecules that protect from apoptosis are engaged in TNF-R2 signaling (costimulation), shifting TNF-R1 signaling slightly to apoptosis. After prestimulation, this effect is intensified and shifts TNF-R1-mediated signaling strongly towards apoptosis. Additionally, prestimulatory TNF-R2 signaling and the thereby evoked gene expression affects and lowers the the TNF-R1-triggered NFκB activation. Details on the implemented reactions are given in Table 20 (Annex C).

Model Simulations Simulation of the implemented logical model could precisely describe the differential NFκB activation as well as the apoptotic cross-talk (Figure 39). Table 8 summarizes the resulting activation values (NFκB, apoptosis) according to the different receptor activation scenarios. Values are in close accordance to those that were experimentally observed and previously reported by Fotin-Mleczek et al. (2002).

Table 8 : Simulations of multi-valued Boolean model with repect to different receptor activation. Scenario 1: TNF-R1 solely; apoptosis: 1, NFκB: 3.Scenario 2: TNF-R2 solely; apoptosis: 0, NFκB: 1. Scenario 3: Costimulation; apoptosis: 3, NFκB: 3. Scenario 4: Prestimulation of TNF-R2; apoptosis: 5, NFκB: 1. Underlying reactions are given in Table 20 (Annex C).

Scenario	TNF-R1 stimulus	TNF-R2 stimulus	apoptosis	NFκB
Scenario 1	1	0	1	3
Scenario 2	0	1	0	1
Scenario 3	1	1	3	3
Scenario 4	1	1	5	1

The established multi-valued Boolean model can serve as a basis for semi-quantitative model simulations and allows the testing of hypotheses on regulatory questions. Ultimately, model development is extend to quantitatively describe the full dynamics of the mutual receptor cross-talk as more detailed time series data for model calibration are available. Data collection and model validation is realized in cooperation with Prof. Wajant (Division of Molecular Internal Medicine, Department of Internal Medicine II, University Hospital Würzburg). Current findings together with data-driven model extensions and predictions will result in a systems biological publication which is currently in preparation.

4.2.3 Clustering of TNF Receptors: A Rule-based Approach

Differential Binding Tumor necrosis factor (TNF) exists as a homo-trimeric molecule that is able to bind up to three moldecules of receptors belonging the TNF receptor superfamily (Smith and Baglioni, 1987; Bazzoni and Beutler, 1996). This implies differential binding characteristics of TNF receptor type 1 (TNF-R1) and type 2 (TNF-R2). Different oligomerization states, in particular trimers of receptor or ligand, modify the binding behavior (Boschert et al., 2010). The affinity of soluble TNF binding to TNF-R1 (dissociation constant $K_D = 1.9 \cdot 10^{-11}$ M) is remarkably high, compared to the significantly lower affinity for TNF-R2 ($K_D = 4.2 \cdot 10^{-10}$ M) (Grell et al., 1998). Besides the causal link to association-dissociation kinetics, the insufficient induction of strong signaling via TNF-R2 by TNFs has been linked to the capability of TNF to form larger and stable signaling clusters (Krippner-Heidenreich et al., 2002).
On the molecular level, the so-called pre-ligand binding assembly domain (PLAD) is critical for cluster formation. Like other receptors of the TNF superfamily, the structure of TNF-R1 contains a PLAD, facilitating the oligomerization prior to ligand binding. Thus, this enables a fast signal processing and transduction (Heidbreder et al., 2012; Chan et al., 2000). These data explain the predominant role of TNF-R1 in mediating cellular responses by TNFs and indicate stable TNF-TNF receptor complexes as plausible cause for differential signaling efficacy. This is particulary important to allow activation of different cell physiological responses such as inflammatory response or apoptosis (Ho and Harrington, 2010).

Models of Receptor Cluster Formation To identify the molecular basis of this differential binding behavior, binding studies including TNF-R1 and TNF-R2 were carried out by our experimental collaborators (Prof. Harald Wajant). Previous studies and experimental data has led us to different models, explaining the differential behavior of TNF in binding to both receptor types (Figure 41).
We compare and model here the behavior of TNF-R1 and TNF-R2 with respect to signal formation at the respective receptor. TNF-R1 activation works already with interacting monomers (receptor, ligand) while TNF-R2 relies on trimer formation (Chan et al., 2000; Mukai et al., 2010). Indeed, experiments showed that preclustering of TNF-R2 monomers increased the affinity for the TNF-homotrimer in comparison with the receptor monomer.

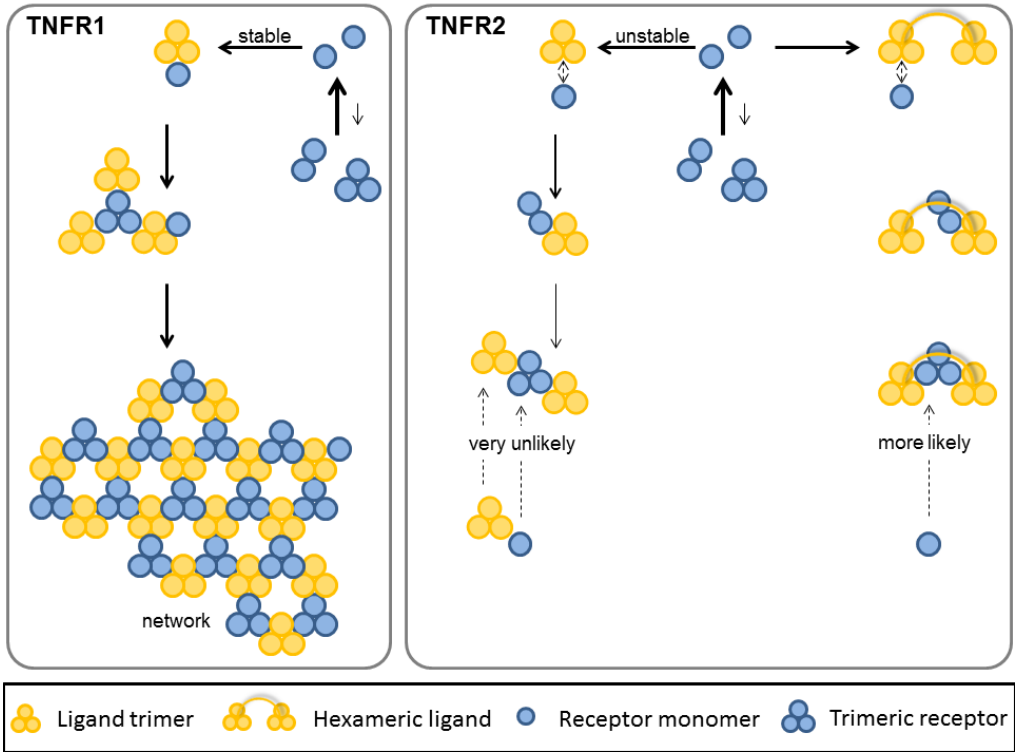

Figure 41: TNF receptor clustering. Model assumptions for differential binding behavior of TNF to TNF-R1 and TNF-R2, respectively. TNF trimers, hexamers are depicted in yellow, distinct receptor conformations in blue.

Moreover, stimulation with a hexameric ligand resulted in a stronger signaling response as well, indicating that this conditions also prefers the trimeric receptor conformation. Differential receptor clustering in small or large aggregates, hence the creation of graded down-stream signal strengths, represents a manipulative and therefore attractive aspect in cell signaling. Thus, testing of different hypotheses experimentally as well as *in silico* is valuable for understanding both, the formation of clusters and their role in signal creation and down-stream signaling.

Rule-based Modeling I applied the rule-based approach to model the multivalent ligand-receptor interactions. As introduced in Section 3.5, this approach appropriately captures structural information about signaling molecules and interactions thereof. Using the rule-based approach, a receptor can be expressed as a molecule comprising three different binding sites, one for the ligand and two for receptors to accomplish the clustering (Figure 42A,B).

Concerning receptor-ligand interactions, these sites are assigned with affinity values (k_i), characterizing the modeled reactions and leading to different cluster sizes, according to the given interaction strengths. This way, all combinations of receptor-ligand configurations can be considered. Moreover, screening over a broad range of affinity values indicate how strong the resulting signal would be generated. This is reflected in the cluster-size that result from simulating the implemented rules. The process of cluster formation is mainly accomplished in three steps: Receptor-ligand binding, further receptor cross-linking and dissociation (Figure 42B).

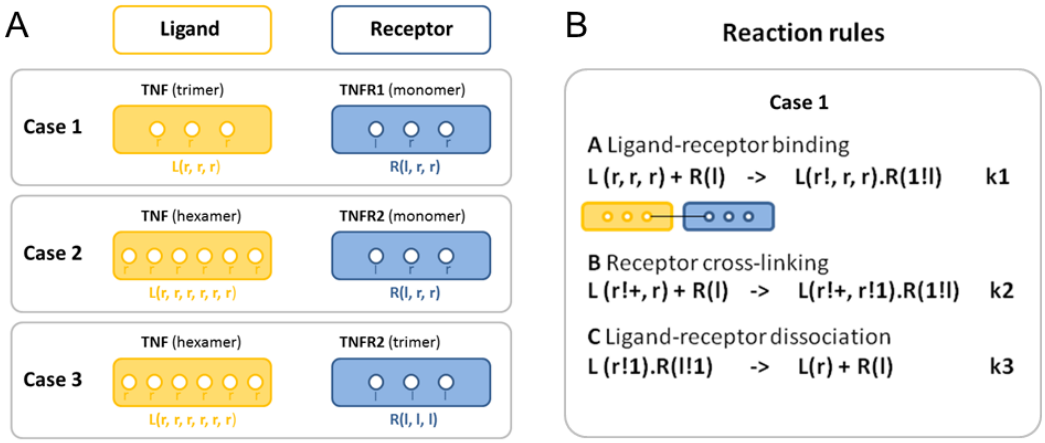

Figure 42: Rule-based moldes of receptor clustering. (A) Assumed cases: combinations of different receptor-ligand conformations. (B) Exemplarly, rules in BioNetGen language (three steps of cluster formation) for simulating case 1. Coefficients k_i characterize the development of connecting receptor R() and ligand L() molecules.

Executing the formulated rules (BioNetGen language) with RuleBender (Xu et al., 2011a), we could indeed show that the stronger the ligand-receptor initial affinity, the greater the resulting cluster size. These preliminary results indicate that modeling is an appropriate method to capture and to study receptor-ligand interactions in more detail. As soon as model refinements and the training against experimental data is perfected, the study can be adapted to other clustering systems such as the Fas receptor (Stel et al., 2007). The achieved systems biological view (data and model) on the differential ligand-receptor binding behavior is furthermore beneficial to test how cluster formation and signaling can be perturbed in the sense of pharmacological interventions.

4.3 Modeling Cell Signaling in Different Cell Types

4.3.1 Introduction

Concepts of mathematical modeling the signal transduction through cells are omnipresent in supporting biological and biomedical research. This ranges from pharmacological and clinically-driven applications to those that are related with the so-called "green systems biology" (Weckwerth, 2011) focusing on the systemic understanding of plants and the ecosystem.
Cell signaling models of different cell types to which I contributed are introduced in the following. Protein-protein interaction (PPI) networks combine experimental observations and give first hints for analyzing information flow in biological networks. In Section 4.3.2 we present such a PPI network that shows the shifted balance between proliferation and apoptosis for TWEAK-treated cardiomyocytes. With respect to green systems biology, I contributed to the development of a Boolean model for mimicking plant-pathogen interactions in *Arabidopsis* (Section 4.3.3). Furthermore, we succeeded in integrating different Boolean models of hepatocyte signaling (Section 4.3.4), a technique which enables the extension and combination of already existing models to enlarge possible model simulation applications and advance biological insights.

4.3.2 Heart Cells and Cardiovascular System

Inflammation and Cardiac Damage Collaborators associated with the SFB688 (Prof. Frantz, University Hospital Würzburg) currently investigate the regulatory and causal connection between inflammation and cardiac damage. The interaction of inflammatory cells e.g. macrophages and neutrophils on the one hand, and of non-inflammatory cells such as fibroblast or cardiomyocytes on the other hand is tightly regulated by paracrine factors. These factors play a key role in cardiac healing as well as in cell responses to injury. Inflammatory mediators regulate involved cell- cell interactions, however, their role in cardiac injury is not yet fully understood. Cytokines, macrophages and neutrophils are among others all part of the so called innate immune response. This indicates that the activation of the innate immune system may play an important role for regulating cell-cell-interactions after cardiac injury (Linde et al., 2007). Activation of inflammatory cytokines, e.g. TNF, interleukins or TWEAK, was reported to be involved in experimental and human heart failure (Aukrust et al., 2005; Anker

and von Haehling, 2004). Furthermore, they all share the downstream activation of the transcription factors such as NFκB, that is activated in heart failure (Frantz et al., 2003). Consecutively, investigation of the cell specific role and regulation of NFκB in cardiac myocytes and inflammatory cells in cardiac ischemic injury is of major clinical importance.

TWEAK-induced Effects The TNF like weak inducer of apoptosis tightly regulates NFκB activation that in turn controls the expression of different proinflammatory cytokines and chemokines. Moreover, the TWEAK/Fn14-system affects cardiac remodeling (Ren and Sui, 2012). Our collaborators have established a mouse *in vivo*-model of myocardial ischemia reperfusion to study the effects of TWEAK treatment and its connection to myocardial infarction. Studies revealed that TWEAK affects the infarct size after ischemia reperfusion as well as the distribution of immune cells e.g. leukocytes in scar cell and raises the occurrence of ruptures (data in the process of being published by Prof. Frantz et al.). Moreover, a statistical evaluation of a cytokine array indicates the upregulation of genes being important for recruitment (namely MIP2, MCP-1 and MCP-5) and differentiation of leukocytes (IL-5, IL-12 and IFNγ) upon TWEAK treatment.

Data Integration For further evaluation and analysis, cytokine array data were mapped on the interactome. The human interactome network including kinases and phosphorylation substrate information was established for the cardiomyocyte as described previously for the platelet (Boyanova et al., 2012). Briefly, different proteome and transcriptome databases were collated regarding protein nodes with expression evidence in the cardiomyocyte. This generates an integrative protein-protein interaction-network focused on the global view of involved signaling cascades and their connectivity (Figure 43). Gray lines indicate protein-protein interactions, red arrows denote phosphorylation reactions. Short gene names are given for each node (protein nodes are shown as circles except kinases which are shown as triangles). Green-labeled proteins indicate upregulation in the TWEAK condition.
Functional clusters denote interleukins and chemokine pathways and entities, connected by the JAK/STAT pathway (Subramaniam et al., 2001), that is stimulated by a variety of chemokines, growth factors or hormones. TWEAK stimulation interacts with the TNF pathways, thereby potentially changing the balance between proliferation and apoptosis. Links to the cy-

tokines and JAK/STAT pathway are given by NFκB and Rac1 (Figure 43). In summary, the shifted balance between proliferation and apoptosis for TWEAK and TWEAK inhibition leads to changes transmitted by the interactome regarding a number of interleukins and chemokines. These findings could not have been observed from the data alone and may be beneficial to create further experiments for elucidating the connection between inflammation and cardiac damage.

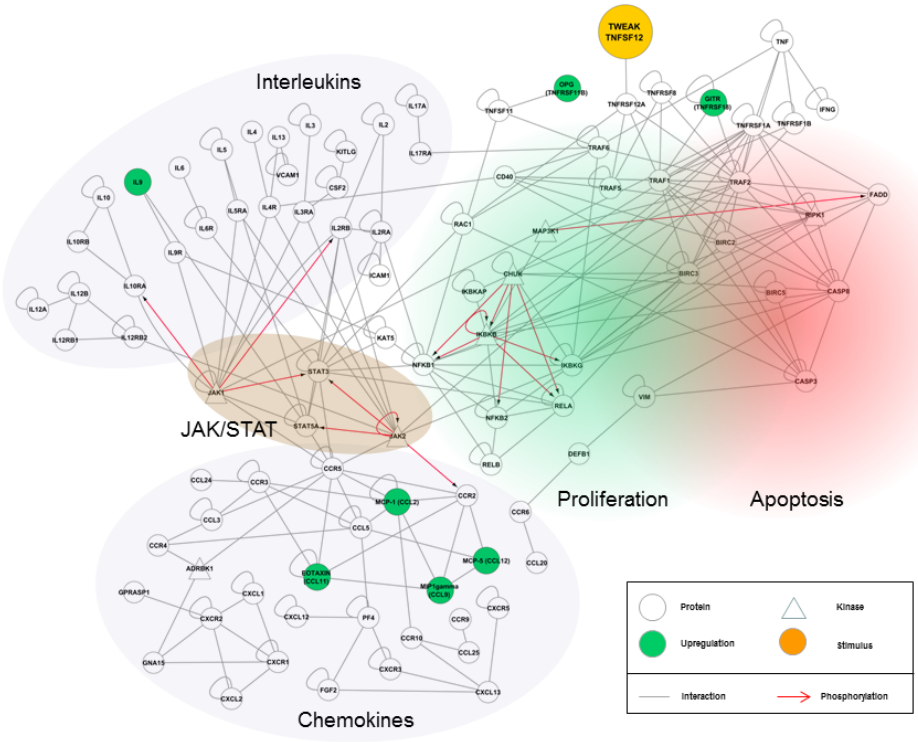

Figure 43 : Protein-protein interaction network. The protein-protein interaction network shows the shifted balance between proliferation (green cloud) and apoptosis (red cloud) and functional context for TWEAK stimulation and TWEAK inhibition. Circles indicate proteins; kinases are depicted in triangular shape, each specified by gene names. They are connected either by gray lines indicating protein-protein interactions or red arrows denoting phosphorylation reactions. The functional entities are highlighted (interleukins, chemokines, JAK/STAT pathway). Green-colored nodes show upregulation in the TWEAK stimulation (orange) condition.

4.3.3 Modeling *Arabidopsis* Immune Response

Phytohormones and Signaling Molecular genetic studies and the completion of the sequencing of the *Arabidopsis thaliana* genome have enormously increased the knowledge of hormonal regulation in plants within the last two decades. This advanced the research on plant signal transduction and gene regulation, however, the understanding of the complex interplay and pathway regulation is yet not fully understood. Thereby, mathematical modeling represents a valuable tool for investigating the pathway dynamics and cross-talks particularly in cases that are not accessible by experiments.
Plant development and immunity is tightly coordinated by plant hormones. Plant immune networks and the ultimate phenotype are often critically determined by small molecules with hormonal properties such as salicylic acid (SA), jasmonic acid (JA), auxin (Aux), ethylene (ET), gibberellic acid (GA), abscisic acid (ABA), and various cytokinins (CK) (Robert-Seilaniantz et al., 2011). The mediated signaling cascades are highly inter-linked (Gazzarrini and McCourt, 2003), maintaining the physiological equilibrium in the plant. Especially the cross-talk regarding auxin and cytokinin (Moubayidin et al., 2009) and the auxin-cytokinin antagonism is important for both, plant development and immunity (Naseem and Dandekar, 2012). Pathogens, e.g. *Pseudomonas syringae* pv tomato DC3000 (*Pst*) that attack the plant enhance host susceptibility by modulating the hormonal balance of the plant cell. This involves cytokinin but its detailed function concerning plant immunity remains to be fully unraveled.

Outline We here present a mathematical model addressing plant immunity in *Arabidopsis*, the model system in green systems biology. Based on extensive data mining, including pathogenicity factors, host regulatory proteins, enzymes of hormone biosynthesis, and signaling components, we set up an integrated signaling network (Naseem et al., 2012). Dynamic simulations and system analysis elucidated the regulatory role of cytokinin and revealed multiple cytokinin-mediated regulatory interactions within plant disease networks. This comprises specific synergism between cytokinin and salicylic acid pathways as well as novel aspects of the antagonistic relation between cytokinin and auxin in plant immunity. Subsequently conducted experiments confirmed the model-based predicted interactions and hormonal effects on plant immunity.

Model Topology and Set-up Taking extensive *a priori* knowledege of hormonal cross-talks in plant signaling and inter-linkage with pathogen *Pst* into account, we set up a comprehensive integrative Boolean model of 105 nodes and 163 edges (Figure 44). It includes biosynthetic pathways of phytohormones with defense signaling, immunologically important receptors, transcription factors, repressor molecules and degradative complexes.

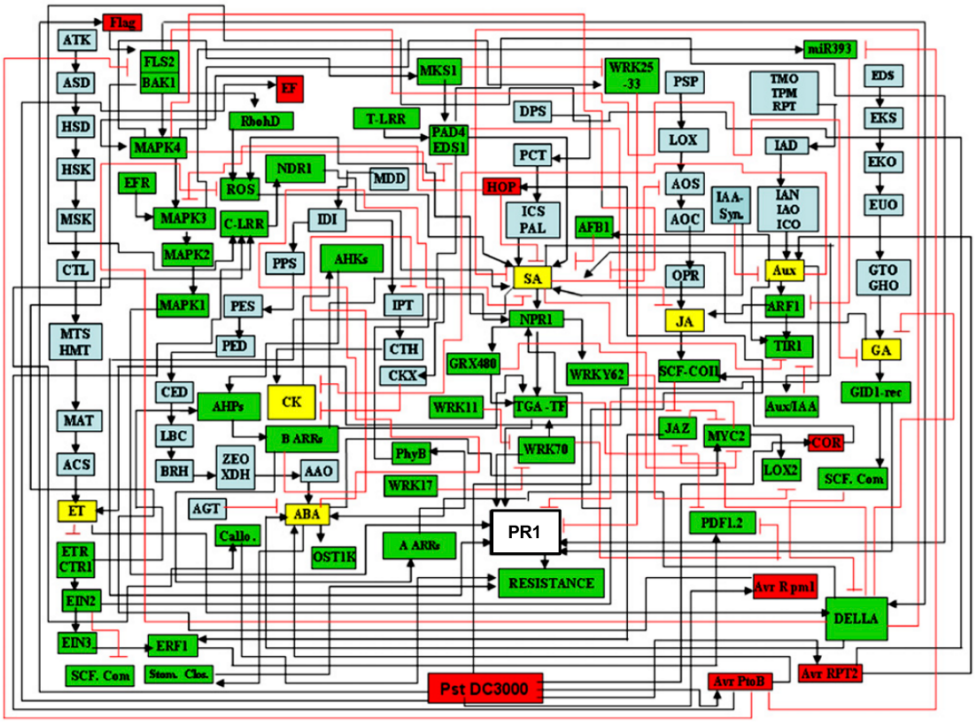

Figure 44: Network topology of *Pst*-mediated hormone disease networks in *Arabidopsis*. Nodes are inter-linked based either on activation (→) or inhibition (—|). Color coding of nodes: light blue, enzymes of hormone biosynthesis and degradation; yellow, active plant hormones; green, host regulatory factors; red, *Pst*-evoked pathogenicity factors responsible for triggering immunity in *Arabidopsis*; white, pathogenesis-related protein 1 (PR1), a marker for immunity against the infection of *Pst* in *Arabidopsis*. See original publication (Naseem et al., 2012) for full names, internodal interactions and literature on the behavior of these interactions. Figure modified after Naseem et al. (2012).

Transforming this literature-based model into a dynamic system using SQUAD (Di Cara et al., 2007), it serves for simulating and investigating various aspects of plant immunity. We applied the dynamic approach, as it is the collective time-dependent dynamic of hormonal effects during infection that determines the outcome of plant-pathogen interactions (Bari and Jones, 2009; Robert-Seilaniantz et al., 2007). Our focus lies on elucidating the role

and impact of cytokinin. It's role has not been assigned a conclusive role in plant pathogen interaction, however, several pathogens pattern the cytokinin secreting capability in plants (Walters and McRoberts, 2006; Pertry et al., 2009). Moreover, cytokinin has been shown to promote resistance in *Arabidopsis thaliana* to *Pst* infection (Choi et al., 2010). Hence, it is plausible that cytokinin signaling has multiple interaction possibilities with respect to plant pathogen immune networks.
Using dynamic simulations of the established logically connected network, we elucidate the complex network interactions around plant immunity after pathogen attack. Main results gained from dynamic simulations are presented in the following. More detailed results including micro array experiments can be found in Naseem et al. (2012)

***Pst* Infection** To assess the dynamic behavior of nodes across the network, we first considered and modeled the effect triggered by plant infection with pathogen *Pst* (Figure 45).

Plant receptors are instrumental in the recognition of pathogen-associated molecular patterns (PAMPs) and effectors (Figure 44, red nodes) that evoke changes in system states of the plant cell. Dynamic simulations of *Pst* infection denoted the resulting activation states for individual nodes across the whole network (Figure 45). Our dynamic model for *Pst* infection showed activation of SA, JA, ET, ABA, and auxin, whereas GA and cytokinin remained unaffected. Furthermore, immunity can be understood as the sum of various components such as PAMP-triggered immunity (PTI) and effector-triggered immunity (ETI) (Jones and Dangl, 2006). Modeling of both forms showed a clear distinction of the corresponding activation patterns with respect to each type of plant immunity and in accordance with current literature (Naseem et al., 2012).

Hormonal and Cytokinin Cross-talk As demonstrated, plant hormones are differentially engaged in plant infection evoked by *Pst*. To model and simulate the hormonal impact on plant immunity, we performed SQUAD simulations by assuming the individual hormones as input nodes while distinguishing between *Pst* presence or absence, respectively. The route of the injected signal can be followed through the network gates reaching the marker node PR1 (Figure 44, white node) that reflects the resulting immunological response of the host plant (Mukhtar et al., 2011).

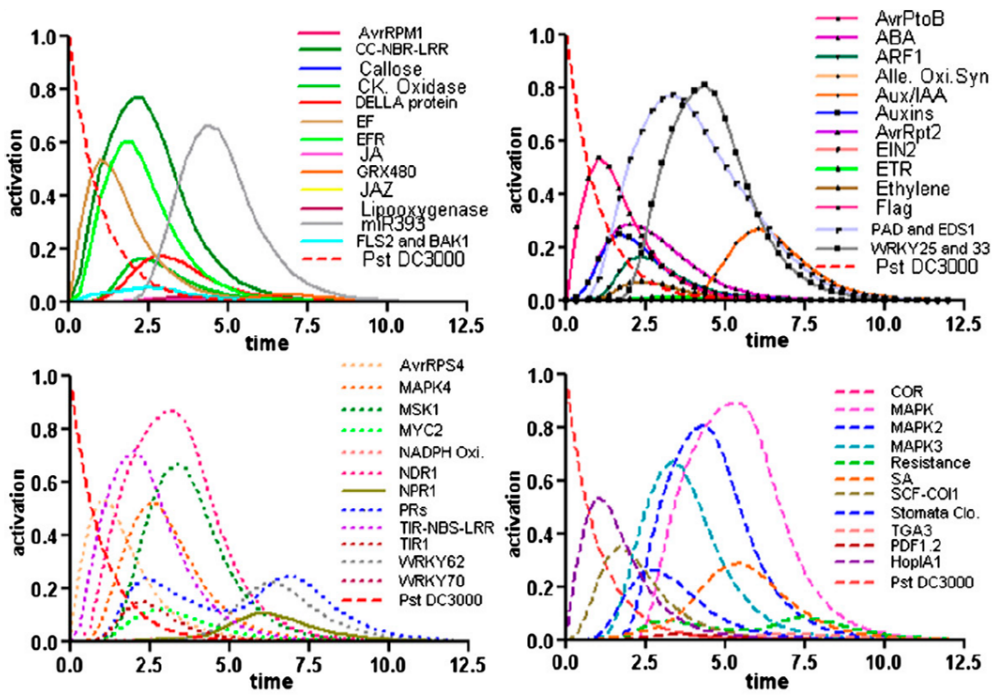

Figure 45: Effects of pathogen *Pst* on components of plant immunity. *Pst* is assumed to be fully active (activation value of 1.0 for simulations, red-dashed line). The dynamic simulation using SQUAD assigns activation states (response curves) to each network node within the assembled network (Figure 44). X-axis: arbitrary units of time (SQUAD simulations are carried out in 12.5 time steps). Y-axis: activation states ranging from no (0) to full (1) activation. Each trajectory represents the response curve of one distinct network node, differentiated by color-codes and line-styles. Full names are given in the supplement of the original publication of Naseem et al. (2012). Figure modified after Naseem et al. (2012).

The activation of PR1 over time was used as an index of plant immunity as a result of different hormone-pathogen inputs, depicted in Figure 46. Simulations indicated three hormones ET, SA, and GA that activate PR1 in contrast to JA, ABA, and auxin (Figure 46A, left panel). Interestingly, SA and GA further enhanced the signal strength of PR1-activity in the presence of *Pst* (Figure 46A, right panel). This sustains the fact that unlike the promoting effect of SA and GA on immunity, auxin, JA, and ABA mediate the susceptibility of *Arabidopsis* against *Pst*-evoked infection. The phytohormone cytokinin thereby seems to have multi-faceted effects on signaling in plant diseases. Regarding their connection to the SA-JA/ET backbone of plant immunity, positive cross-talk between cytokinin and the SA pathway was found (Choi et al., 2010) but also negative cross-talk among them (Argueso et al., 2012). Our own observations from both experiments and modeling intrigued us to investigate the specific cross-talk by cytokinin as this seemed to enhance immunity in plants (Figure 46B).

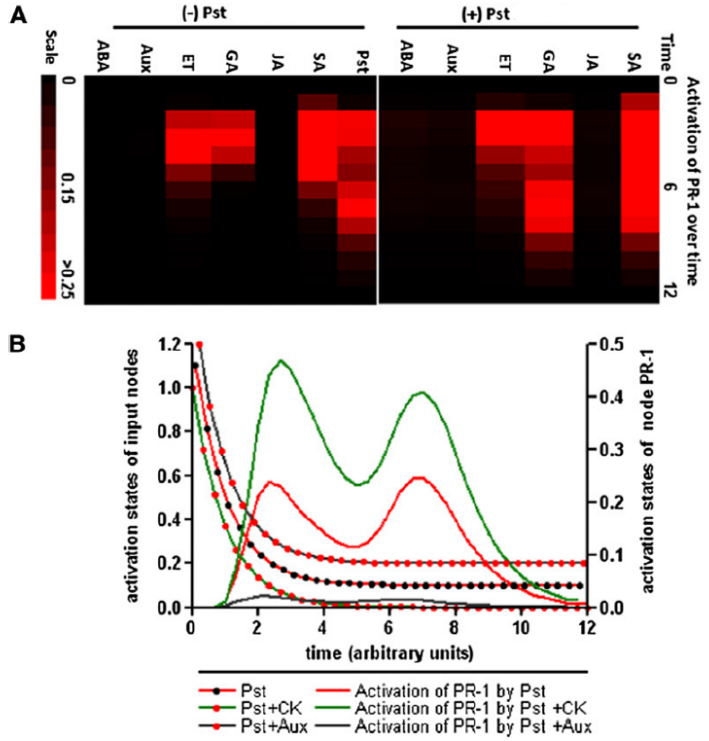

Figure 46: Impact of plant hormones on the pathogenicity of *Pst*. (A) Plant hormones change the immunity of the host which can be monitored by PR1. Activation states of PR1 over arbitrary units of time are shown in form of a heat map for plant hormones with (right panel) and without (left panel) the infection of *Pst*. (B) Impact of cytokinin and auxin regarding the infection by *Pst* in *Arabidopsis* monitored by PR1. Y-axis (left): Activation states of combined input signals or *Pst* infection alone (red line with black dots), with cytokinin (green line with red dots) and with auxin (black line with red dots). Y- axis (right): activity of read-out node PR1 as resonse to *Pst* (red curve), *Pst* with cytokinin (green curve), and *Pst* with auxin (black curve). X-axis: arbitrary units of simulation time. Figure modified after Naseem et al. (2012).

Assuming *Pst* as input together with cytokinin (modeling the increased cytokinin status of the plant during pathogen infection), SQUAD analysis resulted in the activation of nodes including PR1 (Figure 46B). Subsequent simulations also highlighted that cytokinin solely (without *Pst*) is capable to cause the activation of PR1 and hence promote plant immunity. Modeling predictions could nicely be verified by experiments, showing that enhanced plant cytokinin levels boost immunity against infection of *Pst*.

Analogously, modeling and experimental data substantiate that the interaction between cytokinin and SA is down-stream of SA biosynthesis, while increased SA levels only fortify the cytokinin-mediated system state with more extensive protection against infection with *Pst* (Naseem et al., 2012).

Similarly, by modeling and experiments we could show and sustain the importance of cytokinin in promoting PTI.

Auxin-Cytokinin Behavior and Interaction Both, auxin and cytokinin have long been known to be involved in plant growth and development (Liu et al., 2010). On the one hand, auxin promotes *Arabidopsis* susceptibility to infection with *Pst* via multiple cross-talk with JA and SA, respectively (Navarro et al., 2006; Chen et al., 2007; Wang et al., 2007a; Llorente et al., 2008). On the other hand, cytokinin boosts plant immunity against *Pst* (Figure 46). In contrast to their individual roles, the combined effect of auxin and cytokinin in plant immunity is still not entirely known.
To investigate the interplay more closely, we modeled the combined effects of auxin and cytokinin on plant immunity, choosing various input activation values (partial and full activation) for auxin and cytokinin input nodes. Resulting dynamic simulations provided further insights into the contrasting behavior of auxin and cytokinin in plant immunity and into auxin-cytokinin interactions. Partially and fully activated nodes of auxin and cytokinin as combinatory input signal changed the system states across the entire network (Naseem et al., 2012). Again, we monitored the activation course of marker node PR1 as an indicator of immunity status. Resulting time-resolved trajectories for each hormonal combination are depicted in Figure 47A. Simulations revealed that effects on PR1 activity are opposed, depending of the auxin-to-cytokinin ratio: High input activation value of auxin (1.0) and a low value of cytokinin activation (0.5) resulted in low PR1 activity, whereas PR1 gained more activation if the input combination was reversed (Figure 47A). We sampled and combed different activation values for both, auxin and cytokinin. Resulting effects on the PR1-level are depicted as 3D-visualization of the data (Figure 47B). This provides an overview and shows that the auxin-to-cytokinin ratio is crucial for activation of PR1. More precisely, immunity is compromised if auxin supersedes the activation of cytokinin, and immunity is achieved when cytokinin attains higher activation in comparison to auxin.

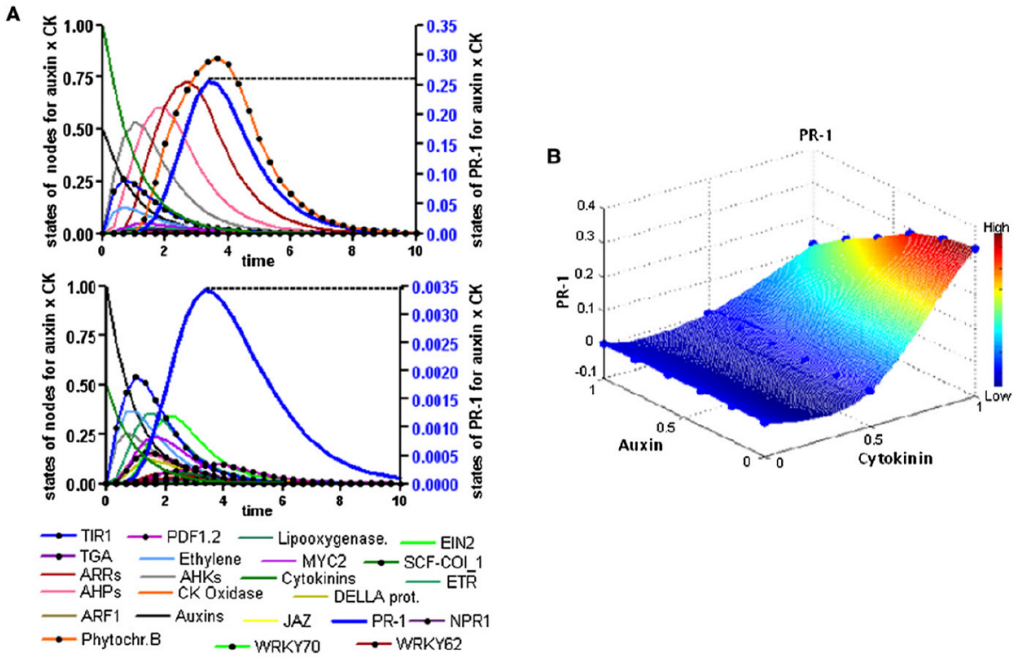

Figure 47: The Interaction between Auxin and Cytokinin Modulates Plant Immunity. (A) SQUAD analysis on the balance between auxin-to-cytokinin (CK) ratio and evoked plant immunity. Top panel: Auxin was partially activated (activation value: 0.5), while cytokinin was assumed fully activated (activation value: 1.0). Bottom panel: Reversed case. Auxin was assumed to be fully activate (activation value: 1.0) whereas cytokinin only to a partial degree (activation value 0.5). The triggered effect on plant system states (key network nodes) is shown concerned to the left y-axis, while immunity in terms of the activity of marker node PR1 (blue curve), with a scaling that belongs to the right y-axis. (B) 3D-visualization of auxin/cytokinin balance and effects on PR1 activation. X-axis: activation values of cytokinin. Y-axis: activation values of auxin. Z-axis: depicts the activation of PR1 at a given auxin-cytokinin input. Figure modified after Naseem et al. (2012).

The entire systems biological study on networking hormones in plan immunity, together with detailed information about experimental data resulted in the comprehensive publication "Integrated Systems View on Networking by Hormones in *Arabidopsis* Immunity Reveals Multiple Crosstalk for Cytokinin" (Naseem et al., 2012). My main scientific contributions to this study include the establishment and adaptation of the applied method of Boolean modeling together with dynamic transformation as well as the subsequent interpretation ans visualization of the resulting model simulations.

4.3.4 Hepatocyte Signal Transduction

Systemic Understanding of Liver Functions Biomedical-driven mathematical modeling of cells and their functions aims at understanding the physiological regulatory processes on the molecular, cellular and ultimately on the organ level. This directs at a systemic comprehension of organ function in normal and diseased states. The liver represents a prime example of bringing these levels together. There is a comprehensive network of German and international research groups actually working on the *Virtual Liver* (`http://www.virtual-liver.de`), a dynamic mathematical model representing, rather than fully replicating human liver physiology, morphology and functions. Several models of liver pathways based on different modeling techniques have already been set up (Philippi et al., 2009; Schlatter et al., 2009; Saez-Rodriguez et al., 2011; Meyer et al., 2012), however, the crucial task is to combine these sub-models into a multi-scale models of liver signaling and function. The work of Krauss et al. (2012) is a recently published example of such a multi-scale model of hepatocyte signaling allowing the quantitative description of metabolic behavior in the context of time-resolved metabolite concentration profiles in the body and in the surrounding liver tissue. Huard et al. (2012) established a large-scale integrated logical model connecting multiple signaling pathways and the cell cycle in hepatocytes.

Integration of Boolean Models Following this integrative aspect, we here demonstrate the coupling of two logical models of different hepatic cell types for describing their interaction. However, for a direct combination of two mathematical models a compatible modeling approach is indispensable. Combination of Boolean models that describe different aspects of the same system is less complex compared the ODE-based model integration, although not trivial. Consistent modeling standards are required for successful combination of Boolean models, independent of the modeling tool. To encourage model convergence towards a more comprehensive overall Boolean model, we proposed conventions on node values, quantitative experimental data, time, input and output as well as on unknown components as detailed in our original paper (Schlatter et al., 2011). We applied the model integration strategy for the liver cell and its cell-cell interactions as exemplified in the following. Cell-type specific SBML models were set up with CellDesigner Version 3.5.1 and their interplay analyzed using SQUAD.

Modeling Cell-Cell Interaction The liver is a multi-cellular organ, comprising hepatocytes and Kupffer cells (Bouwens et al., 1992) among other cell types. We demonstrate here the direct unification of Boolean models of both these cell types by considering aspects of their inter-cellular interaction (Figure 48).

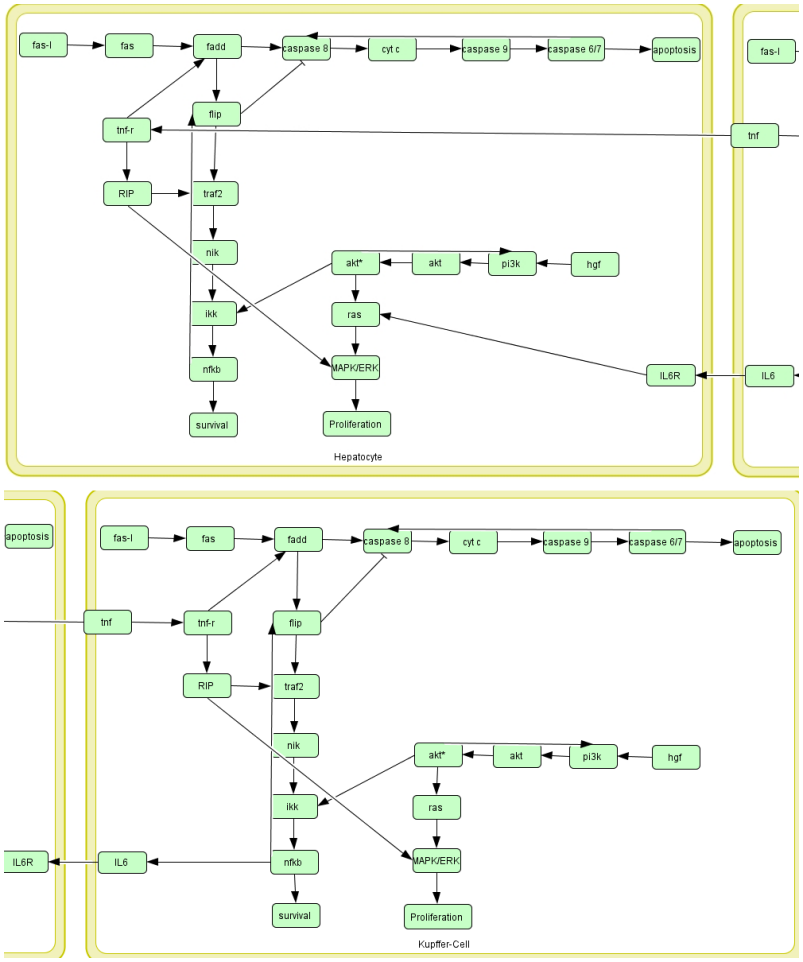

Figure 48 : Topology of the cell-cell interaction network. Hepatocyte-related signaling pathways (apoptosis, proliferation and survival pathways) are shown on the top. Pathways related to the Kupffer cell are shown on the bottom. Two interactions (TNF, IL-6) manifest the inter-cellular interplay connecting both cell types. (Schlatter et al., 2011)

The integrated model was set up on the basis of a mathematical logically connected model, published earlier by our group (Philippi et al., 2009), that models Fas ligand (FasL)-mediated apoptosis in liver cells. SQUAD-based sampling over different network states identified four robust and stable system states including cell survival and apoptosis. Moreover, the model reproduced a number of different conditions around apoptosis involving effects of different growth substrates and viral infections.

First, the signaling of both hepatic cell types was described by a similar model of the FasL, TNF and IL-6 signaling cascades. Thereby, we focused on the Fas-mediated extrinsic apoptotic pathway, the survival pathway that is correlated to NFκB and on the Ras-/MAPK-triggered proliferative pathway. Concerning cell-cell interaction, the integrated model considers two connecting pathways between hepatocytes and Kupffer cells. On the one hand, the activation of NFκB in Kupffer cells goes along with a secretion of IL-6, that itself binds and activates the corresponding IL-6 receptor in hepatocytes. Subsequently, this evokes the activation of the Ras-/MAPK-dependent proliferative pathway in the hepatocyte. On the other hand, secreted TNF from Kupffer cells activates the TNF-R1- induced anti-apoptotic signaling in hepatocytes, forming another way of inter-cellular interplay.

System States Steady state analysis using SQUAD revealed that the integrated cell-cell interaction model demonstrates four different stable states (Table 9).

Table 9: Steady state analyis of the combined cell-cell interaction model. All key nodes are listed together with their activation values for each calculated stable steady state. Values 1 denotes full activation and 0 indicates inactivation. Pathway classifications are only for demonstration issues as in fact, the exact differentiation between the pathways is not trivial. Table: Schlatter et al. (2011).

Steady state	**1**	**2**	**3**	**4**	**Pathway**
Apoptosis	0	0	1	0	Apoptosis
Caspase6/7	0	0	1	0	Apoptosis
Caspase8	0	0	0.93	0	Apoptosis
Caspase9	0	0	1	0	Apoptosis
CytC	0	0	1	0	Apoptosis
IL6	1	1	0	0	Inflammation
IL6R	1	1	0	0	Inflammation
MAPK/ERK	0.93	0.91	0	0	Proliferation
Proliferation	1	1	0	0	Proliferation
AKT	1	0	0	0	Cytoskeleton
AKT*	1	0	0	0	Cytoskeleton
FLIP	0.93	0.93	0	0	Apoptosis
IKK	1	0.93	0	0	Inflammation
NFκB	1	1	0	0	Inflammation
NIK	1	1	0	0	Inflammation
PI3K	0.93	0	0	0	Phosphatidylinositol
RAS	1	0.93	0	0	Proliferation
Survival	1	1	0	0	Survival
TRAF2	0.91	0.91	0	0	Apoptosis

Steady state 1 and 2 are characterized by inactive apoptotic nodes, whereas all nodes of the survival pathway and proliferative nodes are active. Both states can be distinguished by considering the activation of the proliferative pathway. In steady state 1, all activation values of the model nodes except the caspases are positive, denoting activation, and the hepatocyte gets its proliferative signal via hepatocyte growth factor (HGF)-induced stimulation. In contrast, Akt as well as PI3K are inactive in steady state 2, and the hepatocyte gets its proliferation signal from IL-6-triggered stimulation from the Kupffer cell. Considering steady state 3, solely apoptotic nodes are active whereas proliferative and survival nodes are inactive. Finally, steady state 4 represents the balanced state, where all nodes are inactive. Transferred to the physiological level, this situation guarantees stable population of the liver since proliferation and apoptosis are each in cell-specific equilibrations, adjusted by overarching interactions.

Model Simulations The complete cell-cell interaction model directly connects the seperate models and integrates inter- and intra-cellular interactions. It therefore allows model-based simulations of cell-specific signaling as well as the interplay thereof. This offers a dynamic view of how the two different cell types responds with apoptosis (Figure 49) or proliferation and how IL-6 or TNF may influence this interactions.

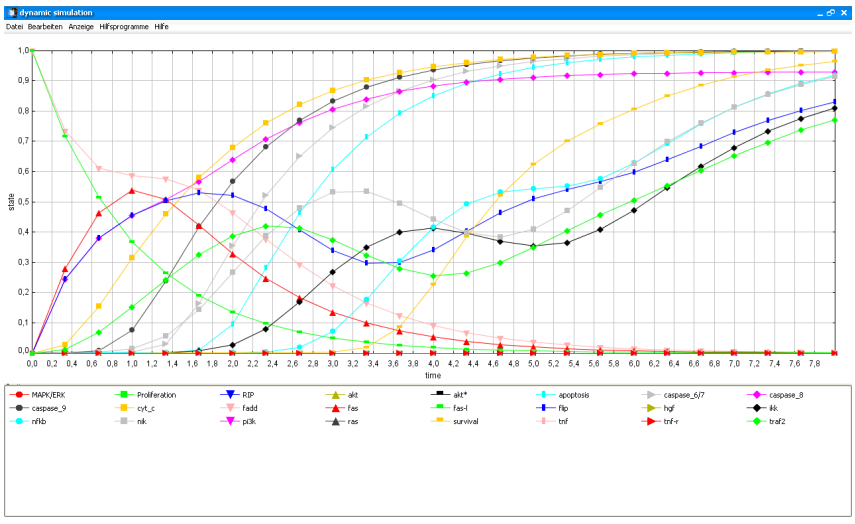

Figure 49: Dynamic simulation. SQUAD simulation of apoptosis in hepatocytes based on the integrated model of two hepatic cell types. Activation values for network nodes are calculated in a time-resolved manner and normalized (values between 0 and 1). One time unit of the simulation (1.0 units) corresponds to one day of hepatocytes in culture as shown according to experimental data. Figure: Schlatter et al. (2011)

Depending on the stimulatory conditions, four distinct system states describe here the principal course of the resulting behavior of the composed cell system. Albeit it is a strong simplification to focus on just two intercellular interactions while describing a interacting cell system, the model represents a valuable approximation: The two key interactions that were chosen to describe the cellular interplay were found to be important in cell co-cultures of hepatocytes and Kupffer cells (Schmich et al., 2011). Moreover, current experimental data available from this system are compatible with the presented behavior that can be concluded from the model. The model predicts well the behavior of hepatocytes under different cultivation conditions regarding viability and apoptosis as well as the intrinsic and extrinsic pathway (Philippi et al., 2009). From that we conclude that the demonstrated strategy for model integration represents a valuable tool to get insights into the mutual interplay of two distinct cell types.

The presented combined model is part of the publication entitled "Integration of Boolean models exemplified on hepatocyte signal transduction" (Schlatter et al., 2011). It reviews in detail the approach of Boolean modeling in cell signaling and presents a strategy for combining distinct Boolean models. The suggested strategy finds its application in two examples of model combination. I scientifically contributed to this study in giving an extensive comparison of existing methods for Boolean modeling and dynamic transformation of discrete systems.

5 Discussion and Conclusion

NOW THIS IS NOT THE END.
IT IS NOT EVEN THE BEGINNING OF THE END.
BUT IT IS, PERHAPS, THE END OF THE BEGINNING.

(*Winston Churchill*)

5.1 Platelet Systems Analysis

5.1.1 Applied Approaches

We introduced a general picture of how mathematical modeling can be applied while studying signaling cascades in thrombocytes, especially in human platelets (Section 4.1). We presented models of platelet signaling that range from large-scale protein-protein models super-imposed with phosphorylation data (Section 4.1.2) over a discrete Boolean network model (Section 4.1.3) to focused continuous ODE-based models (Section 4.1.4). Different modeling approaches serve as a basis for a comprehensive systems analysis of platelets. Each approach bears its predictive power varying from global, interaction-based insights over qualitative to a quantitative description of signaling cascades. The choice of the appropriate modeling approach is highly dependent on the modeling task but also preset by the amount, type and quality of experimental data about the pathway, its components and its interactions. Because of that, the model needs to be validated and adapted in a data-driven way to ensure the reliability of the model-based predictability. Different modeling approaches for the systemic analysis of platelet signaling and results thereof are discussed in detail in the following.

Integrated Networks We started with a static view of signaling network modeling to further describe, analyze and predict platelet functioning. The complexity of signal transduction networks, as outlined before, originates from the large number of interactions and from non-linear network topologies motivating mathematical modeling and network analysis to get deeper insight into the behavior of such networks. Characterizing protein-protein interaction (PPI) networks establishes the global view. PPI networks can be visualized as undirected graphs where nodes represent individual molecular entities (proteins) and edges denote potential interactions within this network. As time is excluded as a parameter, PPI networks are mainly used to statically describe the topology of a network which can by analyzed by means of graph theory. Nonetheless, the analysis of PPI networks sustain the identification of so far unknown interaction partners in the network hence placing functionally uncharacterized proteins in a biological network context as it has been shown for different organisms (Guruharsha et al., 2011; Stelzl et al., 2005; Uetz et al., 2000).
As anucleate platelets are not genetically manipulated, signal transduction mainly occurs through phosphorylation events. Therefore, we superimposed PPI networks and subnetworks thereof, representing functional entities, with phosphorylation data available via *PlateletWeb*. This results in directed graphs, indicating the direction of the transmitted signal flow. Directed networks offer a link between structural properties and their dynamics through e.g. network motifs, forming basic building blocks and patterns such as feed forward loops (Milo et al., 2002). Information of phosphorylation and dephosphorylation is replenished by kinase predictions. Thereby, potential substrate candidates of pivotal platelet kinases such as PKA and PKG can be placed in the functional network context, as we exemplified for platelet activation or inhibition.
Hence, static approaches are particularly informative at the beginning of platelet studies in advancing biological questions like how potential substrates of key kinases can be regulated.
Integrated network analysis together with kinase predictions represent a useful approach for functional exploration of candidate proteins and phosphorylations especially in cases that are not easily accessible by experiments. However it is limited in its predictive power, particularly concerning the dynamic and quantitative behavior of the modeled signaling pathway.

Boolean Modeling We presented a Boolean model of gradual platelet activation, describing and simulating the stepwise activation towards platelet aggregation. Boolean networks become applicable to unravel the dynamical rules that govern biological networks, especially when dynamical parameter values are available only to a minor extend - still a common bottleneck for simulating and predicting the dynamics of signaling networks. Therefore, the Boolean approach is intuitive and well suited to simulate and reproduce the qualitative behavior of networks of cell signaling and has been frequently applied (cf. Morris et al. (2010)).
A dynamic model of platelet phosphoinositide and calcium regulation (P2Y1 activation) has already been established by Purvis et al. (2008), but it only covers a sub-part of platelet activation. In contrast, we focused on the modeling of the gradual platelet activation ultimately leading to platelet aggregation. As information and data on the kinetics have been insufficient to establish a dynamic model to quantitatively predict the signal cross-talk between platelet inhibition and activation and to discriminate between the activation steps, we focused on the Boolean approach combined with time-resolved dynamic simulations using SQUAD (see Section 3.2 and 3.3). Moreover, our group was one of the first to apply the promising combination of Boolean (here multi-valued Boolean) with subsequent semi-quantitative dynamic modeling to cell signaling networks (Philippi et al., 2009).

Multi-valued Boolean Model Boolean models belong to the class of qualitative logical networks used as abstract descriptions where system components are either present or not and dependent on the state of other components of the system. Regarding modeling discrete system behavior, a system is characterized by its states, and by its behavior, which can be interpreted as activities that define a sequence on the set of states. Though Boolean modeling delivers a highly simplified view on the respective system, it has the advantage that no detailed kinetics are necessary and that fast changes can be monitored as different system states. Simulations aim at reproducing the activity of the system entities and thereby monitor the network performance. Via discrete simulation, we here observed the gradual activation steps leading to the activation changes of the system states depending on different initial conditions. To assess the different graduated activation levels we implemented a multi-valued Boolean network. In comparison to pure binary states of Boolean network models, states can be fanned out to a wider range of positive integer-valued values. Simulations of the multi-valued model

indicate and highlight different sub-parts of the network of platelet activation, becoming important during the separate activation phases. In the early phases 0, 1 and 2, the system changes occur rapidly. Such fast kinetics are challenging in terms of time-resolved measuring and dynamic modeling. However, the respective time phases could be directly verified by different phosphorylations and phosphorylation monitoring.

Data-based Dynamic Modeling ODE-based dynamic modeling has emerged as a promising approach for mimicking and analyzing biological systems and signaling pathways (Swameye et al., 2003; Hoffmann et al., 2002; Witt et al., 2009; van Riel, 2006). This approach allows data-based investigation and in particular quantitative predictions of pharmacological effects on cellular signaling cascades in detail. In general, it is most appropriate for investigating moderate-sized networks, where sufficient data are available for model validation and to estimate model parameters in an identifiable way.
In this sense, the cyclic nucleotide signaling pathway in human platelets is especially well-suited for such an approach as there is detailed information on the kinetics *a priori* available connecting the key components.
We present here a mathematical model, based on existing biological knowledge as well as on an extensive set of experimental measurements (cAMP levels). Integrating the *in vitro* data by applying the powerful approach of multi-experiment fitting, we optimized unknown model parameters. We thereby not only estimate predictive model parameters but also statistically verify the validity of a given model (Maiwald and Timmer, 2008; Coleman and Li, 1996). Additionally, this serves as a foundation for data-based discrimination between competing model hypotheses (Cox and Hinkley, 1994). We thereby identified the most parsimonious model explaining the entire set of N = 155 experimental data points (triplicates of cAMP measurements). Models on thrombosis or endothelial function have already been published (Wang et al., 2007b; Xu et al., 2011b) as well as mechanistic models (Wootton et al., 2001; Xu et al., 2008). But we are the first to investigate and model the fine-tuned cAMP mediated signaling in the platelet in detail and in a dynamic, data-based approach.

5.1.2 Model-based Results

Results: Integrated Networks

Network Context and Platelet-specificity Based on protein-protein interaction networks, we here applied an extended, integrative approach. With the *PlateletWeb* knowledge base (Boyanova et al., 2012), we have a unique assembly of data bases and additional information at hand to conduct an integrative platelet-specific network analysis as well as to guide further experiments concerning regulatory questions in human platelets. We showed how potential substrates of PKA and PKG can be integrated into such a PPI network. This results in directing further experiments thereon by providing a functional and platelet-specific network context (e.g. platelet activation, inhibition). Following this approach, our group could predict CLK1 as the kinase responsible for phosphorylating Ser269 on DOK1, a yet functionally uncharacterized phosphorylation site in unstimulated human platelets (Boyanova et al., 2012). DOK1 and its phosphorylation function as a switch for integrin activation as detected in various tissues and cell types (Calderwood et al., 2003) and has also been investigated by means of a rule-based modeling approach (Geier et al., 2011). Kinase CLK1 is expressed in megakaryocytes, proplatelets, and platelets (Schwertz et al., 2006) and can be inhibited by debromohymenialdisine (Bullock et al., 2009), a drug being associated with anti-Alzheimer and anti-osteoarthritis treatment.

Results: Discrete Dynamic Model of Gradual Platelet Activation

Dynamic Transformation and Simulation As outlined before, Boolean networks are mainly qualitative in nature and hence may not cover all features that govern the signaling dynamics. This is partially due to the fact that Boolean networks do not represent realistic time-scales and continuous concentrations of the signaling and its components. The dynamic transformation of our logically connected model into a dynamic system using SQUAD allows the introduction of time-scales and concentrations, albeit in a normalized, semi-quantitative way. Transformed into a continuous dynamic model, its simulations also revealed the necessity of inherent feedback loops for successful platelet aggregation (Mischnik et al., 2013). Furthermore, the transformation allows tracing an activating (GPVI signal) or inhibiting stimulus (PTGDR signal) throughout the network in a dynamic

way. Following a GPVI trigger, the model reacts with activating signaling components being necessary for platelet aggregation and shape change. For the irreversible activation however the increase in input strength by autocrine messengers like ADP and thromboxane is necessary. Physiological conditions also mirror this observation, as the migration of cytosolic vesicles to the plasma membrane is realized by a time-consuming cytoskeletal transport. This needs to be accompanied by at least one additional positive feedback in order to force the platelet to aggregate irreversibly, even in the absence of an inhibitory input. Physiologically, either calcium entry via SOCE or autocrine thromboxane production can accomplish this. Being stimulated with both activatory and inhibitory input signals, the system has to be stabilized by integrin outside-in signaling and a subsequent release of thromboxane to pass the threshold towards irreversible aggregation. Discrete and continuous simulations show that several sub-networks increase the system stability which underpins the platelet's enormous susceptibility to versatile inputs which are integrated over different receptors.

Threshold Behavior and Application Combinatorial effects demonstrate that the relative activating strength ($GPVI_{thr}$/PTGDR) transgressing the threshold diminishes with elevating inhibiting inputs (Mischnik et al., 2013). Thus, the system adapts for higher prostaglandin-concentrations by increasing its sensitivity for activators such as von Willebrand factor and collagen. Thereby it commits platelet-dependent active processes like wound healing even if subsequent prostaglandin-levels in the blood are augmented afterwards. In a model-based way, different efficiencies for various combinations of agonists and antagonists regarding platelet activation can thus be compared, following either over- or sub-threshold behavior. This approach can concretely be applied to model the effect of different prostanoid receptor antagonists that have been experimentally compared for therapeutic strategies (Jones et al., 2011). In general, it can be adapted to various pharmacological conditions, e.g. effects of Aspirin, Milrinone or Iloprost, while modifying the activity of network nodes.

Results: Data-based Dynamic Model

PDE Concentrations Experimental data integrated in a mathematical model can serve as a basis to gain a deeper insight into the basic effects of platelet cyclic nucleotide signaling and the underlying kinetics. Here, simulations of the basal *in silico* model indicate that there is only a very small fraction of the PDEs enzymatically active under resting conditions compared to experimentally measured values (Wangorsch et al., 2011). We speculate that this might be a result of PDE compartmentalization which has been observed for adipocytes (PDE3), HEK293 cells and cardiac myocytes (PDE4) as well as for PDE5 in platelets (Wilson et al., 2008; Baillie, 2009; Houslay, 2010; Shakur et al., 2000).

Pathway Integration Focusing on VASP, a prominent PKA and PKG substrate, we monitored the integration of both branches of cyclic nucleotide signaling in human platelet (cAMP- and cGMP related). Signal integration by the VASP protein, an intensively connected hub protein, relies on the activation of the downstream cytoskeletal regulating signaling cascade (Geiger et al., 2010; Dittrich et al., 2010). Taking into account the differential regulation of the two main known phosphorylation sites of PKA and PKG, respectively (Ser157 and Ser239), we accurately predict and experimentally validate the evoked downstream activation in quantitative terms of specific PKA-mediated phosphorylations on the VASP protein (Wangorsch et al., 2011).

Anti-platelet Drugs and Drug Combinations As platelets play a key role in thrombosis and hemostasis, the maintenance of the intricate balance between activation and inhibition is highly important as well as the avoidance of accidental activation of platelets. Thus, the inhibitory pathway represents a promising starting point for pharmacological fine-tuning of the hemostatic system.
A variety of pharmacological substances affecting cAMP signaling in human platelets (anti-platelet drugs) are in clinical use. They mainly have an impact on the most prominent mechanisms of anti-platelet therapy: the inhibition of P2Y12 receptors (Clopridogrel, Prasugrel, Ticlopidine), of COX1 and thromboxane (Acetylsalicyclic acid), of platelet PDEs (Dipyridamole, Cilostazol, Milrinone) as well as antagonistic effects on integrin αIIbβ3 (Ti-

rofiban, Eptifibatide, Abciximab) (Michelson, 2010; Rao and Xi, 2009). Antagonists of platelet prostaglandin receptor EP3 or ACs as potential drug targets are currently under development (Rao and Xi, 2009; Pierre et al., 2009). Anti-platelet therapy potentially benefits of the over-additive effect of platelet drugs when applied in combination (Michelson, 2010; Lobato et al., 2006). Thus, the investigation of drug interactions (Mackenzie et al., 2010) *in vitro* as well as *in silico* may finally result in decreased drug dosages and undesirable side effects such as bleeding. Hence, an in-depth understanding of the interactions and effects of substances affecting platelet activation and inhibition is not only of scientific interest but also of clinical importance. Having calibrated the model with experimental time-resolved data of different drug effects, we succeed in predicting not only the effect of single drugs but combinations thereof (Wangorsch et al., 2011). Modeling synergistic, additive or antagonistic drug interactions represents a challenging task (Yan et al., 2010; Geva-Zatorsky et al., 2010). We captured combinatorial drug effects by introducing just one unique cAMP-dependent parameter, offering different types of interactions which become apparent on the cAMP level. Albeit the assumed simplification led to reliable and robust predictions compatible with the observed experimental data, we are aware that more complex effects and different modes of action have to be implemented depending on the range of considered anti-platelet drugs.

Feedback-regulated cAMP Level The system analysis based on experiments of platelet stimulation with anti-platelet drugs points to a pivotal role of feedback effects towards AC and PDE. It has been observed that PKA, activated by elevated cAMP concentration, induces the inhibition of AC but activates PDE3 as well (Iwami et al., 1995; Murthy et al., 2002; Hunter et al., 2009). A short-term feedback regulation of cyclic nucleotide concentrations evoked by activation of cAMP-dependent PKA have been indicated in different cell types (rat hepatocytes, adipocytes, myoblasts, smooth muscle cells, osteoclasts, U937 cells) and also in platelets (Macphee et al., 1988; Murthy et al., 2002; Corbin et al., 1985; Gettys et al., 1988; Ball et al., 1980; Alvarez et al., 1995; Ahlstrom and Lamberg-Allardt, 1997) underpinning the ubiquitous nature of this mechanism. The PKA-driven activation of PDE3A and PDE4A has been observed in smooth muscle cells (Murthy et al., 2002). Moreover, it is known that PDE3A is phosphorylated by PKA at phosphosite Ser312 in a response to Forskolin treatment (Pozuelo Rubio et al., 2005)

which entails the activation of PDE3A in human platelets (Macphee et al., 1988). Our model results indicate a greater impact of AC inhibition by PKA-mediated phosphorylation. This inhibitory effect has already been described for adenylyl cyclase subtypes 5 (AC5) and 6 (AC6) in smooth muscle cells (Murthy et al., 2002). Besides the expression of AC subtype 3 and 7 in human platelets, platelet proteomics data indicate the expression AC5 and AC6 as well. Thus, a direct phosphorylation of AC5 or AC6 subtypes by PKA may contribute to the feedback inhibition of cAMP synthesis in human platelets (Iwami et al., 1995; Chen et al., 1997).
Statistical model selection revealed that both described feedback regulations are to be involved to achieve optimal signal strengths becoming apparent on the cAMP level in human platelets. Our data suggest that the inhibitory effect on AC thereby outweighs the positive feedback effect on PDE3 (Table 7).

Cross-talk Raised concentrations of cyclic nucleotides potently contribute to platelet inhibition via targeted cyclic nucleotide-dependent protein kinases (PKA, PKG) which in turn affect and phosphorylate their specific substrates. Via cAMP degrading phosphodiesterases, cGMP is capable to regulate the cAMP level in cardiac cells including platelets (Zaccolo and Movsesian, 2007; Schwarz et al., 2001). Referring to this, we show system state transitions from the non-activated cAMP pathway in platelets to an activated state as well as inhibitory and activatory cross-linking directed from cGMP- and cAMP-branches of the pathway (Figure 37). Data showed that the cAMP pathway is highly specific in human platelets. Even at comparatively high cAMP levels no cross-talk to the cGMP pathway is observed, validated here including experimental measurements.
In contrast, cGMP is known to interact with the cAMP pathway (Aktas et al., 2002; Schwarz et al., 2001), mainly by activating PDE2 and inhibiting PDE3. We speculated on this cross-talk and future model extensions will focus on a data-driven integration of the cGMP branch. Preliminary time-resolved cGMP data have already been collected by our collaborators (team of Dr. Stepan Gambaryan) at the Institute for Clinical Biochemistry and Pathobiochemistry. The quantification and in-depth understanding of cGMP-mediated cross-talk effects is of high clinical relevance, not only in platelets but also in cardiac muscle cells (cardiomyocytes). Here, one has to discriminate between an acute and chronic stimulation of the cAMP pathway (Fischmeister et al., 2006). In the heart, cAMP plays a pi-

votal role in the sympathetic nerve/β-adrenergic receptor (β-AR)/adenylyl cyclase (AC)/protein kinase A (PKA) axis that stimulates cardiac rhythm as well as contractile force and relaxation (Bers, 2002). While an acute stimulation of the cAMP pathway is beneficial for the heart, a sustained activation leads to hypertrophic growth, ventricular dysfunction and to heart failure (Movsesian and Bristow, 2005; Port and Bristow, 2001). In human, different forms of chronic heart failure are all associated with elevated catecholamines (Wehrens et al., 2005; Lohse et al., 2003; Brodde et al., 2006). Catecholamines such as epinephrine, norepinephrine and dopamine stimulate β-adrenoceptor signaling evoking raised cAMP levels and thus PKA activation. To prevent this, blockers of the β-AR are normally administered, which are on the one hand cheap but on the other hand often not well tolerated by the patient and affect globally the entire β-adrenoceptor signaling pathway which bears side-effects. Other starting points to pharmacologically modulate the signal response via β-AR in a more specific way represent the cAMP-degrading PDEs or PKA-affecting steps. Among the PDE isoforms expressed in the heart, PDE2 is unique in being potently stimulated by cGMP, e.g. induced by atrial natriuretic peptide (ANP) (MacFarland et al., 1991). PDE2 activity and ANP production (Takahashi et al., 2003) have been shown to be impaired in human and experimental heart failure. Thus, the research group of Prof. Ali El-Armouche at the Heart Centre Göttingen hypothesizes that a reinforcement of PDE2 may restore part of the dysfunction in the cAMP signaling under heart failure conditions and may protect against arrhythmias. This interesting project will be accompanied by model-based predictions on the impact of cAMP-affecting cross-talk of cGMP, adapting our platelet-focused model to the appropriate conditions in cardiomyocytes. Once calibrated, the model allows the testing of hypotheses supporting the process to answer the question whether enhancing PDEs is a worthwhile therapeutic strategy.

5.2 Modeling Inflammatory Signaling

Modeling Cross-talk between Signaling Pathways Modeling and investigating specific signaling cascades or even parts thereof in a separate manner is useful and can reveal novel regulatory cell-biological insights. The presented model of cAMP signaling pathway as sub-branch of platelet cyclic nucleotide signaling cascade (Section 4.1.4) or mathematical models of the IκB-NFκB- module (Hoffmann et al., 2002) constitute representative examples in this dirtection. However, to understand a cell's systemic response e.g. the overall NFκB activation with respect to inflammation, it is indispensable to consider the signaling cross-talk between the distinct cascades. This becomes particularly evident in addressing apoptotic cross-talks (Fotin-Mleczek et al., 2002; Nakayama et al., 2002). In particular, the apoptotic cross-talk is measurable and quantifiable which is crucial for model calibration and validation.
Multi-valued Boolean model simulation could precisely reproduce the differential effects on NFκB activation and apoptotic cross-talk of TNF-R1 and TNF-R2 (Table 8). Thus, mathematical modeling underpins experimental observations and could serve as a basis for further investigations and for predicting hypotheses of molecular regulations. However, to describe the cross-talk events more precisely, detailed and more specific data are needed not only to further distinguish the receptor effects, but also to validate the already established model. TWEAK stimulation data (gained from Fn14-transfected cells) in combination with TNF-R1 stimulation is of special value as the TWEAK/Fn14-system acts similarly compared to TNF-R2 signaling but TWEAK acts specifically on Fn14. As time-resolved data are available, the model can be trained against and be extended to describe cross-talk dynamics in more detail, as McClean et al. (2007) could realize for the MAP kinase pathways and cross-talk thereof.
Moreover, a detailed understanding of the underlying apoptotic cross-talk is also of great value for therapeutic interventions and represent potential drug targets (Pezzino et al., 2011; Faustman and Davis, 2010). Exemplary, Vince et al. (2008) could show that the Fn14 receptor is expressed by most tumor cell lines and IAP antagonists are beneficial as tumor therapy.

Modeling Cluster Formation We presented a mathematical model to illustrate different scenarios of TNF receptor cluster formation upon ligand binding. The phenomenon of receptor clustering is not restricted to mem-

bers of the TNF receptor family. It is a generally observed process during cell signaling (Stel et al., 2007; Feng et al., 1998; Torres et al., 2011). However, the TNF-R1 and TNF-R2 systems are of key importance as they mediate and regulate NFκB activation, a pivotal transcription factor for several cellular processes.

It is especially the first step of signaling cascade, thus the ligand-receptor-binding, that is crucial for the amplitude and formation of the signal to be transduced. Therefore, a detailed understanding of signal creation at this level is highly important also in the sense of pharmacological intervention. However, identifying receptor properties that tightly determine the processing of ligand-encoded information is still a bottleneck in cell signaling studies. Becker et al. (2010) revealed in a systems biological study the dynamic characteristics of the erythropoietin receptor during signal processing. They used mathematical ODE-based modeling of quantitative data together with experimental validation to investigate the receptor properties. The ODE-based approach however fails in modeling cluster formation, as generally spatial effects or structural features of molecules are neglected. This is mainly due to the fact that each and every state of the molecule and its interactions require a concrete deterministic description. This way, modeling would face a tough combinatorial complexity when addressing cluster formation. Because of that, we opted for the rule-based approach, which is appropriately suited for the structure-orientated modeling task. It has already been successfully applied in a variety of cell signaling studies (Geier et al., 2011; Monine et al., 2010; Hsieh et al., 2010).

On the basis of rule-based modeling, we could simulate the signal processing at TNF-R1 and TNF-R2, using the resulting cluster size as indicator for the processed signal strength. TNF-R2 is different to TNF-R1 as it offers a broad range for evoking TNF-mediated signals. Together with the potential apoptotic cross-talk to TNF-R1 signaling, this renders TNF-R2 a potential drug target. Experimental and computational unraveling the detailed structure of TNF-R2 as well as manipulative contact points to modulate cluster formation may sustain the development of receptor-specific therapies (Mukai et al., 2010). Equally, a meticulous investigation of the PLAD structure of TNF-R1 with respect to cluster formation has led to an improvement in the treatment of autoimmune diseases (Wang et al., 2011).

5.3 Cell Signaling - Models in Different Cell Types

5.3.1 Linking Inflammation and Cardiac Damage

Cardiomyocytes bear several points where mathematical modeling can operate in order to beneficially sustain biomedical research. We mentioned PDE2 and its regulation via cross-talks as a promising target for modulating β-adrenergic receptor signaling. Here, we focused more on inflammation that is highly cross-linked to cardiac damage. TWEAK and inflammatory cytokines in general are supposed to represent new potential drug targets (Givertz and Colucci, 1998; Winkles, 2008). We demonstrated that TWEAK treatment affects infarct size after ischemia reperfusion as well as the distribution of immune cells and leads to the upregulation of genes being important for recruitment (namely MIP2, MCP-1 and MCP-5) and differentiation of leukocytes (IL-5, IL-12 and IFNγ).
By setting these genes into a functional network context, we revealed that TWEAK stimulation interacts with the TNF pathways potentially changing the balance between proliferation and apoptosis. TWEAK tightly regulates the activation of NFκB which, together with Rac1, link cytokines and the JAK/STAT pathway. This connections and pathway inter-linkage could not have been detected from data alone. The network based approach may serve as a basis for the creation of further model-based predictions. Exemplary, this may address the hypothesis whether and to what extent TWEAK-induced apoptotic cross-talk, e.g. to TNF-R1-mediated signaling, is engaged (Nakayama et al., 2002). Moreover, this potential cross-talk pin-points to the increased cardiac ruptures that have been observed under TWEAK treatment conditions. Here, one can also speculate if platelets are involved in the occurrence of cardiac ruptures, as human platelets contain and release TWEAK (Meyer et al., 2010). In general, transferring results that were gained from mice to human is challenging and not trivial. That is why our group is currently developing a mouse-specific knowledge base.

5.3.2 Modeling in Plant Signaling and Immunity

Approach Networking of hormones is a newly emerging aspect in the field of plant immunity where the interplay between growth regulators and stress-specific hormones modulate plant-pathogen interactions. Pathogen infection, as presented in our study on *Pst*, thereby profoundly alters the hormonal profile as well as the network dynamics of the plant cell (Naseem

et al., 2012). Thus, dynamic modeling is a valuable approach for elucidating and a better understanding of hormonal implications in plant immunity. Several mathematical models of plant signaling networks have emerged. Plant signaling models range from logical (Espinosa-Soto et al., 2004), over ODE-based models (Agrawal et al., 2004) to stochastic (Guerriero et al., 2012) and multi-scale models (Grieneisen et al., 2007).
We applied the promising combination of Boolean modeling and dynamic transformation of the resulting logically connected network to simulate and model plant signaling cascades. This is especially appropriate as kinetic data itself are scarce on the complex hormonal interplay. Moreover, the combination of both approaches is ideal to investigate synergistic or antagonistic effects of hormones as shown here for auxin and cytokinin. Respective hormonal or pathogenic factors that serve as input (stimulus) can simply be assigned by activation values of a desired degree, whereas all other factors are switched off by setting them to value zero. Thereby, various effects to the host plant can be investigated and speculated on. We showed several simulation studies with respect to cytokinin, being one of the most important, but immunologically least deciphered plant hormones.

Model-based Results The presented modeling approach illustrates the impact of integrating bacterial effectors and host hormonal cues. The sampling over the whole network documents the eventual outcome for the entire host-pathogen system.
Model simulations revealed the impact of plant hormones on *Pst* infection. JA, auxin and ABA reduce *Pst*-mediated PR1 activation and promote susceptibility, whereas SA and GA further increase PR1 activation and enhance resistance (Figure 46A). Moreover, model-based predictions of increased plant cytokinin with/without the addition of *Pst* regarding plant immunity revealed a boosting effect on plant immunity (Figures 46B). Experiments supported these findings by showing reduced disease symptoms with abrogated *in planta* bacterial multiplication as well as by monitoring higher expression of marker PR1 upon treatment with cytokinin. Additionally, increased cytokinin levels are found to enhance resistance to *Pst* in transgenic plants (Choi et al., 2010) and *Pst tabaci* (Grosskinsky et al., 2011), whereas decreased cytokinin level indicated a reduced expression of marker PR1 (Uchida and Tasaka, 2010).

We took up the challenge to set up a logically connected network to dynamically model these various influences. Simulations reflect that modulation in plant cytokinin changes the infection dynamics in such a way that an increase in cytokinin level favors protection whereas its decrease adds to vulnerability.

The auxin-cytokinin cross-talk is quite prevalent in biological processes related to plant development and growth (Moubayidin et al., 2009; Liu et al., 2010), however literature-based information is scarce regarding its impact on plant immunity. Model-based simulation as well as the subsequent experiments helped in elucidating the interplay between auxin and cytokinin. Moreover, we could thereby reveal a carefully controlled balance of immunity and susceptibility (Figure 47A). Activation states of cytokinin over auxin direct toward resistance whereas the opposite holds true for susceptibility (Figure 47A), which could also be observed experimentally.
Cytokinin is involved in a variety of vital processes such as cell division, tissue differentiation, lateral bud growth, photosynthetic activity and floral development (Kudo et al., 2010). It is complexly engaged in cell signaling, indicating the immense potential in enhancement of crop yield (Gan and Amasino, 1995; Rivero et al., 2007). Resuming this topic, our systems biologically driven experiments and modeling suggest cross-talk possibilities for cytokinin in complex hormonal disease networks that may have implications for advanced yield protection strategies in agriculture.

5.3.3 Modeling Hepatic Cell-Cell-Interaction

Approach We showed the integration of distinct Boolean models of two different hepatic cell types in order to describe their interaction (Schlatter et al., 2011). The combination of partial models into a more comprehensive network model is a crucial move towards a broader level of understanding in the sense of systems biology. Combining dynamic ODE-based models is particularly challenging because of model and kinetic parameters. Moreover, combinatorial explosion of complexity renders a definite parameter estimation in a detailed ODE model of the whole liver cell impossible in the light of current technical possibilities.
Boolean models however allow a comprehensive understanding of the complex signaling network that governs the fate of liver cells, mainly based on the topology rather then on kinetic information. Several integrative Boolean

and discrete models on hepatic signaling have already been established. Saez-Rodriguez et al. (2011) developed a cell-specific Boolean model of immediate-early signaling networks in normal and transformed hepatocytes revealing biochemical differences in signal transduction among normal and tumor cells. Huard et al. (2012) established a large-scale logical model that integrates over a broad variety of receptors and connected signaling pathways and thus provides a broad picture of proliferation control in primary hepatocytes. Moreover, a first multi-scale model includes the quantitative description of metabolic behavior in the context of time-resolved metabolite concentration profiles (Krauss et al., 2012).
We demonstrate that the integration of logical sub-models facilitated by modeling standards is a valuable example for the next step towards a systems biological understanding. The analysis of systems response to different combined inputs or different environmental conditions (e.g. cell cultures) is a special potency that is offered by this approach. Furthermore, the impact of cross-talks is of outstanding importance for the resulting behavior of the cell and the whole organ.
We believe that the presented approach has the potential to be expanded towards a comprehensive cell-covering model structure. Critically validated and trained against biochemical data, comprehensive Boolean models can be transformed into dynamic systems. Thereby, they serve as textures for dynamic ODE-based modeling and sustain the overall long-term goal of a dynamic whole cell and a whole organ model.

Applications Besides Boolean modeling of liver signaling behavior promotes our knowledge about hepatocytes, there are also promising clinical application aspects. Exemplary, viral apoptosis blocking was demonstrated for M36 and M45 cytomegaly virus proteins (Philippi et al., 2009). Furthermore, infection evoked by cytomegaly virus as well as oncolysis by vaccinia virus have been tested (Zhang et al., 2009) and are currently investigated further. Viral infections of liver cells can be better understood on the basis of Boolean cellular models, but now with inclusion of specific cell-cell interactions. This sustains the development of new drugs in general including therapeutic approaches such as the action of an oncolytic virus (Zhang et al., 2009) on liver tissue plus metastases. SMAC-mimetics that are used as anti-cancer treatment are included in the mathematical model of apoptosis (Schlatter et al., 2009) constituting another example of a pharmacology-

driven logical model.
Combined Boolean models are beneficial in immediately generating semi-quantitative data on all involved nodes, highlighting qualitative and even cell-type specific changes in the system. Due to the inherent model features, comprehensive Boolean models can contribute to address important biological research questions. This includes the elucidation of changes induced by the cultivation of cells under distinct conditions, since this modifies the cellular properties and differentiation. Tissue engineering (Schanz et al., 2010) constitutes another field of application for cell-cell interaction models including modified Akt signaling in the different cell types.

5.4 Conclusion and Outlook

For a functional understanding of a single cell, of cellular cross-talks or even of higher organization units, it is often valuable to conceptualize and simplify them as systems of interacting elements or in other words, as models. This especially applies to the process of cell signaling. Signaling cascades play a key role in adapting the cell's behavior to environmental changes, internal stimuli or pharmacological modulation. Such a systems-level description requires knowledge about the identity of model components, their dynamic behavior (e.g. condition-dependent change of concentrations or activity over time) and the kind of interactions between the model components (Kitano, 2002). The quality, amount and accessibility of experimental data is still one of the main limiting factors, not only for model establishment but also for model validation and calibration. Thus, prior knowledge and data explicitly determine the type and scale of a model.

Within the framework of this thesis, we presented main types of mathematical models at different scales that are beneficial for investigating signaling cascades: interaction networks, Boolean models as well as dynamic ODE-based and rule-based models. Each modeling approach provides new insights into the behavior of the system. In particular, every approach bears its predictive power for either qualitative or quantitative forecasts.

Protein-protein interaction networks sustained the systemic view and revealed signaling connections and modules that were not apparent from data alone. Cytokine array data that were gained from experiments in cardiomyocytes was brought into a functional signaling context. Network-based representation advanced the data visualization and showed interconnections to different proliferative and apoptotic signaling pathways. Superimposing protein-protein networks with phosphorylation data and knowledge about drug interactions further enhanced the network information content. Connecting edges are thereby assigned by directions. This includes information about kinases that are directed to their corresponding (de)phosphorylated substrates. In this way, potential substrates of key kinases in human platelets were set in a functional surrounding. Subnetworks comprising key nodes of platelet activation and inhibition formed the basis. Thus, network-based insights sustain the functional integration of signaling proteins or small molecules and guide further experimental investigations.
The power of Boolean dynamic modeling relies on the model construction

itself. Binary model nodes, the components of a signal cascade, are logically connected. Bi-valued model nodes reflect the state "on" or "off", active or inactive, expressed or not expressed, respectively. In the context of signal cascade models, logic connections can be understood as gates through which a signal is propagated. The model structure of Boolean models renders their combination comparatively easy. We demonstrated the coupling of two distinct logic models of different liver cells. From this we conclude that Boolean models are useful precursors for large-scale quantitative models, strengthening the systemic understanding of the liver as a multi-cellular organ.

Multi-valued Boolean models represent a special subtype of Boolean models, where the binary states are fanned out to a wider range of positive integer values. The Boolean approach thereby allows predicting the outcomes of the signal system (steady states), testing of hypotheses (e.g. potential effects of different input stimuli, of knockouts or overexpressed nodes) and directing validating and promising wet lab experiments. Here, we applied Boolean modeling to understand the effect of different input signals and how they cross-talk towards differential cellular responses. First, we elucidated the gradual process of platelet aggregation. Resulting simulation experiments categorized platelet activation into different phases and assigned corresponding key nodes. Second, by applying the multi-valued Boolean approach we established an *in silico* platform for investigating the regulatory cross-talk between two different TNF receptors, TNF-R1 and TNF-R2. Experiments have shown that the signaling of TNF-R2 affects TNF-R1-mediated activation of NFκB and shifts TNF-R1 down-stream signaling to apoptosis. We successfully captured these time-dependent effects in our model that now offers the generation of testable hypotheses about dynamic cross-talk regulations at the molecular level. From these results, we can conclude that (multi-valued) Boolean networks can serve as a basis for modeling interlinked signaling networks. Moreover, detailed continuous models can be built on the foundation of logic models as kinetic and quantitative data become available.

One step towards this goal is the transformation of Boolean models to dynamic semi-quantitative systems. The rapidly increasing number of modeling approaches addressing the dynamic transformation (Stoll et al., 2012; Terfve et al., 2012; MacNamara et al., 2012; Krumsiek et al., 2010; Di Cara et al., 2007) show the need for a dynamic model-based description of sig-

naling pathways if detailed data are lacking. We applied SQUAD (Di Cara et al., 2007), one of the first approaches that evolved, to transform Boolean models and to deduce regulatory insights from dynamic simulations.
Simulation experiments elucidated and separated activatory and inhibitory signaling pathways during the platelet activation process. We concluded a threshold behavior by testing different activation-to-inhibition ratios that served as input for dynamic simulations. In the same way, we tested the impact of hormonal interplay with respect to plant immunity in *Arabidopsis*. Dynamic simulations identified and predicted systems effect and multiple cytokinin-mediated regulatory interactions in plant disease networks. Besides offering insights into the dynamics of regulatory processes, semi-quantitative model predictions are scaled to arbitrary time units and activation values between 0 and 1.

Quantitative prediction can be deduced from models that are based on ordinary differential equations. They comprise kinetic information and parameters of the modeled process. Extensive model calibration on the foundation of time series data of model components allows quantitative predictions such as concentration levels at a realistic time-scale. Sufficient data is needed to estimate unknown model parameter from the data in an identifiable way. Therefore, data-based dynamic modeling mostly focuses on specific parts of signaling pathways. In that way, we modeled the cAMP branch of the platelet inhibitory pathway. We were able to quantify key regulators in platelet signaling from model simulations. For the first time, active concentrations of cAMP-regulating phosphodiesterases could be predicted and quantified. Comprehensive calibration of the model with time-series data from cAMP-elevating drugs revealed a feed-back regulation of cAMP levels in the platelet. From statistical analyses we concluded that two feedback effects are involved. On this basis, the established model serves for quantitatively predicting various effects of anti-platelet drugs in a dose-dependent manner. Simulations deciphered synergistic effects among drug combinations and showed that the raise of cAMP-levels leaves the cGMP branch of the signaling cascade unaffected. These findings are sustained by predicting phosphorylation effects on VASP, a protein that is capable to integrate down-stream effects from both branches. The reverse cross-talk from cGMP to the cAMP branch is known. Due to the lack of dynamic data, we could not quantify the cross-talk effect but simulate the possible impact at a realistic time-scale.

Furthermore, adapting the observations we derived from the quantitative platelet model to cardiomyocytes will probably offer novel starting points for pharmacological interventions. Here, phosphodiesterases and their cross-talk between cyclic nucleotides are involved in transmitting signals from the β-adrenergic receptor that plays a pivotal role in heart failure. Quantitative model predictions of this interplay will support the investigation of new types of therapeutic strategies in this connection.

Besides the enormous predictive power of data-based dynamic models, they bear the problem of combinatorial complexity as each state of a model component has to be defined deterministically. Therefore, we opted for the structure-orientated rule-based approach for modeling cluster formation at TNF receptors. This process seems to be critical for the creation of a proper ligand-encoded signal at TNF-R1 and TNF-R2. On the basis of rule-based modeling, we could simulate the signal creation at both receptor types. The resulting cluster size thereby indicates the evoked signal strength. Together with the potential apoptotic cross-talk to TNF-R1 signaling, this renders TNF-R2 and the PLAD structure of TNF-R1 a potential drug target.

I close by referring to the famous quote of the statistician George Box:

"All models are wrong, but some are useful" (Box, 1976).

Results from this thesis show that indeed every mathematical model is "wrong" in being a simplification, or better a compromise, that weights up *a priori* knowledge and data against preciseness, predictability and computational complexity. However, by choosing the appropriate approach, models are "useful" in assigning a physiological and functional context, uncovering regulatory principles, generating testable hypotheses and model predictions. Hence, mathematical modeling and computational systems biology are and will be a substantial element in pharmacological and clinical research.

References

Abrahamsen, H., Vang, T., and Taskén, K. (2003). Protein kinase a intersects src signaling in membrane microdomains. *J Biol Chem*, 278(19):17170–17177.

Agrawal, V., Zhang, C., Shapiro, A. D., and Dhurjati, P. S. (2004). A dynamic mathematical model to clarify signaling circuitry underlying programmed cell death control in arabidopsis disease resistance. *Biotechnol Prog*, 20(2):426–442.

Ahlstrom, M. and Lamberg-Allardt, C. (1997). Rapid protein kinase a–mediated activation of cyclic AMP-phosphodiesterase by parathyroid hormone in UMR-106 osteoblast-like cells. *Journal of bone and mineral research : the official journal of the American Society for Bone and Mineral Research*, 12:172–8. 2.

Akaike, H. (1973). Information theory and an extension of the maximum likelihood principle. In *2nd International Symposium on Information Theory*.

Akaike, H. (1974). A new look at the statistical model identification. *IEEE Transactions on Automatic Control*, 19(6):716 – 723.

Aktas, B., Honig-Liedl, P., Walter, U., and Geiger, J. (2002). Inhibition of platelet P2Y12 and alpha2A receptor signaling by cGMP-dependent protein kinase. *Biochemical pharmacology*, 64:433–9. 3.

Aktas, B., Utz, A., Hoenig-Liedl, P., Walter, U., and Geiger, J. (2003). Dipyridamole enhances NO/cGMP-mediated vasodilator-stimulated phosphoprotein phosphorylation and signaling in human platelets: in vitro and in vivo/ex vivo studies. *Stroke*, 34:764–9. 3.

Albert, I., Thakar, J., Li, S., Zhang, R., and Albert, R. (2008). Boolean network simulations for life scientists. *Source Code Biol Med*, 3:16.

Aldridge, B. B., Burke, J. M., Lauffenburger, D. A., and Sorger, P. K. (2006). Physicochemical modelling of cell signalling pathways. *Nat Cell Biol*, 8(11):1195–1203.

Altschuler, D. and Lapetina, E. G. (1993). Mutational analysis of the camp-dependent protein kinase-mediated phosphorylation site of rap1b. *J Biol Chem*, 268(10):7527–7531.

Alvarez, R., Sette, C., Yang, D., Eglen, R. M., Wilhelm, R., Shelton, E. R., and Conti, M. (1995). Activation and selective inhibition of a cyclic AMP-specific phosphodiesterase, PDE-4D3. *Molecular pharmacology*, 48:616–22. 4.

Andrews, R. K., Harris, S. J., McNally, T., and Berndt, M. C. (1998). Binding of purified 14-3-3 zeta signaling protein to discrete amino acid sequences within the cytoplasmic domain of the platelet membrane glycoprotein ib-ix-v complex. *Biochemistry*, 37(2):638–647.

Anker, S. D. and von Haehling, S. (2004). Inflammatory mediators in chronic heart failure: an overview. *Heart*, 90(4):464–470.

Antl, M., von Brühl, M.-L., Eiglsperger, C., Werner, M., Konrad, I., Kocher, T., Wilm, M., Hofmann, F., Massberg, S., and Schlossmann, J. (2007). Irag mediates no/cgmp-dependent inhibition of platelet aggregation and thrombus formation. *Blood*, 109(2):552–559.

Arehart, E., Stitham, J., Asselbergs, F. W., Douville, K., MacKenzie, T., Fetalvero, K. M., Gleim, S., Kasza, Z., Rao, Y., Martel, L., Segel, S., Robb, J., Kaplan, A., Simons, M., Powell, R. J., Moore, J. H., Rimm, E. B., Martin, K. A., and Hwa, J. (2008). Acceleration of cardiovascular disease by a dysfunctional prostacyclin receptor mutation: potential implications for cyclooxygenase-2 inhibition. *Circulation research*, 102:986–93. 8.

Argueso, C. T., Ferreira, F. J., Epple, P., To, J. P. C., Hutchison, C. E., Schaller, G. E., Dangl, J. L., and Kieber, J. J. (2012). Two-component elements mediate interactions between cytokinin and salicylic acid in plant immunity. *PLoS Genet*, 8(1):e1002448.

Arrell, D. K. and Terzic, A. (2012). Systems proteomics for translational network medicine. *Circ Cardiovasc Genet*, 5(4):478.

Ashburner, M., Ball, C. A., Blake, J. A., Botstein, D., Butler, H., Cherry, J. M., Davis, A. P., Dolinski, K., Dwight, S. S., Eppig, J. T., Harris, M. A., Hill, D. P., Issel-Tarver, L., Kasarskis, A., Lewis, S., Matese, J. C., Richardson, J. E., Ringwald, M., Rubin, G. M., and Sherlock, G. (2000). Gene ontology: tool for the unification of biology. the gene ontology consortium. *Nat Genet*, 25(1):25–29.

Assmann, S. M. and Albert, R. (2009). Discrete dynamic modeling with asynchronous update, or how to model complex systems in the absence of quantitative information. *Methods Mol Biol*, 553:207–225.

Aszódi, A., Pfeifer, A., Ahmad, M., Glauner, M., Zhou, X. H., Ny, L., Andersson, K. E., Kehrel, B., Offermanns, S., and Fässler, R. (1999). The vasodilator-stimulated phosphoprotein (vasp) is involved in cgmp- and camp-mediated inhibition of agonist-induced platelet aggregation, but is dispensable for smooth muscle function. *EMBO J*, 18(1):37–48.

Aukrust, P., Gullestad, L., Ueland, T., Dam?s, J. K., and Yndestad, A. (2005). Inflammatory and anti-inflammatory cytokines in chronic heart failure: potential therapeutic implications. *Ann Med*, 37(2):74–85.

Authi, K. S. and Crawford, N. (1985). Inositol 1,4,5-trisphosphate-induced release of sequestered ca2+ from highly purified human platelet intracellular membranes. *Biochem J*, 230(1):247–253.

Authi, K. S., Evenden, B. J., and Crawford, N. (1986). Metabolic and functional consequences of introducing inositol 1,4,5-trisphosphate into saponin-permeabilized human platelets. *Biochem J*, 233(3):707–718.

Bailey, J. M., Levy, J. H., Kikura, M., Szlam, F., and Hug, C. C. (1994). Pharmacokinetics of intravenous milrinone in patients undergoing cardiac surgery. *Anesthesiology*, 81(3):616–622.

Baillie, G. S. (2009). Compartmentalized signalling: spatial regulation of cAMP by the action of compartmentalized phosphodiesterases. *FEBS J*, 276:1790–9. 7.

Ball, E. H., Seth, P. K., and Sanwal, B. D. (1980). Regulatory mechanisms involved in the control of cyclic adenosine 3':5'-monophosphate phosphodiesterases in myoblasts. *The Journal of biological chemistry*, 255:2962–8. 7.

Balsinde, J., Balboa, M. A., and Dennis, E. A. (1998). Functional coupling between secretory phospholipase a2 and cyclooxygenase-2 and its regulation by cytosolic group iv phospholipase a2. *Proc Natl Acad Sci U S A*, 95(14):7951–7956.

Banno, A. and Ginsberg, M. H. (2008). Integrin activation. *Biochem Soc Trans*, 36(Pt 2):229–234.

Barabási, A. and Oltvai, Z. N. (2004). Network biology: understanding the cell's functional organization. *Nat Rev Genet*, 5(2):101–113.

Bari, R. and Jones, J. D. G. (2009). Role of plant hormones in plant defence responses. *Plant Mol Biol*, 69(4):473–488.

Battinelli, E. M., Hartwig, J. H., and Italiano, Jr, J. E. (2007). Delivering new insight into the biology of megakaryopoiesis and thrombopoiesis. *Curr Opin Hematol*, 14(5):419–426.

Bauman, A. L., Soughayer, J., Nguyen, B. T., Willoughby, D., Carnegie, G. K., Wong, W., Hoshi, N., Langeberg, L. K., Cooper, D. M. F., Dessauer, C. W., and Scott, J. D. (2006). Dynamic regulation of camp synthesis through anchored pka-adenylyl cyclase v/vi complexes. *Mol Cell*, 23(6):925–931.

Bazzoni, F. and Beutler, B. (1996). The tumor necrosis factor ligand and receptor families. *N Engl J Med*, 334(26):1717–1725.

Beazely, M. A., Alan, J. K., and Watts, V. J. (2005). Protein kinase c and epidermal growth factor stimulation of raf1 potentiates adenylyl cyclase type 6 activation in intact cells. *Mol Pharmacol*, 67(1):250–259.

Beck, I. M. E., Vanden Berghe, W., Vermeulen, L., Yamamoto, K. R., Haegeman, G., and De Bosscher, K. (2009). Crosstalk in inflammation: the interplay of glucocorticoid receptor-based mechanisms and kinases and phosphatases. *Endocr Rev*, 30(7):830–882.

Becker, V., Schilling, M., Bachmann, J., Baumann, U., Raue, A., Maiwald, T., Timmer, J., and Klingmüller, U. (2010). Covering a broad dynamic range: information processing at the erythropoietin receptor. *Science*, 328(5984):1404–1408.

Bell, E. T. (1986). *Men of Mathematics*. Touchstone.

Bender, A. T. and Beavo, J. A. (2006). Cyclic nucleotide phosphodiesterases: molecular regulation to clinical use. *Pharmacol Rev*, 58:488–520. 3.

Bergmeier, W., Oh-Hora, M., McCarl, C.-A., Roden, R. C., Bray, P. F., and Feske, S. (2009). R93w mutation in orai1 causes impaired calcium influx in platelets. *Blood*, 113(3):675–678.

Bers, D. M. (2002). Cardiac excitation-contraction coupling. *Nature*, 415(6868):198–205.

Beyer, E. M. and MacBeath, G. (2012). Cross-talk between receptor tyrosine kinase and tumor necrosis factor-? signaling networks regulates apoptosis but not proliferation. *Mol Cell Proteomics*, 11(6):M111.013292.

Billah, M. M., Lapetina, E. G., and Cuatrecasas, P. (1980). Phospholipase a2 and phospholipase c activities of platelets. differential substrate specificity, ca2+ requirement, ph dependence, and cellular localization. *J Biol Chem*, 255(21):10227–10231.

Bilodeau, M. L. and Hamm, H. E. (2007). Regulation of protease-activated receptor (par) 1 and par4 signaling in human platelets by compartmentalized cyclic nucleotide actions. *J Pharmacol Exp Ther*, 322(2):778–788.

Blank, U., Karlsson, G., and Karlsson, S. (2008). Signaling pathways governing stem-cell fate. *Blood*, 111(2):492–503.

Blumer, K. J. and Thorner, J. (1991). Receptor-g protein signaling in yeast. *Annu Rev Physiol*, 53:37–57.

Bodnar, R. J., Xi, X., Li, Z., Berndt, M. C., and Du, X. (2002). Regulation of glycoprotein ib-ix-von willebrand factor interaction by camp-dependent protein kinase-mediated phosphorylation at ser 166 of glycoprotein ib(beta). *J Biol Chem*, 277(49):47080–47087.

Boess, F. G., Hendrix, M., van der Staay, F.-J., Erb, C., Schreiber, R., van Staveren, W., de Vente, J., Prickaerts, J., Blokland, A., and Koenig, G. (2004). Inhibition of phosphodiesterase 2 increases neuronal cgmp, synaptic plasticity and memory performance. *Neuropharmacology*, 47(7):1081–1092.

Boole, G. (1847). *The Mathematical Analysis of Logic*. Barclay and Macmillan, Cambridge.

Boole, G. (1848). The calculus of logic. *Cambridge and Dublin Mathematical Journal*, 3:183–98.

Boole, G. (1854). *An investigation of the laws of thought: on which are founded the mathematical theories of logic and probabilities.* Walton and Maberly.

Boschert, V., Krippner-Heidenreich, A., Branschädel, M., Tepperink, J., Aird, A., and Scheurich, P. (2010). Single chain tnf derivatives with individually mutated receptor binding sites reveal differential stoichiometry of ligand receptor complex formation for tnfr1 and tnfr2. *Cell Signal*, 22(7):1088–1096.

Bouwens, L., De Bleser, P., Vanderkerken, K., Geerts, B., and Wisse, E. (1992). Liver cell heterogeneity: functions of non-parenchymal cells. *Enzyme*, 46(1-3):155–168.

Box, G. E. P. (1976). Science and statistics. *Journal of the American Statistical Association*, 71:791–799.

Boyanova, D., Nilla, S., Birschmann, I., Dandekar, T., and Dittrich, M. (2012). Plateletweb: a systems biologic analysis of signaling networks in human platelets. *Blood*, 119(3):e22–e34.

Bradley, J. R. (2008). Tnf-mediated inflammatory disease. *J Pathol*, 214(2):149–160.

Braun, A., Varga-Szabo, D., Kleinschnitz, C., Pleines, I., Bender, M., Austinat, M., Bösl, M., Stoll, G., and Nieswandt, B. (2009). Orai1 (cracm1) is the platelet soc channel and essential for pathological thrombus formation. *Blood*, 113(9):2056–2063.

Briggs, G. E. and Haldane, J. B. (1925). A note on the kinetics of enzyme action. *Biochem J*, 19(2):338–339.

Brodde, O.-E., Bruck, H., and Leineweber, K. (2006). Cardiac adrenoceptors: physiological and pathophysiological relevance. *J Pharmacol Sci*, 100(5):323–337.

Broos, K., De Meyer, S. F., Feys, H. B., Vanhoorelbeke, K., and Deckmyn, H. (2012). Blood platelet biochemistry. *Thromb Res*, 129(3):245–249.

Buck, L. B. (2000). The molecular architecture of odor and pheromone sensing in mammals. *Cell*, 100(6):611–618.

Bullock, A. N., Das, S., Debreczeni, J. E., Rellos, P., Fedorov, O., Niesen, F. H., Guo, K., Papagrigoriou, E., Amos, A. L., Cho, S., Turk, B. E., Ghosh, G., and Knapp, S. (2009). Kinase domain insertions define distinct roles of clk kinases in sr protein phosphorylation. *Structure*, 17(3):352–362.

Burnham, K. P. and Anderson, D. R. (2002). *Model Selection and Multi-Model Inference: A Practical Information-Theoretic Approach*. Springer.

Butt, E., Abel, K., Krieger, M., Palm, D., Hoppe, V., Hoppe, J., and Walter, U. (1994). cAMP- and cGMP-dependent protein kinase phosphorylation sites of the focal adhesion vasodilator-stimulated phosphoprotein (VASP) in vitro and in intact human platelets. *J Biol Chem*, 269:14509–17. 20.

Butt, E., Gambaryan, S., Göttfert, N., Galler, A., Marcus, K., and Meyer, H. E. (2003). Actin binding of human lim and sh3 protein is regulated by cgmp- and camp-dependent protein kinase phosphorylation on serine 146. *J Biol Chem*, 278(18):15601–15607.

Butt, E., Immler, D., Meyer, H. E., Kotlyarov, A., Laass, K., and Gaestel, M. (2001). Heat shock protein 27 is a substrate of cgmp-dependent protein kinase in intact human platelets: phosphorylation-induced actin polymerization caused by hsp27 mutants. *J Biol Chem*, 276(10):7108–7113.

Butt, E. and Walter, U. (1997). Platelet phosphodiesterases. *Handbook of experimental pharmacology*, 126:219–230.

Cabal-Hierro, L. and Lazo, P. S. (2012). Signal transduction by tumor necrosis factor receptors. *Cell Signal*, 24(6):1297–1305.

Calderwood, D. A., Fujioka, Y., de Pereda, J. M., García-Alvarez, B., Nakamoto, T., Margolis, B., McGlade, C. J., Liddington, R. C., and Ginsberg, M. H. (2003). Integrin beta cytoplasmic domain interactions with phosphotyrosine-binding domains: a structural prototype for diversity in integrin signaling. *Proc Natl Acad Sci U S A*, 100(5):2272–2277.

Campbell, P. (1999). Can physics deliver another biological revolution? *Nature*, 397(6715):89.

Carlotti, F., Dower, S. K., and Qwarnstrom, E. E. (2000). Dynamic shuttling of nuclear factor kappa b between the nucleus and cytoplasm as a consequence of inhibitor dissociation. *J Biol Chem*, 275(52):41028–41034.

Cattaneo, M., Canciani, M. T., Lecchi, A., Kinlough-Rathbone, R. L., Packham, M. A., Mannucci, P. M., and Mustard, J. F. (1990). Released adenosine diphosphate stabilizes thrombin-induced human platelet aggregates. *Blood*, 75(5):1081–1086.

Cattaneo, M. and Gachet, C. (2001). The platelet adp receptors. *Haematologica*, 86(4):346–348.

Cer, R. Z., Mudunuri, U., Stephens, R., and Lebeda, F. J. (2009). Ic50-to-ki: a web-based tool for converting ic50 to ki values for inhibitors of enzyme activity and ligand binding. *Nucleic Acids Res*, 37(Web Server issue):W441–W445.

Chan, F. K., Chun, H. J., Zheng, L., Siegel, R. M., Bui, K. L., and Lenardo, M. J. (2000). A domain in tnf receptors that mediates ligand-independent receptor assembly and signaling. *Science*, 288(5475):2351–2354.

Chatterjee, M. S., Denney, W. S., Jing, H., and Diamond, S. L. (2010). Systems biology of coagulation initiation: kinetics of thrombin generation in resting and activated human blood. *PLoS Comput Biol*, 6(9).

Chen, G. and Goeddel, D. V. (2002). Tnf-r1 signaling: a beautiful pathway. *Science*, 296(5573):1634–1635.

Chen, M. and Stracher, A. (1989). In situ phosphorylation of platelet actin-binding protein by camp-dependent protein kinase stabilizes it against proteolysis by calpain. *J Biol Chem*, 264(24):14282–14289.

Chen, W. W., Niepel, M., and Sorger, P. K. (2010). Classic and contemporary approaches to modeling biochemical reactions. *Genes Dev*, 24(17):1861–1875.

Chen, Y., Harry, A., Li, J., Smit, M. J., Bai, X., Magnusson, R., Pieroni, J. P., Weng, G., and Iyengar, R. (1997). Adenylyl cyclase 6 is selectively regulated by protein kinase a phosphorylation in a region involved in galphas stimulation. *Proceedings of the National Academy of Sciences of the United States of America*, 94:14100–4. 25.

Chen, Z., Agnew, J. L., Cohen, J. D., He, P., Shan, L., Sheen, J., and Kunkel, B. N. (2007). Pseudomonas syringae type iii effector avrrpt2 alters arabidopsis thaliana auxin physiology. *Proc Natl Acad Sci U S A*, 104(50):20131–20136.

Cheong, R., Hoffmann, A., and Levchenko, A. (2008). Understanding nf-kappab signaling via mathematical modeling. *Mol Syst Biol*, 4:192.

Choi, J., Huh, S. U., Kojima, M., Sakakibara, H., Paek, K.-H., and Hwang, I. (2010). The cytokinin-activated transcription factor arr2 promotes plant immunity via tga3/npr1-dependent salicylic acid signaling in arabidopsis. *Dev Cell*, 19(2):284–295.

Chuang, H.-Y., Hofree, M., and Ideker, T. (2010). A decade of systems biology. *Annu Rev Cell Dev Biol*, 26:721–744.

Cicmil, M., Thomas, J. M., Leduc, M., Bon, C., and Gibbins, J. M. (2002). Platelet endothelial cell adhesion molecule-1 signaling inhibits the activation of human platelets. *Blood*, 99(1):137–144.

Cohen, J. E. (2004). Mathematics is biology's next microscope, only better; biology is mathematics' next physics, only better. *PLoS Biol*, 2(12):e439.

Coleman, T. F. and Li, A. Y. (1996). An interior trust region approach for nonlinear minimization subject to bounds. *SIAM Journal on Optimization*, 6:418–455.

Colvin, J., Monine, M. I., Gutenkunst, R. N., Hlavacek, W. S., Von Hoff, D. D., and Posner, R. G. (2010). Rulemonkey: software for stochastic simulation of rule-based models. *BMC Bioinformatics*, 11:404.

Corbin, J. D., Beebe, S. J., and Blackmore, P. F. (1985). cAMP-dependent protein kinase activation lowers hepatocyte cAMP. *The Journal of biological chemistry*, 260:8731–5. 15.

Cornish-Bowden, A. (2012). *Fundamentals of enzyme kinetics*. Wiley-VCH.

Coussens, L. M. and Werb, Z. (2002). Inflammation and cancer. *Nature*, 420(6917):860–867.

Cox, D. R. and Hinkley, D. V. (1974). *Theoretical Statistics*. Chapman & Hall.

Cox, D. R. and Hinkley, D. V. (1994). *Theoretical Statistics*. Chapman and Hall, New York.

Crittenden, J. R., Bergmeier, W., Zhang, Y., Piffath, C. L., Liang, Y., Wagner, D. D., Housman, D. E., and Graybiel, A. M. (2004). Caldag-gefi integrates signaling for platelet aggregation and thrombus formation. *Nat Med*, 10(9):982–986.

Croft, M. (2009). The role of tnf superfamily members in t-cell function and diseases. *Nat Rev Immunol*, 9(4):271–285.

Daniel, J. L., Dangelmaier, C., Jin, J., Ashby, B., Smith, J. B., and Kunapuli, S. P. (1998). Molecular basis for adp-induced platelet activation. i. evidence for three distinct adp receptors on human platelets. *J Biol Chem*, 273(4):2024–2029.

Daniel, J. L., Dangelmaier, C., Jin, J., Kim, Y. B., and Kunapuli, S. P. (1999). Role of intracellular signaling events in adp-induced platelet aggregation. *Thromb Haemost*, 82(4):1322–1326.

Danos, V., Feret, J., Fontana, W., Harmer, R., and Krivine, J. (2007). Rule-based modelling of cellular signalling. *CONCUR 2007–Concurrency Theory*, pages 17–41.

Davi, G. and Patrono, C. (2007). Platelet activation and atherothrombosis. *N Engl J Med*, 357(24):2482–2494.

de Almagro, M. C. and Vucic, D. (2012). The inhibitor of apoptosis (iap) proteins are critical regulators of signaling pathways and targets for anti-cancer therapy. *Exp Oncol*, 34(3):200–211.

De Jong, H., Geiselmann, J., Hernandez, C., and Page, M. (2003). Genetic network analyzer: qualitative simulation of genetic regulatory networks. *Bioinformatics*, 19(3):336–344.

Di Cara, A., Garg, A., De Micheli, G., Xenarios, I., and Mendoza, L. (2007). Dynamic simulation of regulatory networks using squad. *BMC Bioinformatics*, 8:462.

Diamond, S. L. (2009). Systems biology to predict blood function. *J Thromb Haemost*, 7 Suppl 1:177–180.

Dittrich, M., Birschmann, I., Mietner, S., Sickmann, A., Walter, U., and Dandekar, T. (2008). Platelet protein interactions: map, signaling components, and phosphorylation groundstate. *Arterioscler Thromb Vasc Biol*, 28:1326–31. 7.

Dittrich, M., Birschmann, I., Pfrang, J., Herterich, S., Smolenski, A., Walter, U., and Dandekar, T. (2006). Analysis of SAGE data in human platelets: features of the transcriptome in an anucleate cell. *Thromb Haemost*, 95:643–51. 4.

Dittrich, M., Strassberger, V., Fackler, M., Tas, P., Lewandrowski, U., Sickmann, A., Walter, U., Dandekar, T., and Birschmann, I. (2010). Characterization of a novel interaction between vasodilator-stimulated phosphoprotein and abelson interactor 1 in human platelets: a concerted computational and experimental approach. *Arterioscler Thromb Vasc Biol*, 30:843–50. 4.

Dohlman, H. G., Thorner, J., Caron, M. G., and Lefkowitz, R. J. (1991). Model systems for the study of seven-transmembrane-segment receptors. *Annu Rev Biochem*, 60:653–688.

Dragovich, T., Rudin, C. M., and Thompson, C. B. (1998). Signal transduction pathways that regulate cell survival and cell death. *Oncogene*, 17(25):3207–3213.

Dunkern, T. R. and Hatzelmann, A. (2005). The effect of sildenafil on human platelet secretory function is controlled by a complex interplay between phosphodiesterases 2, 3 and 5. *Cell Signal*, 17(3):331–339.

Ea, C.-K., Deng, L., Xia, Z.-P., Pineda, G., and Chen, Z. J. (2006). Activation of ikk by tnfalpha requires site-specific ubiquitination of rip1 and polyubiquitin binding by nemo. *Mol Cell*, 22(2):245–257.

Eigenthaler, M., Nolte, C., Halbrügge, M., and Walter, U. (1992). Concentration and regulation of cyclic nucleotides, cyclic-nucleotide-dependent protein kinases and one of their major substrates in human platelets. estimating the rate of camp-regulated and cgmp-regulated protein phosphorylation in intact cells. *Eur J Biochem*, 205(2):471–481.

El-Daher, S. S., Patel, Y., Siddiqua, A., Hassock, S., Edmunds, S., Maddison, B., Patel, G., Goulding, D., Lupu, F., Wojcikiewicz, R. J., and Authi, K. S. (2000). Distinct localization and function of (1,4,5)ip(3) receptor subtypes and the (1,3,4,5)ip(4) receptor gap1(ip4bp) in highly purified human platelet membranes. *Blood*, 95(11):3412–3422.

Enyedi, A., Sarkadi, B., Földes-Papp, Z., Monostory, S., and Gárdos, G. (1986). Demonstration of two distinct calcium pumps in human platelet membrane vesicles. *J Biol Chem*, 261(20):9558–9563.

Erdoes, P. and Renyi, A. (1960). On the evolution of random graphs. *Publ Math Inst Hung Acad Sci*, 5:17–61.

Espinosa-Soto, C., Padilla-Longoria, P., and Alvarez-Buylla, E. R. (2004). A gene regulatory network model for cell-fate determination during arabidopsis thaliana flower development that is robust and recovers experimental gene expression profiles. *Plant Cell*, 16(11):2923–2939.

Euler, L. (1736). Solutio Problematis ad Geometriam Situs Pertinentis, Commentarii Academiae Scientiarum Imperialis Petropolitanae. *Commentarii Academiae Scientiarum Imperialis Petropolitanae*, 8:128–140.

Ewens, W. J. (1972). The sampling theory of selectively neutral alleles. *Theor Popul Biol*, 3(1):87–112.

Eykhoff, P. (1974). *System Identification: Parameter and State Estimation.* John Wiley & Sons.

Faeder, J. R., Blinov, M. L., and Hlavacek, W. S. (2009). Rule-based modeling of biochemical systems with bionetgen. *Methods Mol Biol*, 500:113–167.

Faustman, D. and Davis, M. (2010). Tnf receptor 2 pathway: drug target for autoimmune diseases. *Nat Rev Drug Discov*, 9(6):482–493.

Feijge, M. A., Ansink, K., Vanschoonbeek, K., and Heemskerk, J. W. (2004). Control of platelet activation by cyclic AMP turnover and cyclic nucleotide phosphodiesterase type-3. *Biochem Pharmacol*, 67:1559–67. 8.

Feng, G., Tintrup, H., Kirsch, J., Nichol, M. C., Kuhse, J., Betz, H., and Sanes, J. R. (1998). Dual requirement for gephyrin in glycine receptor clustering and molybdoenzyme activity. *Science*, 282(5392):1321–1324.

Fink, L., Hölschermann, H., Kwapiszewska, G., Muyal, J. P., Lengemann, B., Bohle, R. M., and Santoso, S. (2003). Characterization of platelet-specific mrna by real-time pcr after laser-assisted microdissection. *Thromb Haemost*, 90(4):749–756.

Fischmeister, R., Castro, L. R. V., Abi-Gerges, A., Rochais, F., Jurevicius, J., Leroy, J., and Vandecasteele, G. (2006). Compartmentation of cyclic nucleotide signaling in the heart: the role of cyclic nucleotide phosphodiesterases. *Circ Res*, 99(8):816–828.

Floreani, M., Fossa, P., Gessi, S., Mosti, L., Borea, P. A., and Dorigo, P. (2003). New milrinone analogues: in vitro study of structure-activity relationships for positive inotropic effect, antagonism towards endogenous adenosine, and inhibition of cardiac type iii phosphodiesterase. *Naunyn Schmiedebergs Arch Pharmacol*, 367(2):109–118.

Fontana, D., Wong, T. Y., Theibert, A., and Devreotes, P. (1986). Cell-cell interactions in the development of dictyostelium. *Dev Biol (N Y 1985)*, 3:261–281.

Forsell, P. K. A., Olsson, A. O., Andersson, E., Nallan, L., and Gelb, M. H. (2005). Polychlorinated biphenyls induce arachidonic acid release in human platelets in a tamoxifen sensitive manner via activation of group iva cytosolic phospholipase a2-alpha. *Biochem Pharmacol*, 71(1-2):144–155.

Fotin-Mleczek, M., Henkler, F., Hausser, A., Glauner, H., Samel, D., Graness, A., Scheurich, P., Mauri, D., and Wajant, H. (2004). Tumor necrosis factor receptor-associated factor (traf) 1 regulates cd40-induced traf2-mediated nf-kappab activation. *J Biol Chem*, 279(1):677–685.

Fotin-Mleczek, M., Henkler, F., Samel, D., Reichwein, M., Hausser, A., Parmryd, I., Scheurich, P., Schmid, J. A., and Wajant, H. (2002). Apoptotic crosstalk of tnf receptors: Tnf-r2-induces depletion of traf2 and iap proteins and accelerates tnf-r1-dependent activation of caspase-8. *J Cell Sci*, 115(Pt 13):2757–2770.

Frantz, S., Fraccarollo, D., Wagner, H., Behr, T. M., Jung, P., Angermann, C. E., Ertl, G., and Bauersachs, J. (2003). Sustained activation of nuclear factor kappa b and activator protein 1 in chronic heart failure. *Cardiovasc Res*, 57(3):749–756.

Fraser, I. D. C. and Germain, R. N. (2009). Navigating the network: signaling cross-talk in hematopoietic cells. *Nat Immunol*, 10(4):327–331.

Funahashi, A., Matsuoka, Y., Jouraku, A., Morohashi, M., Kikuchi, N., and Kitano, H. (2008). Celldesigner 3.5 : A versatile modeling tool for biochemical networks. *Proceedings of the IEEE*, 96:1254–1265.

Gambaryan, S., Kobsar, A., Hartmann, S., Birschmann, I., Kuhlencordt, P. J., Müller-Esterl, W., Lohmann, S. M., and Walter, U. (2008). No-synthase-/no-independent regulation of human and murine platelet soluble guanylyl cyclase activity. *J Thromb Haemost*, 6(8):1376–1384.

Gambaryan, S., Kobsar, A., Rukoyatkina, N., Herterich, S., Geiger, J., Smolenski, A., Lohmann, S. M., and Walter, U. (2010). Thrombin and collagen induce a feedback inhibitory signaling pathway in platelets involving dissociation of the catalytic subunit of protein kinase a from an nfkappab-ikappab complex. *J Biol Chem*, 285(24):18352–18363.

Gan, S. and Amasino, R. M. (1995). Inhibition of leaf senescence by autoregulated production of cytokinin. *Science*, 270(5244):1986–1988.

Garcia, A., Kim, S., Bhavaraju, K., Schoenwaelder, S. M., and Kunapuli, S. P. (2010). Role of phosphoinositide 3-kinase beta in platelet aggregation and thromboxane a2 generation mediated by gi signalling pathways. *Biochem J*, 429(2):369–377.

Garcia, A., Prabhakar, S., Brock, C. J., Pearce, A. C., Dwek, R. A., Watson, S. P., Hebestreit, H. F., and Zitzmann, N. (2004). Extensive analysis of the human platelet proteome by two-dimensional gel electrophoresis and mass spectrometry. *Proteomics*, 4(3):656–668.

Garg, A., Xenarios, I., Mendoza, L., and DeMicheli, G. (2007). *An efficient method for dynamic analysis of gene regulatory networks. In: Lecture Notes in Computer Science (Vol. 4453)*. Springer.

Gazzarrini, S. and McCourt, P. (2003). Cross-talk in plant hormone signalling: what arabidopsis mutants are telling us. *Ann Bot*, 91(6):605–612.

Geier, F., Fengos, G., and Iber, D. (2011). A computational analysis of the dynamic roles of talin, dok1, and pipki for integrin activation. *PLoS One*, 6(11):e24808.

Geiger, J., Brandmann, T., Hubertus, K., Tjahjadi, B., Schinzel, R., and Walter, U. (2010). A protein phosphorylation-based assay for screening and monitoring of drugs modulating cyclic nucleotide pathways. *Anal Biochem*, 407:261–9. 2.

Geiger, J., Honig-Liedl, P., Schanzenbacher, P., and Walter, U. (1998). Ligand specificity and ticlopidine effects distinguish three human platelet ADP receptors. *European journal of pharmacology*, 351:235–46. 2.

Gettys, T. W., Vine, A. J., Simonds, M. F., and Corbin, J. D. (1988). Activation of the particulate low km phosphodiesterase of adipocytes by addition of cAMP-dependent protein kinase. *The Journal of biological chemistry*, 263:10359–63. 21.

Geva-Zatorsky, N., Dekel, E., Cohen, A. A., Danon, T., Cohen, L., and Alon, U. (2010). Protein dynamics in drug combinations: a linear superposition of individual-drug responses. *Cell*, 140:643–51. 5.

Ghosh, S. and Karin, M. (2002). Missing pieces in the nf-kappab puzzle. *Cell*, 109 Suppl:S81–S96.

Gillespie, D. T. (2007). Stochastic simulation of chemical kinetics. *Annu Rev Phys Chem*, 58:35–55.

Givertz, M. M. and Colucci, W. S. (1998). New targets for heart-failure therapy: endothelin, inflammatory cytokines, and oxidative stress. *Lancet*, 352 Suppl 1:SI34–SI38.

Goh, K.-I., Cusick, M. E., Valle, D., Childs, B., Vidal, M., and Barabási, A.-L. (2007). The human disease network. *Proc Natl Acad Sci U S A*, 104(21):8685–8690.

Gomberg-Maitland, M. and Olschewski, H. (2008). Prostacyclin therapies for the treatment of pulmonary arterial hypertension. *The European respiratory journal : official journal of the European Society for Clinical Respiratory Physiology*, 31:891–901. 4.

Gonzalez, A. G., Naldi, A., Sánchez, L., Thieffry, D., and Chaouiya, C. (2006). Ginsim: a software suite for the qualitative modelling, simulation and analysis of regulatory networks. *Biosystems*, 84(2):91–100.

Grell, M. (1995). Tumor necrosis factor (tnf) receptors in cellular signaling of soluble and membrane-expressed tnf. *J Inflamm*, 47(1-2):8–17.

Grell, M., Douni, E., Wajant, H., Löhden, M., Clauss, M., Maxeiner, B., Georgopoulos, S., Lesslauer, W., Kollias, G., Pfizenmaier, K., and Scheurich, P. (1995). The transmembrane form of tumor necrosis factor is the prime activating ligand of the 80 kda tumor necrosis factor receptor. *Cell*, 83(5):793–802.

Grell, M. and Scheurich, P. (1997). *Growth Factors and Cytokines in Health and Disease*. JAI Press Inc., Greenwich, CT.

Grell, M., Wajant, H., Zimmermann, G., and Scheurich, P. (1998). The type 1 receptor (cd120a) is the high-affinity receptor for soluble tumor necrosis factor. *Proc Natl Acad Sci U S A*, 95(2):570–575.

Grieneisen, V. A., Xu, J., Marée, A. F. M., Hogeweg, P., and Scheres, B. (2007). Auxin transport is sufficient to generate a maximum and gradient guiding root growth. *Nature*, 449(7165):1008–1013.

Grima, R. and Schnell, S. (2006). A systematic investigation of the rate laws valid in intracellular environments. *Biophys Chem*, 124(1):1–10.

Gross, L. (2006). When evidence is scant, mathematical modeling offers a roadmap for discovery. *PLoS Biol*, 4(10):e323.

Grosse, J., Braun, A., Varga-Szabo, D., Beyersdorf, N., Schneider, B., Zeitlmann, L., Hanke, P., Schropp, P., Mühlstedt, S., Zorn, C., Huber, M., Schmittwolf, C., Jagla, W., Yu, P., Kerkau, T., Schulze, H., Nehls, M., and Nieswandt, B. (2007). An ef hand mutation in stim1 causes premature platelet activation and bleeding in mice. *J Clin Invest*, 117(11):3540–3550.

Grosskinsky, D. K., Naseem, M., Abdelmohsen, U. R., Plickert, N., Engelke, T., Griebel, T., Zeier, J., Novák, O., Strnad, M., Pfeifhofer, H., van der Graaff, E., Simon, U., and Roitsch, T. (2011). Cytokinins mediate resistance against pseudomonas syringae in tobacco through increased antimicrobial phytoalexin synthesis independent of salicylic acid signaling. *Plant Physiol*, 157(2):815–830.

Guerriero, M. L., Pokhilko, A., Fernández, A. P., Halliday, K. J., Millar, A. J., and Hillston, J. (2012). Stochastic properties of the plant circadian clock. *J R Soc Interface*, 9(69):744–756.

Guldberg, C. M. and Waage, P. (1864). Studies concerning affinities. *Forhandlinger: Videnskabs-Selskabet i Christiana*, 35.

Guldberg, C. M. and Waage, P. (1879). Über die chemische Affinität. *Journal fuer Praktische Chemie*, 19:69.

Guruharsha, K. G., Rual, J.-F., Zhai, B., Mintseris, J., Vaidya, P., Vaidya, N., Beekman, C., Wong, C., Rhee, D. Y., Cenaj, O., McKillip, E., Shah, S., Stapleton, M., Wan, K. H., Yu, C., Parsa, B., Carlson, J. W., Chen, X., Kapadia, B., VijayRaghavan, K., Gygi, S. P., Celniker, S. E., Obar, R. A., and Artavanis-Tsakonas, S. (2011). A protein complex network of drosophila melanogaster. *Cell*, 147(3):690–703.

Haberstock-Debic, H., Andre, P., Mills, S., Phillips, D. R., and Conley, P. B. (2011). A clopidogrel-insensitive inducible pool of p2y12 receptors contributes to thrombus formation: inhibition by elinogrel, a direct-acting, reversible p2y12 antagonist. *J Pharmacol Exp Ther*, 339(1):54–61.

Halbrügge, M. and Walter, U. (1989). Purification of a vasodilator-regulated phosphoprotein from human platelets. *Eur J Biochem*, 185(1):41–50.

Hall, P. and Wilson, S. R. (1991). Two guidelines for bootstrap hypothesis testing. *Biometrics*, 47:757 – 762.

Hanada, T. and Yoshimura, A. (2002). Regulation of cytokine signaling and inflammation. *Cytokine Growth Factor Rev*, 13(4-5):413–421.

Hanson, M. S., Stephenson, A. H., Bowles, E. A., Sridharan, M., Adderley, S., and Sprague, R. S. (2008). Phosphodiesterase 3 is present in rabbit and human erythrocytes and its inhibition potentiates iloprost-induced increases in cAMP. *Am J Physiol Heart Circ Physiol*, 295:H786–93. 2.

Harbeck, B., Hüttelmaier, S., Schluter, K., Jockusch, B. M., and Illenberger, S. (2000). Phosphorylation of the vasodilator-stimulated phosphoprotein regulates its interaction with actin. *J Biol Chem*, 275(40):30817–30825.

Hardy, G. H. (1908). Mendelian proportions in a mixed population. *Science*, 28(706):49–50.

Haslam, R. J., Dickinson, N. T., and Jang, E. K. (1999). Cyclic nucleotides and phosphodiesterases in platelets. *Thromb Haemost*, 82(2):412–423.

Hassock, S. R., Zhu, M. X., Trost, C., Flockerzi, V., and Authi, K. S. (2002). Expression and role of trpc proteins in human platelets: evidence that trpc6 forms the store-independent calcium entry channel. *Blood*, 100(8):2801–2811.

Hathaway, D. R. and Adelstein, R. S. (1979). Human platelet myosin light chain kinase requires the calcium-binding protein calmodulin for activity. *Proc Natl Acad Sci U S A*, 76(4):1653–1657.

Hauser, W., Knobeloch, K. P., Eigenthaler, M., Gambaryan, S., Krenn, V., Geiger, J., Glazova, M., Rohde, E., Horak, I., Walter, U., and Zimmer, M. (1999). Megakaryocyte hyperplasia and enhanced agonist-induced platelet activation in vasodilator-stimulated phosphoprotein knockout mice. *Proc Natl Acad Sci U S A*, 96(14):8120–8125.

Hayden, M. S. and Ghosh, S. (2004). Signaling to nf-kappab. *Genes Dev*, 18(18):2195–2224.

Hechler, B. and Gachet, C. (2011). P2 receptors and platelet function. *Purinergic Signal*, 7(3):293–303.

Hechler, B., Léon, C., Vial, C., Vigne, P., Frelin, C., Cazenave, J. P., and Gachet, C. (1998). The p2y1 receptor is necessary for adenosine 5′-diphosphate-induced platelet aggregation. *Blood*, 92(1):152–159.

Heemskerk, J. W. M., Bevers, E. M., and Lindhout, T. (2002). Platelet activation and blood coagulation. *Thromb Haemost*, 88(2):186–193.

Heidbreder, M., Zander, C., Malkusch, S., Widera, D., Kaltschmidt, B., Kaltschmidt, C., Nair, D., Choquet, D., Sibarita, J.-B., and Heilemann, M. (2012). Tnf-? influences the lateral dynamics of tnf receptor i in living cells. *Biochim Biophys Acta*, 1823(10):1984–1989.

Heinrich, R. and Schuster, S. (1996). *The Regulation Of Cellular Systems*. Chapman & Hall.

Hengl, S., Kreutz, C., Timmer, J., and Maiwald, T. (2007). Data-based identifiability analysis of non-linear dynamical models. *Bioinformatics*, 23(19):2612–2618.

Herget, S., Lohse, M. J., and Nikolaev, V. O. (2008). Real-time monitoring of phosphodiesterase inhibition in intact cells. *Cell Signal*, 20(8):1423–1431.

Hettasch, J. M. and Sellers, J. R. (1991). Caldesmon phosphorylation in intact human platelets by camp-dependent protein kinase and protein kinase c. *J Biol Chem*, 266(18):11876–11881.

Heyninck, K. and Beyaert, R. (2005). A20 inhibits nf-kappab activation by dual ubiquitin-editing functions. *Trends Biochem Sci*, 30(1):1–4.

Hines, L. M. and Tabakoff, B. (2005). Platelet adenylyl cyclase activity: a biological marker for major depression and recent drug use. *Biological psychiatry*, 58:955–62. 12.

Hlavacek, W. S., Faeder, J. R., Blinov, M. L., Perelson, A. S., and Goldstein, B. (2003). The complexity of complexes in signal transduction. *Biotechnol Bioeng*, 84(7):783–794.

Hlavacek, W. S., Faeder, J. R., Blinov, M. L., Posner, R. G., Hucka, M., and Fontana, W. (2006). Rules for modeling signal-transduction systems. *Sci STKE*, 2006(344):re6.

Ho, K. L. and Harrington, H. A. (2010). Bistability in apoptosis by receptor clustering. *PLoS Comput Biol*, 6(10):e1000956.

Hoffmann, A., Levchenko, A., Scott, M. L., and Baltimore, D. (2002). The IkappaB-NF-kappaB signaling module: temporal control and selective gene activation. *Science*, 298(5596):1241–1245.

Hoffmeister, M., Riha, P., Neumüller, O., Danielewski, O., Schultess, J., and Smolenski, A. P. (2008). Cyclic nucleotide-dependent protein kinases inhibit binding of 14-3-3 to the gtpase-activating protein rap1gap2 in platelets. *J Biol Chem*, 283(4):2297–2306.

Hofmann, F. (2005). The biology of cyclic gmp-dependent protein kinases. *J Biol Chem*, 280(1):1–4.

Hornbeck, P. V., Chabra, I., Kornhauser, J. M., Skrzypek, E., and Zhang, B. (2004). Phosphosite: A bioinformatics resource dedicated to physiological protein phosphorylation. *Proteomics*, 4(6):1551–1561.

Hornberg, J. J., Bruggeman, F. J., Binder, B., Geest, C. R., de Vaate, A. J. M. B., Lankelma, J., Heinrich, R., and Westerhoff, H. V. (2005). Principles behind the multifarious control of signal transduction. erk phosphorylation and kinase/phosphatase control. *FEBS J*, 272(1):244–258.

Hotamisligil, G. S. (2003). Inflammatory pathways and insulin action. *Int J Obes Relat Metab Disord*, 27 Suppl 3:S53–S55.

Hotamisligil, G. S. (2006). Inflammation and metabolic disorders. *Nature*, 444(7121):860–867.

Houslay, M. D. (2010). Underpinning compartmentalised cAMP signalling through targeted cAMP breakdown. *Trends Biochem Sci*, 35:91–100. 2.

Hoylaerts, M. F., Oury, C., Toth-Zsamboki, E., and Vermylen, J. (2000). Adp receptors in platelet activation and aggregation. *Platelets*, 11(6):307–309.

Hsieh, M. Y., Yang, S., Raymond-Stinz, M. A., Edwards, J. S., and Wilson, B. S. (2010). Spatio-temporal modeling of signaling protein recruitment to EGFR. *BMC Syst Biol*, 4:57.

Huard, J., Mueller, S., Gilles, E. D., Klingmüller, U., and Klamt, S. (2012). An integrative model links multiple inputs and signaling pathways to the onset of dna synthesis in hepatocytes. *FEBS J*, 279(18):3290–3313.

Hubertus, K. (2012). *Regulation of cAMP level and signaltransduction in human platelets by prostanoid-receptors*. PhD thesis, University of Wuerzburg, Faculty of Biology.

Hunter, R. W., Mackintosh, C., and Hers, I. (2009). Protein kinase c-mediated phosphorylation and activation of PDE3A regulate cAMP levels in human platelets. *J Biol Chem*, 284:12339–48. 18.

Iadevaia, S., Lu, Y., Morales, F. C., Mills, G. B., and Ram, P. T. (2010). Identification of optimal drug combinations targeting cellular networks: integrating phospho-proteomics and computational network analysis. *Cancer Res*, 70(17):6704–6714.

Ishii-Watabe, A., Uchida, E., Mizuguchi, H., and Hayakawa, T. (2001). Involvement of a calcium-independent pathway in plasmin-induced platelet shape change. *Life Sci*, 69(8):945–960.

Iwami, G., Kawabe, J., Ebina, T., Cannon, P. J., Homcy, C. J., and Ishikawa, Y. (1995). Regulation of adenylyl cyclase by protein kinase a. *J Biol Chem*, 270:12481–4. 21.

Iyú, D., Glenn, J. R., White, A. E., Fox, S. C., Dovlatova, N., and Heptinstall, S. (2011). P2y12 and ep3 antagonists promote the inhibitory effects of natural modulators of platelet aggregation that act via camp. *Platelets*, 22(7):504–515.

Iyu, D., Jüttner, M., Glenn, J. R., White, A. E., Johnson, A. J., Fox, S. C., and Heptinstall, S. (2011). Pge1 and pge2 modify platelet function through different prostanoid receptors. *Prostaglandins Other Lipid Mediat*, 94(1-2):9–16.

Jay, D., García, E. J., Lara, J. E., Medina, M. A., and de la Luz Ibarra, M. (2000). Determination of a camp-dependent protein kinase phosphorylation site in the c-terminal region of human endothelial actin-binding protein. *Arch Biochem Biophys*, 377(1):80–84.

Jensen, F. V. (1996). *An Introduction To Bayesian Networks*. UCL Press.

Jeyaraj, S. C., Unger, N. T., and Chotani, M. A. (2011). Rap1 gtpases: an emerging role in the cardiovasculature. *Life Sci*, 88(15-16):645–652.

Jin, J., Quinton, T. M., Zhang, J., Rittenhouse, S. E., and Kunapuli, S. P. (2002). Adenosine diphosphate (adp)-induced thromboxane a(2) generation in human platelets requires coordinated signaling through integrin alpha(iib)beta(3) and adp receptors. *Blood*, 99(1):193–198.

Jin, Z. and El-Deiry, W. S. (2005). Overview of cell death signaling pathways. *Cancer Biol Ther*, 4(2):139–163.

Jones, C. I., Barrett, N. E., Moraes, L. A., Gibbins, J. M., and Jackson, D. E. (2012). Endogenous inhibitory mechanisms and the regulation of platelet function. *Methods Mol Biol*, 788:341–366.

Jones, J. D. G. and Dangl, J. L. (2006). The plant immune system. *Nature*, 444(7117):323–329.

Jones, R. L., Woodward, D. F., Wang, J. W., and Clark, R. L. (2011). Roles of affinity and lipophilicity in the slow kinetics of prostanoid receptor antagonists on isolated smooth muscle preparations. *Br J Pharmacol*, 162(4):863–879.

Jordan, J. D., Landau, E. M., and Iyengar, R. (2000). Signaling networks: the origins of cellular multitasking. *Cell*, 103(2):193–200.

Juska, A. and Farndale, R. W. (1999). Inhibition of human platelet adenylate cyclase activity by adrenaline, thrombin and collagen: analysis and reinterpretation of experimental data. *The Biochemical journal*, 340 (Pt 1):245–53.

Kahlem, P. and Birney, E. (2006). Dry work in a wet world: computation in systems biology. *Mol Syst Biol*, 2:40.

Karniguian, A., Grelac, F., Levy-Toledano, S., Legrand, Y. J., and Rendu, F. (1990). Collagen-induced platelet activation mainly involves the protein kinase c pathway. *Biochem J*, 268(2):325–331.

Kauffman, S. A. (1969). Metabolic stability and epigenesis in randomly constructed genetic nets. *J Theor Biol*, 22(3):437–467.

Kawata, M., Kikuchi, A., Hoshijima, M., Yamamoto, K., Hashimoto, E., Yamamura, H., and Takai, Y. (1989). Phosphorylation of smg p21, a ras p21-like gtp-binding protein, by cyclic amp-dependent protein kinase in a cell-free system and in response to prostaglandin e1 in intact human platelets. *J Biol Chem*, 264(26):15688–15695.

Kenyon, C. J. (2010). The genetics of ageing. *Nature*, 464(7288):504–512.

Keshava Prasad, T. S., Goel, R., Kandasamy, K., Keerthikumar, S., Kumar, S., Mathivanan, S., Telikicherla, D., Raju, R., Shafreen, B., Venugopal, A., Balakrishnan, L., Marimuthu, A., Banerjee, S., Somanathan, D. S., Sebastian, A., Rani, S., Ray, S., Harrys Kishore, C. J., Kanth, S., Ahmed, M., Kashyap, M. K., Mohmood, R., Ramachandra, Y. L., Krishna, V., Rahiman, B. A., Mohan, S., Ranganathan, P., Ramabadran, S., Chaerkady, R., and Pandey, A. (2009). Human protein reference database–2009 update. *Nucleic Acids Res*, 37(Database issue):D767–D772.

Kholodenko, B. N. (2006). Cell-signalling dynamics in time and space. *Nat Rev Mol Cell Biol*, 7(3):165–176.

Kirk, R. I., Sanderson, M. R., and Lerea, K. M. (2000). Threonine phosphorylation of the beta 3 integrin cytoplasmic tail, at a site recognized by pdk1 and akt/pkb in vitro, regulates shc binding. *J Biol Chem*, 275(40):30901–30906.

Kitano, H. (2002). Systems biology: a brief overview. *Science*, 295(5560):1662–1664.

Klamt, S., Saez-Rodriguez, J., and Gilles, E. D. (2007). Structural and functional analysis of cellular networks with cellnetanalyzer. *BMC Syst Biol*, 1:2.

Klipp, E., Liebermeister, W., Wierling, C., Kowald, A., Lehrach, H., and Herwig, R. (2009). *Systems Biology: A Textbook*. WILEY-VCH.

Kloeze, J. (1966). *Influence of prostaglandins on platelet adhesiveness and platelet aggregation. In: Bergström S, Samuelsson B, eds. Prostaglandins: Proceedings of the 2nd Nobel Symposium*. Almqvist and Wicksell.

Knox, C., Law, V., Jewison, T., Liu, P., Ly, S., Frolkis, A., Pon, A., Banco, K., Mak, C., Neveu, V., Djoumbou, Y., Eisner, R., Guo, A. C., and Wishart, D. S. (2011). Drugbank 3.0: a comprehensive resource for 'omics' research on drugs. *Nucleic Acids Res*, 39(Database issue):D1035–D1041.

Kohn, A. D., Takeuchi, F., and Roth, R. A. (1996). Akt, a pleckstrin homology domain containing kinase, is activated primarily by phosphorylation. *J Biol Chem*, 271(36):21920–21926.

Kollmann, M., L?vdok, L., Bartholomé, K., Timmer, J., and Sourjik, V. (2005). Design principles of a bacterial signalling network. *Nature*, 438(7067):504–507.

Kopelman, R. (1988). Fractal reaction kinetics. *Science*, 241(4873):1620–1626.

Krauss, M., Schaller, S., Borchers, S., Findeisen, R., Lippert, J., and Kuepfer, L. (2012). Integrating cellular metabolism into a multiscale whole-body model. *PLoS Comput Biol*, 8(10):e1002750.

Krippner-Heidenreich, A., Tübing, F., Bryde, S., Willi, S., Zimmermann, G., and Scheurich, P. (2002). Control of receptor-induced signaling complex formation by the kinetics of ligand/receptor interaction. *J Biol Chem*, 277(46):44155–44163.

Krumsiek, J., Pölsterl, S., Wittmann, D. M., and Theis, F. J. (2010). Odefy–from discrete to continuous models. *BMC Bioinformatics*, 11:233.

Kudo, T., Kiba, T., and Sakakibara, H. (2010). Metabolism and long-distance translocation of cytokinins. *J Integr Plant Biol*, 52(1):53–60.

Lalli, E. and Sassone-Corsi, P. (1994). Signal transduction and gene regulation: the nuclear response to camp. *J Biol Chem*, 269(26):17359–17362.

Lapetina, E. G., Lacal, J. C., Reep, B. R., and Molina y Vedia, L. (1989). A ras-related protein is phosphorylated and translocated by agonists that increase camp levels in human platelets. *Proc Natl Acad Sci U S A*, 86(9):3131–3134.

Lapetina, E. G., Reep, B., Ganong, B. R., and Bell, R. M. (1985). Exogenous sn-1,2-diacylglycerols containing saturated fatty acids function as bioregulators of protein kinase c in human platelets. *J Biol Chem*, 260(3):1358–1361.

Lewandrowski, U., Wortelkamp, S., Lohrig, K., Zahedi, R. P., Wolters, D. A., Walter, U., and Sickmann, A. (2009). Platelet membrane proteomics: a novel repository for functional research. *Blood*, 114(1):e10–e19.

Li, Y., Tai, B.-C., Sia, W., Phua, Q.-H., Richards, M. A., Low, A., Chan, K.-H., Teo, S.-G., Sim, T.-B., Lee, C.-H., Roe, M. T., Yeo, T.-C., Tan, H.-C., and Chan, M. Y. (2012). Angiographic and platelet reactivity outcomes with prasugrel 60 mg pretreatment and clopidogrel 600 mg pretreatment in primary percutaneous coronary intervention. *J Thromb Thrombolysis*, 34(4):499–505.

Liebenhoff, U., Greinacher, A., and Presek, P. (1994). The protein tyrosine kinase pp60c-src is activated upon platelet stimulation. *Cell Mol Biol (Noisy-le-grand)*, 40(5):645–652.

Linde, A., Mosier, D., Blecha, F., and Melgarejo, T. (2007). Innate immunity and inflammation–new frontiers in comparative cardiovascular pathology. *Cardiovasc Res*, 73(1):26–36.

Lindemann, S., Tolley, N. D., Dixon, D. A., McIntyre, T. M., Prescott, S. M., Zimmerman, G. A., and Weyrich, A. S. (2001a). Activated platelets mediate inflammatory signaling by regulated interleukin 1beta synthesis. *J Cell Biol*, 154(3):485–490.

Lindemann, S., Tolley, N. D., Eyre, J. R., Kraiss, L. W., Mahoney, T. M., and Weyrich, A. S. (2001b). Integrins regulate the intracellular distribution of eukaryotic initiation factor 4e in platelets. a checkpoint for translational control. *J Biol Chem*, 276(36):33947–33951.

Linding, R., Jensen, L. J., Ostheimer, G. J., van Vugt, M. A. T. M., J?rgensen, C., Miron, I. M., Diella, F., Colwill, K., Taylor, L., Elder, K., Metalnikov, P., Nguyen, V., Pasculescu, A., Jin, J., Park, J. G., Samson, L. D., Woodgett, J. R., Russell, R. B., Bork, P., Yaffe, M. B., and Pawson, T. (2007). Systematic discovery of in vivo phosphorylation networks. *Cell*, 129(7):1415–1426.

Lipniacki, T., Paszek, P., Brasier, A. R. A. R., Luxon, B., and Kimmel, M. (2004). Mathematical model of nf-kappab regulatory module. *J Theor Biol*, 228(2):195–215.

Liu, J., Fitzgerald, M. E., Berndt, M. C., Jackson, C. W., and Gartner, T. K. (2006). Bruton tyrosine kinase is essential for botrocetin/vwf-induced signaling and gpib-dependent thrombus formation in vivo. *Blood*, 108(8):2596–2603.

Liu, J., Mehdi, S., Topping, J., Tarkowski, P., and Lindsey, K. (2010). Modelling and experimental analysis of hormonal crosstalk in arabidopsis. *Mol Syst Biol*, 6:373.

Liu, J., Pestina, T. I., Berndt, M. C., Steward, S. A., Jackson, C. W., and Gartner, T. K. (2004). The roles of adp and txa in botrocetin/vwf-induced aggregation of washed platelets. *J Thromb Haemost*, 2(12):2213–2222.

Llorente, F., Muskett, P., Sánchez-Vallet, A., López, G., Ramos, B., Sánchez-Rodríguez, C., Jordá, L., Parker, J., and Molina, A. (2008). Repression of the auxin response pathway increases arabidopsis susceptibility to necrotrophic fungi. *Mol Plant*, 1(3):496–509.

Lobato, E. B., Beaver, T., Muehlschlegel, J., Kirby, D. S., Klodell, C., and Sidi, A. (2006). Treatment with phosphodiesterase inhibitors type III and v: milrinone and sildenafil is an effective combination during thromboxane-induced acute pulmonary hypertension. *British journal of anaesthesia*, 96:317–22. 3.

Lohmann, S. M. and Walter, U. (2005). Tracking functions of cgmp-dependent protein kinases (cgk). *Front Biosci*, 10:1313–1328.

Lohse, M. J., Engelhardt, S., and Eschenhagen, T. (2003). What is the role of beta-adrenergic signaling in heart failure? *Circ Res*, 93(10):896–906.

Léon, C., Hechler, B., Freund, M., Eckly, A., Vial, C., Ohlmann, P., Dierich, A., LeMeur, M., Cazenave, J. P., and Gachet, C. (1999). Defective platelet aggregation and increased resistance to thrombosis in purinergic p2y(1) receptor-null mice. *J Clin Invest*, 104(12):1731–1737.

Lorenz, K., Schmitt, J. P., Schmitteckert, E. M., and Lohse, M. J. (2009). A new type of erk1/2 autophosphorylation causes cardiac hypertrophy. *Nat Med*, 15(1):75–83.

Lotka, A. J. (1925). *Elements of physical biology*. Baltimore: Williams and Wilkins.

MacFarland, R. T., Zelus, B. D., and Beavo, J. A. (1991). High concentrations of a cgmp-stimulated phosphodiesterase mediate anp-induced decreases in camp and steroidogenesis in adrenal glomerulosa cells. *J Biol Chem*, 266(1):136–142.

Mackenzie, I. S., Coughtrie, M. W., MacDonald, T. M., and Wei, L. (2010). Antiplatelet drug interactions. *Journal of internal medicine*, 268:516–29. 6.

MacNamara, A., Terfve, C., Henriques, D., Bernabé, B. P., and Saez-Rodriguez, J. (2012). State-time spectrum of signal transduction logic models. *Phys Biol*, 9(4):045003.

Macphee, C. H., Reifsnyder, D. H., Moore, T. A., Lerea, K. M., and Beavo, J. A. (1988). Phosphorylation results in activation of a cAMP phosphodiesterase in human platelets. *J Biol Chem*, 263:10353–8. 21.

Maglott, D., Ostell, J., Pruitt, K. D., and Tatusova, T. (2007). Entrez gene: gene-centered information at ncbi. *Nucleic Acids Res*, 35(Database issue):D26–D31.

Mahoney, D. J., Cheung, H. H., Mrad, R. L., Plenchette, S., Simard, C., Enwere, E., Arora, V., Mak, T. W., Lacasse, E. C., Waring, J., and Korneluk, R. G. (2008). Both ciap1 and ciap2 regulate tnfalpha-mediated nf-kappab activation. *Proc Natl Acad Sci U S A*, 105(33):11778–11783.

Maiwald, T. and Timmer, J. (2008). Dynamical modeling and multi-experiment fitting with potterswheel. *Bioinformatics*, 24(18):2037–2043.

Malumbres, M. and Barbacid, M. (2009). Cell cycle, cdks and cancer: a changing paradigm. *Nat Rev Cancer*, 9(3):153–166.

Mangan, S. and Alon, U. (2003). Structure and function of the feed-forward loop network motif. *Proc Natl Acad Sci U S A*, 100(21):11980–11985.

Manganello, J. M., Djellas, Y., Borg, C., Antonakis, K., and Le Breton, G. C. (1999). Cyclic amp-dependent phosphorylation of thromboxane a(2) receptor-associated galpha(13). *J Biol Chem*, 274(39):28003–28010.

Manganello, J. M., Huang, J.-S., Kozasa, T., Voyno-Yasenetskaya, T. A., and Le Breton, G. C. (2003). Protein kinase a-mediated phosphorylation of the galpha13 switch i region alters the galphabetagamma13-g protein-coupled receptor complex and inhibits rho activation. *J Biol Chem*, 278(1):124–130.

Manning, G., Whyte, D. B., Martinez, R., Hunter, T., and Sudarsanam, S. (2002). The protein kinase complement of the human genome. *Science*, 298(5600):1912–1934.

Marchetti, L., Klein, M., Schlett, K., Pfizenmaier, K., and Eisel, U. L. M. (2004). Tumor necrosis factor (tnf)-mediated neuroprotection against glutamate-induced excitotoxicity is enhanced by n-methyl-d-aspartate receptor activation. essential role of a tnf receptor 2-mediated phosphatidylinositol 3-kinase-dependent nf-kappa b pathway. *J Biol Chem*, 279(31):32869–32881.

Margarucci, L., Roest, M., Preisinger, C., Bleijerveld, O. B., van Holten, T. C., Heck, A. J. R., and Scholten, A. (2011). Collagen stimulation of platelets induces a rapid spatial response of camp and cgmp signaling scaffolds. *Mol Biosyst*, 7(7):2311–2319.

Markov, A. A. (1906). Extension of the law of large numbers to dependent quantities. *Izvestiia Fiz Matem Obsch Kazan Univ*, 15:135–156.

Marks, F., Klingmüller, U., and Müller-Decker, K. (2009). *Cellular Signal Processing*. Garland Science.

Marquis, N. R., Vigdahl, R. L., and Tavormina, P. A. (1969). Platelet aggregation. i. regulation by cyclic amp and prostaglandin e1. *Biochem Biophys Res Commun*, 36(6):965–972.

Marshall, S. J., Senis, Y. A., Auger, J. M., Feil, R., Hofmann, F., Salmon, G., Peterson, J. T., Burslem, F., and Watson, S. P. (2004). GPIb-dependent platelet activation is dependent on src kinases but not map kinase or cgmp-dependent kinase. *Blood*, 103(7):2601–2609.

Massberg, S., Grüner, S., Konrad, I., Garcia Arguinzonis, M. I., Eigenthaler, M., Hemler, K., Kersting, J., Schulz, C., Muller, I., Besta, F., Nieswandt, B., Heinzmann, U., Walter, U., and Gawaz, M. (2004). Enhanced in vivo platelet adhesion in vasodilator-stimulated phosphoprotein (vasp)-deficient mice. *Blood*, 103(1):136–142.

MATLAB (2010). *version 7.10.0 (R2010a)*. The MathWorks Inc, Natick, Massachusetts.

Matsumoto, T., Kobayashi, T., and Kamata, K. (2003). Phosphodiesterases in the vascular system. *Journal of smooth muscle research = Nihon Heikatsukin Gakkai kikanshi*, 39:67–86. 4.

Maurice, D. H. (2003). Does sildenafil indirectly inhibit phosphodiesterase 3 in vascular smooth muscle? *Hypertension*, 41(3):e2.

May, F., Hagedorn, I., Pleines, I., Bender, M., Vögtle, T., Eble, J., Elvers, M., and Nieswandt, B. (2009). Clec-2 is an essential platelet-activating receptor in hemostasis and thrombosis. *Blood*, 114(16):3464–3472.

Mazzucato, M., Pradella, P., Cozzi, M. R., De Marco, L., and Ruggeri, Z. M. (2002). Sequential cytoplasmic calcium signals in a 2-stage platelet activation process induced by the glycoprotein ibalpha mechanoreceptor. *Blood*, 100(8):2793–2800.

McClean, M. N., Mody, A., Broach, J. R., and Ramanathan, S. (2007). Cross-talk and decision making in map kinase pathways. *Nat Genet*, 39(3):409–414.

Mellion, B. T., Ignarro, L. J., Ohlstein, E. H., Pontecorvo, E. G., Hyman, A. L., and Kadowitz, P. J. (1981). Evidence for the inhibitory role of guanosine 3′, 5′-monophosphate in adp-induced human platelet aggregation in the presence of nitric oxide and related vasodilators. *Blood*, 57(5):946–955.

Mendoza, L. and Xenarios, I. (2006). A method for the generation of standardized qualitative dynamical systems of regulatory networks. *Theor Biol Med Model*, 3:13.

Menten, L. and Michaelis, M. (1913). Die Kinetik der Invertinwirkung. *Biochem Z*, 49:333–369.

Meyer, R., D'Alessandro, L. A., Kar, S., Kramer, B., She, B., Kaschek, D., Hahn, B., Wrangborg, D., Karlsson, J., Kvarnström, M., Jirstrand, M., Lehmann, W.-D., Timmer, J., Höfer, T., and Klingmüller, U. (2012). Heterogeneous kinetics of akt signaling in individual cells are accounted for by variable protein concentration. *Front Physiol*, 3:451.

Meyer, T., Amaya, M., Desai, H., Robles-Carrillo, L., Hatfield, M., Francis, J. L., and Amirkhosravi, A. (2010). Human platelets contain and release tweak. *Platelets*, 21(7):571–574.

Michelson, A. D. (2006). *Platelets*. Academic Press.

Michelson, A. D. (2010). Antiplatelet therapies for the treatment of cardiovascular disease. *Nature reviews. Drug discovery*, 9:154–69. 2.

Miller, M. L., Jensen, L. J., Diella, F., J?rgensen, C., Tinti, M., Li, L., Hsiung, M., Parker, S. A., Bordeaux, J., Sicheritz-Ponten, T., Olhovsky, M., Pasculescu, A., Alexander, J., Knapp, S., Blom, N., Bork, P., Li, S., Cesareni, G., Pawson, T., Turk, B. E., Yaffe, M. B., Brunak, S., and Linding, R. (2008). Linear motif atlas for phosphorylation-dependent signaling. *Sci Signal*, 1(35):ra2.

Milo, R., Shen-Orr, S., Itzkovitz, S., Kashtan, N., Chklovskii, D., and Alon, U. (2002). Network motifs: simple building blocks of complex networks. *Science*, 298(5594):824–827.

Mischnik, M., Boyanova, D., Hubertus, K., Geiger, J., Philippi, N., Dittrich, M., Wangorsch, G., TImmer, J., and Dandekar, T. (2013). A boolean view separates platelet activatory and inhibitory signalling as verified by phosphorylation monitoring including threshold behaviour and integrin modulation. *Mol Biosyst*, page (accepted).

Monine, M. I., Posner, R. G., Savage, P. B., Faeder, J. R., and Hlavacek, W. S. (2010). Modeling multivalent ligand-receptor interactions with steric constraints on configurations of cell-surface receptor aggregates. *Biophys J*, 98(1):48–56.

Moore, C., Tymvios, C., and Emerson, M. (2010). Functional regulation of vascular and platelet activity during thrombosis by nitric oxide and endothelial nitric oxide synthase. *Thromb Haemost*, 104(2):342–349.

Morris, M. K., Saez-Rodriguez, J., Sorger, P. K., and Lauffenburger, D. A. (2010). Logic-based models for the analysis of cell signaling networks. *Biochemistry*, 49(15):3216–3224.

Moser, M., Nieswandt, B., Ussar, S., Pozgajova, M., and Fässler, R. (2008). Kindlin-3 is essential for integrin activation and platelet aggregation. *Nat Med*, 14(3):325–330.

Moubayidin, L., Di Mambro, R., and Sabatini, S. (2009). Cytokinin-auxin crosstalk. *Trends Plant Sci*, 14(10):557–562.

Movsesian, M. A. and Bristow, M. R. (2005). Alterations in camp-mediated signaling and their role in the pathophysiology of dilated cardiomyopathy. *Curr Top Dev Biol*, 68:25–48.

Mukai, Y., Nakamura, T., Yoshikawa, M., Yoshioka, Y., Tsunoda, S.-i., Nakagawa, S., Yamagata, Y., and Tsutsumi, Y. (2010). Solution of the structure of the tnf-tnfr2 complex. *Sci Signal*, 3(148):ra83.

Mukhtar, M. S., Carvunis, A.-R., Dreze, M., Epple, P., Steinbrenner, J., Moore, J., Tasan, M., Galli, M., Hao, T., Nishimura, M. T., Pevzner, S. J., Donovan, S. E., Ghamsari, L., Santhanam, B., Romero, V., Poulin, M. M., Gebreab, F., Gutierrez, B. J., Tam, S., Monachello, D., Boxem, M., Harbort, C. J., McDonald, N., Gai, L., Chen, H., He, Y., , E. U. E. C., Vandenhaute, J., Roth, F. P., Hill, D. E., Ecker, J. R., Vidal, M., Beynon, J., Braun, P., and Dangl, J. L. (2011). Independently evolved virulence effectors converge onto hubs in a plant immune system network. *Science*, 333(6042):596–601.

Mullershausen, F., Friebe, A., Feil, R., Thompson, W. J., Hofmann, F., and Koesling, D. (2003). Direct activation of pde5 by cgmp: long-term effects within no/cgmp signaling. *J Cell Biol*, 160(5):719–727.

Murray, J. D. (2003). *Mathematical Biology: Spatial models and biomedical applications.* Springer.

Murthy, K. S. and Zhou, H. (2003). Selective phosphorylation of the ip3r-i in vivo by cgmp-dependent protein kinase in smooth muscle. *Am J Physiol Gastrointest Liver Physiol*, 284(2):G221–G230.

Murthy, K. S., Zhou, H., and Makhlouf, G. M. (2002). PKA-dependent activation of PDE3A and PDE4 and inhibition of adenylyl cyclase V/VI in smooth muscle. *American journal of physiology. Cell physiology*, 282:C508—C517. 3.

Nakahata, N. (2008). Thromboxane a2: physiology/pathophysiology, cellular signal transduction and pharmacology. *Pharmacol Ther*, 118(1):18–35.

Nakayama, M., Ishidoh, K., Kayagaki, N., Kojima, Y., Yamaguchi, N., Nakano, H., Kominami, E., Okumura, K., and Yagita, H. (2002). Multiple pathways of tweak-induced cell death. *J Immunol*, 168(2):734–743.

Naseem, M. and Dandekar, T. (2012). The role of auxin-cytokinin antagonism in plant-pathogen interactions. *PLoS Pathog*, 8(11):e1003026.

Naseem, M., Philippi, N., Hussain, A., Wangorsch, G., Ahmed, N., and Dandekar, T. (2012). Integrated systems view on networking by hormones in arabidopsis immunity reveals multiple crosstalk for cytokinin. *Plant Cell*.

Natarajan, M., Lin, K.-M., Hsueh, R. C., Sternweis, P. C., and Ranganathan, R. (2006). A global analysis of cross-talk in a mammalian cellular signalling network. *Nat Cell Biol*, 8(6):571–580.

Naudé, P. J. W., den Boer, J. A., Luiten, P. G. M., and Eisel, U. L. M. (2011). Tumor necrosis factor receptor cross-talk. *FEBS J*, 278(6):888–898.

Navarro, L., Dunoyer, P., Jay, F., Arnold, B., Dharmasiri, N., Estelle, M., Voinnet, O., and Jones, J. D. G. (2006). A plant mirna contributes to antibacterial resistance by repressing auxin signaling. *Science*, 312(5772):436–439.

Nelson, J. (2009). *Structure and Funtion in Cell Signalling*. John Wiley and Sons.

Netherton, S. J., Jimmo, S. L., Palmer, D., Tilley, D. G., Dunkerley, H. A., Raymond, D. R., Russell, J. C., Absher, P. M., Sage, E. H., Vernon, R. B., and Maurice, D. H. (2002). Altered phosphodiesterase 3-mediated cAMP hydrolysis contributes to a hypermotile phenotype in obese JCR:LA-cp rat aortic vascular smooth muscle cells: implications for diabetes-associated cardiovascular disease. *Diabetes*, 51:1194–200. 4.

Newman, M. E. J. (2003). The structure and function of complex networks. *SIAM reviews*, 45:167 – 256.

Newman, P. J. (1999). Switched at birth: a new family for pecam-1. *J Clin Invest*, 103(1):5–9.

Nikolsky, Y. and Kleemann, R. (2010). Systems biology approaches to the study of cardiovascular drugs. *Methods Mol Biol*, 662:221–243.

Nolte, C., Eigenthaler, M., Horstrup, K., Honig-Liedl, P., and Walter, U. (1994). Synergistic phosphorylation of the focal adhesion-associated vasodilator-stimulated phosphoprotein in intact human platelets in response to cGMP- and cAMP-elevating platelet inhibitors. *Biochem Pharmacol*, 48:1569–75. 8.

Oeckinghaus, A., Hayden, M. S., and Ghosh, S. (2011). Crosstalk in nf-kb signaling pathways. *Nat Immunol*, 12(8):695–708.

Offermanns, S. (2006). Activation of platelet function through g protein-coupled receptors. *Circ Res*, 99(12):1293–1304.

Omori, K. and Kotera, J. (2007). Overview of PDEs and their regulation. *Circulation research*, 100:309–27. 3.

Ozüyaman, B., Gödecke, A., Küsters, S., Kirchhoff, E., Scharf, R. E., and Schrader, J. (2005). Endothelial nitric oxide synthase plays a minor role in inhibition of arterial thrombus formation. *Thromb Haemost*, 93(6):1161–1167.

Parsian, A., Todd, R. D., Cloninger, C. R., Hoffman, P. L., Ovchinnikova, L., Ikeda, H., and Tabakoff, B. (1996). Platelet adenylyl cyclase activity in alcoholics and subtypes of alcoholics. WHO/ISBRA study clinical centers. *Alcohol Clin Exp Res*, 20:745–51. 4.

Patrignani, P., Di Febbo, C., Tacconelli, S., Douville, K., Guglielmi, M. D., Horvath, R. J., Ding, M., Sierra, K., Stitham, J., Gleim, S., Baccante, G., Moretta, V., Di Francesco, L., Capone, M. L., Porreca, E., and Hwa, J. (2008). Differential association between human prostacyclin receptor polymorphisms and the development of venous thrombosis and intimal hyperplasia: a clinical biomarker study. *Pharmacogenetics and genomics*, 18:611–20. 7.

Pearson, K. and Lee, A. (1903). On the laws of inheritance in man: I. inheritance of physical characters. *Biometrika*, 2(4):pp. 357–462.

Pearson, T. A., Mensah, G. A., Alexander, R. W., Anderson, J. L., Cannon, 3rd, R. O., Criqui, M., Fadl, Y. Y., Fortmann, S. P., Hong, Y., Myers, G. L., Rifai, N., Smith, Jr, S. C., Taubert, K., Tracy, R. P., Vinicor, F., , C. f. D. C., Prevention, and , A. H. A. (2003). Markers of inflammation and cardiovascular disease: application to clinical and public health practice: A statement for healthcare professionals from the centers for disease control and prevention and the american heart association. *Circulation*, 107(3):499–511.

Perrault, C., Mangin, P., Santer, M., Baas, M.-J., Moog, S., Cranmer, S. L., Pikovski, I., Williamson, D., Jackson, S. P., Cazenave, J.-P., and Lanza, F. (2003). Role of the intracellular domains of gpib in controlling the adhesive properties of the platelet gpib/v/ix complex. *Blood*, 101(9):3477–3484.

Pertry, I., Václavíková, K., Depuydt, S., Galuszka, P., Spíchal, L., Temmerman, W., Stes, E., Schmülling, T., Kakimoto, T., Van Montagu, M. C. E., Strnad, M., Holsters, M., Tarkowski, P., and Vereecke, D. (2009). Identification of rhodococcus fascians cytokinins and their modus operandi to reshape the plant. *Proc Natl Acad Sci U S A*, 106(3):929–934.

Petrich, B. G., Marchese, P., Ruggeri, Z. M., Spiess, S., Weichert, R. A. M., Ye, F., Tiedt, R., Skoda, R. C., Monkley, S. J., Critchley, D. R., and Ginsberg, M. H. (2007). Talin is required for integrin-mediated platelet function in hemostasis and thrombosis. *J Exp Med*, 204(13):3103–3111.

Pezzino, S., Paratore, S., and Cavallaro, S. (2011). Systems biology of apoptosis and survival: implications for drug development. *Curr Pharm Des*, 17(3):190–203.

Philippi, N., Walter, D., Schlatter, R., Ferreira, K., Ederer, M., Sawodny, O., Timmer, J., Borner, C., and Dandekar, T. (2009). Modeling system states in liver cells: survival, apoptosis and their modifications in response to viral infection. *BMC Syst Biol*, 3:97.

Pierre, S., Eschenhagen, T., Geisslinger, G., and Scholich, K. (2009). Capturing adenylyl cyclases as potential drug targets. *Nature reviews. Drug discovery*, 8:321–35. 4.

Podzuweit, T., Nennstiel, P., and Müller, A. (1995). Isozyme selective inhibition of cgmp-stimulated cyclic nucleotide phosphodiesterases by erythro-9-(2-hydroxy-3-nonyl) adenine. *Cell Signal*, 7(7):733–738.

Poppe, H., Rybalkin, S. D., Rehmann, H., Hinds, T. R., Tang, X. B., Christensen, A. E., Schwede, F., Genieser, H. G., Bos, J. L., Doskeland, S. O., Beavo, J. A., and Butt, E. (2008). Cyclic nucleotide analogs as probes of signaling pathways. *Nature methods*, 5:277–8. 4.

Port, J. D. and Bristow, M. R. (2001). beta-adrenergic receptors, transgenic mice, and pharmacological model systems. *Mol Pharmacol*, 60(4):629–631.

Pozuelo Rubio, M., Campbell, D. G., Morrice, N. A., and Mackintosh, C. (2005). Phosphodiesterase 3A binds to 14-3-3 proteins in response to PMA-induced phosphorylation of ser428. *The Biochemical journal*, 392:163–72. Pt 1.

Premsler, T., Lewandrowski, U., Sickmann, A., and Zahedi, R. P. (2011). Phosphoproteome analysis of the platelet plasma membrane. *Methods Mol Biol*, 728:279–290.

Purvis, J. E., Chatterjee, M. S., Brass, L. F., and Diamond, S. L. (2008). A molecular signaling model of platelet phosphoinositide and calcium regulation during homeostasis and p2y1 activation. *Blood*, 112(10):4069–4079.

Qiao, J., Holian, O., Lee, B.-S., Huang, F., Zhang, J., and Lum, H. (2008). Phosphorylation of gtp dissociation inhibitor by pka negatively regulates rhoa. *Am J Physiol Cell Physiol*, 295(5):C1161–C1168.

Ramsey, S. A., Gold, E. S., and Aderem, A. (2010). A systems biology approach to understanding atherosclerosis. *EMBO Mol Med*, 2(3):79–89.

Rao, Y. J. and Xi, L. (2009). Pivotal effects of phosphodiesterase inhibitors on myocyte contractility and viability in normal and ischemic hearts. *Acta pharmacologica Sinica*, 30:1–24. 1.

Raue, A., Kreutz, C., Maiwald, T., Bachmann, J., Schilling, M., Klingmüller, U., and Timmer, J. (2009). Structural and practical identifiability analysis of partially observed dynamical models by exploiting the profile likelihood. *Bioinformatics*, 25(15):1923–1929.

Rauert, H., Wicovsky, A., Müller, N., Siegmund, D., Spindler, V., Waschke, J., Kneitz, C., and Wajant, H. (2010). Membrane tumor necrosis factor (tnf) induces p100 processing via tnf receptor-2 (tnfr2). *J Biol Chem*, 285(10):7394–7404.

Ren, M.-Y. and Sui, S.-J. (2012). The role of tweak/fn14 in cardiac remodeling. *Mol Biol Rep*, 39(11):9971–9977.

Riba, R., Oberprieler, N. G., Roberts, W., and Naseem, K. M. (2006). Von willebrand factor activates endothelial nitric oxide synthase in blood platelets by a glycoprotein ib-dependent mechanism. *J Thromb Haemost*, 4(12):2636–2644.

Riba, R., Sharifi, M., Farndale, R. W., and Naseem, K. M. (2005). Regulation of platelet guanylyl cyclase by collagen: evidence that glycoprotein vi mediates platelet nitric oxide synthesis in response to collagen. *Thromb Haemost*, 94(2):395–403.

Rink, T. J., Smith, S. W., and Tsien, R. Y. (1982). Cytoplasmic free ca2+ in human platelets: Ca2+ thresholds and ca-independent activation for shape-change and secretion. *FEBS Lett*, 148(1):21–26.

Rittenhouse, S. E. and Sasson, J. P. (1985). Measurement of ip3 mass as a monitor of phospholipase c activation in stimulated human platelets. *Nouv Rev Fr Hematol*, 27(4):239–242.

Rivero, R. M., Kojima, M., Gepstein, A., Sakakibara, H., Mittler, R., Gepstein, S., and Blumwald, E. (2007). Delayed leaf senescence induces extreme drought tolerance in a flowering plant. *Proc Natl Acad Sci U S A*, 104(49):19631–19636.

Rivet-Bastide, M., Vandecasteele, G., Hatem, S., Verde, I., Bénardeau, A., Mercadier, J. J., and Fischmeister, R. (1997). cgmp-stimulated cyclic nucleotide phosphodiesterase regulates the basal calcium current in human atrial myocytes. *J Clin Invest*, 99(11):2710–2718.

Robert-Seilaniantz, A., Grant, M., and Jones, J. D. G. (2011). Hormone crosstalk in plant disease and defense: more than just jasmonate-salicylate antagonism. *Annu Rev Phytopathol*, 49:317–343.

Robert-Seilaniantz, A., Navarro, L., Bari, R., and Jones, J. D. G. (2007). Pathological hormone imbalances. *Curr Opin Plant Biol*, 10(4):372–379.

Rodius, S., Chaloin, O., Moes, M., Schaffner-Reckinger, E., Landrieu, I., Lippens, G., Lin, M., Zhang, J., and Kieffer, N. (2008). The talin rod ibs2 alpha-helix interacts with the beta3 integrin cytoplasmic tail membrane-proximal helix by establishing charge complementary salt bridges. *J Biol Chem*, 283(35):24212–24223.

Rolf, M. G., Brearley, C. A., and Mahaut-Smith, M. P. (2001). Platelet shape change evoked by selective activation of p2x1 purinoceptors with alpha,beta-methylene atp. *Thromb Haemost*, 85(2):303–308.

Rolf, M. G. and Mahaut-Smith, M. P. (2002). Effects of enhanced p2x1 receptor ca2+ influx on functional responses in human platelets. *Thromb Haemost*, 88(3):495–502.

Rosen, O. M. (1987). After insulin binds. *Science*, 237(4821):1452–1458.

Rota, G., Kac, M., and Schwartz, J. T. (1986). *Discrete Thoughts: Essays on Mathematics, Science and Philosophy*. Birkhaeuser Boston.

Rothe, M., Pan, M. G., Henzel, W. J., Ayres, T. M., and Goeddel, D. V. (1995a). The tnfr2-traf signaling complex contains two novel proteins related to baculoviral inhibitor of apoptosis proteins. *Cell*, 83(7):1243–1252.

Rothe, M., Sarma, V., Dixit, V. M., and Goeddel, D. V. (1995b). Traf2-mediated activation of nf-kappa b by tnf receptor 2 and cd40. *Science*, 269(5229):1424–1427.

Rowley, J. W., Oler, A. J., Tolley, N. D., Hunter, B. N., Low, E. N., Nix, D. A., Yost, C. C., Zimmerman, G. A., and Weyrich, A. S. (2011). Genome-wide rna-seq analysis of human and mouse platelet transcriptomes. *Blood*, 118(14):e101–e111.

Rual, J.-F., Venkatesan, K., Hao, T., Hirozane-Kishikawa, T., Dricot, A., Li, N., Berriz, G. F., Gibbons, F. D., Dreze, M., Ayivi-Guedehoussou, N., Klitgord, N., Simon, C., Boxem, M., Milstein, S., Rosenberg, J., Goldberg, D. S., Zhang, L. V., Wong, S. L., Franklin, G., Li, S., Albala, J. S., Lim, J., Fraughton, C., Llamosas, E., Cevik, S., Bex, C., Lamesch, P., Sikorski, R. S., Vandenhaute, J., Zoghbi, H. Y., Smolyar, A., Bosak, S., Sequerra, R., Doucette-Stamm, L., Cusick, M. E., Hill, D. E., Roth, F. P., and Vidal, M. (2005). Towards a proteome-scale map of the human protein-protein interaction network. *Nature*, 437(7062):1173–1178.

Ruggeri, Z. M. and Mendolicchio, G. L. (2007). Adhesion mechanisms in platelet function. *Circ Res*, 100(12):1673–1685.

Rukoyatkina, N., Walter, U., Friebe, A., and Gambaryan, S. (2011). Differentiation of cgmp-dependent and -independent nitric oxide effects on platelet apoptosis and reactive oxygen species production using platelets lacking soluble guanylyl cyclase. *Thromb Haemost*, 106(5):922–933.

Saez-Rodriguez, J., Alexopoulos, L. G., Epperlein, J., Samaga, R., Lauffenburger, D. A., Klamt, S., and Sorger, P. K. (2009). Discrete logic modelling as a means to link protein signalling networks with functional analysis of mammalian signal transduction. *Mol Syst Biol*, 5:331.

Saez-Rodriguez, J., Alexopoulos, L. G., Zhang, M., Morris, M. K., Lauffenburger, D. A., and Sorger, P. K. (2011). Comparing signaling networks between normal and transformed hepatocytes using discrete logical models. *Cancer Res*, 71(16):5400–5411.

Saez-Rodriguez, J., Simeoni, L., Lindquist, J. A., Hemenway, R., Bommhardt, U., Arndt, B., Haus, U.-U., Weismantel, R., Gilles, E. D., Klamt, S., and Schraven, B. (2007). A logical model provides insights into t cell receptor signaling. *PLoS Comput Biol*, 3(8):e163.

Saitoh, T., Nakayama, M., Nakano, H., Yagita, H., Yamamoto, N., and Yamaoka, S. (2003). Tweak induces nf-kappab2 p100 processing and long lasting nf-kappab activation. *J Biol Chem*, 278(38):36005–36012.

Samaga, R., Saez-Rodriguez, J., Alexopoulos, L. G., Sorger, P. K., and Klamt, S. (2009). The logic of egfr/erbb signaling: theoretical properties and analysis of high-throughput data. *PLoS Comput Biol*, 5(8):e1000438.

Santner, A. and Estelle, M. (2009). Recent advances and emerging trends in plant hormone signalling. *Nature*, 459(7250):1071–1078.

Sauro, H. M. and Kholodenko, B. N. (2004). Quantitative analysis of signaling networks. *Prog Biophys Mol Biol*, 86(1):5–43.

Savageau, M. A. (1995). Michaelis-menten mechanism reconsidered: implications of fractal kinetics. *J Theor Biol*, 176(1):115–124.

Savi, P., Labouret, C., Delesque, N., Guette, F., Lupker, J., and Herbert, J. M. (2001). P2y(12), a new platelet adp receptor, target of clopidogrel. *Biochem Biophys Res Commun*, 283(2):379–383.

Sawyers, C. (2004). Targeted cancer therapy. *Nature*, 432(7015):294–297.

Schanz, J., Pusch, J., Hansmann, J., and Walles, H. (2010). Vascularised human tissue models: a new approach for the refinement of biomedical research. *J Biotechnol*, 148(1):56–63.

Schäfer, A., Burkhardt, M., Vollkommer, T., Bauersachs, J., Münzel, T., Walter, U., and Smolenski, A. (2003). Endothelium-dependent and -independent relaxation and vasp serines 157/239 phosphorylation by cyclic nucleotide-elevating vasodilators in rat aorta. *Biochem Pharmacol*, 65(3):397–405.

Schinner, E., Salb, K., and Schlossmann, J. (2011). Signaling via irag is essential for no/cgmp-dependent inhibition of platelet activation. *Platelets*, 22(3):217–227.

Schlatter, R., Philippi, N., Wangorsch, G., Pick, R., Sawodny, O., Borner, C., Timmer, J., Ederer, M., and Dandekar, T. (2011). Integration of boolean models exemplified on hepatocyte signal transduction. *Brief Bioinform*.

Schlatter, R., Schmich, K., Avalos Vizcarra, I., Scheurich, P., Sauter, T., Borner, C., Ederer, M., Merfort, I., and Sawodny, O. (2009). On/off and beyond–a boolean model of apoptosis. *PLoS Comput Biol*, 5(12):e1000595.

Schmich, K., Schlatter, R., Corazza, N., Sá Ferreira, K., Ederer, M., Brunner, T., Borner, C., and Merfort, I. (2011). Tumor necrosis factor ? sensitizes primary murine hepatocytes to fas/cd95-induced apoptosis in a bim- and bid-dependent manner. *Hepatology*, 53(1):282–292.

Schmidt, K., Schrammel, A., Koesling, D., and Mayer, B. (2001). Molecular mechanisms involved in the synergistic activation of soluble guanylyl cyclase by YC-1 and nitric oxide in endothelial cells. *Molecular pharmacology*, 59:220–4. 2.

Schnell, S. and Turner, T. E. (2004). Reaction kinetics in intracellular environments with macromolecular crowding: simulations and rate laws. *Prog Biophys Mol Biol*, 85(2-3):235–260.

Schultess, J., Danielewski, O., and Smolenski, A. P. (2005). Rap1gap2 is a new gtpase-activating protein of rap1 expressed in human platelets. *Blood*, 105(8):3185–3192.

Schulz, R. and Heusch, G. (2009). Tumor necrosis factor-alpha and its receptors 1 and 2: Yin and yang in myocardial infarction? *Circulation*, 119(10):1355–1357.

Schwarz, G. (1978). Estimating the dimension of a model. *Annals of Statistics*, 6(2):461 – 464.

Schwarz, U. R., Geiger, J., Walter, U., and Eigenthaler, M. (1999). Flow cytometry analysis of intracellular vasp phosphorylation for the assessment of activating and inhibitory signal transduction pathways in human platelets–definition and detection of ticlopidine/clopidogrel effects. *Thromb Haemost*, 82(3):1145–1152.

Schwarz, U. R., Walter, U., and Eigenthaler, M. (2001). Taming platelets with cyclic nucleotides. *Biochemical pharmacology*, 62:1153–61. 9.

Schwertz, H., Tolley, N. D., Foulks, J. M., Denis, M. M., Risenmay, B. W., Buerke, M., Tilley, R. E., Rondina, M. T., Harris, E. M., Kraiss, L. W., Mackman, N., Zimmerman, G. A., and Weyrich, A. S. (2006). Signal-dependent splicing of tissue factor pre-mrna modulates the thrombogenicity of human platelets. *J Exp Med*, 203(11):2433–2440.

Seber, G. A. F. and Wild, C. J. (1989). *Nonlinear regression*. New York: Wiley.

Self, S. G. and Liang, K. Y. (1987). Asymptotic properties of maximum likelihood estimators and likelihood ratio tests under nonstandard conditions. *Journal of the American Statistical Association*, 82:605 – 610.

Seybold, J., Thomas, D., Witzenrath, M., Boral, S., Hocke, A. C., Bürger, A., Hatzelmann, A., Tenor, H., Schudt, C., Krüll, M., Schütte, H., Hippenstiel, S., and Suttorp, N. (2005). Tumor necrosis factor-alpha-dependent expression of phosphodiesterase 2: role in endothelial hyperpermeability. *Blood*, 105(9):3569–3576.

Shakur, Y., Takeda, K., Kenan, Y., Yu, Z. X., Rena, G., Brandt, D., Houslay, M. D., Degerman, E., Ferrans, V. J., and Manganiello, V. C. (2000). Membrane localization of cyclic nucleotide phosphodiesterase 3 (PDE3). two n-terminal domains are required for the efficient targeting to, and association of, PDE3 with endoplasmic reticulum. *The Journal of biological chemistry*, 275:38749–61. 49.

Shannon, P., Markiel, A., Ozier, O., Baliga, N. S., Wang, J. T., Ramage, D., Amin, N., Schwikowski, B., and Ideker, T. (2003). Cytoscape: a software environment for integrated models of biomolecular interaction networks. *Genome Res*, 13(11):2498–2504.

Shattil, S. J., Kim, C., and Ginsberg, M. H. (2010). The final steps of integrin activation: the end game. *Nat Rev Mol Cell Biol*, 11(4):288–300.

Shattil, S. J. and Newman, P. J. (2004). Integrins: dynamic scaffolds for adhesion and signaling in platelets. *Blood*, 104(6):1606–1615.

Siess, W., Winegar, D. A., and Lapetina, E. G. (1990). Rap1-b is phosphorylated by protein kinase a in intact human platelets. *Biochem Biophys Res Commun*, 170(2):944–950.

Silvey, S. D. (1975). *Statistical Inference*. Chapman & Hall.

Sim, D. S., Merrill-Skoloff, G., Furie, B. C., Furie, B., and Flaumenhaft, R. (2004). Initial accumulation of platelets during arterial thrombus formation in vivo is inhibited by elevation of basal camp levels. *Blood*, 103(6):2127–2134.

Smith, A. M., Xu, W., Sun, Y., Faeder, J. R., and Marai, G. E. (2012). Rulebender: integrated modeling, simulation and visualization for rule-based intracellular biochemistry. *BMC Bioinformatics*, 13 Suppl 8:S3.

Smith, R. A. and Baglioni, C. (1987). The active form of tumor necrosis factor is a trimer. *J Biol Chem*, 262(15):6951–6954.

Smolenski, A. (2012). Novel roles of camp/cgmp-dependent signaling in platelets. *J Thromb Haemost*, 10(2):167–176.

Smolenski, A., Bachmann, C., Reinhard, K., Honig-Liedl, P., Jarchau, T., Hoschuetzky, H., and Walter, U. (1998). Analysis and regulation of vasodilator-stimulated phosphoprotein serine 239 phosphorylation in vitro and in intact cells using a phosphospecific monoclonal antibody. *J Biol Chem*, 273:20029–35. 32.

Smoot, M. E., Ono, K., Ruscheinski, J., Wang, P.-L., and Ideker, T. (2011). Cytoscape 2.8: new features for data integration and network visualization. *Bioinformatics*, 27(3):431–432.

Sneddon, M. W., Faeder, J. R., and Emonet, T. (2011). Efficient modeling, simulation and coarse-graining of biological complexity with nfsim. *Nat Methods*, 8(2):177–183.

Soderling, S. H., Bayuga, S. J., and Beavo, J. A. (1998). Identification and characterization of a novel family of cyclic nucleotide phosphodiesterases. *J Biol Chem*, 273(25):15553–8. 0021-9258 (Print) Journal Article Research Support, U.S. Gov't, P.H.S.

Sontag, E. D. (2002). For differential equations with r parameters, 2r+1 experiments are enough for identification. *Journal of Nonlinear Science*, 12 (6):553 – 583.

Stegner, D. and Nieswandt, B. (2011). Platelet receptor signaling in thrombus formation. *J Mol Med (Berl)*, 89(2):109–121.

Stel, A. J., Ten Cate, B., Jacobs, S., Kok, J. W., Spierings, D. C. J., Dondorff, M., Helfrich, W., Kluin-Nelemans, H. C., de Leij, L. F. M. H., Withoff, S., and Kroesen, B. J. (2007). Fas receptor clustering and involvement of the death receptor pathway in rituximab-mediated apoptosis with concomitant sensitization of lymphoma b cells to fas-induced apoptosis. *J Immunol*, 178(4):2287–2295.

Stelzl, U., Worm, U., Lalowski, M., Haenig, C., Brembeck, F. H., Goehler, H., Stroedicke, M., Zenkner, M., Schoenherr, A., Koeppen, S., Timm, J., Mintzlaff, S., Abraham, C., Bock, N., Kietzmann, S., Goedde, A., Toksöz, E., Droege, A., Krobitsch, S., Korn, B., Birchmeier, W., Lehrach, H., and Wanker, E. E. (2005). A human protein-protein interaction network: a resource for annotating the proteome. *Cell*, 122(6):957–968.

Stoll, G., Viara, E., Barillot, E., and Calzone, L. (2012). Continuous time boolean modeling for biological signaling: application of gillespie algorithm. *BMC Syst Biol*, 6:116.

Subramaniam, P. S., Torres, B. A., and Johnson, H. M. (2001). So many ligands, so few transcription factors: a new paradigm for signaling through the stat transcription factors. *Cytokine*, 15(4):175–187.

Suzuki, K., Saito, S.-y., and Ishikawa, T. (2012). Involvement of phosphatidylcholine-specific phospholipase c in thromboxane a2 receptor-mediated extracellular ca? influx in rat aorta. *Eur J Pharmacol*, 677(1-3):123–130.

Suzuki, Y., Yamamoto, M., Wada, H., Ito, M., Nakano, T., Sasaki, Y., Narumiya, S., Shiku, H., and Nishikawa, M. (1999). Agonist-induced regulation of myosin phosphatase activity in human platelets through activation of rho-kinase. *Blood*, 93(10):3408–3417.

Swameye, I., Muller, T. G., Timmer, J., Sandra, O., and Klingmuller, U. (2003). Identification of nucleocytoplasmic cycling as a remote sensor in cellular signaling by databased modeling. *Proc Natl Acad Sci U S A*, 100:1028–33. 3.

Takahashi, M., Takeda, S., Kurokawa, S., Kubo, T., Fukuda, N., and Izumi, T. (2003). Cyclic gmp production by anp, bnp, and no during worsening and improvement of chronic heart failure. *Jpn Heart J*, 44(5):713–724.

Tang, K. M., Jang, E. K., and Haslam, R. J. (1994). Photoaffinity labelling of cyclic gmp-inhibited phosphodiesterase (pde iii) in human and rat platelets and rat tissues: effects of phosphodiesterase inhibitors. *Eur J Pharmacol*, 268(1):105–114.

Tansey, M. G. and Szymkowski, D. E. (2009). The tnf superfamily in 2009: new pathways, new indications, and new drugs. *Drug Discov Today*, 14(23-24):1082–1088.

Terfve, C. D. A., Cokelaer, T., Henriques, D., Macnamara, A., Gonçalves, E., Morris, M. K., van Iersel, M., Lauffenburger, D. A., and Saez-Rodriguez, J. (2012). Cellnoptr: a flexible toolkit to train protein signaling networks to data using multiple logic formalisms. *BMC Syst Biol*, 6(1):133.

Tertyshnikova, S., Yan, X., and Fein, A. (1998). cgmp inhibits ip3-induced Ca2+ release in intact rat megakaryocytes via cgmp- and camp-dependent protein kinases. *J Physiol*, 512 (Pt 1):89–96.

Thakar, J., Schleinkofer, K., Borner, C., and Dandekar, T. (2006). Rip death domain structural interactions implicated in tnf-mediated proliferation and survival. *Proteins*, 63(3):413–423.

Timmer, J. and Mueller, T. G. (2004). Modeling the nonlinear dynamics of cellular signal transduction. *International Journal of Bifurcation and Chaos*, 14:2069 – 2079.

Timmer, J., Rust, H., Horbelt, W., and Voss, H. U. (2000). Parametric, nonparametric and parametric modelling of a chaotic circuit time series. *Physics Letters A*, 274:123 – 134.

Tokunaga, F. and Iwai, K. (2012). Lubac, a novel ubiquitin ligase for linear ubiquitination, is crucial for inflammation and immune responses. *Microbes Infect*, 14(7-8):563–572.

Tolhurst, G., Carter, R. N., Amisten, S., Holdich, J. P., Erlinge, D., and Mahaut-Smith, M. P. (2008). Expression profiling and electrophysiological studies suggest a major role for orai1 in the store-operated ca2+ influx pathway of platelets and megakaryocytes. *Platelets*, 19(4):308–313.

Torres, A. J., Holowka, D., and Baird, B. A. (2011). Micropatterned ligand arrays to study spatial regulation in fc receptor signaling. *Methods Mol Biol*, 748:195–207.

Tracey, K. J. and Cerami, A. (1993). Tumor necrosis factor, other cytokines and disease. *Annu Rev Cell Biol*, 9:317–343.

Turner, T. E., Schnell, S., and Burrage, K. (2004). Stochastic approaches for modelling in vivo reactions. *Comput Biol Chem*, 28(3):165–178.

Uchida, N. and Tasaka, M. (2010). Intersections between immune responses and morphological regulation in plants. *J Exp Bot*, 61(10):2539–2547.

Uetz, P., Giot, L., Cagney, G., Mansfield, T. A., Judson, R. S., Knight, J. R., Lockshon, D., Narayan, V., Srinivasan, M., Pochart, P., Qureshi-Emili, A., Li, Y., Godwin, B., Conover, D., Kalbfleisch, T., Vijayadamodar, G., Yang, M., Johnston, M., Fields, S., and Rothberg, J. M. (2000). A comprehensive analysis of protein-protein interactions in saccharomyces cerevisiae. *Nature*, 403(6770):623–627.

Ulitsky, I., Gat-Viks, I., and Shamir, R. (2008). Metareg: a platform for modeling, analysis and visualization of biological systems using large-scale experimental data. *Genome Biol*, 9(1):R1.

Vallabhapurapu, S. and Karin, M. (2009). Regulation and function of nf-kappab transcription factors in the immune system. *Annu Rev Immunol*, 27:693–733.

van Riel, N. A. (2006). Dynamic modelling and analysis of biochemical networks: mechanism-based models and model-based experiments. *Brief Bioinform*, 7:364–74. 4.

Vandamme, J., Castermans, D., and Thevelein, J. M. (2012). Molecular mechanisms of feedback inhibition of protein kinase a on intracellular camp accumulation. *Cell Signal*, 24(8):1610–1618.

Varga-Szabo, D., Braun, A., and Nieswandt, B. (2009). Calcium signaling in platelets. *J Thromb Haemost*, 7(7):1057–1066.

Varga-Szabo, D., Pleines, I., and Nieswandt, B. (2008). Cell adhesion mechanisms in platelets. *Arterioscler Thromb Vasc Biol*, 28(3):403–412.

Verhulst, P. F. (1838). Notice sur la loi que la population suit dans son accroissement. correspondance mathematique et physique publiee par a. *Quetelet*, 10:113–121.

Vince, J. E., Chau, D., Callus, B., Wong, W. W.-L., Hawkins, C. J., Schneider, P., McKinlay, M., Benetatos, C. A., Condon, S. M., Chunduru, S. K., Yeoh, G., Brink, R., Vaux, D. L., and Silke, J. (2008). Tweak-fn14 signaling induces lysosomal degradation of a ciap1-traf2 complex to sensitize tumor cells to tnfalpha. *J Cell Biol*, 182(1):171–184.

Volterra, V. (1931). *Variations and fluctuations of the number of individuals in animal species living together*.

von Neumann, J. and Morgenstern, O. (1953). *Theory of Games and Economic Behavior*. John Wiley and Sons.

Vuong, Q. H. (1989). Likelihood ratio tests for model selection and non-nested hypotheses. *Econometrica*, 57(2):307 – 333.

Wajant, H. (2011). Increasing complexity in tnfr1 signaling. *FEBS J*, 278(6):861.

Wajant, H. and Scheurich, P. (2001). Tumor necrosis factor receptor-associated factor (traf) 2 and its role in tnf signaling. *Int J Biochem Cell Biol*, 33(1):19–32.

Wajant, H. and Scheurich, P. (2011). Tnfr1-induced activation of the classical nf-?b pathway. *FEBS J*, 278(6):862–876.

Walter, U. and Gambaryan, S. (2009). cgmp and cgmp-dependent protein kinase in platelets and blood cells. *Handb Exp Pharmacol*, (191):533–548.

Walters, D. R. and McRoberts, N. (2006). Plants and biotrophs: a pivotal role for cytokinins? *Trends Plant Sci*, 11(12):581–586.

Wang, D., Pajerowska-Mukhtar, K., Culler, A. H., and Dong, X. (2007a). Salicylic acid inhibits pathogen growth in plants through repression of the auxin signaling pathway. *Curr Biol*, 17(20):1784–1790.

Wang, L., Du, F., and Wang, X. (2008). Tnf-alpha induces two distinct caspase-8 activation pathways. *Cell*, 133(4):693–703.

Wang, S., Liu, Z., Wang, L., and Zhang, X. (2009). Nf-kappab signaling pathway, inflammation and colorectal cancer. *Cell Mol Immunol*, 6(5):327–334.

Wang, Y., Aguda, B. D., and Friedman, A. (2007b). A continuum mathematical model of endothelial layer maintenance and senescence. *Theor Biol Med Model*, 4:30.

Wang, Y.-L., Chou, F.-C., Chen, S.-J., Lin, S.-H., Chang, D.-M., and Sytwu, H.-K. (2011). Targeting pre-ligand assembly domain of tnfr1 ameliorates autoimmune diseases - an unrevealed role in downregulation of th17 cells. *J Autoimmun*, 37(3):160–170.

Wangorsch, G., Butt, E., Mark, R., Hubertus, K., Geiger, J., Dandekar, T., and Dittrich, M. (2011). Time-resolved in silico modeling of fine-tuned cAMP signaling in platelets: feedback loops, titrated phosphorylations and pharmacological modulation. *BMC Syst Biol*, 5:178.

Wardell, M. R., Reynolds, C. C., Berndt, M. C., Wallace, R. W., and Fox, J. E. (1989). Platelet glycoprotein ib beta is phosphorylated on serine 166 by cyclic amp-dependent protein kinase. *J Biol Chem*, 264(26):15656–15661.

Watanabe, N., Bodin, L., Pandey, M., Krause, M., Coughlin, S., Boussiotis, V. A., Ginsberg, M. H., and Shattil, S. J. (2008). Mechanisms and consequences of agonist-induced talin recruitment to platelet integrin alphaiibbeta3. *J Cell Biol*, 181(7):1211–1222.

Weber, A. A., Hohlfeld, T., and Schrör, K. (1999). camp is an important messenger for adp-induced platelet aggregation. *Platelets*, 10(4):238–241.

Weckwerth, W. (2011). Green systems biology - from single genomes, proteomes and metabolomes to ecosystems research and biotechnology. *J Proteomics*, 75(1):284–305.

Wehrens, X. H. T., Lehnart, S. E., and Marks, A. R. (2005). Intracellular calcium release and cardiac disease. *Annu Rev Physiol*, 67:69–98.

Weinberg, W. (1908). Ueber den nachweis der vererbung beim menschen. *Jahreshefte d Ver f vaterlaendische Naturkunde in Wuerttemberg*, 64:368–82.

Wertz, I. E., O'Rourke, K. M., Zhou, H., Eby, M., Aravind, L., Seshagiri, S., Wu, P., Wiesmann, C., Baker, R., Boone, D. L., Ma, A., Koonin, E. V., and Dixit, V. M. (2004). De-ubiquitination and ubiquitin ligase domains of a20 downregulate nf-kappab signalling. *Nature*, 430(7000):694–699.

Weyrich, A. S., Lindemann, S., Tolley, N. D., Kraiss, L. W., Dixon, D. A., Mahoney, T. M., Prescott, S. P., McIntyre, T. M., and Zimmerman, G. A. (2004). Change in protein phenotype without a nucleus: translational control in platelets. *Semin Thromb Hemost*, 30(4):491–498.

White, J. S. (1999). The 1653 english edition of de motu cordis, shown to be harvey's vernacular original and revealing crucial aspects of his pre-circulation theory and its connection to the discovery of the circulation of the blood. *Hist Philos Life Sci*, 21(1):65–91.

Wicovsky, A., Henkler, F., Salzmann, S., Scheurich, P., Kneitz, C., and Wajant, H. (2009a). Tumor necrosis factor receptor-associated factor-1 enhances proinflammatory tnf receptor-2 signaling and modifies tnfr1-tnfr2 cooperation. *Oncogene*, 28(15):1769–1781.

Wicovsky, A., Salzmann, S., Roos, C., Ehrenschwender, M., Rosenthal, T., Siegmund, D., Henkler, F., Gohlke, F., Kneitz, C., and Wajant, H. (2009b). Tnf-like weak inducer of apoptosis inhibits proinflammatory tnf receptor-1 signaling. *Cell Death Differ*, 16(11):1445–1459.

Willoughby, S., Holmes, A., and Loscalzo, J. (2002). Platelets and cardiovascular disease. *Eur J Cardiovasc Nurs*, 1(4):273–288.

Wilson, L. S., Elbatarny, H. S., Crawley, S. W., Bennett, B. M., and Maurice, D. H. (2008). Compartmentation and compartment-specific regulation of PDE5 by protein kinase g allows selective cGMP-mediated regulation of platelet functions. *Proc Natl Acad Sci U S A*, 105:13650–5. 36.

Winkles, J. A. (2008). The tweak-fn14 cytokine-receptor axis: discovery, biology and therapeutic targeting. *Nat Rev Drug Discov*, 7(5):411–425.

Witt, J., Barisic, S., Schumann, E., Allgower, F., Sawodny, O., Sauter, T., and Kulms, D. (2009). Mechanism of PP2A-mediated IKK beta dephosphorylation: a systems biological approach. *BMC Syst Biol*, 3:71.

Wong, C., Liu, Y., Yip, J., Chand, R., Wee, J. L., Oates, L., Nieswandt, B., Reheman, A., Ni, H., Beauchemin, N., and Jackson, D. E. (2009). Ceacam1 negatively regulates platelet-collagen interactions and thrombus growth in vitro and in vivo. *Blood*, 113(8):1818–1828.

Wootton, D. M., Markou, C. P., Hanson, S. R., and Ku, D. N. (2001). A mechanistic model of acute platelet accumulation in thrombogenic stenoses. *Ann Biomed Eng*, 29(4):321–329.

World Health Organization (2011). Fact sheet nr. 310.

Worth, D. C., Hodivala-Dilke, K., Robinson, S. D., King, S. J., Morton, P. E., Gertler, F. B., Humphries, M. J., and Parsons, M. (2010). Alpha v beta3 integrin spatially regulates vasp and riam to control adhesion dynamics and migration. *J Cell Biol*, 189(2):369–383.

Wu, C. C., Ko, F. N., Kuo, S. C., Lee, F. Y., and Teng, C. M. (1995). YC-1 inhibited human platelet aggregation through NO-independent activation of soluble guanylate cyclase. *British journal of pharmacology*, 116:1973–8. 3.

Wu, C.-J., Conze, D. B., Li, T., Srinivasula, S. M., and Ashwell, J. D. (2006). Sensing of lys 63-linked polyubiquitination by nemo is a key event in nf-kappab activation [corrected]. *Nat Cell Biol*, 8(4):398–406.

Xiang, B., Zhang, G., Liu, J., Morris, A. J., Smyth, S. S., Gartner, T. K., and Li, Z. (2010). A g(i) -independent mechanism mediating akt phosphorylation in platelets. *J Thromb Haemost*, 8(9):2032–2041.

Xu, W., Smith, A. M., Faeder, J. R., and Marai, G. E. (2011a). Rulebender: a visual interface for rule-based modeling. *Bioinformatics*, 27(12):1721–1722.

Xu, Z., Chen, N., Kamocka, M. M., Rosen, E. D., and Alber, M. (2008). A multiscale model of thrombus development. *J R Soc Interface*, 5:705—722. 24.

Xu, Z., Kamocka, M., Alber, M., and Rosen, E. D. (2011b). Computational approaches to studying thrombus development. *Arterioscler Thromb Vasc Biol*, 31(3):500–505.

Yan, H., Zhang, B., Li, S., and Zhao, Q. (2010). A formal model for analyzing drug combination effects and its application in TNF-alpha-induced NFkappaB pathway. *BMC Syst Biol*, 4:50.

Zaccolo, M. and Movsesian, M. A. (2007). cAMP and cGMP signaling cross-talk: role of phosphodiesterases and implications for cardiac pathophysiology. *Circ Res*, 100:1569–78. 11.

Zahedi, R., Lewandrowski, U., Wiesner, J., Wortelkamp, S., Moebius, J., Schütz, C., Walter, U., Gambaryan, S., and Sickmann, A. (2008). Phosphoproteome of resting human platelets. *J Proteome Res*, 7(2):526–534.

Zhang, G., Xiang, B., Dong, A., Skoda, R. C., Daugherty, A., Smyth, S. S., Du, X., and Li, Z. (2011). Biphasic roles for soluble guanylyl cyclase (sgc) in platelet activation. *Blood*, 118(13):3670–3679.

Zhang, Q., Liang, C., Yu, Y. A., Chen, N., Dandekar, T., and Szalay, A. A. (2009). The highly attenuated oncolytic recombinant vaccinia virus glv-1h68: comparative genomic features and the contribution of f14.5l inactivation. *Mol Genet Genomics*, 282(4):417–435.

Zhang, W. and Colman, R. W. (2007). Thrombin regulates intracellular cyclic amp concentration in human platelets through phosphorylation/activation of phosphodiesterase 3a. *Blood*, 110(5):1475–1482.

Zhang, W., Ke, H., and Colman, R. W. (2002). Identification of interaction sites of cyclic nucleotide phosphodiesterase type 3a with milrinone and cilostazol using molecular modeling and site-directed mutagenesis. *Mol Pharmacol*, 62(3):514–520.

Zhao, H., Quilley, J., Montrose, D. C., Rajagopalan, S., Guan, Q., and Smith, C. J. (2007). Differential effects of phosphodiesterase pde-3/pde-4-specific inhibitors on vasoconstriction and camp-dependent vasorelaxation following balloon angioplasty. *Am J Physiol Heart Circ Physiol*, 292(6):H2973–H2981.

List of Figures

List of Tables

List of Abbreviations

Pst ..... *Pseudomonas syringae* pv tomato DC3000
ABA ..... abscisic acid
AC ..... adenylyl cyclase
ADP ..... adenosine diphosphate
AIC ..... Akaike information criterion
AKAP ..... A-kinase anchoring protein
AMP ..... adenosine monophosphate
ANP ..... atrial natriuretic peptide
ARAC ..... arachidonic acid
ATP ..... adenosine triphosphate
Aux ..... auxin
BCA ..... bicinchoninic acid
BID ..... BH3 interacting-domain death agonist
BTK ..... Bruton's tyrosine kinase
CalDAG-GEFI Ca^{2+} and diacylglycerol regulated guanine nucleotide exchange factor I
cAMP ..... cyclic adenosine monophosphate
CEACAM1 ... carcinoembryonic antigen cell adhesion molecule 1
cGMP ..... cyclic guanosine monophosphate
cIAP ..... cellular inhibitor of apoptosis protein
cIAP1 ..... cellular inhibitors of apoptosis 1
cIAP2 ..... cellular inhibitors of apoptosis 2
CK ..... cytokinin
CLEC2 ..... C-type lectin receptor
CLP ..... Common lymphoid progenitor
CMP ..... Common myeloid progenitor
CO ..... carbon monoxide
DAG 1,2-diacylglycerol
df ..... degree of freedom
e.g. ..... exempli gratia
ECM ..... extracellular matrix
EDRF ..... endothelium-derived relaxing factor
EGF ..... epidermal growth factor
eNOS ..... endothelial NO synthase
ET ..... ethylene
ETI ..... effector-triggered immunity

FADD ..... Fas-associated death domain
FasL ..... Fas ligand
GA ..... gibberellic acid
GC ..... guanylyl cyclase
GDP ..... guanosine diphosphosphate
GKAP ..... G-kinase anchoring protein
GMP ..... Granulocyte/macrophage progenitor
GMP ..... guanosine monophosphate
GP ..... glycoprotein
GPCR ..... G protein-coupled receptor
GR ..... glucocordocoid receptor
GTP ..... guanosine triphosphate
H_2S ..... hydrogen sulphide
HGF ..... hepatocyte growth factor
HSC ..... Hematopoietic stem cell
IκB ..... inhibitor of κB proteins
IFNγ ..... interferon gamma
IL-1 ..... interleukin-1
IP_3 ..... inositol 1,4,5 triphosphate
IP_3R ..... IP_3 receptor
IPKB ..... Ingenuity Pathways Knowledge Base
IPTG ..... Isopropyl-β-D-thiogalactopyranosid
ITAM ..... immunoreceptor tyrosine activation motif
JA ..... jasmonic acid
KEGG ..... Kyoto Encyclopedia of Genes and Genomes
LASP ..... Lim and SH3 domain protein
LRT ..... likelihood ratio test
LUBAC ..... linear ubiquitin chain assembly complex
LXR ..... liver X receptor
memTNF .... membranous TNF
MEP ..... Megakaryocyte/erythrocyte progenitor
ML ..... maximum likelihood
mRNA ..... messenger RNA
NEMO ..... NFκB essential modulator
NIK ..... NFκB-inducing kinase
NO ..... nitric oxide
NRD1 ..... Nardilysin

ODE ..... ordinary differential equation
PAMP ..... pathogen-associated molecular pattern
PAR ..... protease-activated receptor
PDE ..... phosphodiesterase
PECAM-1 .... platelet-endothelial cell adhesion molecule-1
PGI_2 ..... prostaglandin I_2
PI3Kβ ..... phosphoinositide 3-kinase β
PIP2 ..... phosphatidylinositol 4,5 bisphosphate
PITPNM2 .... phosphatidylinositol transfer protein, membrane-associated 2
PKA ..... cAMP-dependent protein kinase
PKC ..... protein kinase C
PKG ..... cGMP-dependent protein kinase
PLA_2 ..... phospholipase A_2
PLAD ..... pre-ligand binding assembly domain
PLCβ2 ..... phospholipase Cβ2
PLCγ2 ..... phospholipase Cγ2
PMCA ..... plasma membrane Ca^{2+} ATPase
PPAR ..... peroxisome proliferator-activated receptor
PPI ..... protein-protein interaction
PR1 ..... pathogenesis-related protein 1
PTGDR ..... prostaglandin receptor
PTI ..... PAMP-triggered immunity
PYK2 ..... protein tyrosine kinase 2
RBM ..... Rule-based modeling
RhoK ..... Rho kinase
RIAM ..... Rap1-interacting adapter molecule
RIP ..... receptor-interacting protein
ROC ..... receptor-operated calcium
RXR ..... retinoic X receptor
SA ..... salicylic acid
SD ..... standard deviation
SEM ..... standard error of the mean
SERCA ..... sarcoplasmic/endoplasmic Ca^{2+} ATPase
sGC ..... soluble guanylyl cyclase
SOC ..... store-operated calcium
SOCE ..... store-operated calcium entry

STIM1 ..... stromal interaction molecule-1
STKE ..... Signal Transduction Knowledge Environment
STMN1 ..... Stathmin
sTNF ..... soluble TNF
Tab2 ..... Tak1 binding proteins 2
TACE ..... TNF alpha converting enzyme
Tak1 ..... TGFβ-activated kinase 1
TF ..... tissue factor
TGF ..... transforming growth factor
TNF ..... tumor necrosis factor
TNF-R1 ..... tumor necrosis factor receptor 1
TNF-R2 ..... tumor necrosis factor receptor 2
TRADD ..... TNF receptor-associated death domain
TRAF ..... TNF receptor-associated factor
TRAF1 ..... TNF receptor-associated factor 1
TRAF2 ..... TNF receptor-associated factor 2
TRPC6 ..... canonial transient receptor potential channel 6
TWEAK ..... TNF-like weak inducer of apoptosis
TXA_2 ..... thromboxane
VASP ..... vasodilator stimulated phosphoprotein
vWF ..... von Willebrand factor
XIAP ..... X-linked inhibitor of apoptosis protein

Annex

Annex A: Statistics

Annex A.1: Log-likelihood-ratio of a model is χ^2-distributed

Here it will be shown that the log-likelihood-ratio between the likelihood of a true parameter set θ_0 and the estimated parameter vector θ_{ML} follows a χ^2-distribution. This holds if the parameters are identifiable and are not located at the border of the parameter space. Moreover it is assumed that θ_{ML} are normally distributed around θ_0 with covariance matrix $\mathbf{C}$:

$$P(\theta_{ML} - \theta_0) = \frac{1}{\sqrt{2\pi}} |\mathbf{C}|^{-\frac{1}{2}} \mathrm{e}^{\left(-\frac{1}{2}(\theta_{ML}-\theta_0)^T \mathbf{C}^{-1}(\theta_{ML}-\theta_0)\right)},$$

with

$$\mathbf{C}_{i,j} = -\left(\frac{\partial^2 \mathcal{L}(\theta_{ML}|M,D)}{\partial\theta_i \partial\theta_j}\right)^{-1}.$$

Covariance matrix $\mathbf{C}$ is given by the inverse of the Hessian matrix.
The log-Likelihood $\mathcal{L}(\theta_0|M,D)$ can be approximated using the Taylor-expansion

$$\begin{aligned} \mathcal{L}(\theta_0|M,D) \approx \quad & \mathcal{L}(\theta_{ML}|M,D) + \frac{\partial \mathcal{L}(\theta_{ML}|M,D)}{\partial\theta}(\theta_0 - \theta_{ML}) \\ & + \frac{1}{2}(\theta_0 - \theta_{ML})^T \frac{\partial^2 \mathcal{L}(\theta_{ML}|M,D)}{\partial\theta_i \partial\theta_j}(\theta_0 - \theta_{ML}). \end{aligned} \tag{5.1}$$

The first derivatives $\frac{\partial \mathcal{L}(\theta_{ML}|M,D)}{\partial\theta}$ equal zero at maximum likelihood, so that the formula (5.1) reduces to

$$\mathcal{L}(\theta_0|M,D) \approx \mathcal{L}(\theta_{ML}|M,D) - \frac{1}{2}(\theta_0 - \theta_{ML})^T \mathbf{C}^{-1}(\theta_0 - \theta_{ML}).$$

Concerning the log-Likelihood-ratio, this yields

$$2\left(\mathcal{L}(\theta_{ML}|M,D) - \mathcal{L}(\theta_0|M,D)\right) \approx (\theta_0 - \theta_{ML})^T \mathbf{C}^{-1}(\theta_0 - \theta_{ML}). \tag{5.2}$$

As the covariance is symmetric and positive definite, there exists a transformation $\mathbf{U}$ under which $\mathbf{C}$ as well as the transformed inverse is diagonal with

$$\mathbf{U}^T\mathbf{C}^{-1}\mathbf{U} =: \widetilde{\mathbf{C}}^{-1} = \text{diag}(1/\upsilon_1, 1/\upsilon_2, \ldots, 1/\upsilon_r).$$

Thus, equation (5.2) can be reformulated as:

$$\begin{aligned} 2\left(\mathcal{L}(\theta_{ML}|M,D) - \mathcal{L}(\theta_0|M,D)\right) \approx & \quad (\theta_0 - \theta_{ML})^T\mathbf{U}\widetilde{\mathbf{C}}^{-1}\mathbf{U}^T(\theta_0 - \theta_{ML}) \\ = & \quad \sum_{i=1}^{r} \frac{1}{\upsilon_i}\left(\mathbf{U}^T(\theta_0 - \theta_{ML})\right)_i^2 . \end{aligned}$$

Transformation $\mathbf{U}$ was constructed such that the components of the transformed parameter differences $\left(\mathbf{U}^T(\theta_0 - \theta_{ML})\right)_i$ have a variance υ_i but no covariances. Hence, the log-Likelihood-ratio can be expressed as a sum of r normalized Gaussian distributed random numbers which is χ^2-distributed with r degrees of freedom.
This relation (Burnham and Anderson, 2002; Cox and Hinkley, 1994) is also applied while comparing nested models (Annex A.2).

Annex A.2: Comparison of Nested Models

Assuming one compares two nested models, meaning model M_2 comprising r_2 parameters is a reduction of model M_1 having p_1 parameters. Hence, in comparison to model M_2 Model M_1 has additional $r_1 - r_2$ parameters. The log-ratio of their likelihoods under the null hypothesis that M_2 represents the true model follows also a χ^2-distribution. Following Annex A.1, this becomes evident using the Taylor-expansion of both the log-likelihoods:

$$\begin{aligned}\mathcal{L}(\theta_{1,0}|M_1, D) &\approx \mathcal{L}(\theta_{1,ML}|M_1, D) - \frac{1}{2}(\theta_{1,0} - \theta_{1,ML})^T \mathbf{C}_1^{-1}(\theta_{1,0} - \theta_{1,ML}) \\ \mathcal{L}(\theta_{2,0}|M_2, D) &\approx \mathcal{L}(\theta_{2,ML}|M_2, D) - \frac{1}{2}(\theta_{2,0} - \theta_{2,ML})^T \mathbf{C}_2^{-1}(\theta_{2,0} - \theta_{2,ML}).\end{aligned}$$

The first terms (log-likelihoods) $\mathcal{L}(\theta_{1,0}|M_1, D)$ and $\mathcal{L}(\theta_{2,0}|M_2, D)$ of these series are equal, as model M_1 has the same solution under the null hypothesis explaining the data equally well, so that:

$$\begin{aligned}\mathcal{L}(\theta_{1,ML}|M_1, D) - \frac{1}{2}(\theta_{1,0} - \theta_{1,ML})^T \mathbf{C}_1^{-1}(\theta_{1,0} - \theta_{1,ML}) &\approx \\ \mathcal{L}(\theta_{2,ML}|M_2, D) - \frac{1}{2}(\theta_{2,0} - \theta_{2,ML})^T \mathbf{C}_2^{-1}(\theta_{2,0} - \theta_{2,ML}).\end{aligned}$$

This can be reformulated as:

$$\begin{aligned}2(\mathcal{L}(\theta_{1,ML}|M_1, D) - \mathcal{L}(\theta_{2,ML}|M_2, D)) &\approx \\ (\theta_{1,0} - \theta_{1,ML})^T \mathbf{C}_1^{-1}(\theta_{1,0} - \theta_{1,ML}) &- (\theta_{2,0} - \theta_{2,ML})^T \mathbf{C}_2^{-1}(\theta_{2,0} - \theta_{2,ML}).\end{aligned} \tag{5.3}$$

As the first r_2 parameters of model M_1 equal the parameters of M_2, these r_2 values vanish in the scalar product in (5.3). Consequently, only the remaining $r_1 - r_2$ parameters contribute to the log-likelihood-ratio. Thus, the log-ratio (5.3) follows a χ^2-distribution with $r_1 - r_2$ degrees of freedom:

$$2(\mathcal{L}(M_1) - \mathcal{L}(M_2)) \sim \chi^2_{r_1 - r_2}.$$

Annex A.3: Akaike's Information Criterion (AIC)

Information criteria are based on information theory and give indication of the discrepancy between the truth and the estimated model. Here, the Kullback-Leibler distance (5.4) plays a essential role, being a a measure for the difference between two probability distributions (Burnham and Anderson, 2002) - the true and the estimated distribution of the data:

$$KL = \int P_t(D) \log \left(\frac{P_t(D)}{P_M(D|M,\theta)} \right) \mathrm{d}D, \tag{5.4}$$

with P_t and P_M are the respective probability distributions. The Kullack-Leibler distance thus expresses the information that is "lost" when approximating the truth by use of the model. Equation 5.4 can be expanded to:

$$KL = \int P_t(D) \log P_t(D) \mathrm{d}D - \int P_t(D) \log P_M(D|M,\theta) \mathrm{d}D. \tag{5.5}$$

As the first term of the right hand side of 5.5 is constant (true), only the second term contributes to the evaluation of the difference. This which can be formulated as:

$$\int P_t(D) \log P_M(D|M,\theta) \mathrm{d}D = \int P_t(D) \mathcal{L}(\theta|M,D) \mathrm{d}D, \tag{5.6}$$

with log-likelihood $\mathcal{L}$ weighted with the probability distribution of the true model.
For the computation of 5.6, two problems arise: $P_t(D)$ is not known as well as the best set of parameters, which however can be estimated by maximization of the likelihood. Akaike (1973) found that term (see 5.6) can be approximated by

$$\mathcal{L}(\theta_{ML}|M,D) - r, \tag{5.7}$$

with r being the count of parameters of model M (Akaike, 1973, 1974).
Since usually χ^2-values are computed during the fitting process, the formula 5.7 was multiplied by -2 (see equation 3.6). Hence, the value of AIC can be expressed as:

$$AIC = -2\mathcal{L}(\theta_{ML}|M,D) + 2 \cdot r = \chi^2 + 2 \cdot r. \tag{5.8}$$

Regarding model selection, this suggests to use the model with the lowest AIC value.

Annex B: Platelet Signaling

Annex B.1: Boolean Model - Edges

The Boolean model is also available as xml-file and CellNetAnalyzer-files (Annex D).

Table 10 : Boolean model of platelet activation - modeled edges.

Edge	Reference
GPVI→PLCB	(Karniguian et al., 1990)
PLCB→IP3	(Rittenhouse and Sasson, 1985)
PLCB→DAG	(Billah et al., 1980)
DAG→PKC	(Lapetina et al., 1985)
IP3→IP3R	(Authi et al., 1986; Braun et al., 2009)
IP3R→CaC	(Authi et al., 1986; Braun et al., 2009)
CaC→Orai1	(Braun et al., 2009)
Orai1→CaC	(Braun et al., 2009)
P2X1→CaC	(Hoylaerts et al., 2000)
PKC→SRC	(Liebenhoff et al., 1994)
PI3→Akt	(Kohn et al., 1996)
Src→Akt	(Xiang et al., 2010)
CaC→ADP	(Cattaneo et al., 1990; Daniel et al., 1998)
ADP→P2Y1	(Hechler et al., 1998)
ADP→P2Y12	(Savi et al., 2001)
CaC→CalDAG	(Zahedi et al., 2008)
CalDAG→RAP1	(Zahedi et al., 2008)
RAP1→Talin	(Watanabe et al., 2008)
ATP→P2X1	(Rolf and Mahaut-Smith, 2002)
P2X1→CaC	(Rolf and Mahaut-Smith, 2002)
P2Y1→PLCB	(Hechler et al., 1998; Daniel et al., 1999)
P2Y12→cAMP	(Daniel et al., 1999)
P2Y12→PI3	(Daniel et al., 1999)
P2Y1→PLA2	(Liu et al., 2004)
PLA2→ARAC	(Forsell et al., 2005; Balsinde et al., 1998)
ARAC→TXA	(Balsinde et al., 1998)
TXA2R→PLCB	(Suzuki et al., 2012)
TXA2R→RhoK	(Suzuki et al., 1999; Nakahata, 2008)
RhoK→cellshape	(Suzuki et al., 1999; Ishii-Watabe et al., 2001)
Talin→Inta2b3	(Petrich et al., 2007)
PTGDR→cAMP	(Marquis et al., 1969; Iyu et al., 2011; Weber et al., 1999)
cAMP→PKA	(Murthy et al., 2002)
PKA→Rap1	(Siess et al., 1990)
PKA→VASP	(Butt et al., 1994; Weber et al., 1999)
PKA→RhoK	(Qiao et al., 2008)
PKA→PDE3	(Murthy et al., 2002)
Akt→Inta2b3	(Kirk et al., 2000)
PKA→IP3R	(Murthy and Zhou, 2003)
PKA→Src	(Abrahamsen et al., 2003)
Inta2b3→ARAC	(Jin et al., 2002)
Inta2b3→aggregation	(Shattil and Newman, 2004)

Annex B.2: Boolean Model - Logical Connections

Table 11 : Multi-valued Boolean model - logical connections.

Reaction	Logical connection	Phase
ADP	1 GPVI = 1 ADP	1
aggregation	5 Inta2b3 = 1 irrev.agg	3
Akt_activation	1 PI3 = 1 Akt	0
Akt_activation2	1 Src +2 PI3 = 2 Akt	1
Akt_activation3	2 Src + 2 PI3 = 3 Akt	3
ARAC_recruitment	1 PLA2 + 4 Inta2b3 = 1 ARAC	3
CaC	1 IP3R = 1 CaC	0
CaC2	2 IP3R + 1 P2X1 = 2 CaC	1
CaC3	1 Orai1 = 3 CaC	2
CaC4	3 IP3R + 1 P2X1 + 1 Orai1 = 4 CaC	3
CalDAG_activation	1 CaC = 1 CalDAG	0
CalDAG_activation2	2 CaC = 2 CalDAG	1
CalDAG_activation3	3 CaC = 3 CalDAG	2
CalDAG_activation4	4 CaC = 4 CalDAG	3
cAMP_production	1 !P2Y12 + 1 PTGDR + 1 !PDE3 = 1 cAMP	0
cellshape	1 CaC + 1 RAP1 + A !VASP = 1 cellshape	0
cellshape2	2 CaC + 2 RAP1 = 1 cellshape	1
cellshape3	2 CaC + 2 RAP1 + 1 RhoK = 2 cellshape	3
DAG_production	1 PLCB = 1 DAG	0
DAG_production2	2 PLCB = 2 DAG	1
DAG_production3	3 PLCB = 3 DAG	3
GPVI_activation	= 1 GPVI	0 (INPUT)
Int_activation_talin	1 Talin = 1 Inta2b3	0
Int_activation_Akt	1 Akt = 1 Inta2b3	0
Int_activation_combi1	1 AKt + 1 Talin = 2 Inta2b3	0
Int_activation_combi2	2 Akt + 2 Talin = 3 Inta2b3	1
Int_activation_combi3	2 Akt + 3 Talin = 4 Inta2b3	2
Int_activation_combi4	3 AKT + 3 Talin = 5 Inta2b3	3
IP3_production	1 PLCB = 1 IP3	0
IP3_production2	2 PLCB = 2 IP3	1
IP3_production3	3 PLCB = 3 IP3	3
IP3R_activation	1 PKC + 1 IP3 + 1 !PKA = 1 IP3R	0
IP3R_activation2	2 PKC + 2 IP3 = 2 IP3R	1
IP3R_activation3	3 PKC + 3 IP3 = IP3R	3
Orai1_activation	2 CaC = 1 Orai1	2
P2X1	1 ADP = 1 P2X1	0
P2Y1	1 ADP = 1 P2Y1	1
P2Y12_activation	1 ADP = 1 P2Y12	1

Continued on next page

Table 11 – *continued from previous page*

Reaction	Logical connection	Phase
PDE3	1 PKA = 1 PDE3	2
PI3_activation	1 IP3 = 1 PI3	0
PI3_activation2	1 IP3 + 1 P2Y12 = 2 PI3	1
PKA_activation	1 cAMP = 1 PKA	0
PKC_activation	1 DAG = 1 PKC	0
PKC_activation2	1 CaC + 2 DAG = 2 PKC	1
PKC_activation3	3 CaC + 2 DAG = 3 PKC	2
PLA2_activation	1 P2Y1 = 1 PLA2	1
PLCB_activation2	1 P2Y1 = 2 PLCB	1
PLCB_activation3	1 TBXA2R = 2 PLCB	3
PLCB_GPVI	1 GPVI = 1 PLCB	0
PTGDR_activation	= 1 PTGDR	0 (INPUT)
RAP1_activation1	1 CalDAG + 1 !PKA = 1 RAP1	0
RAP1_activation2	2 CalDAG + 1 PKA = 1 RAP1	1
RAP1_activation3	2 CalDAG + 1 !PKA = 2 RAP1	1
RAP1_activation4	3 CalDAG + 1 !PKA = 4 RAP1	2
RAP1_activation5	3 CalDAG + 1 PKA = 2 RAP1	2
RAP1_activation6	4 CalDAG = 4 RAP1	3
RhoK_activation	1 TBXA2R + 1 !PKA = 1 RhoK	3
Src_activation	1 PKC + 1 !PKA = 1 Src	0
Src_activation2	2 PKC = 1 Src	1
Src_activation3	3 PKC = 2 Src	2
Talin_activation	1 RAP1 = 1 Talin	0
Talin_activation2	2 RAP1 = 2 Talin	1
Talin_activation3	3 RAP1 = 3 Talin	2
Talin_activation4	4 RAP1 = 4 Talin	2
TBXA2R_activation	1 TXA = 1 TBXA2R	3
TXA_production	1 ARAC = 1 TXA	3
VASP_activation	1 PKA = 1 VASP	0

Annex B.3: Substrates for PKA and PKG in Platelets

Substrate	Phosphosite	PKA	PKG	Role of phosphorylation	Reference
G-proteins/Signaling regulators					
Rap1B	Ser179	✓	✓	Detachment of Rap1B from the plasma membrane	(Lapetina et al., 1989; Altschuler and Lapetina, 1993) (Kawata et al., 1989)
Rap1GAP2	Ser7	✓	✓	Disruption of complex with 14-3-3 reduced Rap1 function, reduced cell adhesion	(Schultess et al., 2005; Hoffmeister et al., 2008)
$G_{\alpha_{13}}$	Thr203	✓	?	Inhibition of RhoA activity	(Manganello et al., 1999, 2003)
IP_3R	?	✓	✓	Inhibition of Ca^{2+} release	(Tertyshnikova et al., 1998; El-Daher et al., 2000)
IRAG	Ser664	?	✓	Inhibition of Ca^{2+} release	(Antl et al., 2007; Schinner et al., 2011)
	Ser677	?	✓		
TRPC6	?	✓	✓	Not known	(Hassock et al., 2002)
PDE5A	Ser92	-	✓	Increased degradation of cGMP	(Mullershausen et al., 2003)
PDE3A	Ser312	✓	?	Increased degradation of cAMP	(Hunter et al., 2009; Macphee et al., 1988)
GPIbβ	Ser166	✓	?	Regulation of cell adhesion	(Wardell et al., 1989; Bodnar et al., 2002) (Perrault et al., 2003; Andrews et al., 1998)
Actin-binding proteins					
VASP	Ser157	✓	✓	Regulation of actin dynamics	(Halbrügge and Walter, 1989; Butt et al., 1994) (Smolenski et al., 1998)
	Ser239	✓	✓		(Harbeck et al., 2000; Worth et al., 2010)
LASP	Ser146	✓	✓	Reduced F-actin binding	(Butt et al., 2003)
HSP27	Thr143	✓	✓	Reduced actin polimerization	(Butt et al., 2001)
Filamin-A	Ser2152	✓	?	Protection against proteolysis	(Chen and Stracher, 1989; Jay et al., 2000)
Caldesmon	?	✓	?	Not known	(Hettasch and Sellers, 1991)

Glycoprotein (GP), heat shock protein 27 (HSP27), inositol 1,4,5-trisphosphate receptor (IP_3R), Lim and SH3 domain protein (LASP), phosphodiesterase (PDE), transient receptor potential channel 6 (TRPC6), vasodilator-stimulated phosphoprotein (VASP).
PKA and PKG columns indicate whether the substrates have been shown to be phosphorylated by PKA or by PKG, respectively.
Question marks denote that no data on phosphorylation in platelets have been published.

Table 12 : Substrates for PKA and PKG in platelets. Table adapted from Smolenski (2012)

Annex B.4: Model Components and Parameter

Table 13 : Model components and specific parameter values.

Component, parameter	Parameter Values	Reference
Cyclases and cyclic nucleotides		
Adenylate cyclase (AC)		HPRD, (Boyanova et al., 2012)
ADCY3, ADCY5, ADCY6, ADCY7		
Basal AC activity	15.9 pmol/mg/min=7.16 μM/min	(Hines and Tabakoff, 2005)
	12.4 pmol/mg/min=5.6 μM/min	(Parsian et al., 1996)
	0.0376 amol/min/platelet=7.23 μM/min	(Juska and Farndale, 1999)
cAMP	4.4 $\pm$ 1.0 μM/min	(Eigenthaler et al., 1992)
Guanylyl cyclase (sGC)		HPRD, (Boyanova et al., 2012)
GUCY1A3, GUCY1B3		
Basal sGC activity	0.6 - 1 μM/min	(Schmidt et al., 2001)
cGMP	0.4 $\pm$ 0.1 μM/min	(Eigenthaler et al., 1992)
Phosphodiesterases (PDEs)		
PDE2A, cGMP stimulated		HPRD
(allosterically)		
PDE2-specific parameters:		(Butt and Walter, 1997)
		(Bender and Beavo, 2006)
PDE2 concentration	63.46 mg/l	This study
Hill coefficient	2	
K_m-value (cAMP turnover)	50 μM	
V_{max}-value (cAMP turnover)	120µmol/min/mg	
K_m-value (cGMP turnover)	35 μM	
V_{max}-value (cGMP turnover)	120 µmol/min/mg	
PDE3A, cGMP-inhibitied		HPRD
PDE3-specific parameters:		(Butt and Walter, 1997)
		(Bender and Beavo, 2006)
PDE3 concentration	225 mg/l	This study
K_m-value (cAMP turnover)	0.2 μM	
V_{max}-value (cAMP turnover)	3 µmol/min/mg	
K_m-value (cGMP turnover)	0.02 μM	
V_{max}-value (cGMP turnover)	0.3 µmol/min/mg	
PDE5A, cGMP specific		HPRD
PDE5-specific parameters:		(Butt and Walter, 1997)
PDE5 concentration	1359 mg/l	This study
K_m-value (cGMP turnover)	5 μM	
V_{max}-value (cGMP turnover)	5 µmol/min/mg	
PDE7A, PDE8B, PDE9A		(Dittrich et al., 2006)
Vasodilator-stimulated phosphoprotein (VASP)		
VASP		HPRD
VASP-specific parameters:		
Phosphorylation sites:		(Smolenski et al., 1998)
Ser157, Ser239, Thr278		(Butt et al., 1994)
VASP concentration	25.2 $\pm$ 7.6 μM	(Eigenthaler et al., 1992)
Protein kinases (PKA/PKG)		
PKA concentration	3.1 $\pm$ 0.6 μM	(Eigenthaler et al., 1992)
PKG concentration	7.3 $\pm$ 0.8 μM	(Eigenthaler et al., 1992)

Annex B.5: ODE Model Adapted to Anti-platelet Conditions

Core models (Matlab (PottersWheel) model definition files) as well as xml-files of the basal and extended model are available (Annex D).

Variables, Constants, Rates and System of ODEs (PDE3 inhibition)

Variables and constants of modeled reactions (see Figure 29A,B) are listed in Table 14.

Variables and Constants (PDE Inhibition Model)

Table 14 : Set of variables and constants for mathematical model of PDE inhibition.

Dynamic variables	**Values** and **fitting range**	**Remarks**
x_1: c(PDE2) active	$[0.005, 0.2]$ mg/l	
x_2: c(PDE3) active	$[1.7, 3.5]$ mg/l	
x_3: c(PDE2) inactive	$[(63.46 - \mathrm{c(PDE2)}), 63.46]$ mg/l	
x_4: c(PDE3) inactive	$[(225 - \mathrm{c(PDE3)}), 225]$ mg/l	
x_5: c(cAMP)	µmol, simulated Startvalue: 4 μM	
x_6: c(AMP)	μM	
Input		
u_1: c(Cilostamide)	0.5, 1, 5, 10, 50 μM	PDE3 inhibitor
u_2: c(Milrinone)	1, 5, 10, 50, 100 μM	
Constants		
k_1: V_{max} PDE2	120 µmol/min/mg; fix	
k_2: K_m PDE2	50 μM; fix	cAMP turnover
k_3: V_{max} PDE3	3 µmol/min/mg; fix	
k_4: Feedback regulation	$[0, 0.2]$ µmol^{-1}	Activation of PDE3 via cAMP
k_5: K_m PDE3	0.2 μM; fix	cAMP turnover
k_6: kcAMP	$[5, 9]$ µmol/min	Basal influx of cAMP (AC)
k_7: hPDE2	2 ; fix	Hill coefficient (PDE2)
k_8: Deactivation of PDE2 k_9: Activation of PDE2 k_{10}: Deactivation of PDE3 k_{11}: Activation of PDE3	$[0, 1]$ min^{-1}	
k_{12_1}: k_i Cilostamide k_{12_2}: k_i Milrinone	[0.00001, 1] μM	Inhibition constant (PDE3)

Parameter x_1, x_2, k_4, k_6, $k_8 - k_{12_2}$ fit to cAMP concentration measurements at several time points using parameter values given in Table 13.

Reaction Fate Formalism (PDE3 inhibition)

$$
\begin{array}{lll}
\text{Basal AC influx of cAMP (r1)}: & \nu_1 = k_6; & \\
\text{cAMP turnover via PDE2 (r2)}: & \nu_2 = k_1 \cdot x_5^{k_7} \cdot x_1/(k_2 + x_5^{k_7}); & \\
\text{(De)activation of PDE (r3-r6)}: & \begin{cases} \nu_3 = k_9 \cdot x_3; \\ \nu_4 = k_8 \cdot x_1; \\ \nu_5 = k_{11} \cdot x_4; \\ \nu_6 = k_{10} \cdot x_2; \end{cases} & \\
\text{cAMP turnover via PDE3 (r7)}: & \nu_7 = (k_3 + k_4 \cdot x_5) \cdot x_5 \cdot x_2/((1.0 + (u_i/k_{12_i})) \cdot k_5 + x_5); & \\
 & \text{with } u_i : \text{c(PDE3 inhibitor)},\ k_{12_i} : \text{Inhibition constant}, i = 1, 2. &
\end{array}
\tag{5.9}
$$

System of Differential Equations (PDE3 inhibition)

Variables are defined in Table 14.

$$
\begin{aligned}
\frac{\mathrm{d}x_1}{\mathrm{d}t} &= +\nu_3 - \nu_4; \\
\frac{\mathrm{d}x_2}{\mathrm{d}t} &= +\nu_5 - \nu_6; \\
\frac{\mathrm{d}x_3}{\mathrm{d}t} &= -\nu_3 + \nu_4; \\
\frac{\mathrm{d}x_4}{\mathrm{d}t} &= -\nu_5 + \nu_6; \\
\frac{\mathrm{d}x_5}{\mathrm{d}t} &= +\nu_1 - \nu_2 - \nu_7; \\
\frac{\mathrm{d}x_6}{\mathrm{d}t} &= +\nu_2 + \nu_7;
\end{aligned}
\tag{5.10}
$$

Variables, Constants, Rates and System of ODEs (AC activation)

Variables and constants of modeled reactions (see Figure 29) are listed in Table 15.

Variables and Constants (AC activation model)

Table 15: Set of variables and constants for mathematical model of adenylyl cyclase activation.

Dynamic variables	**Values** and **fitting range**	**Remarks**
x_1: c(PDE2) active	$[0.005, 0.2]$ mg/l	
x_2: c(PDE3) active	$[1.7, 3.5]$ mg/l	
x_3: c(PDE2) inactive	$[(63.46 - \text{c(PDE2)}), 63.46]$ mg/l	
x_4: c(PDE3) inactive	$[(225 - \text{c(PDE3)}), 225]$ mg/l	
x_{5_1}: $\text{AC}_{\textbf{Forskolin}}$	$[0, 5000]$ µmol/min	Response to Foskolin doses
x_{5_2}: $\text{AC}_{\textbf{Iloprost}}$		Response to Iloprost doses
x_6: c(cAMP)	μM, simulated Startvalue: 4 μM	
x_7: c(AMP)	μM	
Constants		
k_1: V_{max} PDE2	120 µmol/min/mg; fix	
k_2: K_m PDE2	50 μM; fix	cAMP turnover
k_3: V_{max} PDE3	3 µmol/min/mg; fix	
k_4: Feedback regulation	$[0, 0.2]$ μmol^{-1}	Activation of PDE3 via cAMP
k_5: K_m PDE3	0.2 μM; fix	cAMP turnover
k_6: kcAMP	$[5, 9]$ µmol/min	Basal influx of cAMP (AC)
k_7: hPDE2	2 ; fix	Hill coefficient (PDE2)
k_8: Deactivation of PDE2		
k_9: Activation of PDE2	$[0, 1]$ min^{-1}	
k_{10}: Deactivation of PDE3		
k_{11}: Activation of PDE3		
k_{12_1}: Activation constant	1 min^{-1}; fix	Via Forskolin
k_{12_2}: of AC		Via Iloprost
k_{13}: Inhibition of AC	$[0, 10000]$ min^{-1}	Via cAMP (PKA)

Parameter x_1, x_2, k_4, k_6, $k_8 - k_{11}$, k_{13} fit to cAMP concentration measurements at several time points using parameter values given in Table 13.

Reaction Rate Formalism (AC activation)

$$
\begin{aligned}
&\text{Basal AC influx of cAMP (r1)}: && \nu_1 = k_6;\\
&\text{cAMP turnover via PDE2 (r2)}: && \nu_2 = k_1 \cdot x_6^{k7} \cdot x_1/(k_2 + x_6^{k7});\\
&\text{cAMP turnover via PDE3 (r3)}: && \nu_3 = (k_3 + k_4 \cdot x_6) \cdot x_6 \cdot x_2/(k_5 + x_6);\\
&\text{(De)activation of PDE (r4-r7)}: && \begin{cases} \nu_4 = k_9 \cdot x_3; \\ \nu_5 = k_8 \cdot x_1; \\ \nu_6 = k_{11} \cdot x_4; \\ \nu_7 = k_{10} \cdot x_2; \end{cases}\\
&\text{cAMP influx via activated AC (r8)}: && \nu_8 = k_{12_i} \cdot x_{5_i} - k_{13} \cdot x_6;\\
& && \text{with } x_{5_i} : \text{AC}_{\textbf{Forskolin}}, \text{AC}_{\textbf{Iloprost}}, k_{12_i} : \text{Activation constant of AC, } i = 1, 2.
\end{aligned}
\tag{5.11}
$$

System of Differential Equations (AC activation)

Variables are defined in Table 15.

$$
\begin{aligned}
\frac{\mathrm{d}x_1}{\mathrm{d}t} &= &&+ \nu_4 - \nu_5;\\
\frac{\mathrm{d}x_2}{\mathrm{d}t} &= &&+ \nu_6 - \nu_7;\\
\frac{\mathrm{d}x_3}{\mathrm{d}t} &= &&- \nu_4 + \nu_5;\\
\frac{\mathrm{d}x_4}{\mathrm{d}t} &= &&- \nu_6 + \nu_7;\\
\frac{\mathrm{d}x_5}{\mathrm{d}t} &= &&0;\\
\frac{\mathrm{d}x_6}{\mathrm{d}t} &= &&+ \nu_1 - \nu_2 - \nu_3 + \nu_8;\\
\frac{\mathrm{d}x_7}{\mathrm{d}t} &= &&+ \nu_2 + \nu_3;
\end{aligned}
\tag{5.12}
$$

Variables, Constants, Rates and System of ODEs (VASP phosphorylations 1)

Variables and constants of the underlying modeled reactions (see Figure 50) are listed in Table 16.

Reaction Scheme

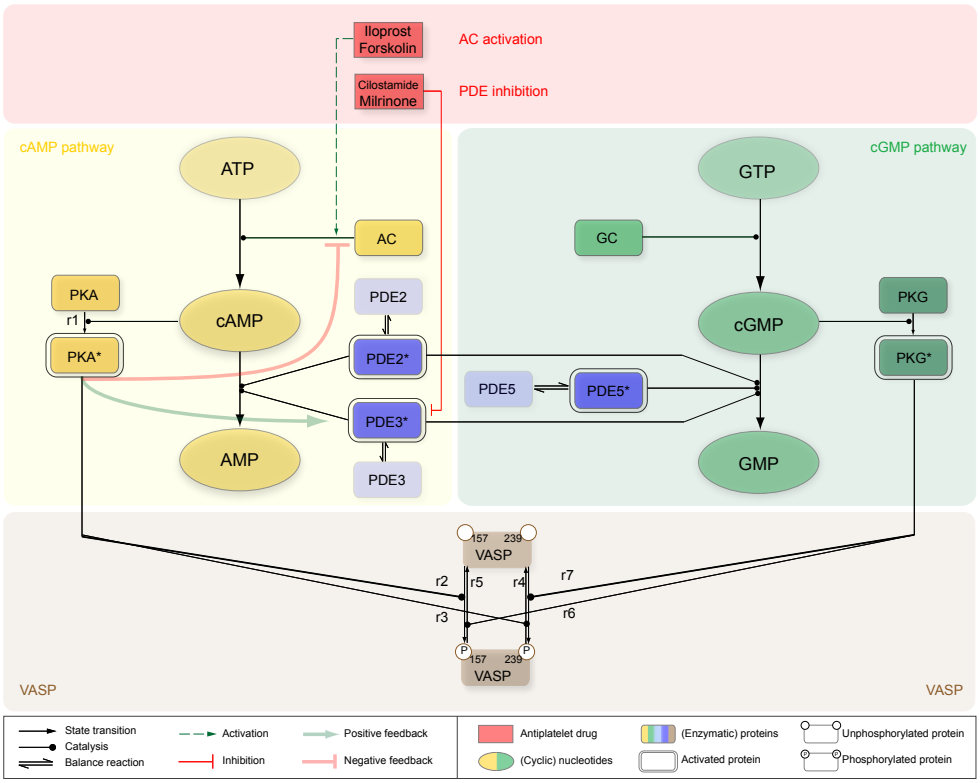

Figure 50: Reaction scheme of VASP phosphorylation - modeled reactions.

Variables and Constants (VASP Phosphorylations 1)

Table 16 : Set of variables and constants for the mathematical model of VASP activation.

Dynamic variables	**Values** and **fitting range**	**Remarks**
x_1: c(PKAα) inactive	Startvalue: 6.2 μM; fix	Catalytic subunit PKAα
x_2: c(VASP)	Startvalue: 25 μM; fix	Intracellular VASP concentration
x_3: c(VASP$_{Ser157}$) unphosphorylated	Startvalue: 25 μM;	Concentration of unphosphorylated VASP$_{Ser157}$
x_4: c(VASP$_{Ser239}$) unphosphorylated	Range: [0, 25] μM	Concentration of unphosphorylated VASP$_{Ser239}$
x_5: c(PKG) active	Startvalue: 1 μM; fix	Active c(PKG) due to basal cGMP level
x_6: c(PKAα) active	Simulated	
x_7: c(VASP$_{Ser157}$) phosphorylated	Simulated	Concentration of phosphorylated VASP$_{Ser157}$
x_8: c(VASP$_{Ser239}$) phosphorylated		Concentration of phosphorylated VASP$_{Ser239}$
Constants		
k_1: $kPKA\alpha_{act}$	Startvalue: 1 Range: [0, 1000]	Activation of PKA through cAMP
k_2: $kVASP_{inact}$	Startvalue: 1 Range: [0, 1000000]	Inactivation (dephosphorylation) of VASP
k_3: K_m VASP$_{Ser239}$	Startvalue: 10 Range: [0, 10000]	PKA-specific
k_4: V_{max} VASP$_{Ser239}$	Startvalue: 1 Range: [0, 10000]	
k_5: K_m VASP$_{Ser157}$	Startvalue: 0.1 Range: [0, 10000]	
k_6: V_{max} VASP$_{Ser157}$	Startvalue: 1 Range: [0, 10000]	
k_7: K_m VASP$_{Ser239}$	Startvalue: 10 Range: [0, 10000]	PKG-specific
k_8: V_{max} VASP$_{Ser239}$	Startvalue: 10 Range: [0, 10000]	
k_9: K_m VASP$_{Ser157}$	Startvalue: 10 Range: [0, 1000]	
k_{10}: V_{max} VASP$_{Ser157}$	Startvalue: 10 Range: [0, 10000]	
Assignment rules		
a_1: Ratio of VASP$_{Ser157}$ to VASP		Experimental measurement
a_2: Ratio of VASP$_{Ser239}$ to VASP		
Driving input		
u_1: cAMP level Time series within $[0, 10]$ min		Due to Iloprost stimulation (2, 5, 10 nM)
Parameters $k_1 - k_{10}$ were fit to measured relations of phosphorylated VASP (Ser157, Ser239) to unphosphorylated VASP at several time points.		

Reaction Rate Formalism (VASP Phosphorylations 1)
Defining the observed ratio between phosphorylated VASP and VASP in total (important for the fitting procedure):

$$\begin{aligned} &\text{Ratio of VASP}_{Ser157} \text{ to VASP:} \qquad a_1 = \frac{x_7}{x_2}; \\ &\text{Ratio of VASP}_{Ser239} \text{ to VASP:} \qquad a_2 = \frac{x_8}{x_2}; \end{aligned} \tag{5.13}$$

$$\begin{aligned} &\text{Activation of PKA via cAMP} && \text{(r1)}: && \nu_1 = k_1 \cdot x_1 \cdot u_1; \\ &\text{Phosphorylation of VASP}_{Ser157} \text{ by PKA}\alpha && \text{(r2)}: && \nu_2 = k_6 \cdot x_3 \cdot x_6/(k_5 + x_3); \\ &\text{Phosphorylation of VASP}_{Ser239} \text{ by PKA}\alpha && \text{(r3)}: && \nu_3 = k_4 \cdot x_4 \cdot x_6/(k_3 + x_4); \\ &\text{Dephosphorylation of VASP}_{Ser239} && \text{(r4)}: && \nu_4 = k_2 \cdot x_8; \\ &\text{Dephosphorylation of VASP}_{Ser157} && \text{(r5)}: && \nu_5 = k_2 \cdot x_7; \\ &\text{Phosphorylation of VASP}_{Ser157} \text{ by PKG} && \text{(r6)}: && \nu_6 = k_{10} \cdot x_3 \cdot x_5/(k_9 + x_3); \\ &\text{Phosphorylation of VASP}_{Ser239} \text{ by PKG} && \text{(r7)}: && \nu_7 = k_8 \cdot x_4 \cdot x_5/(k_7 + x_4); \end{aligned} \tag{5.14}$$

System of Differential Equations (VASP Phosphorylations 1)
Variables are defined in Table 16.

$$\begin{aligned} \frac{\mathrm{d}x_1}{\mathrm{d}t} &= -\nu_1; \\ \frac{\mathrm{d}x_2}{\mathrm{d}t} &= 0.0; \\ \frac{\mathrm{d}x_3}{\mathrm{d}t} &= -\nu_2 + \nu_5 - \nu_6; \\ \frac{\mathrm{d}x_4}{\mathrm{d}t} &= -\nu_3 + \nu_4 - \nu_7; \\ \frac{\mathrm{d}x_5}{\mathrm{d}t} &= 0.0; \\ \frac{\mathrm{d}x_6}{\mathrm{d}t} &= +\nu_1; \\ \frac{\mathrm{d}x_7}{\mathrm{d}t} &= +\nu_2 - \nu_5 + \nu_6; \\ \frac{\mathrm{d}x_8}{\mathrm{d}t} &= +\nu_3 - \nu_4 + \nu_7; \end{aligned} \tag{5.15}$$

Variables, Constants, Rates and System of ODEs (VASP Phosphorylations 2)

Reaction Scheme

Similarly, we here consider the modeling of VASP phosphorylation as downstream event but with two distinct variants of PKA (Figure 51) of different activity. Variables and constants of the underlying modeled reaction are listed in Table 17. Available data was not sufficient to discriminate between the two VASP phosphorylation approaches.

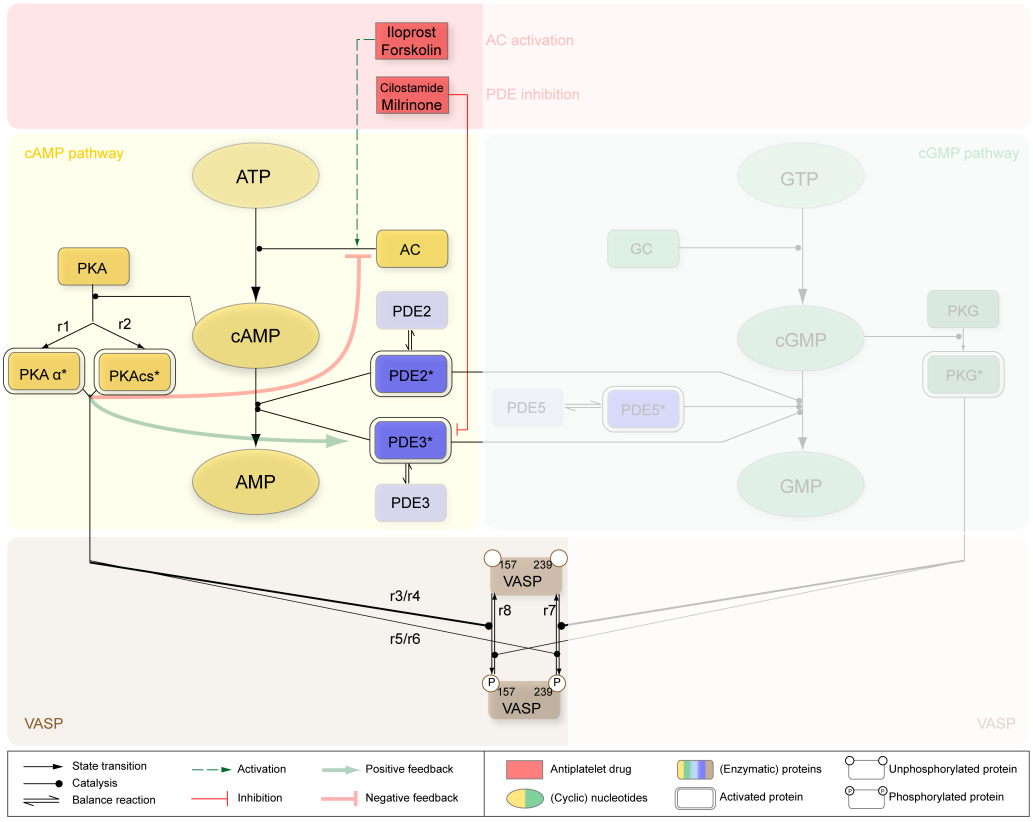

Figure 51 : Reaction scheme of VASP phosphorylation - modeled reactions.

Variables and Constants (VASP Phosphorylations 2)

Table 17 : Set of variables and constants for the mathematical model of VASP activation.

Dynamic variables	**Values** and **fitting range**	**Remarks**
x_1: c(PKAα) inactive	Startvalue: 6.2 μM; fix	Catalytic subunit PKAα
x_2: c(PKAcs) inactive	Startvalue: 6.2 μM; fix	Distinct catalytic subunit of PKA
x_3: c(VASP)	Startvalue: 25 μM; fix	Intracellular VASP concentration
x_4: c(VASP$_{Ser157}$) unphosphorylated	Startvalue: 25 μM;	Concentration of unphosphorylated VASP$_{Ser157}$
x_5: c(VASP$_{Ser239}$) unphosphorylated	Range: [0, 25] μM	Concentration of unphosphorylated VASP$_{Ser239}$
x_6: c(PKAα) active	Simulated	Catalytic subunit PKAα
x_7: c(PKAcs) active		Catalytic subunit of PKA
x_8: c(VASP$_{Ser157}$) phosphorylated	Simulated	Concentration of phosphorylated VASP$_{Ser157}$
x_9: c(VASP$_{Ser239}$) phosphorylated		Concentration of phosphorylated VASP$_{Ser239}$
Constants		
k_1: $kPKA\alpha_{act}$	Startvalue: 1 Range: $[0, 1000]$	Activation of PKAα through cAMP
k_2: $kPKAcs_{act}$	Startvalue: 1 Range: $[0, 1000]$	Activation of PKAcs through cAMP
k_3: $kVASP_{inact}$	Startvalue: 1 Range: $[0, 1000000]$	Inactivation (dephosphorylation) of VASP
k_4: K_m VASP$_{Ser239}$	Startvalue: 10 Range: $[0, 1000000]$	PKAα-specific
k_5: V_{max} VASP$_{Ser239}$	Startvalue: 1 Range: $[0, 100000]$	
k_6: K_m VASP$_{Ser157}$	Startvalue: 0.1 Range: $[0, 100000]$	
k_7: V_{max} VASP$_{Ser157}$	Startvalue: 1 Range: $[0, 100000]$	
k_8: K_m VASP$_{Ser239}$	Startvalue: 1 Range: $[0, 1000000]$	PKAcs-specific
k_9: V_{max} VASP$_{Ser239}$	Startvalue: 1 Range: $[0, 1000000]$	
k_{10}: K_m VASP$_{Ser157}$	Startvalue: 0.1 Range: $[0, 100000]$	
k_{11}: V_{max} VASP$_{Ser157}$	Startvalue: 1 Range: $[0, 1000000]$	
Assignment rules		
a_1: Ratio of VASP$_{Ser157}$ to VASP		Experimental measurement
a_2: Ratio of VASP$_{Ser239}$ to VASP		
Driving input		
u_1: cAMP level Time series within $[0, 10]$ min		Due to Iloprost stimulation (2, 5, 10 nM)
Parameters $k_1 - k_{11}$ were fit to measured relations of phosphorylated VASP (Ser157, Ser239) to unphosphorylated VASP at several time points.		

Reaction Rate Formalism (VASP Phosphorylations 2)
Defining the observed ratio between phosphorylated VASP and VASP in total (necessary for the fitting procedure):

$$\begin{aligned} \text{Ratio of VASP}_{Ser157} \text{ to VASP:} \quad & a_1 = \frac{x_8}{x_3}; \\ \text{Ratio of VASP}_{Ser239} \text{ to VASP:} \quad & a_2 = \frac{x_9}{x_3}; \end{aligned} \tag{5.16}$$

$$\begin{aligned} \text{Activation of PKA}\alpha \text{ via cAMP (r1)} : \quad & \nu_1 = k_1 \cdot x_1 \cdot u_1; \\ \text{Activation of PKA}cs \text{ via cAMP (r2)} : \quad & \nu_2 = k_2 \cdot x_2 \cdot u_1; \\ \text{Phosphorylation of VASP}_{Ser157} \text{ by PKA}\alpha \text{ (r3)} : \quad & \nu_3 = k_7 \cdot x_4 \cdot x_6/(k_6 + x_4); \\ \text{Phosphorylation of VASP}_{Ser157} \text{ by PKA}cs \text{ (r4)} : \quad & \nu_4 = k_{11} \cdot x_4 \cdot x_7/(k_{10} + x_4); \\ \text{Phosphorylation of VASP}_{Ser239} \text{ by PKA}\alpha \text{ (r5)} : \quad & \nu_5 = k_5 \cdot x_5 \cdot x_6/(k_4 + x_5); \\ \text{Phosphorylation of VASP}_{Ser239} \text{ by PKA}cs \text{ (r6)} : \quad & \nu_6 = k_9 \cdot x_5 \cdot x_7/(k_8 + x_5); \\ \text{Dephosphorylation of VASP}_{Ser239} \text{ (r7)} : \quad & \nu_7 = k_3 \cdot x_9; \\ \text{Dephosphorylation of VASP}_{Ser157} \text{ (r8)} : \quad & \nu_8 = k_3 \cdot x_8; \end{aligned} \tag{5.17}$$

System of Differential Equations (VASP Phosphorylations 2)
Variables are defined Table 17.

$$\begin{aligned} \frac{\mathrm{d}x_1}{\mathrm{d}t} &= -\nu_1; \\ \frac{\mathrm{d}x_2}{\mathrm{d}t} &= -\nu_2 \\ \frac{\mathrm{d}x_3}{\mathrm{d}t} &= 0.0; \\ \frac{\mathrm{d}x_4}{\mathrm{d}t} &= -\nu_3 - \nu_4 + \nu_7; \\ \frac{\mathrm{d}x_5}{\mathrm{d}t} &= -\nu_5 - \nu_6 + \nu_7; \\ \frac{\mathrm{d}x_6}{\mathrm{d}t} &= +\nu_1; \\ \frac{\mathrm{d}x_7}{\mathrm{d}t} &= +\nu_2 \\ \frac{\mathrm{d}x_8}{\mathrm{d}t} &= +\nu_3 + \nu_4 - \nu_8; \\ \frac{\mathrm{d}x_9}{\mathrm{d}t} &= +\nu_5 - \nu_6 - \nu_7; \end{aligned} \tag{5.18}$$

Annex B.6: Fitted Parameters

Table 18 : Fitted parameter values.

Parameter description	Symbol	Value (best 50% of 1000 fits)	Value (best fit)
PDE inhibition and AC activation			
cAMP influx via AC in response to	$AC_{F(500)}$	595.60 ± 2.99 µmol/min	621.75 µmol/min
several application concentrations	$AC_{F(200)}$	386.83 ± 2.01 µmol/min	403.01 µmol/min
of Forskolin:	$AC_{F(100)}$	85.84 ± 0.36 µmol/min	87.89 µmol/min
(1 - 500 μM)	$AC_{F(30)}$	55.07 ± 0.30 µmol/min	55.60 µmol/min
	$AC_{F(10)}$	29.20 ± 0.18 µmol/min	28.56 µmol/min
	$AC_{F(3)}$	3.18 ± 0.14 µmol/min	2.10 µmol/min
	$AC_{F(1)}$	6.32 ± 0.13 µmol/min	5.22 µmol/min
cAMP influx via AC in response to	$AC_{I(100)}$	116.23 ± 0.75 µmol/min	119.82 µmol/min
several application concentrations	$AC_{I(50)}$	117.33 ± 0.75 µmol/min	120.93 µmol/min
of Iloprost:	$AC_{It(10)}$	68.21 ± 0.43 µmol/min	69.57 µmol/min
(1 - 100 nM)	$AC_{I(5)}$	53.18 ± 0.35 µmol/min	53.89 µmol/min
	$AC_{I(1)}$	4.63 ± 0.12 µmol/min	3.53 µmol/min
Inhibition of AC	k_{13}	0.86 ± 0.017 min^{-1}	0.69 min^{-1}
k_i Milrinone	k_{12_2}	0.16 ± 0.003 μM	0.14 μM
c(PDE2)	x_1	0.02 ± 0.003 µg/l	0.005 µg/l
c(PDE3)	x_2	1.78 ± 0.07 µg/l	1.70 µg/l
k_i Cilostamide	k_{12_1}	0.99 ± 0.003 μM	1 μM
Deactivation of PDE2	k_8	0.56 ± 0.018 min^{-1}	0.67 min^{-1}
Activation of PDE2	k_9	$0.0007 \pm 2.25 \cdot 10^{-5}$ min^{-1}	0.0008 min^{-1}
Deactivation of PDE3	k_{10}	0.02 ± 0.04 min^{-1}	0.95 min^{-1}
Activation of PDE3	k_{11}	$6.39 \cdot 10^{-5} \pm 0.0002$ min^{-1}	0.0046 min^{-1}
Basal influx of cAMP	k_6	8.93 ± 0.1 µmol/min	8.99 µmol/min
feedback regulation	k_4	0.01 ± 0.01 µmol^{-1}	0.2 µmol^{-1}
(cAMP $\rightarrow$ PDE3)			
VASP - model PKA and PKG			
kPKAα_{act} (2 nM)	k_1	$0.00028 \pm 1.64 \cdot 10^{-5}$ min^{-1}	0.00026 min^{-1}
kPKAα_{act} (5 nM)	k_1	0.008 ± 0.0015 min^{-1}	0.006 min^{-1}
kPKAα_{act} (10 nM)	k_1	0.04 ± 0.01 min^{-1}	0.03 min^{-1}
kVASP$_{\text{inact}}$	k_2	2.31 ± 0.53 min^{-1}	3.26 min^{-1}
K_mVASP$_{Ser239}$ (PKA$_\alpha$)	k_3	135.59 ± 61.32 μM	197.01 μM
V_{max}VASP$_{Ser239}$ (PKA$_\alpha$)	k_4	48.00 ± 22.95 µmol/min/mg	104.31 µmol/min/mg
K_mVASP$_{Ser157}$ (PKA$_\alpha$)	x_5	88.11 ± 38.07 μM	130.42 μM
V_{max}VASP$_{Ser157}$ (PKA$_\alpha$)	x_6	49.65 ± 22.05 µmol/min/mg	107.95 µmol/min/mg
K_mVASP$_{Ser239}$ (PKG)	k_7	12.36 ± 38.09 μM	2.05 μM
V_{max}VASP$_{Ser239}$ (PKG)	k_8	1.90 ± 2.45 µmol/min/mg	1.73 µmol/min/mg
K_mVASP$_{Ser157}$ (PKG)	x_9	158.28 ± 133.33 μM	214.44 μM
V_{max}VASP$_{Ser157}$ (PKG)	x_{10}	62.73 ± 47.46 µmol/min/mg	115.86 µmol/min/mg
VASP - model with two distinct catalytic PKA subunits			
kPKAα_{act} (2 nM)	k_1	63.54 ± 300.7 min^{-1}	0.18 min^{-1}
kPKAα_{act} (5 nM)	k_1	113.41 ± 390.59 min^{-1}	34.86 min^{-1}
kPKAα_{act} (10 nM)	k_1	930.42 ± 1670.26 min^{-1}	1.02 min^{-1}
kPKAcs$_{act}$ (2 nM)	k_2	$0.00033 \pm 3.99 \cdot 10^{-5}$ min^{-1}	0.00033 min^{-1}
kPKAcs$_{act}$ (5 nM)	k_2	0.0068 ± 0.001 min^{-1}	0.005 min^{-1}
kPKAcs$_{act}$ (10 nM)	k_2	0.02 ± 0.002 min^{-1}	0.02 min^{-1}

Continued on next page

Table 18 – ***continued from previous page***

Parameter description	Symbol	Value (best 50% of 1000 fits)	Value (best fit)
kVASP$_{\text{inact}}$	k_3	491.28 ± 168.90 min^{-1}	318.16 min^{-1}
K_mVASP$_{Ser239}$ (PKA$_\alpha$)	k_4	6.70 ± 11.49 μM	31.48 μM
V_{max}VASP$_{Ser239}$ (PKA$_\alpha$)	k_5	54.02 ± 20.16 µmol/min/mg	63.66 µmol/min/mg
K_mVASP$_{Ser157}$ (PKA$_\alpha$)	x_6	1.49 ± 4.58 μM	1.80 μM
V_{max}VASP$_{Ser157}$ (PKA$_\alpha$)	x_7	249.56 ± 85.36 µmol/min/mg	173.28 µmol/min/mg
K_mVASP$_{Ser239}$ (PKAcs)	k_8	0.76 ± 1.98 μM	0.01 μM
V_{max}VASP$_{Ser239}$ (PKAcs)	k_9	1041.23 ± 374.71 µmol/min/mg	676.98 µmol/min/mg
K_mVASP$_{Ser157}$ (PKAcs)	x_{10}	890.20 ± 445.65 μM	1805.42 μM
V_{max}VASP$_{Ser157}$ (PKAcs)	x_{11}	87429.4 ± 37233.7 µmol/min/mg	114700 µmol/min/mg

Annex B.7: Drug-specific Parameter Values

Table 19 : Drug-specific parameters.

Drug	Pathway effect	Drug specific parameter	Reference
		Modeled	
Milrinone	PDE3 inhibition (cAMP)	IC50: 56 $\pm$ 12 nM	(Tang et al., 1994)
		IC50: 0.3 μM	(Bailey et al., 1994)
		IC50: 0.49 μM	(Zhao et al., 2007)
		IC50: 7.0 $\pm$ 0.9 μM resulting in k_i values:	(Herget et al., 2008)
		(0.05 - 0.3) μM	(Cer et al., 2009)
		k_i: 0.55 μM	(Floreani et al., 2003)
		k_i: 0.66 μM	(Zhang et al., 2002)
		here: k_i: 0.15 μM	(k_{12_2}); Table 18[1]
Cilostamide		IC50: 70 $\pm$ 9 nM	(Tang et al., 1994)
		IC50: 0.37 $\pm$ 0.005 μM	(Herget et al., 2008)
		k_i: 1 μM	(k_{12_1}); Table 18[1]
Iloprost	AC stimulation (through GPCR)	k_{12_i}	section 4.3
Forskolin	AC stimulation (direct)		
		General/predictive	
EHNA	PDE2 inhibition (cAMP)	IC50: 1 μM	(Soderling et al., 1998)
		IC50: 0.8 - 4 μM	(Podzuweit et al., 1995)
Oxindole		IC50: 40 nM	(Rivet-Bastide et al., 1997)
Bay-60 7550		IC50: 4.7 nM	(Boess et al., 2004)
PDP		IC50: 0.6 nM	(Seybold et al., 2005)
Trequisin	PDE3 inhibition (cAMP)	IC50: 13 $\pm$ 2 nM	(Tang et al., 1994)
Lixazinone		IC50: 22 $\pm$ 4 nM	(Tang et al., 1994)
IBMX		IC50: 3950 $\pm$ 22 nM	(Tang et al., 1994)
Siguazodan		IC50: 0.117 $\pm$ 0.029 μM	(Tang et al., 1994)
Zaprinast	PDE5 inhibition (cGMP)	IC50: 0.76 μM	(Soderling et al., 1998)
Dipyridamole		IC50: 0.9 μM	(Soderling et al., 1998) (Herget et al., 2008)
Vardenafil		IC50: 0.16 $\pm$ 0.03 μM	(Herget et al., 2008)
Sildenafil		IC50: 1.9 $\pm$ 0.4 μM	(Herget et al., 2008)
Milrinone-like agonists	PDE3 inhibition	Variation of ${k_{12_2}}^2$	see section 3.3, (r7)
Cilostamide-like agonists		Variation of ${k_{12_1}}^2$	
Iloprost-like agonists	AC stimulation	Variation of ${k_{12_2}}^2$	see section 4.3, (r8)
Forskolin-like agonists		Variation of ${k_{12_1}}^2$	
		Modeling drug combinations	
Milrinone/Iloprost synergistic	PDE3 inhibition / AC stimulation	Modified AC activation by $k_{12} = 1.443 = \frac{\text{cAMP}}{{k_{\text{syn}}}^1} > 1$	see section 4.3, (r8)
Cilostamide/Iloprost synergistic	PDE3 inhibition AC stimulation	Modified AC activation $k_{12} = 1.443 = \frac{\text{cAMP}}{{k_{\text{syn}}}^1} > 1$	see section 4.3, (r8)
Milrinone/AC inhibitor	PDE3 inhibition/ AC inhibition	k_3 (AC inhibitor (I) dependent) here: $k_3 = 0.5$	AC influx = $k_6 - k_3 \cdot \log(c(I))$, k_6: basal AC influx of cAMP

Continued on next page

Table 19 – *continued from previous page*

Drug	Pathway effect	Drug specific parameter	Reference
Forskolin/Milrinone synergistic	PDE3 inhibition/ AC stimulation	Modified AC activation by $k_{12} = 1.443 = \frac{\text{cAMP}}{k_{\text{syn}}^{\text{I}}} > 1$	see section 4.3, (r8)
Single drugs with additive interaction		$k_{12} = 1$	see section 4.3, (r8)
Single drugs with antagonistic interaction	PDE3 inhibition/ PDE5 inhibition	$k_{12} = \frac{1}{1.443} < 1$	see section 4.3, (r8) (Maurice, 2003)

[1]Estimated from experimental data

[2]Range according to pharmacological relevant differences in agonist strengths

Annex C: Cross-talk Model (TNF receptors)

CellNetAnalyzer-files are available (Annex D).

Table 20 : Cross-talk model - modeled logical connections.

Reactions:	**Logical connection for simulation**
Reaction 1: TNFR1_Stimulation :	TNFR1_stimulus = TNFR1
Reaction 2: TNFR1_Stimulation_TNF :	TNF = TNFR1
Reaction 3: TNFR2_Stimulation :	TNFR2_stimulus = TNFR2
Reaction 4: TNFR2_Stimulation_TNF :	TNF = TNFR2
Reaction 5: R1_RIP_activation :	TNFR1 = RIP
Reaction 6: R1_TRAF2_cIAP1/2_recrution :	TNFR1 = 3 TRAF2_cIAP1/2_TNFR1
Reaction 7: LUBAC_complex :	RIP + TRAF2_cIAP1/2_TNFR1 + TRAF1_TRAF2_cIAP1/2_TNFR1 = 3 TAK1_TAB2_LUBAC
Reaction 8: R1_TRAF1_TRAF2_cIAP1/2_recrution :	TNFR1 = 3 TRAF1_TRAF2_cIAP1/2_TNFR1
Reaction 9: R1_RIP_caspase8_complex :	!TNFR2_stimulus + RIP + cIAP2 = RIP_caspase8
Reaction 10: R1_TRADD_FADD_caspase8_complex :	TNFR1 + !TNFR2_stimulus + cIAP2 = TRADD_FADD_caspase8
Reaction 11: R1_effector_caspase_activation :	!TNFR2_stimulus + RIP_caspase8 = effector_caspases
Reaction 12: R1R2_effector_caspases_activation_FADD :	3 TRADD_FADD_caspase8 = 3 effector_caspases
Reaction 13: R1_apoptosis :	!TNFR2_stimulus + effector_caspases = apoptosis
Reaction 14: R1_NEMO_complex_activation :	TNFR1 + 3 TAK1_TAB2_LUBAC = 3 NEMO_IKK1_IKK2
Reaction 15: R2_p65_p50_IkB_phospho :	TNFR2 + NEMO_IKK1_IKK2 = p65_p50_IkB_p
Reaction 16: R2_p65_p50_IkB_p_Ubi :	TNFR2 + p65_p50_IkB_p = p65_p50_IkB_p_Ub
Reaction 17: R2_p65_p50 :	TNFR2 + p65_p50_IkB_p_Ub = p65_p50
Reaction 18: R2_IkB_p_Ub :	TNFR2 + p65_p50_IkB_p_Ub = IkB_p_Ub
Reaction 19: R2_IkB_degradation :	TNFR2 + IkB_p_Ub = IkB_deg
Reaction 20: R2_nuclear_shuttle :	TNFR2 + p65_p50 = p65_p50_nuc
Reaction 21: induction_Cyld/A20 :	p65_p50_nuc = Cyld/A20
Reaction 22: induction_cIAP2 :	p65_p50_nuc = cIAP2
Reaction 23: induction_TRAF1 :	p65_p50_nuc = TRAF1
Reaction 24: induction_FLIP :	p65_p50_nuc = FLIP
Reaction 25: induction_TNF :	p65_p50_nuc = TNF_sec
Reaction 26: R2_TRAF_cIAP12_recrution :	TNFR2 = TRAF2_cIAP1/2
Reaction 27: INPUT_TNFR1_Stimulus :	= TNFR1_stimulus
Reaction 28: INPUT_TNFR2_stimulus :	= TNFR2_stimulus
Reaction 29: INPUT_TNF :	= TNF
Reaction 30: TRAF1/2_recr_TNFR2 :	TNFR2 = TRAF1_TRAF2_cIAP1/2
Reaction 31: alt_NFkB_reg2 :	TRAF1_TRAF2_cIAP1/2 + !TRAF1TRAF2cIAP1/2 = alt_NFkB
Reaction 32: MAPKKK_activation :	TRAF2_cIAP1/2 = MAPKKK
Reaction 33: MAPKKK_activation2 :	TRAF1_TRAF2_cIAP1/2 = MAPKKK
Reaction 34: R2_NEMO_complex_activation :	TNFR2 + MAPKKK = NEMO_IKK1_IKK2
Reaction 35: R1_p65_p50_IkB_phospho :	3 NEMO_IKK1_IKK2 = 3 p65_p50_IkB_p
Reaction 36: Proteasomal_degradation1 :	TRAF1_TRAF2_cIAP1/2 = prot_deg
Reaction 37: Proteasomal_degradation2 :	TRAF2_cIAP1/2 = prot_deg
Reaction 38: R1_p65_p50_IkB_p_Ubi :	3 p65_p50_IkB_p = 3 p65_p50_IkB_p_Ub
Reaction 39: R1_p65_p50 :	3 p65_p50_IkB_p_Ub = 3 p65_p50

Continued on next page

Table continued from previous page

Reactions:	**Logical connection for simulation**
Reaction 40: R1_IkB_p_Ub :	3 p65_p50_IkB_p_Ub = 3 IkB_p_Ub
Reaction 41: R1_nuclear_shuttle :	3 p65_p50 = 3 p65_p50_nuc
Reaction 42: R1_IkB_degradation :	3 IkB_p_Ub = 3 IkB_deg
Reaction 43: R1R2_RIP_caspase_complex :	TNFR2 + RIP + cIAP2 = 3 RIP_caspase8
Reaction 44: R1R2_effector_caspase_activation :	3 RIP_caspase8 = 3 effector_caspases
Reaction 45: R1R2_apoptosis :	3 effector_caspases ==> 3 apoptosis
Reaction 46: R1R2_TRADD_FADDcaspase8_complex :	TNFR1 + TNFR2 + cIAP2 = 3 TRADD_FADD_caspase8
Reaction 47: R1_effector_caspase_activation_FADD :	!TNFR2_stimulus + TRADD_FADD_caspase8 = effector_caspases
Reaction 48: Pre :	TNFR2 + TNFR1_stimulus = TNFR1
Reaction 49: Pre_caspase8 :	TNFR1 + TNFR2 + RIP + cIAP2 = 5 RIP_caspase8
Reaction 50: Pre_effector_caspase_activation :	5 RIP_caspase8 = 5 effector_caspases
Reaction 51: Pre_apoptosis :	5 effector_caspases = 5 apoptosis
Reaction 52: Pre_TRADD_FADDcaspase8_complex :	TNFR1 + TNFR2 + cIAP2 = 5 TRADD_FADD_caspase8
Reaction 53: Pre_TRAF1_TRAF2_cIAP1/2_recrution :	TNFR1 + TNFR2 = TRAF1_TRAF2_cIAP1/2_TNFR1
Reaction 54: Pre_TRAF2_cIAP1/2_recrution :	TNFR1 + TNFR2 = TRAF2_cIAP1/2_TNFR1
Reaction 55: Pre_LUBAC_complex :	RIP + TRAF2_cIAP1/2_TNFR1 + TRAF1_TRAF2_cIAP1/2_TNFR1 = TAK1_TAB2_LUBAC
Reaction 56: Pre_NEMO_complex_activation :	TNFR1 + TNFR2 + TAK1_TAB2_LUBAC = NEMO_IKK1_IKK2
Reaction 57: Pre_p65_p50_IkB_phospho :	NEMO_IKK1_IKK2 = p65_p50_IkB_p
Reaction 58: Pre_p65_p50_IkB_p_Ubi :	p65_p50_IkB_p = p65_p50_IkB_p_Ub
Reaction 59: Pre_p65_p50 :	p65_p50_IkB_p_Ub = p65_p50
Reaction 60: Pre_nuclear_shuttle :	p65_p50 = p65_p50_nuc
Reaction 61: Pre_IkB_p_Ub :	p65_p50_IkB_p_Ub = IkB_p_Ub
Reaction 62: Pre_IkB_degradation :	IkB_p_Ub = IkB_deg
Reaction 63: Pre_effector_caspases_activation_FADD :	5 TRADD_FADD_caspase8 = 5 effector_caspases

Annex D: Model Files

Affidavit / Eidesstattliche Erklärung

English:

I hereby confirm that my thesis entitled "Mathematical Modeling of Cellular Signal Transduction" is the result of my own work. I did not receive any help or support from commercial consultants. All sources and / or materials applied are listed and specified in the thesis.

Furthermore, I confirm that this thesis has not yet been submitted as part of another examination process neither in identical nor in similar form.

Signature: _____

_____ (Gaby Wangorsch)

Place, Date

Deutsch:

Hiermit erkläre ich an Eides statt, die Dissertation „Mathematische Modellierung der zellulärer Signaltransduktion“ eigenständig, d.h. insbesondere selbständig und ohne Hilfe eines kommerziellen Promotionsberaters, angefertigt und keine anderen als die von mir angegebenen Quellen und Hilfsmittel verwendet zu haben.

Ich erkläre außerdem, dass die Dissertation weder in gleicher noch in ähnlicher Form bereits in einem anderen Prüfungsverfahren vorgelegen hat.

Unterschrift: _____

_____ (Gaby Wangorsch)

Ort, Datum

List of Publications

Mischnik, M., Boyanova, D., Hubertus, K., Geiger, J., Philippi, N., Dittrich, M., **Wangorsch, G.**, Timmer, J., and Dandekar, T. (2013). A Boolean view separates platelet activatory and inhibitory signalling as verified by phosphorylation monitoring including threshold behaviour and integrin modulation. *Mol. BioSyst.*. (Accepted Manuscript).
URL `http://pubs.rsc.org/en/content/articlelanding/2013/MB/C3MB25597B`

Naseem, M., Philippi, N., Hussain, A., **Wangorsch, G.**, Ahmed, N., and Dandekar, T. (2012). Integrated Systems View on Networking by Hormones in *Arabidopsis* Immunity Reveals Multiple Crosstalk for Cytokinin. *Plant Cell*.
URL `http://www.plantcell.org/content/early/2012/05/27/tpc.112.098335.short?keytype=ref&ijkey=oBzmQMaXbrBA7X4.`

Schlatter, R., Philippi, N., **Wangorsch, G.**, Pick, R., Sawodny, O., Borner, C., Timmer, J., Ederer, M., and Dandekar, T. (2011). Integration of Boolean models exemplified on hepatocyte signal transduction. *Brief Bioinform*.
URL `http://dx.doi.org/10.1093/bib/bbr065.`

Wangorsch, G., Butt, E., Mark, R., Hubertus, K., Geiger, J., Dandekar, T., and Dittrich, M. (2011). Time-resolved *in silico* modeling of fine-tuned cAMP signaling in platelets: feedback loops, titrated phosphorylations and pharmacological modulation. *BMC Syst Biol*, 5: 178.
URL `http://dx.doi.org/10.1186/1752-0509-5-178.`

Manuscripts - in preparation

Wangorsch, G., Dandekar, T., and Wajant, H. (2013). Clustering of TNF receptors 1 and 2: modeling and experimental data show different phase states.

Wangorsch, G., Dittrich, M., Wajant, H., and Dandekar, T. (2013). TNFR1 and TNFR2 cross-talk modeling reveals condition-dependent antagonism and synergy.

Pachel, C., **Wangorsch, G.**, Dandekar, T., and Frantz, S. (2013). TWEAK and its inhibition in an *in vivo*-model of myocardial ischemia reperfusion.